Oriol Gomis-Bellmunt
Lucio Flavio Campanile

Design Rules for Actuators in Active Mechanical Systems

Springer

Design Rules for Actuators in Active Mechanical Systems

Oriol Gomis-Bellmunt • Lucio Flavio Campanile

Design Rules for Actuators in Active Mechanical Systems

Springer

Oriol Gomis-Bellmunt, Dr.
CITCEA-UPC (Technical University of Catalonia)
Avinguda Diagonal, 647
08028 Barcelona
Spain
oriol.gomis@upc.edu

Lucio Flavio Campanile, Dr.
Swiss Federal Laboratories for Materials Testing and Research (EMPA)
Überlandstrasse 129
8600 Dübendorf
Switzerland
flavio.campanile@empa.ch

ISBN 978-1-84882-613-7 e-ISBN 978-1-84882-614-4
DOI 10.1007/978-1-84882-614-4
Springer London Dordrecht Heidelberg New York

British Library Cataloguing in Publication Data
A catalogue record for this book is available from the British Library

Library of Congress Control Number: 2009939257

Cover design: eStudioCalamar, Figueres/Berlin

Printed on acid-free paper

Springer is part of Springer Science+Business Media (www.springer.com)

Unseren kleinen Clara und Giulia
A les nostres petites Clara i Giulia
To our little Clara and Giulia

Preface

The seed of this book was set in 2003, at the Institute of Structural Mechanics of the German Aerospace Center (DLR) in Braunschweig. Oriol joined the Institute as a Marie Curie Fellow and Flavio, as a member of the Center of Excellence "Adaptronics" at DLR, was in charge of coordinating the Marie Curie Training Site "Smart lightweight structures and transportation application". The "daily bread" of the Center of Excellence and, as a consequence, the focus of the Marie Curie Training Site, was solid-state actuation, in particular piezoceramic actuation.

While working with solid-state actuation, scientists always encounter (sooner or later) fancy histograms or tables showing the comparison between different actuator principles on a quantitative and seemingly objective basis. After having seen such comparisons a couple of times, (and at latest after a couple of lectures or conference talks in which he shows such a histograms or table himself) the scientist begins to wonder what is behind those numbers, which claim, for instance, that the performance of Shape-Memory-Alloy actuators is, say, twice as large as the one of hydraulic cylinders.

And since we could not find an exhaustive answer in published literature, we tried to compute performance quantities for conventional actuators on a model basis, in the way we knew from solid-state actuators. We realized soon that the designer of solid-state actuators lives in a quite ideal and comfortable universe, in which powerful design rules and meaningful performance quantities can be obtained, on the basis of simple assumptions, in a straightforward way. For conventional actuation things revealed definitely more complicated, and intriguing enough to be worth starting a research project. This project eventually became part of Oriol's doctoral thesis, and we kept working on this topic after he went back to Catalonia to get involved in CITCEA-UPC and Flavio took a new professional challenge at Empa in Dübendorf, Switzerland.

The model-based definition of performance quantities implies dealing with the whole design and optimization process of actuators in a systematic way, which gave added value to this work and taught us a lot of new things on solid-state actuation as well. Last year, we finally decided that the topic of model-based design rules for

actuators (conventional as well as solid-state ones) could be an interesting topic for a book.

Besides the original issue, i.e. on which objective and quantitative basis different actuator principles can be compared to each other, the contents of this book tries to give an answer to the following questions, which are strongly related to the above mentioned one:

- which is the dependance of the actuator's primary output quantities force and stroke from the mechanical load applied to the actuator?
- for a given actuator kind (i.e. actuators based on the same principle), which is the relationship between actuator geometry and primary output quantities?
- how scalable are actuators of a given kind?
- how are energetic output quantities (work and power) related to mechanical load and geometry?
- how should actuators be designed and sized to obtain the best performance for the chosen actuator kind and for a given application?

Of course it was not possible to answer the above mentioned questions in an exhaustive way and for all existing actuator classes in the time and space framework which was available for this book. So we had to limit the range of our treatment in a twofold sense:

- we reduced the number of dimensions of the design space by successive optimization: after having identified proper specific quantities, we look for the best combination between actuator and load, then we analyze the optimal value of the specific quantities with respect to the actuator design variables;
- we restricted our focus to four actuator principles: solenoid actuators, voice-coil actuators, hydraulic actuators and solid-state, strain-induction based actuators.

The reader who will make it to the end of this book will discover three distinct parts:

In the first one, the most common actuator principles are introduced, and the philosophy behind the above sketched actuator analysis is described in detail. The second one is dedicated to the application of the described analysis procedure to three classes of conventional actuators: solenoid, voice-coil and hydraulic actuators. The third part, dedicated to solid state actuation, is – paradoxically – of more conventional nature in the context of this book. As mentioned above, model-based analysis of solid-state actuator is a common tool and several papers or book chapters can be found in literature which deal with the basic concept treated in part three, like blocking force, free stroke, energy density or design of a pre-stressed solid-state actuator. Additionally, due to the exact mechanical scalability of solid-state actuators (under the assumptions of the prescribed-strain theory) the design analysis introduced in Chapter 2 and applied to conventional actuators in Chapters 3 to 5 reduces to a few quite simple concepts when applied to solid-state actuators. In order to make things more interesting, we put this material in an unusual form by introducing a new kind of graphic representation and by complementing the classic issues with

some remarks on hybrid actuators relying on a compliant passive element as well as on design analysis for solid-state actuators for dynamic applications.

We believe that this book can be of interest for anyone dealing with actuator design, and in particular:

- as a textbook for undergraduate and graduate students of mechanical engineering, aerospace engineering, mechatronics control and virtually all other specializations dealing with actuators and active materials; in particular, the graphic representation introduced in Chapter 6 can be an useful didactic tool to learn – by solving exercises – how to analyze solid-state actuators coupled with passive structural elements;
- as a reference for engineers dealing with the design of conventional as well as solid-state actuators;
- as a basis for researchers operating in the fascinating areas of smart mechanical systems as well as coupled mechanical design and optimization, who can profit from some criteria and general concepts exposed in this book, in particular while approaching – in a simultaneous way – the design of passive and active components of mechatronic and adaptive structural systems.

We are aware of the fact that if no book at all is perfect, a book which was compiled in one – even if intensive – year is quite far from being perfect. We are therefore thankful for any suggestion and comment which can help us to improve and enrich possible new editions of this work.

Dübendorf, Switzerland *Lucio Flavio Campanile*
Barcelona, Spain *Oriol Gomis-Bellmunt*
November 2008

Acknowledgements

Part of this book is a result of a research training project which has been developed in the DLR (German Aerospace Center) in Braunschweig (Germany) and supported by a Marie Curie Fellowship of the European Community program *Smart Lightweight Structures And Transportation Application* under the contract number HPMT-CT-2001-00298.

Contents

List of Figures

List of Tables

Part I
Introductory Remarks

Chapter 1
Actuator Principles and Classification

An actuator can be defined [16, 15] as an energy converter which transforms energy from an external source into mechanical energy in a controllable way. The actuator input quantities depend on the type of energy used and can be chosen among all the quantities involved in the energy conversion from the energy source to the output mechanical quantities. For electromagnetic, piezoelectric and magnetostrictive actuators the input quantities can be the current, the charge or the voltage; for fluid power actuators the fluid pressure or the flow; for shape memory alloys and thermal expansion actuators the temperature. The output quantities are of mechanical nature. We will distinguish among *(primary)* output quantities (actuator *force* and *stroke*), and *(derived)* output quantities, which can be computed on the basis of the primary quantities. The most used derived output quantities are the actuator *work* and the actuator *power*.

Actuators play a decisive role in industrial mechatronic systems. They are responsible of moving the load to the required set point transforming an input energy source into mechanical energy. This can be done transferring energy from the power source to the mechanical load when working as motors or actuators, but also returning the energy to the power source when they have to brake, operating as generators.

A typical mechatronic system scheme can be seen in Figure 1.2, including the usual elements:

- The *power source* provides the energy needed to drive the *actuator*. In industrial systems the most common power sources are electrical or fluid power.
- The *power converter* supplies (or returns) the energy from the power source to the actuator according to the controller orders. Some industrial examples of power converters are electrical inverters or hydraulic proportional valves.
- The *actuator* is the energy converter which converts the power source energy into mechanical energy.
- The *mechanical load* is the mechanical system being driven.
- The *controller* is responsible of making the whole system follow the reference set points established by an external system operator. This is achieved by sensing the critical quantities and applying appropriate control algorithms.

Fig. 1.1 Example industrial system. Press transfer system in sheet-metal working. Courtesy of Bosch Rexroth AG

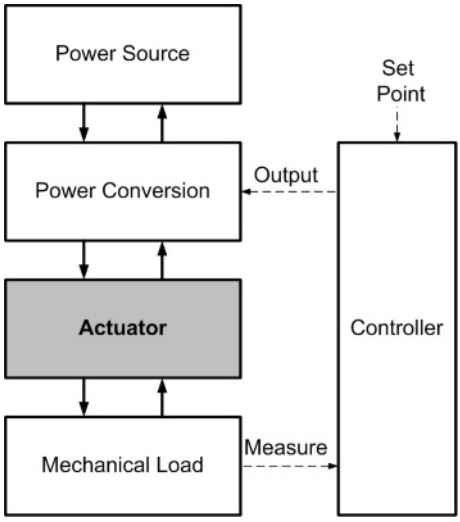

Fig. 1.2 Usual block diagram of a mechatronic system

The present chapter deals with actuator principles and classification. Firstly, different actuator principles and technologies are described. Then the main distinction between conventional and solid-state actuators is introduced and discussed.

1.1 Actuator Principles

As it has been stated, actuators convert a given kind of energy into mechanical energy. Depending on the physical principle on which the energy conversion is based, different classes of actuators can be identified. The present section deals with the actuator classes which are most relevant to the scope of this book. Some of them (electromagnetic actuators, electrostatic actuators, hydraulic actuators, pneumatic actuators, thermal expansion actuators) are state-of-the art in industrial applications; other are emerging actuator technologies in the main focus of past and current research (piezoelectric actuators magnetostrictive actuators, thermally-induced shape memory alloy actuators and electroactive polymer actuators based on dielectric elastomers). Other, less common, actuator classes like magnetic shape-memory alloys, electrochemical actuators as well as ionic electroactive polymers will not be treated here. The reader can refer to specific literature [21] to this purpose. Semi-active devices like magnetorheological and electrorheological devices are not actuators in the above mentioned sense and will be not considered in this book.

1.1.1 Electromagnetic Actuators

Electromechanic actuators convert electrical or magnetic energy to mechanical energy. The energy conversion takes place in the so-called *air gap* which separates the moving part of the actuator and the fixed part of the actuator.

Electromechanic actuators can be classified between electromagnetic and electrostatic actuators [5]. Electromagnetic actuators produce force and torque by means of magnetic energy while electrostatic and piezoelectric actuators employ directly electrical energy. The present section analyzes firstly electromagnetic actuators to later deal with electrostatic and piezoelectric actuators.

Electromagnetic actuators are commonly used in many engineering fields. They feature good force and work densities, although not as high as hydraulic actuators. They are easily controllable, since the electrical which drive the actuators may be established by means of power converters. Moreover, the power source providing the energy can be placed as far away as necessary. They permit power flow in both directions allowing to use the actuators as generators to brake whenever it is necessary. Their use must be avoided when their environment must be free of electromagnetic fields or interferences.

Electromagnetic actuators have two important circuits to take into account: the electrical circuit which establishes the currents and voltages according to the well known electrical circuit analysis laws, and the magnetic circuit which establishes the magnetic flux and magnetic field strength. The magnetic flux ϕ and magnetic flux density $\overrightarrow{B}$ is produced by the magnetic field strength $\overrightarrow{H}$ as

$$\overrightarrow{B} = \mu_r(\overrightarrow{H})\mu_0\overrightarrow{H} \tag{1.1}$$

where $\mu_0 = 4\pi 10^{-7} NA^{-2}$ is the permeability constant and μ_r is the relative permeability of the material and its dependance on $\overrightarrow{H}$ is usually analyzed by means of $B-H$ or $\mu-H$ curves.

An scalar expression, analogous to the Ohm law for electrical circuits, can be used by considering the electrical-magnetic analogy. For coil-type circuits the magnetic flux can be considered a current, the magnetomotive force $\mathfrak{F}$ is considered a voltage (with $\mathfrak{F} = Ni$ being N the number of turns and i the electrical current flowing in the coil) and the magnetic reluctance $\mathfrak{R}$ is considered as a resistance. The relationship between $\mathfrak{F}$ and ϕ yields

$$\mathfrak{F} = \mathfrak{R}\phi \tag{1.2}$$

where the reluctance can be defined for a constant section element as

$$\mathfrak{R} = \frac{l}{\mu_0 \mu_r A} \tag{1.3}$$

where l corresponds to the element length in the direction of the flux flow and A is the cross-section being crossed by the flux.

The fundamental principles for electromagnetic actuators are the *Lorentz law*, the *Faraday law* and the *Biot-Savart law*. The Lorentz law states that a current i flowing in a conductor $\overrightarrow{L}$ in the presence of a magnetic flux density $\overrightarrow{B}$ produces a force $\overrightarrow{F}$ given by

$$\overrightarrow{F} = i\overrightarrow{L} \times \overrightarrow{B} \tag{1.4}$$

which in a number of cases where $\overrightarrow{B}$ and $\overrightarrow{L}$ are orthogonal can be rewritten as

$$F = BLi \tag{1.5}$$

considering $\overrightarrow{F}$ orthogonal to both $\overrightarrow{B}$ and $\overrightarrow{L}$.

Faraday law is also known as electromagnetic induction law. It states that the induced voltage in a closed circuit is equal to the time rate of change of the magnetic flux through the circuit

$$e = -\frac{d\phi}{dt} \tag{1.6}$$

The Biot-Savart law describes the magnetic field generated by an electrical current. For a straight long (assumed infinite) conductor, it yields

$$B = \frac{\mu_r \mu_0}{2\pi r} i \tag{1.7}$$

where r is the distance to the conductor.

In the case of a solenoid, it yields

$$B = \mu_0 \mu_r \frac{Ni}{L} \tag{1.8}$$

where N is the number of turns and L the solenoid length.

1.1.1.1 Electrical Motors

Michael Faraday built the first electric motor in 1831. Since then, electrical motors have been increasingly used in more and more applications, becoming the most generalized actuators. Electrical motors can be classified according to a number of different criteria:

Fig. 1.3 Industrial DC motor. Courtesy of BEI Kimco Magnetics

- Depending on the command input type electrical motors can be classified in DC or AC motors. The first DC motor was proposed in 1831 by Michael Faraday while the first AC motor was presented in 1887 by Nikola Tesla. While DC motors (Figure 1.3) have been extensively used for many years, nowadays the use of AC motors is becoming more significant. The main advantage of DC motors based on its ease of control has been overcome by the powerful control devices available at reduced price. Moreover, some AC machines are brushless with the corresponding maintenance cost reduction.
- Depending on how the magnetic field is created, electrical motors can be classified between those using permanent magnets, those using electromagnets or induction principles.
- In AC machines, synchronization between mechanical and electrical frequencies is another important issue. AC motors can be classified according to this criterion as:
  - Synchronous motors present a mechanical speed ω_m of $\omega_m = P\omega_e$ where ω_e is the electrical pulsation and P is the number of pole pairs of the motor. The torque is proportional to the angle between the rotating field and the rotor position, while the mechanical speed is constant as long as the motor is operating stably. The synchronous motor field can be created by either a permanent magnet (typical brushless AC or DC motors) or by an electromagnet. The use of electromagnets allow to change the magnetic field as desired at the cost of needing a connection between static and rotating parts or more complex induction-based excitation systems.
  - Induction or asynchronous motors present a mechanical speed ω_m of $\omega_m = (1-s)P\omega_e$ where ω_e is the electrical pulsation, s is the so-called slip and P

is the number of pole pairs of the motor. The motor slip characterizes its behavior so that the higher the slip the higher the motor torque, which is zero for $s = 0$. Therefore, an induction motor rotating at synchronous speed does not produce any torque. The magnetic field of such induction machines is created by the currents induced in the rotor. this is the reason why asynchronous motors are called induction motors.

- Other motor concepts include:
  - Stepper motors based on a permanent magnet. The stator windings provide the magnetic field which is followed by the permanent magnet rotor. A sequence is applied to the different stator windings in order to move the rotor to a given position step by step. There are different well-known sequences to be used in this class of motors:
    - Wave drive: the different windings are excited during a certain period of time. Only one winding is excited each time.
    - Full step drive: two consecutive windings are excited each cycle, producing a higher torque.
    - Half step drive: the two previous drive modes are alternated, achieving double resolution at the cost of torque pulsation.
  - Reluctance motors: reluctance motors are based on a variable airgap reluctance which makes the rotor move to the less reluctance position.

  Detailed analysis on electrical motors can be found in [7, 22].

1.1.1.2 Solenoid Actuators

Solenoid actuators (Figure 1.4) provide motion exciting a magnetic field where a plunger (movable part) tries to minimize the reluctance (i.e. the air gap) moving to the less reluctance position. Solenoid actuators are analyzed in Chapter 3.

Fig. 1.4 Industrial solenoid actuators. Courtesy of NSF Controls Ltd

1.1.1.3 Moving Coil Actuators

Moving coil actuators are based on the interaction of a magnetic flux provided by a permanent magnet and the electrical current flowing in the so-called moving coil, described in the Lorenz force law. The force can be expressed by

$$F = Bl_w i \tag{1.9}$$

where B is the field density provided by the permanent magnet, l_w is the length of the wire and i the current flowing in the wire.

Typical industrial moving coil actuators are shown in Figure 1.5 and analyzed in Chapter 4.

Fig. 1.5 Industrial moving coil actuators. Courtesy of BEI Kimco Magnetics

1.1.1.4 Thermal Effects in Electromagnetic Actuators

The electrical circuit of an electromagnetic actuator supplies current to the coils. This current flows through wires and produces heat due to the well known Joule effect. Different materials can be employed for the wires but usually copper, silver or aluminium are used because they present the lowest resistivity (see Table 1.1). New technologies with superconductor materials (of extremely low resistivity) are being developed, but they are beyond the scope of this work.

The magnetic circuit provides the flux and the force also producing heat due to the magnetic losses in the magnetic circuit. Different materials can be used in the magnetic circuit depending on their magnetic permeability as illustrated in Table 1.2.

Electromechanical actuators have an electrical and a magnetic circuit. Such circuits are built together, and therefore, the heat generated in the coils by Joule effect must flow through part of the magnetic circuit. The heat transfer circuit includes all the components of the actuator and depends on the geometry of each of them. Although different materials can be used in both the electric and magnetic circuit, it is common to talk about copper for the electric circuit and iron for the magnetic circuit.

Table 1.1 Resistivity of different materials

Material	Resistivity [Ω m]
Silver	1.59×10^{-8}
Copper	1.68×10^{-8}
Gold	2.44×10^{-8}
Aluminium	2.65×10^{-8}
Tungsten	5.6×10^{-8}
Iron	9.71×10^{-8}
Platinum	1.06×10^{-7}
Lead	2.2×10^{-7}
Mercury	9.8×10^{-7}
Silicon	6.4×10^{2}
Glass	10^{10}-10^{14}
Teflon	10^{22}-10^{24}

Table 1.2 Magnetic permeability of different materials

Material	μ_r
Iron (99.91 %)	200
Ferrite M33	750
Nickel	600
Ferrite N41	3000
Iron (99.95 %)	5000
Ferrite T38	10000
Permalloy 78	20000
Silicon GO steel	40000
Supermalloy	100000

Although some magnetic (demagnetization, saturation and magnetization hysteresis) and mechanical (friction and mechanical stress) effects are important in electromagnetical actuators, this work assumes that the temperature is the quantity that limits the available force. Therefore, to maximize the force, a study of the heat transfer phenomenon is to be done. Although there are losses caused by the magnetic hysteresis, eddy currents and friction, the resistive losses are dominant in the considered actuators operation, and hence, only such resistive losses are considered. An expression of the maximum current or current density allowed in an actuator in order to keep the temperature under the safety threshold has been developed. For the sake of simplicity, continuous operation (100 % duty cycle) has been assumed, nonetheless the case of non-continuous operation can be considered by using the RMS current. The model will be valid as long as the thermal transients are significantly slower than the mechanical. Otherwise (for fast temperature transients), the worst case should be considered, and thus, the maximum current of the cycle should be chosen instead of the RMS current.

1.1.2 Fluid Power Actuators

Fluid power actuators use the fluid power to provide mechanical work; the difference between the pressures P in two different chambers results in a relative pressure which produces a force F in a given surface S which yields

$$F = PS \tag{1.10}$$

Fluid power actuators employed in the industry are mainly classified according the state of the fluid employed: *hydraulic actuators* employ an incompressible liquid (usually oil), while *pneumatic actuators* employ a compressible gas (air).

1.1.2.1 Hydraulic Actuators

Hydraulic actuators are commonly used in many engineering fields. They feature the following advantages:

- very good force and work densities (more than any other actuator).
- strokes as long as necessary (if enough fluid is supplied).
- easily controllable.
- the power source providing the energy can be placed far away from the actuator (but not as far as with the electromagnetic actuators).

Their main disadvantages are:

- the safety problems generated by the high pressures needed (the same fact that provides the advantages).
- the leakage flow (that can become an important problem for actuator performance, safety conditions and environmental issues).
- the inflammability of the oil employed.

An example hydraulic cylinder is shown in Figure 1.6, while the detailed parts composing such cylinder are sketched in Figure 1.7. Hydraulic actuators are further analyzed in Chapter 5.

1.1.2.2 Pneumatic Actuators

Pneumatic actuators are also used in many engineering fields. They present the following advantages:

- good force and work densities, even though not as high as the hydraulic actuators.
- able to perform strokes as long as needed like their hydraulic counterparts.
- easily controllable.
- the power source providing the energy can be placed far away from the actuator.
- able to work at higher temperatures than hydraulic actuators.

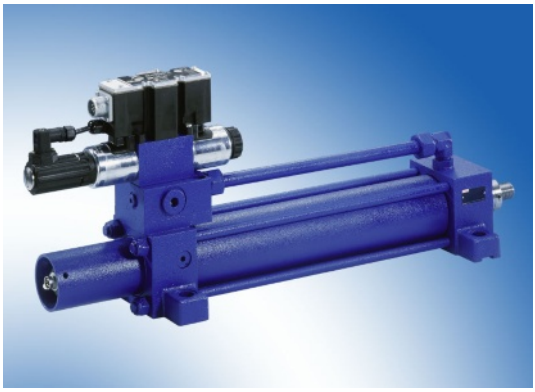

Fig. 1.6 Example hydraulic cylinder. Courtesy of Bosch Rexroth AG

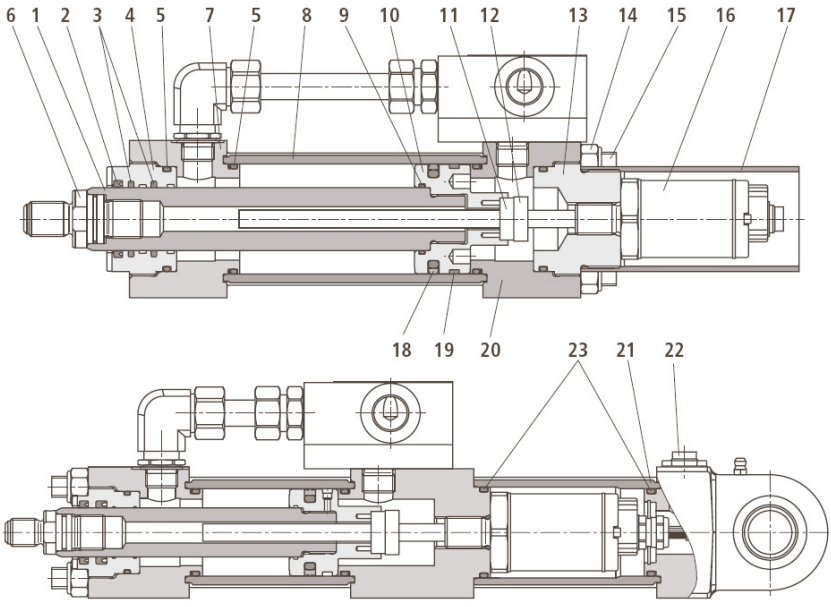

Fig. 1.7 Hydraulic cylinder parts. Courtesy of Bosch Rexroth AG

Pneumatic actuators present the following drawbacks:

- not able to work with pressures as high as the hydraulic actuators because of the problems derived from the high compressibility of the gases.

- less fast and less stiff against perturbations than their hydraulic counterparts.
- less efficient than hydraulic actuators. It is caused by the losses of energy due to the heat transfer (in the air cooling), higher leakage and worse lubrication which occurs in the pneumatic systems.

An example pneumatic cylinder is shown in Figure 1.8.

Fig. 1.8 Example pneumatic cylinder. Courtesy of Bosch Rexroth AG

1.1.3 Piezoelectric Actuators

Piezoelectric and electrostatic actuators convert electrical energy to mechanical energy without the need of using magnetic energy. The word *Piezo* derives from the Greek *piezein*, which means to squeeze or press. When joined with *electricity* forming *piezoelectricity* it stands for the material property that links directly the mechanical and electrical states. The piezoelectric effect was firstly described in 1880 by Jacques and Pierre Curie [10]. In certain materials with crystalline non-symmetrical structure, dipoles are formed when the material is deformed, i.e. a mechanical strain produces an electrical field, reciprocally the application of an electric field produces a strain.

Although the piezoelectric behavior observed is highly nonlinear, linear equations are presented in [19, 28, 27] introducing the direct and inverse piezoelectric effect:

$$\mathbf{D} = \mathbf{d}^{\mathbf{T}}\mathbf{T} + \varepsilon\mathbf{E} \tag{1.11}$$

$$\mathbf{S} = \mathbf{s}\mathbf{T} + \mathbf{d}\mathbf{E} \tag{1.12}$$

where:

- $\mathbf{d}$ is defined as the piezoelectric coefficients matrix.
- ε is the piezoelectric permittivity matrix.
- $\mathbf{s}$ is the compliance of the material matrix.
- $\mathbf{T}$ is the vector including the six components of the mechanical stress.
- $\mathbf{S}$ is the vector of mechanical strain.

- **E** is the vector including the three components of the electric field.
- **D** is the vector with the components of the electric displacement.

All the expressions can be written in matrix form. Using the tetragonal crystal system [19]:

$$\begin{pmatrix} S_1 \\ S_2 \\ S_3 \\ S_4 \\ S_5 \\ S_6 \end{pmatrix} = \begin{bmatrix} s_{11} & s_{12} & s_{13} & 0 & 0 & 0 \\ s_{12} & s_{11} & s_{13} & 0 & 0 & 0 \\ s_{13} & s_{13} & s_{33} & 0 & 0 & 0 \\ 0 & 0 & 0 & s_{44} & 0 & 0 \\ 0 & 0 & 0 & 0 & s_{44} & 0 \\ 0 & 0 & 0 & 0 & 0 & s_{66} \end{bmatrix} \times \begin{pmatrix} T_1 \\ T_2 \\ T_3 \\ T_4 \\ T_5 \\ T_6 \end{pmatrix} + \begin{bmatrix} 0 & 0 & d_{31} \\ 0 & 0 & d_{31} \\ 0 & 0 & d_{33} \\ 0 & d_{15} & 0 \\ d_{15} & 0 & 0 \\ 0 & 0 & 0 \end{bmatrix} \times \begin{pmatrix} E_1 \\ E_2 \\ E_3 \end{pmatrix} \quad (1.13)$$

Analogously:

$$\begin{pmatrix} D_1 \\ D_2 \\ D_3 \end{pmatrix} = \begin{bmatrix} 0 & 0 & 0 & 0 & d_{15} & 0 \\ 0 & 0 & 0 & d_{15} & 0 & 0 \\ d_{31} & d_{31} & d_{33} & 0 & 0 & 0 \end{bmatrix} \times \begin{pmatrix} T_1 \\ T_2 \\ T_3 \\ T_4 \\ T_5 \\ T_6 \end{pmatrix} + \begin{bmatrix} \varepsilon_{11} & 0 & 0 \\ 0 & \varepsilon_{11} & 0 \\ 0 & 0 & \varepsilon_{33} \end{bmatrix} \times \begin{pmatrix} E_1 \\ E_2 \\ E_3 \end{pmatrix} \quad (1.14)$$

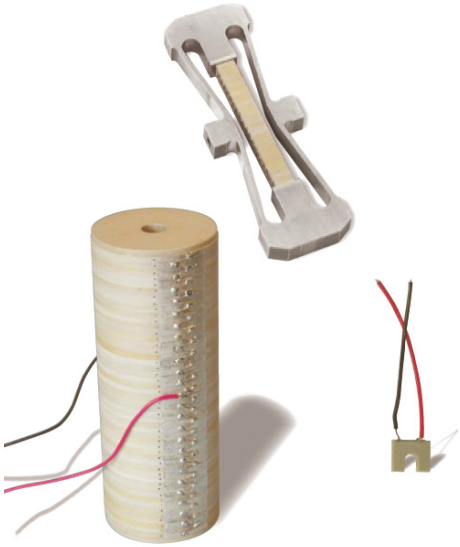

Fig. 1.9 Sample piezoelectric actuators. Courtesy of Noliac

Fig. 1.10 Sample piezoelectric actuators. Courtesy of Cedrat

1.1.3.1 Deformation Modes

The deformation directions are shown in Figure 1.11. It is important to note that all the parameters used in (1.12) have to be considered in the different deformation directions.

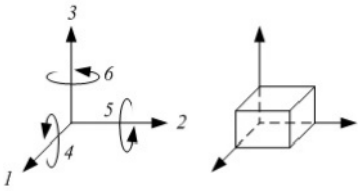

Fig. 1.11 Axes and deformation directions

Depending on the electrical field application and the deformation of interest, piezoelectric actuators can be employed using different modes:

- Longitudinal mode d_{33}. See Figure 1.12(a). Expression (1.13) turns into:

$$S_3 = \sum_{i=1}^{6} (s_{3i} T_i) + d_{33} E_3 \tag{1.15}$$

- Transverse mode d_{31}. See Figure 1.12(b). Expression (1.13) turns into:

$$S_1 = \sum_{i=1}^{6} (s_{1i} T_i) + d_{31} E_3 \tag{1.16}$$

- Shear mode d_{15}. See Figure 1.12(c). Expression (1.13) turns into:

$$S_5 = \sum_{i=1}^{6} (s_{5i} T_i) + d_{15} E_1 \tag{1.17}$$

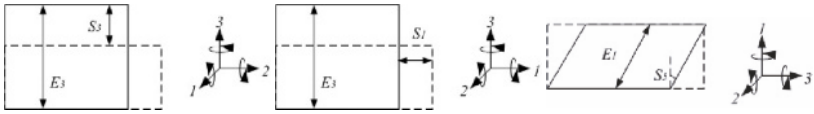

(a) (b) (c)

Fig. 1.12 Different deformation modes: (a) longitudinal mode, (b) transverse mode, (c) shear mode

1.1.3.2 Simplified Model

A piezoelectric element can be modeled from (1.12) as the association in parallel of a capacitor and a charge source, since the charge can be obtained from the electric displacement D, and the voltage can be derived from the electrical field E, assuming that it is uniformly distributed in a length l ($V = E/l$). Expression (1.12) can be written as:

$$\frac{Q_e}{A} = d\frac{F}{A} + \varepsilon\frac{V}{z} \tag{1.18}$$

$$\frac{x}{l_0} = s\frac{F}{A} + d\frac{V}{z} \tag{1.19}$$

where Q_e is the electrical charge, A is the cross-section in the movement direction, F is the force, V is the applied voltage, l_0 is the initial length in the movement axis and z is the thickness in electrical field direction. Expression (1.18), (known as the sensor expression) can be written as:

$$Q_e = dF + \varepsilon\frac{A}{z}V = dF + CV \tag{1.20}$$

where $C = \varepsilon A/z$ is the equivalent capacitance.

Equation 1.19, (known as the actuator expression) can be written as:

$$x = sl_0\frac{F}{A} + Vd\frac{l_0}{z} = k^{-1}F + d\frac{l_0}{z}V \tag{1.21}$$

where $k = A/sl_0$ is the equivalent stiffness constant. Note that in the longitudinal mode, the electrical field is applied in the motion direction and thus:

$$x = k^{-1}F + dV \tag{1.22}$$

The approximations of (1.20), (1.21) and (1.22) apply for low frequencies. When the dynamic behavior for higher frequencies (close to the mechanical resonance frequency) is concerned, the model from [30] characterized in Figure 1.13 has to be used. It includes the equivalent capacitor and a RLC branch in parallel where R_1 includes the mechanical losses, L_1 is the equivalent inductance of the mechanical circuit and C_1 the capacitance of the mechanical circuit. Each branch has a mechanical resonance at $f_i = 1/2\pi\sqrt{L_i C_i}$. A current (or charge) source can be added if the system is mechanically loaded. More branches can be added corresponding to the resonance frequencies of the mechanical system.

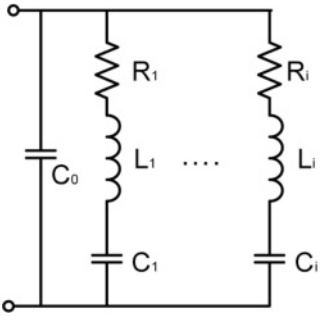

Fig. 1.13 Equivalent circuit of a piezoelectric element excited at high frequency

1.1.3.3 Load Dependance

The relationship between force and displacement can be extracted from expression (1.21). Manufacturers usually provide the force with no displacement and the free displacement. Defining F_0 as the force with no displacement (clamped actuator) and x_0 the free displacement with no force:

$$x_0 = dV\frac{l_0}{z} \tag{1.23}$$

$$F_0 = dV\frac{A}{zs} \tag{1.24}$$

Hence expression (1.21) can be rewritten as:

$$F = \frac{F_0}{x_0}(x_0 - x) \tag{1.25}$$

where both F_0 and x_0 depend linearly on the applied voltage. Note that the previously defined stiffness constant k, can be expressed as F_0/x_0 and does not depend

on the voltage but on the material stiffness. An alternative expression of (1.25) is:

$$F = k\,(x_0 - x) = F_0 - kx \tag{1.26}$$

Example 1.1. An example can be shown with a sample actuator working in the transversal mode. The parameters are:

$$\begin{aligned} l_0 &= 50 \cdot 10^{-3} m \\ z_0 &= 0.2 \cdot 10^{-3} m \\ A &= 6 \cdot 10^{-6} m^2 \\ s_{31} &= 15 \cdot 10^{-12} m^2/N \\ d_{31} &= -250 \cdot 10^{-12} m/V \end{aligned}$$

Then:

$$k = \frac{A}{s_E \cdot l_0} = \frac{6 \cdot 10^{-6}}{15 \cdot 10^{-12} \cdot 50 \cdot 10^{-3}} = 8 \cdot 10^6 N/m$$

For $V = 400\,V$:

$$\begin{aligned} x_0 &= d \cdot V \cdot \tfrac{l_0}{z_0} = -250 \cdot 10^{-12} \cdot 400 \cdot \tfrac{50 \cdot 10^{-3}}{0.2 \cdot 10^{-3}} = 25 \cdot 10^{-6} m \\ F_0 &= x_0 \cdot k = 200N \end{aligned}$$

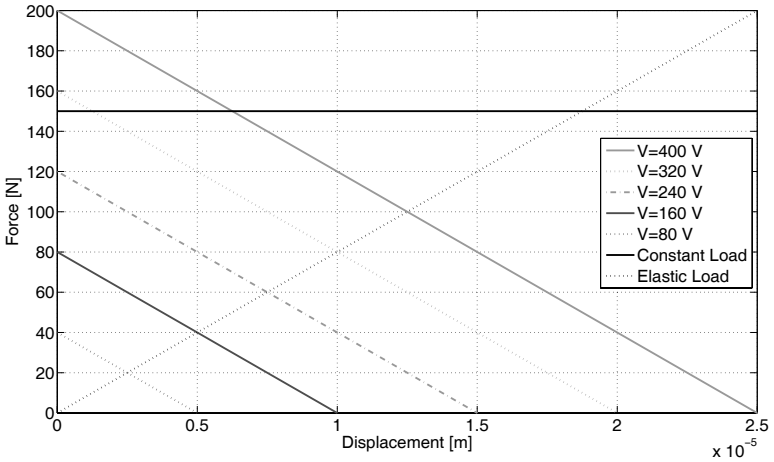

Fig. 1.14 Displacement-force curves

In Figure 1.14 the load-displacement characteristic for different voltages can be seen. Also the load-displacement characteristic for different voltages under a constant load and linear load (for example a spring or a attached structure) are shown.

1.1.3.4 Piezoelectric Materials

The piezoelectric materials are divided in single-crystal materials, piezoceramics, piezopolymers, piezocomposites and piezofilms. Comprehensive information about them may be found in [27]. The most significant parameters employed to describe piezoelectric actuators can be found in Table 1.3. The most relevant properties of some piezoelectric materials are shown in Table 1.4.

Table 1.3 Piezoelectric material relevant parameters

Quantity	Description	Units
d_{ij}	Piezoelectric Strain Constant	C/N
g_{ij}	Piezoelectric Voltage Constant	Vm/N
k_t	Thickness-extensional coupling factor	
k_p	Planar coupling factor	
ε	Relative permittivity	
Q_m	Mechanical Quality Factor	
T_C	Curie Temperature	$^\circ C$

Table 1.4 Piezoelectric material properties [27]

Parameter	Quartz	$BaTiO_3$	PZT 4	PST 5H	(Pb,Sm) TiO_3	PVDF TrFE
d_{33} pC/N	2.3	190	289	593	65	33
g_{33} $10^{-3}Vm/N$	57.8	12.6	26.1	19.7	42	380
k_t	0.09	0.38	0.51	0.50	0.50	0.30
k_p		0.33	0.58	0.65	0.03	
ε	5	1700	1300	3400	175	6
Q_m	$> 10^5$		500	65	900	3-10
T_C $^\circ C$		120	328	193	355	

1.1.3.5 Applications

The employment of piezoelectric actuators has been increased in the last decades. The main advantages [26] shown by the piezoelectric actuators are:

- High resolution: a piezoelectric actuator can perform very small and precise position changes to the subnanometer range.
- Easy miniaturization: The fact that they are solid state actuators allows to miniaturize them and allow their application to micro and nano-scale applications. This advantage is very significative in comparison with their electromagnetic counterparts [16].

- Work in different directions: it is not necessarily an advantage but it certainly allows a wide range of applications, not only longitudinal traction.
- Large force generation: piezoelectric actuators generate large forces. It leads to high energy and power densities.
- Very rapid response: piezoelectric actuators offer very fast time response. It enables to be used in applications requiring very high frequencies.
- Absence of magnetic fields: piezoelectric actuators are especially indicated for applications where magnetic fields are not allowed.
- Low power consumption: the piezoelectric effect converts directly electrical energy to motion. The electrical energy is consumed only during the motion. The static losses can be considered very low in comparison with other kinds of actuators.
- Compatible with vacuum and clean rooms: piezoelectric actuators use ceramic elements which do not need lubrication and exhibit no wear or abrasion. This makes them clean-room compatible and ideally suited for ultra-high-vacuum applications.

The main drawbacks include:

- Reduced displacement: the piezoelectric actuators range is small in comparison with other actuators. The maximum typical deformation is approximately < 0.2 %.
- High voltage operation: to obtain a certain displacement usually requires high voltage operation, with all the drawbacks involved.
- High nonlinearity: piezoelectric actuators show an elevated nonlinearity due to hysteresis and creep.

The mentioned advantages make piezoelectric actuators appropriated for a wide range of applications. They are summarized in Table 1.5.

1.1.4 Thermal Shape Memory Alloy Actuators

The shape memory effect was firstly observed in 1932 by A. Ölander in a gold-cadmium alloy. The shape memory effect is the property of some materials to recover a predefined memorized shape once they have deformed. Such an effect is based on solid-solid phase transition and it occurs in a given temperature interval [21]. The most known kind of shape memory alloys is nickel-titanium alloy, however other alloys as copper-zinc-aluminum-nickel and copper-aluminum-nickel also reproduce a similar behavior and can be used at higher temperatures than nickel-titanium alloys.

The employment of shape memory alloys as actuators reside in their capability of return to the original shape when they are heated up and move from martensite to austenitic structure producing high force. While shape memory alloy actuators present many advantages including easy miniaturization, high energy density and

Table 1.5 Main applications of piezoelectric devices

Linear actuator	Bending actuator	Generator sensor	Transformer sensor/actuator
Fuel injection	Drug dispensers	Accelerometers	LCD backlighting
Printers	Valves	Force sensor	Ion generators
Microscopes	Pumps	Pressure sensor	Power supplies
Micropositioning	Micropositioning	Knock sensors	
Nanopositioning	Nanopositioning	Gyroscopes	
Tunable lasers	Textile machines	Medical	
Ultrasonic motors	Optics	Gas ignition	
Micro pumps	Micro pumps	Sonars	
Ultrasound scanners	Vibration control	Medical scanners	
Droplet dispensing	Droplet dispensing	Blood flow meters	
Hard disc drives	Wire bonding	Distance sensors	
Process control	Tunable lasers		
Mechatronics	Mechatronics		
Optics	Optics		
Vibration control	Vibration control		
Ultrasound welding	Telecommunication		
Ultrasound cleaning	Moving opt. fibres		
Stretching opt. fibers			

flexible configuration, they present some important drawbacks related to their low speed, temperature dependance and low efficiency.

Shape memory alloy actuators are used in a broad range of engineering applications including among others, medical equipment, robotics and aeronautics applications. Some shape memory alloys components used in medical applications can be seen in Figures 1.15 and 1.16.

Fig. 1.15 Shape memory alloy actuator used in medical applications. It consists in a tissue spreader used in open heart surgery. Courtesy of Memory Metalle GmbH

Fig. 1.16 Shape memory alloy parts. Courtesy of Memory Metalle GmbH

1.1.5 Other Actuators

1.1.5.1 Electrostatic Actuators

Electrostatic actuators are based on the well-known Coulomb law, which was reported in 1780 and describes the force between two electrical charges as

$$F = \frac{1}{4\pi\varepsilon_0}\frac{Q_1 Q_2}{r^2} \tag{1.27}$$

where Q_1 and Q_2 are the interacting electrical charges, r is the distance between such charges and ε_0 is the electric constant, which yields $\varepsilon_0 = 8.854 \times 10^{-12}$. When the charges are of the same sign there is a positive force which implies a repulsion. If the charges are of opposite sign, there is a negative force implying attraction.

In practice, a number of electrostatic actuators are based on capacitive actuators. They use the energy stored E_C by a capacitor of capacitance C, which yields $E_C = (1/2)CV^2$, being V the applied voltage. Considering two opposite parallel plates, the capacitance C can be expressed as $C = \varepsilon A/r$,where ε is the dielectric permittivity, A is the plate surface and r the distance between plates.

The force between plates yields:

$$F_C = -\frac{\varepsilon A V^2}{2r^2} \tag{1.28}$$

Because electrostatic actuators show lower energy density than their magnetic counterparts [5], their use is restricted to micromechanical actuators, like the well-known comb actuators [1] of Figure 1.17.

1.1.5.2 Magnetostrictive Actuators

A magnetic field applied to ferromagnetic materials produces magnetostriction, which forces the expansion (in the case of positive magnetostriction) or contraction (for negative magnetostriction) of the element which is subjected to a longitudinal static magnetic field [21]. It is actually the same effect that produces the well-known undesired transformer hum. Regardless the direction of the magnetic field, magne-

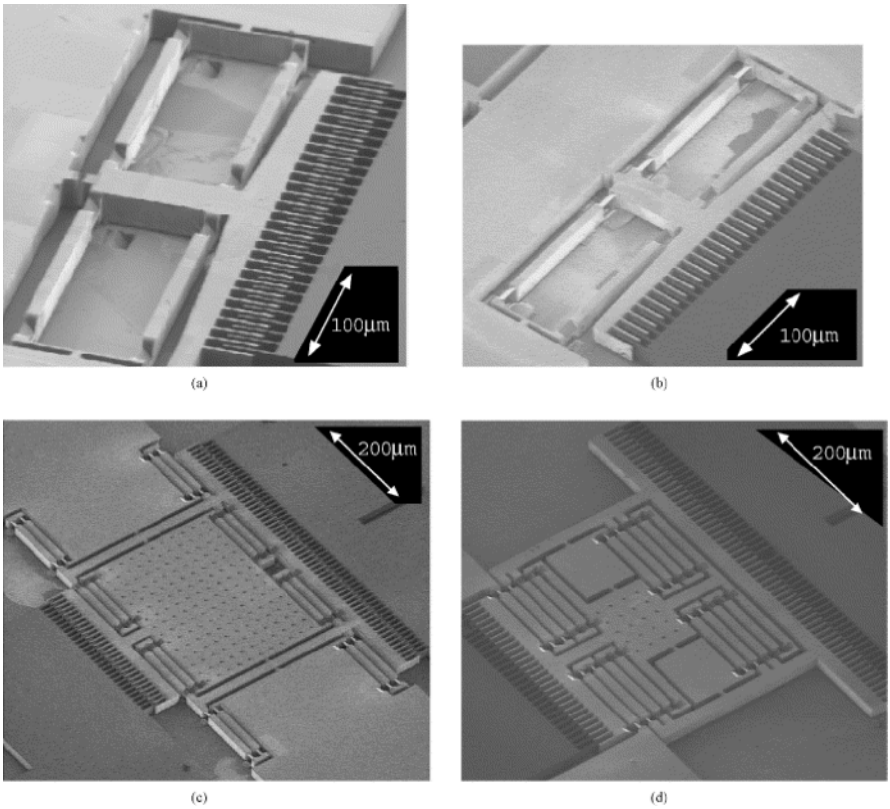

Fig. 1.17 Comb actuator by Ando et al. [1]

tostriction is experienced always in the same direction and shows a quadratic relationship between strain and magnetic field. Magnetostriction was first observed with nickel by James Joule in 1842.

According to [17] some relevant data on magnetostrictive maximum strains for some materials is given in Table 1.6. It can be noted that some materials like nickel show negative magnetostriction like others as Terfenol-D show positive magnetostriction.

Table 1.6 Magnetostrictive maximum strain. Data from [17]

Material	Max. strain (ppm)
Ni	-50
Fe	-14
Fe_3O_4	60
Terfenol-D	2000
$Tb_{0.5}Zn_{0.5}$	5500
$Tb_{0.5}Dy_xZn$	5000

Magnetostrictive actuators (Figure 1.18) feature larger strains than their piezoelectric counterparts and therefore they can be used in applications where piezoelectric actuators are used, ranging from ultrasonic motors (Figure 1.19) to miniature micro-actuators. Furthermore, magnetostrictive actuators show less hysteresis than piezoelectric actuators. The main drawback is the cost and volume implied by the need of a solenoid or a another device to produce the magnetic field.

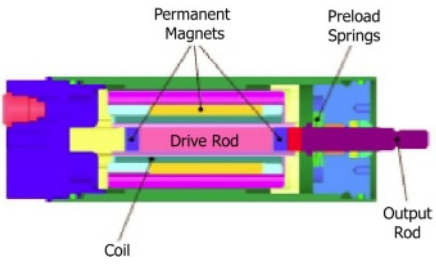

Fig. 1.18 Magnetostrictive actuator concept. Courtesy of ETREMA Products, Inc.

Fig. 1.19 Ultrasonic magnetostrictive actuator. Courtesy of ETREMA Products, Inc.

1.1.5.3 Thermal Expansion Actuators

Thermal expansion actuators are usually designed using thermal bimorphs. In such actuators, two bonded element expand at different rates when temperature changes and therefore a stress is produced in the bimorph and it curves to one side.

The typical expression for the curvature radius yields

$$\Re = \frac{(w_1 + w_2)^2}{6(\alpha_1 - \alpha_2)\Delta T w_1 w_2} \tag{1.29}$$

where w_1 and w_2 are the thicknesses of the two bonded elements, α_i is the material thermal expansion coefficient and ΔT is the temperature increment.

Thermal expansion actuators feature strong forces and relatively large displacements. The main drawbacks are their temperature dependency, slow actuation and control difficulties.

1.2 Solid-State versus Conventional Actuation

Piezoceramic actuators are *solid-state* actuators, since they exploit a material effect. They are inherently monolithic, while conventional actuators like hydraulic cylinders or solenoid actuator need moveable or sliding parts.

The basic ingredient of a solid-state actuator is an *active material*[1] . Active materials typically respond, when unconstrained, with the generation of a mechanical strain to an input of non-mechanical nature (e.g. a change in the electric or thermal field). Due to this reason, the term "induced-strain actuators" is often used to denote solid-state actuators. When the strain generation is hindered, mechanical stresses are generated (according to the stress-strain behavior of the material). Besides the active material, the solid-state actuator is provided with elements apt to produce the non-mechanical input (electrodes, coils, leading wires) and to transfer the mechanical output (forces and displacements) to the host system. Finally, auxiliary components like insulation elements or casing complete the device.

Besides piezoceramic actuators, the most common kind of solid-state actuators are thermal shape-memory alloy actuators. Electrostrictive and magnetostrictive actuators also belong to this actuator class. Despite of their monolithic nature, Electroactive Polymers based on dielectric elastomers cannot be considered as solid-state actuator in the sense introduced above, since they do not operate according to the strain induction principle, but they are stress inducing instead. An electrostatic force is primarily generated and the dielectric elastomer works essentially in a passive way (as an insulator as well as a mechanical transmission element).

Solid state actuators and the closely related area of smart structural systems constitute a very broad field involving a large number of disciplines. It has experienced a strong growth in the last ten to twenty years, and the amount of available literature is correspondingly very large. Within the scope of this book, only a few aspects can be discussed in detail, mainly related to simple rules for the preliminary design

[1] In the literature devoted to active or adaptive structures, several (more or less equivalent) denominations are used for active materials. The terms "smart materials" and "intelligent materials" are widely used, despite of their inconsistence (the materials as such are neither intelligent nor smart, but allow for interfacing a structural system with the "intelligence" or smartness of a control algorithm). The same holds for the term "adaptive materials", since adaptivity is not a property of the material, but of the system or structure which incorporates the material. A more lucky choice is represented by the term "multifunctional materials", which points at the fact that active materials join the conventional load-carrying function of a passive, construction material with actuating or sensing capabilities.

of single actuators. The interested reader can find plenty of details on solid-state actuation and smart structures in [8, 2, 13, 25, 11, 29, 24, 3, 9, 12, 4].

Solid-state actuators present some peculiar advantages with respect to conventional actuators [6]:

- *Configurability*. Since they are material-based, solid-state actuators profit from a high level of configurability: They can be virtually shaped in any form and be therefore easily customized for a particular application.
- *Multifunctionality*. Solid-state actuators are load-carrying elements. This feature involves two distinct aspects: firstly, while conventional actuators are built to carry loads in one single mode, a solid-state actuator virtually interacts with its mechanical environment by means of distributed stresses and strains and offers therefore the possibility of carrying loads in multiple directions; secondly, in its main loading mode and due strain induction, a solid-state actuator stiffens the host structure without requiring additional mechanical energy to work "against" this stiffness contribution. Additionally, the load-carrying function of a solid-state actuator is present even if the actuator input (e.g. electrical tension) is switched off.
- *Integrability*. Solid-state actuators can be better integrated into structures. They can be virtually distributed over the structure, in a continuous fashion or as arrays of miniaturized actuators. This helps reducing load concentrations and saving structural weight.
- *Scalability*. Solid-state actuators are mechanically scalable. This implies the possibility of realizing small-scale actuators (useful for the above mentioned distributed actuation) as well as the possibility of realizing full functional, reduced-scale models of active structural systems for investigation purposes (e.g. wind tunnel models).
- *Damage tolerance*. Solid-state actuators can experience a partial mechanical failure and still being able to operate. A typical case is represented by piezoceramic plate actuators which break in several pieces due to excessive bending and still work (each piece operates as a single actuator).
- *High specific performance*. Due to the strain-induction principle, actuator forces per unit area are of the order of magnitude of the modulus of elasticity times the active strain. This leads to a high static specific performance (energy density, see Section 6.4.1) for high-strain materials like Shape Memory Alloys and to a high dynamic performance (deliverable power per unit volume or weight) for fast reacting materials like piezoceramics [23, 20, 18, 14].
- *Compactness*. Solid-state actuators are of inherently monolithic nature: they show no backlash, are wear and lubrication free and profit from a reduced need for assembly.
- *Simple modeling.* This is the most relevant feature in the context of this book. Solid-state actuation can be modeled at the material level, which makes the analysis of the actuator performance as a function of its geometry straightforward (at least within the limits of a linear theory based on the prescribed-strain approach). This presents large advantages for preliminary design of actuators as well as for the coupled optimization of actuator and structure.

The theory of single-stroke linear solid-state actuators as well as the design rules presented in Chapter 6 are limited to materials and actuators based on the strain induction principle. Moreover, we will explicitly refer to single-stroke actuators, i.e. actuators which interface with the host mechanical systems through one single force and one single stroke. A SMA wire and a piezoceramic stack actuator are common examples of single-stroke solid-state actuators. Even if some of the mentioned advantages (mainly related to multifunctionality and integrability) of solid-state actuation are put into perspective for this class of actuators, this restriction allows for formulating simple and expedient design rules. Most of the documented applications of solid-state actuators are still kept at a relatively low integration level, and even in the case of higher integration (e.g. piezoelectric patches glued on the surface of a thin-walled structure), the interaction between actuator and host structure can often be regarded, as a first approximation, as of single-stroke nature, which makes the single-stroke assumption useful in most cases of practical relevance.

References

1. Ando Y, Ikehara T, Matsumoto S (2002) Design, fabrication and testing of new comb actuators realizing three-dimensional continuous motions. Sensors and Actuators A: Physical 97-98:579–586
2. Auricchio F (2005) Shape memory alloys: applications, micromechanics, macromodeling and numerical simulations. PhD thesis, University of California at Berkeley
3. Banks HT, Smith RC, Wang Y (1996) Smart Material Structures Modeling, Estimation and Control. Wiley, New York
4. Birman V (1997) Review of mechanics of shape memory alloy structures. Applied Mechanics Reviews 50:629–645
5. Bishop RH (ed) (2002) The Mechatronics Handbook. CRC Press
6. Campanile LF (2007) Adaptive Structures: Engineering applications, John Wiley and Sons, chap Lightweight shape-adaptable airfoils: a new challenge for an old dream, pp 89–135
7. Chapman S (2004) Electric Machinery Fundamentals. McGraw-Hill Professional
8. Chopra I (2002) Review of state of art of smart structures and integrated systems. AIAA Journal 40(11):2145–2187
9. Culshaw B (1996) Smart Structures and Materials. Artech House Optoelectronics Library, Boston
10. Curie J, Curie P (1880) Développement par compression de l'électricité polaire dans les cristaux hémièdres à faces inclinées. Bulletin de la Société Minéralogique de France 3:90–93
11. Duerig T, Melton K, Stockel D, Wayman C (eds) (1990) Engineering Aspects of Shape Memory Alloys. Butterworth-Heinemann, London
12. Fremond M, Miyazaki S (1996) Shape Memory Alloys. Springer-Verlag, New York
13. Funakubo H (ed) (1987) Shape memory alloys. Gordon and Breach Science Publishers, New York
14. Giurgiutiu V, Rogers CA (1996) Energy based comparision of solid state induced strain actuators. Journal of intelligent material systems and structures 7
15. Gomis-Bellmunt O (2007) Design, modeling, identification and control of mechatronic systems. PhD thesis, Technical University of Catalonia

16. Gomis-Bellmunt O, Galceran-Arellano S, Sudrià-Andreu A, Montesinos-Miracle D, Campanile LF (2007) Linear electromagnetic actuator modeling for optimization of mechatronic and adaptronic systems. Mechatronics 17:153–163
17. Grunwald A, Olabi A (2008) Design of a magnetostrictive (ms) actuator. Sensors and Actuators A: Physical 144:161–175
18. Huber JE, Fleck NA, Ashby MF (1997) The selection of mechanical actuators based on performance indices. Proc R Soc Lond A 453:2185–2205
19. IEEE Ultrasonics F, Society FC (1987) IEEE Standards on Piezoelectricity. IEEE
20. Jänker P, Martin W (1993) Performance and characteristics of actuator material. In: Proc. of the 4th International Conference on Adaptive Structures, Cologne, Germany, pp 126–138
21. Janocha H (2000) Adaptronics and Smart Structures. Springer Verlag
22. Krause P (1986) Analysis of Electric Machinery. McGraw-Hill
23. Kuribayashi K (1993) Criteria for the evaluation of new actuators as energy converters. Advanced robotics 7(4):289–307
24. Matsuzaki Y (1997) Smart structures research in Japan. Smart Materials and Structures 6:R1–R10
25. Otsuka K, Ren X (2005) Physical metallurgy of Ti-Ni-based shape memory alloys. Progress in Materials Science 50(5):511–678
26. PI PI (2005-2006) The world of Micro- and Nanopositioning
27. Uchino K (1997) Piezoelectric Actuators and Ultrasonic Motors. Kluwer Academic Publishers
28. Uchino K (2000) Ferroelectric Devices. Marcel Dekker Inc.
29. Utku S (1998) Theory of Adaptive Structures. CRC Press, New York
30. Waanders J (1991) Piezoelectric Ceramics. Properties and Applications, 1st edn. Philips Components, Eindhoven

Chapter 2
Actuator Design Analysis

2.1 Nature and Objectives of Actuator Design Analysis

The primary quantities of an actuator depend on

1. the actuator principle or class (e.g. piezoceramic stack actuator, solenoid actuator, hydraulic cylinder);
2. a set of non-geometrical design variables (e.g. the kind of active material used, the amount of pre-strain of a Shape-Memory wire);
3. a set of geometrical variables;
4. the actuator input quantity;
5. the external load.

While designing an actuator for a particular application, the engineer deals explicitly or implicitly with this multi-variable dependency. Even with the help of formal optimization algorithms, the design task can reveal extremely challenging if no preliminary information is made available to the engineers as a guide to effectively move in the highly multidimensional design space the actuator. With limited resources for the design procedure, the result is inevitably a sub-optimal actuator device. Things become even more complex if the actuator is to be designed together with the host mechanical system.

The scope of this study is to provide such a guide by analyzing the above listed dependencies in a systematic and general way, discerning strong trends from the weak ones and finally extracting rules and criteria to be used as a basis for a powerful and efficient design process.

In particular, those rules and criteria should guide the engineer in:

- choosing the proper actuator class or principle for a given application.
- optimizing the actuator size and geometry for given output quantities.
- perform a simultaneous design of the actuator's geometry and of its interface with a given host mechanical system (in this case the required actuator output quantities are not defined explicitly but are function of the actuator position and

of the direction of the actuator forces, which are among the unknowns of the problem).
- perform a coupled optimization with the external system in which the whole system is to be concurrently designed.

For some design tasks it can be useful not to refer to the primary output quantities, but to derived quantities, mostly of energetic nature, like work or power. The work performed by the actuator against an external load will depend on all the variables listed above, with the difference that on point d. not a single value of the input quantity is to be considered but a defined change of the input quantity between a minimum and a maximum value. The actuator power will be defined by a cyclic variation of the input quantity as a function of time instead.

The key facts which will be considered in the actuator design analysis presented in this chapter are discussed in the following:

- **Effect of the external load**. For a given choice of the variables on items 1 to 4, the actuator defines a relationship between the primary output quantities. The actual value of the actuator force and stroke are only defined if the characteristic curve of the external load is considered, which provides a second relationship between those quantities. While considering a parametric choice of possible loads (e.g. all linear elastic springs, defined by their spring constant) the primary output quantities can be usually maximized with respect to the load. The same applies to derived quantities (with the adjustments discussed above). The maximum values of the considered output quantities are taken into a second step of the design analysis; the optimal load for a given quantity to be maximized gives a valuable insight on how actuator and host system have to be adapted to another in order to exploit the chosen actuation principle in an efficient way.
- **Thresholds on the input quantities**. While considering now the maximum values resulting by the above described load analysis, these will depend only on the variables listed on items 1 to 4. The dependency on the input variable chosen to drive the actuator will usually be of monotonic nature but just up to a threshold value beyond which the input variable cannot be increased. By analyzing the threshold effects and identifying the limit values the design space can be reduced by a further dimension.
- **Geometrical parameterization**. The maximum output quantities resulting by the threshold analysis can now be analyzed as a function of the actuator geometry (for a fixed choice of the variables on items 1 and 2). The first step of the geometry analysis is the identification of a global representative length which defines the actuator size and of an appropriate number of aspect ratios which relate the actuator size to a corresponding number of reference lengths along different axes. The further geometrical variables are then related to the reference lengths on the same axis by additional non-dimensional variables. In most cases, these additional variables express the relationship between an active length, area or quantity of active material to the length, area or quantity of a passive component. We will therefore use the name filling factors for geometrical ratios defined on the same axis, implicitly including geometrical ratios of different nature.

- **Size analysis**. Since the output quantities are expected to increase indefinitely as a function of the actuator size, the next step in the actuator design analysis is to identify the law which rules the dependency of the maximum output quantities on the size and try to separate, if possible, this dependency from the dependency on aspect ratios and filling factors. If the dependency on size is defined, the analysis can now be reduced to the study of the dependency of the maximum output quantities for a given size as a function of aspect ratios, filling factors and finally the non-geometrical variables listed on items 1 and 2.
- **Scalability**. One important implication of size analysis is the scalability issue. It deals with the question if the output quantities are mechanically scalable, i.e. if they change with size like in a passive mechanical system which can be analyzed by continuum mechanics. This implies forces to scale with the square of size and strokes linearly with the size. As a consequence, work scales with the cube of the size. Mechanical scalability is quite relevant for mechatronic and adaptronic systems, since it allows to globally scale the whole active system consisting of a passive and an active part.
- **Shape analysis**. Once the output quantities have gone through the successive steps of load optimization, input quantity threshold and size analysis, the optimal aspect ratios and filling factors can be found, in order to finally achieve a set of performance quantities which are representative for the chosen actuator principle (item 1) and only depend on non-geometrical design variables (item 2).
- **Actuator principle analysis**. This is the final step of the actuator design analysis, in which the chosen actuator principle can be analyzed on a general basis, independently on geometry, thresholds and loads. After having performed – if possible – an optimization with respect to the non-geometrical design variables of item 2, indexes of merit for the chosen actuator principle can be defined on an objective and quantitative basis, which helps comparing different possible choices for a given application.

The designer can take advantage from the described design analysis as a whole or in part, making use of intermediate results and integrating them with conventional design procedures based on statistical methods or on trial-and-error techniques. In order to get familiar with the proposed design philosophy, we will summarize it in form of a stepwise design algorithm which essentially reproduces the successive reduction of the design space described above.

This algorithm will be applied once the designer chooses a certain class of actuator and defines a first sketch of the actuator geometry as illustrated in Figure 2.1. After applying the algorithm, the actuator designer can decide whether the obtained actuator performance is optimum or not and to introduce or change the actuator class or geometry and start the procedure again. The procedure can be repeated until it becomes clear that the best actuator has been chosen for the given application.

The forthcoming sections illustrate the different methodology steps, stressing the most important concepts which are to become relevant in the design of the actuator. The different step procedures are explained and illustrated by means of examples. Although the whole methodology is described, it has to be noted that for some classes of actuators not all the steps will have the same importance. Dimensional

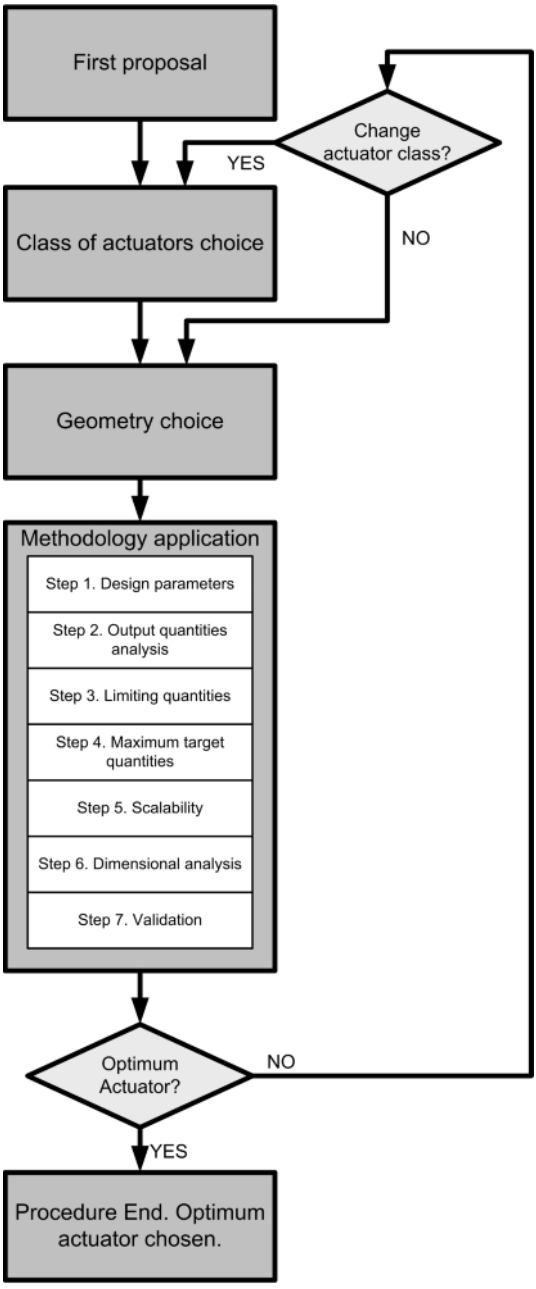

Fig. 2.1 Actuator design procedure

analysis, for example, may become valuable in some applications related to fluid power or thermal transfer and may provide trivial results when dealing with other kind of actuator applications. In any case, it is strongly recommended to follow all the steps, since some relevant non-expected results may be obtained in certain cases.

Although the present chapter describes different examples to illustrate the methodology, a detailed analysis of three classes of conventional actuators (solenoid, moving coil and hydraulic actuators) will be developed in the following Chapters 3, 4 and 5. The application to solid-state actuators will be the topic of Chapter 6.

2.2 Performance Indexes

Before explaining the actuator design analysis philosophy in more detail, we will shortly review some published results on actuator performance indexes, which somehow represent the state of the art on the issue of quantitative comparison of different actuator class and principles.

As a rule, published performance indexes of actuators are based on statistical methods, with the exception of solid-state actuators for which a model-based analysis is quite straightforward and customary. With the design analysis described later in the chapter we aim to provide a novel contribution to this topic by extending model-based techniques to conventional actuator principles.

The data presented in this section are taken from [5, 4, 11], where the reader can find more details on the definition of the used performance indexes and on how the quantitative results were obtained.

The basic characteristics of actuators are well defined as the stress σ and the strain ε. As stress and strain apply for a broad range of actuator sizes, for a specific application it is common to use the force F and displacement or stroke x. Stress and force are linked by the section A as $F = \sigma A$, while strain and displacement are linked by the reference length l as $x = \varepsilon l$.

The present Section analyzes and compares different actuator classes according to different performance criteria. When an actuator has to be chosen for a given application, the designer has to decide what the relevant criteria are and choose one actuator or the other according to it.

The analyzed classes of actuators are:

1. Low strain piezoelectric actuators
2. High strain piezoelectric actuators
3. Polymeric piezoelectric actuators
4. Thermal expansion actuators 10 K
5. Thermal expansion actuators 100 K
6. Magnetostrictive actuators
7. Shape memory alloy based actuators
8. Moving coil actuators
9. Solenoid actuators
10. Muscles

11. Pneumatic actuators
12. Hydraulic actuators

The different actuator classes have been compared using different performance indices. Such indices include:

1. Maximum strain
2. Maximum stress
3. Maximum frequency
4. Maximum volumetric power density
5. Maximum mass power density
6. Efficiency
7. Resolution

A plot showing the different maximum strain versus maximum stress is shown in Figure 2.2. It can be noted that the diagonal lines from left-top to right-bottom show constant volumetric energy. It implies that a certain actuator can move along this diagonal by using mechanical amplification or reduction. For example, a high strain piezoelectric actuator performs strains in the range of 10^{-4}. If a mechanical amplification is added it can increase notably the strain at the cost of reducing the stress in the same proportion.

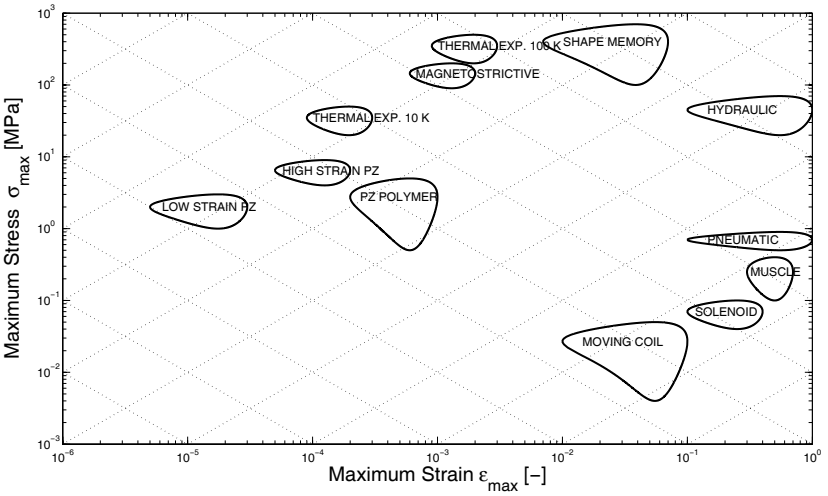

Fig. 2.2 Maximum stress versus maximum strain for different classes of actuators (Data extracted from [5])

Another important quantity is the maximum available frequency. Some actuators can provide large strains, while others feature high frequencies. Again, mechanical transmissions can be used in order to increase frequency or strain, but they increase the volume, weight and cost of actuation system chosen. Figure 2.3 illustrates the

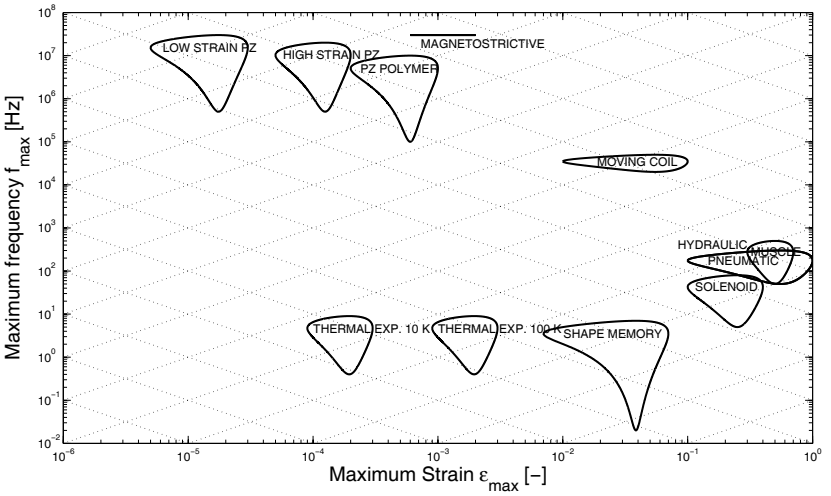

Fig. 2.3 Maximum frequency versus maximum strain for different classes of actuators (Data extracted from [5])

maximum frequency versus the maximum strain for different classes of actuators. It can be seen that the actuators featuring the best frequency to strain ratio are moving coil actuators, muscles, pneumatic actuators, hydraulic actuators and magnetostrictive actuators. The thermal expansion actuator 10 K is the worst positioned according to this index.

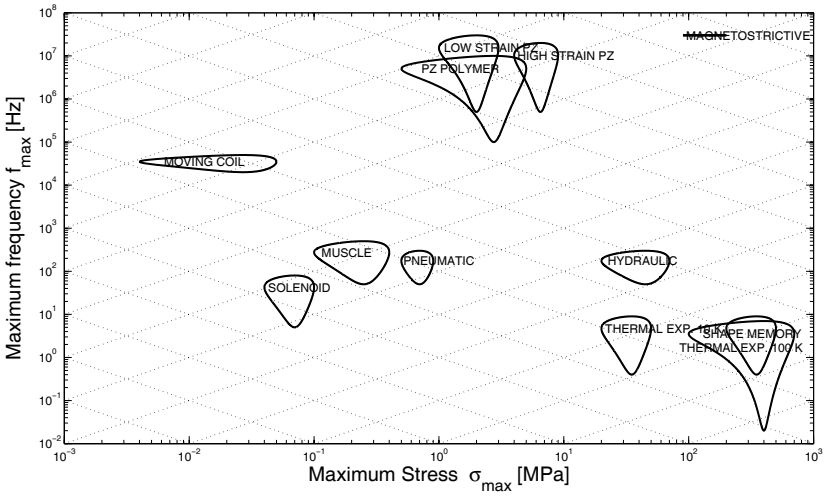

Fig. 2.4 Maximum frequency versus maximum stress for different classes of actuators (Data extracted from [5])

It can be also useful to see the maximum frequency against the maximum stress, as shown in Figure 2.4. It can be noted that the actuator featuring a best frequency to stress ratio is the magnetostrictive actuator, while the solenoid actuator is the worst positioned according to this index.

The maximum power density is an extremely important quantity since it expresses the maximum power that can be provided per unit of volume or mass. Figure 2.5 shows the maximum volumetric power density versus maximum strain while Figure 2.6 shows the maximum mass power density versus maximum strain. Hydraulic actuators dominate both volumetric and mass power density to strain ratios, while thermal expansion 10 K actuators feature the worst power density to strain ratio.

Multiplying the maximum strain times the maximum stress another interesting quantity is obtained, which corresponds to the volumetric work. The plot linking power density and volumetric work of Figure 2.7 shows that the actuator featuring a best ratio is again the hydraulic actuator, while moving coils, solenoid and thermal expansion actuators 10 K show the worst ratios.

The resolution versus the maximum strain is illustrated in Figure 2.8. It should be noted that the resolution is expressed as the minimum controllable strain and therefore the smaller the value the better the resolution is. It can be seen that the worst resolutions are obtained by the actuators that provide large strains, like the muscles or the solenoid actuators, while the best resolution is obtained by low strain piezoelectric actuators. The diagonal lines bottom-left to up-right show the number available and controllable positions where the actuator can be moved. The number of positions is obtained by dividing the strain into the resolution. It can be noted that the maximum number of positions is obtained by the different piezoelectric actuators, moving coils and pneumatic and hydraulic actuators, while the thermal expansion 10 K actuator feature the worst number of positions. Therefore, such thermal expansion 10 K actuators will be recommended for applications requiring a low number of positions, such as bistable switches.

The efficiency versus the maximum mass power density is illustrated in Figure 2.9. It can be noted that the actuators with higher efficiency are the piezoelectric, magnetostrictive and hydraulic actuators.

2.3 Design Parameters

The first step introduces the relevant design parameters in the construction of the actuator. A detailed schematic drawing is presented showing the geometric quantities and the materials used. In order to obtain a clear design parameterization *geometrical factors*, *aspect ratios* and *filling factors* are used.

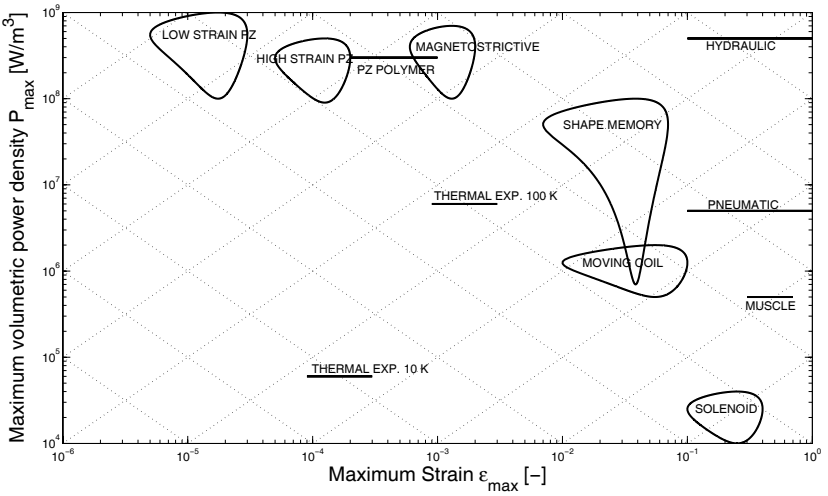

Fig. 2.5 Maximum volumetric power density versus maximum strain for different classes of actuators (Data extracted from [5])

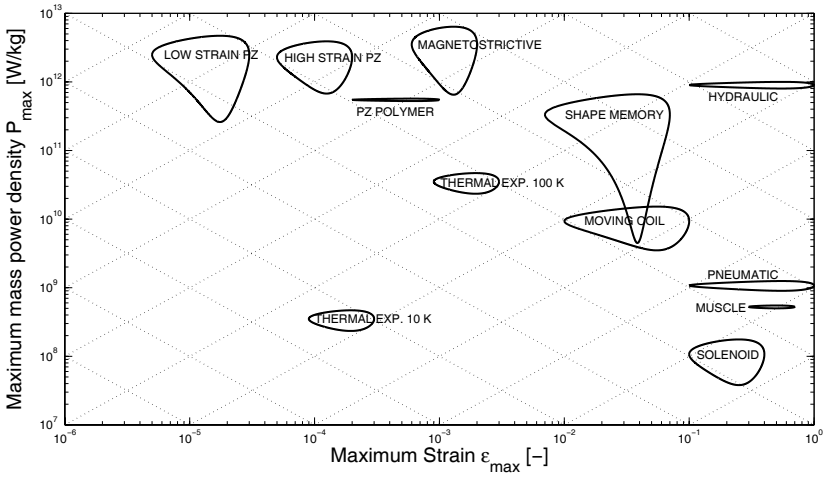

Fig. 2.6 Maximum mass power density versus maximum strain for different classes of actuators (Data extracted from [5])

2.3.1 Geometrical Factors

Geometrical factors define the ratio between any geometrical dimension and a reference geometrical dimension in the same axis.

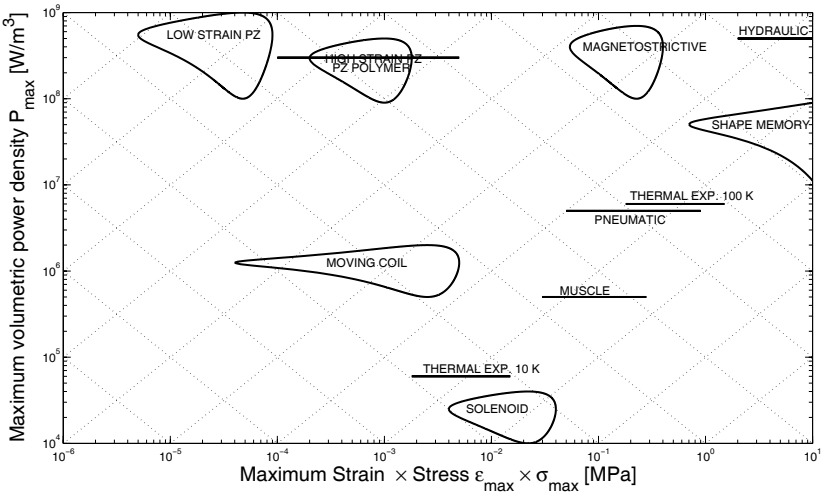

Fig. 2.7 Maximum volumetric power density versus maximum strain times maximum stress for different classes of actuators (Data extracted from [5])

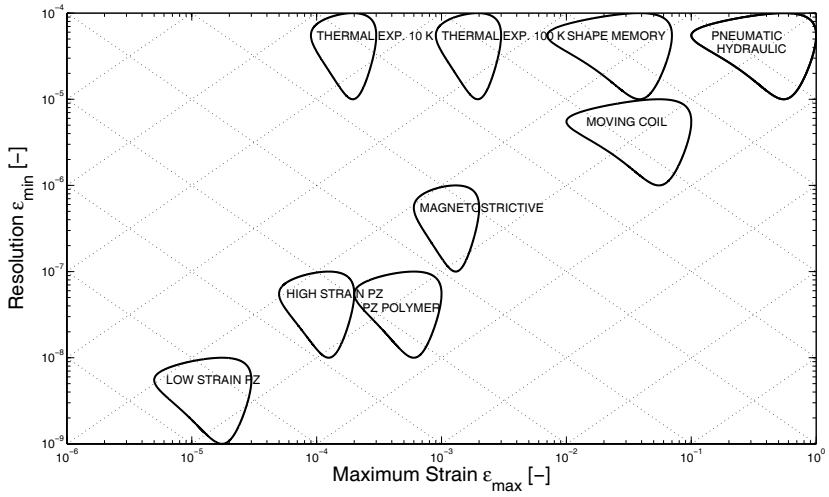

Fig. 2.8 Resolution versus maximum strain for different classes of actuators (Data extracted from [5])

A non-dimensional geometrical factor k_i is obtained for each length l_i as a quotient of this length and the reference length l in its axis as:

$$k_i = \frac{l_i}{l} \rightarrow l_i = k_i l \tag{2.1}$$

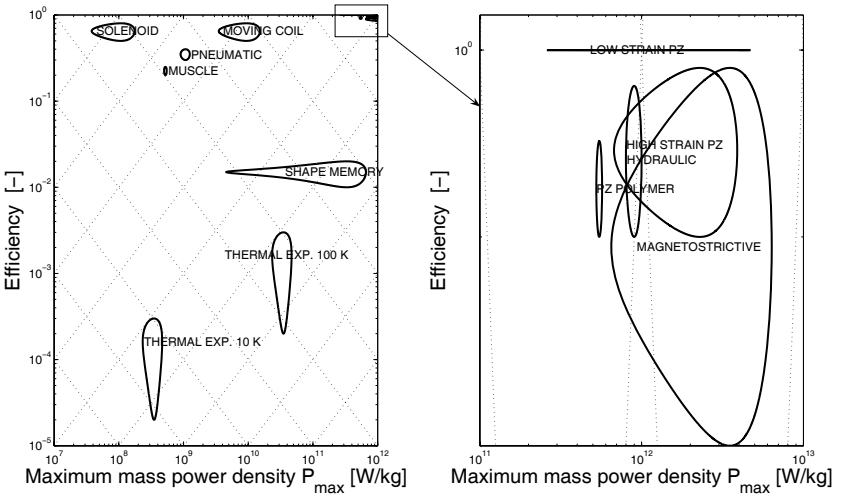

Fig. 2.9 Efficiency versus maximum mass power density for different classes of actuators (Data extracted from [5])

Using these factors, all the lengths in the same axis can be related to one single length, simplifying the analysis of the size dependance of different quantities. The number n of independent reference lengths depend on the degrees of symmetry of the actuator. An actuator with cylindrical shape presents two different reference lengths ($n = 2$, since a cross-section diameter and a length define a cylinder), a spherical actuator would be defined with one reference length ($n = 1$, only a diameter defines a sphere).

Example 2.1. Evaluate the mass of a hollow sphere.

A hollow sphere can be characterized by the outer diameter D_2 and the inner diameter D_1. Considering the material density ρ the mass m_{sphere} of the sphere can be expressed as:

$$m_{sphere} = \rho \frac{\pi}{6}(D_2^3 - D_1^3) \tag{2.2}$$

The previously mentioned number of independent reference lengths is $n = 1$ in this case. Using the geometrical factor $k_1 = D_1/D_2$ the dependance on D_1 can be removed, allowing to express (2.2) as

$$m_{sphere} = \rho \frac{\pi}{6} D_2^3 (1 - k_1^3) \tag{2.3}$$

2.3.2 Aspect Ratios

The proportions between different axes can be characterized by means of aspect ratios.

Aspect ratios express the relationship between different reference lengths as:

$$\eta = \frac{\chi_i}{\chi} \tag{2.4}$$

where χ_i refers to the reference length corresponding to the axis i, while χ corresponds to the absolute reference length, as a function of whom all the other geometric quantities will be expressed.

For the cylindrical coordinates case, it yields:

$$\eta = \frac{r}{l} \tag{2.5}$$

where r corresponds to the main *radial* reference length and l corresponds to the main *axial* reference length.

If n independent reference dimensions are necessary, $n-1$ aspect ratios are to be defined. The combination of the previous two concepts implies that all the geometric dimensions are expressed as a function of one single reference length, which is associated to the size of the actuator and allows the independent study of the performance of an actuator with a limited size and the actuator performance when the size is changed.

Example 2.2. Evaluate the weight of the pipe illustrated in Figure 2.10.

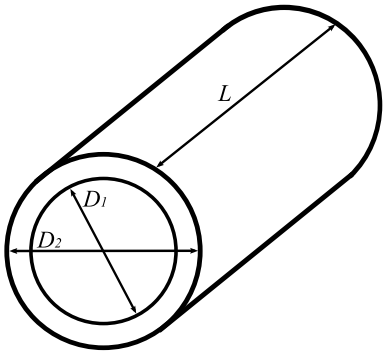

Fig. 2.10 Pipe analyzed in Example 2.2

The pipe can be characterized by the geometrical quantities D_1, D_2 and L. Considering the material density ρ the mass m_{pipe} of the pipe can be expressed as:

$$m_{pipe} = \rho\pi\frac{(D_2^2 - D_1^2)L}{4} \tag{2.6}$$

The previously mentioned number of independent reference lengths is $n = 2$ in this case. Using the geometrical factor $k_1 = D_1/D_2$ the dependance on D_1 can be removed. As we need $n - 1 = 1$ aspect ratios to express the weight as a function of a single geometrical quantity, an aspect ratio $\eta = D_2/L$ can be defined, allowing to express (2.6) as

$$m_{pipe} = \rho \pi D_2^3 \frac{(1 - k_1^2)}{4\eta} \tag{2.7}$$

where it can be noted that the pipe mass is expressed as a function of a single length D_2, a material property ρ, the defined geometrical relationship k_1 and the aspect ratio η.

2.3.3 Filling Factors

The filling factor provides the portion of usable material against the total needed material. This is of great importance when dealing with multiple conductors, since they usually need isolation from the surrounding conductors losing also some space due to construction issues or the design of the actuator. Such multiple conductors can be found in a broad range of actuators technologies, from the electrical conductors employed in an inductance or an electromagnet to the fluid conductors of pneumatic or hydraulic systems. In the mentioned cases the entire cross-section designed for the conductors wires is not employed.

Filling factors express the relationship between the usable area and the total area as:

$$k_{ff} = \frac{S_{use}}{S_{total}} \tag{2.8}$$

where S_{use} is the usable cross-section, S_{total} is the total cross-section and k_{ff} depends not only on the isolators width but in the distribution of the wires or conductors. If squared or rectangular conductors are used, the most optimum filling factors are obtained, since no space is lost as it happens with circular or elliptic conductors. For such squared conductors the ratio between the usable surface of $D_1 \times D_1$ and the total surface of $D_2 \times D_2$ would be $k_{ff} = k_1^2$, being $k_1 = D_1/D_2$.

For the example of an electrical coil illustrated in Figures 2.11 and 2.12, $S_{use} = S_{copper}$ is the copper section and S_{total} the overall cross-section of the coil. The filling factor depends on the configuration of the wires in the available space.

If the configuration of Figure 2.11 is used, the filling factor can be defined as

$$k_{ff} = \frac{S_{copper}}{S_{total}} = \frac{mn\pi D_1^2/4}{mnD_2^2} = \frac{\pi}{4} k_1^2 \tag{2.9}$$

Using the configuration of Figure 2.12, S_{total} can be expressed as

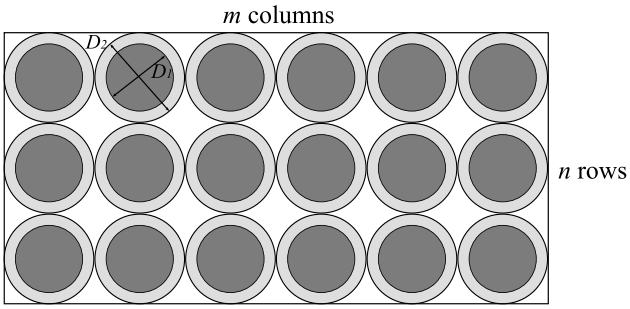

Fig. 2.11 Coil wiring scheme employed in the k_{ff} calculation developed in (2.9)

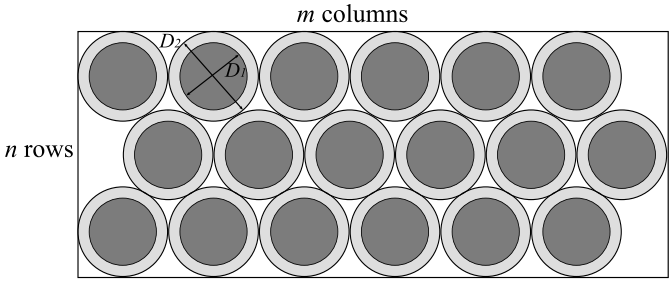

Fig. 2.12 Coil wiring scheme employed in the k_{ff} calculation developed in (2.11)

$$S_{total} = D_2\left(m+\frac{1}{2}\right)\left(D_2 + D_2\,(n-1)\sin\left(\frac{\pi}{3}\right)\right) = D_2^2\left(m+\frac{1}{2}\right)\left(1+\frac{n-1}{2}\sqrt{3}\right) \tag{2.10}$$

for $n > 1$ and $m > 1$.

The filling factor

$$k_{ff} = \frac{S_{copper}}{S_{total}} = \frac{mn\pi D_1^2/4}{D_2^2\left(m+\frac{1}{2}\right)\left(1+\frac{n-1}{2}\sqrt{3}\right)} = \frac{mn\pi}{4\left(m+\frac{1}{2}\right)\left(1+\frac{n-1}{2}\sqrt{3}\right)}k_1^2 \tag{2.11}$$

In order to compare the different configurations regardless coefficient k_1, the previously defined filling factors can be expressed as $k_{ffi} = \alpha_i k_1^2$. Comparing the α_i parameters for squared conductors ($i = 0$), circular placed as in Figure 2.11 ($i = 1$) and circular placed as in Figure 2.12 ($i = 2$), the results displayed in Figure 2.13 are obtained, where it can be noted that squared conductors do not loose any space due to their configuration and the configuration sketched in Figure 2.12 performs better than that of Figure 2.11 when the number of conductors is large enough. It can also be observed that for $i = 0$ $\alpha_0 = 1$ and for $i = 1$ $\alpha_1 = \pi/4 \approx 0.7854$. For $i = 2$ α_2 is a monotonically increasing function, with an horizontal asymptote at $\alpha_3 = \pi/(2\sqrt{3}) \approx 0.9069$.

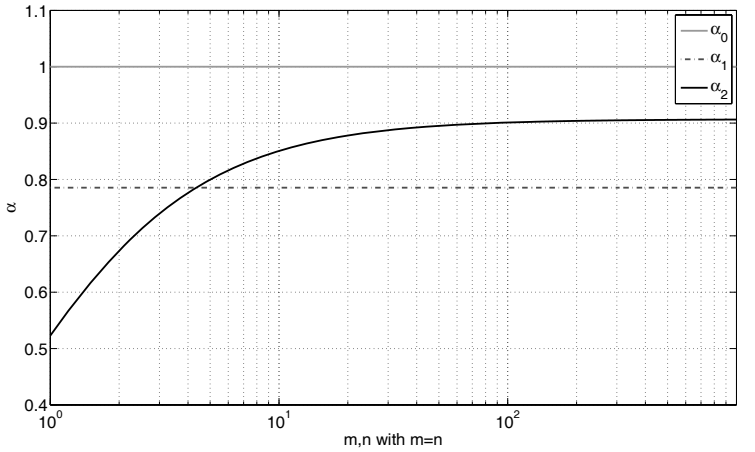

Fig. 2.13 Comparison of the α_i parameters of the different exposed conductor configurations

Although it has been shown that the filling factor depends significantly on the wiring configuration coefficient α, it is usually considered as a constant known value between 0.75 and 0.8.

2.4 Output Quantities

An actuator can be defined as an energy converter which transforms energy from an external source into mechanical energy in a controllable way. The actuator input quantities depend on the type of energy used and include all the quantities involved in the energy conversion from the energy source to the output mechanical quantities. For electromagnetic, piezoelectric and magnetostrictive actuators the input quantities can be the current, the charge or the voltage; for fluid power actuators the fluid pressure or the flow; for shape memory alloys and thermal expansion actuators the temperature. The output quantities are the relevant mechanical quantities *force*, *stroke*, *work* or *power*.

2.4.1 Output Quantities Expression

The output quantities developed by an actuator can be controlled by modifying the input quantities described in Table 2.1. Such input quantities are provided by a control system which lead output quantities to the referenced values. Such quantities are ruled by the mechanical load system or structure, which defines the relationship

between the force and the stroke. The integration of actuators and loads in a mechatronic or adaptronic[1] system allows the conception of a unique system which is to be analyzed.

Table 2.1 Actuator drive input quantities for different actuator technologies

Actuator technology	Actuator drive input quantity
Electromagnetic actuators	Electrical voltages and currents
Electrostatic actuators	Electrical voltages and currents
Hydraulic actuators	Oil pressure
Pneumatic actuators	Air pressure
Thermal expansion actuators	Temperature
Piezoelectric actuators	Electrical voltage and charge
Magnetostrictive actuators	Electrical voltages and currents
Magnetorheological actuators	Electrical voltages and currents
Electrorheological actuators	Electrical voltages and currents
Shape memory alloy actuators	Temperature

A general expression of output quantities as a function of all input quantities involved is developed in the second step. These expressions are taken from the general physics laws ruling the actuators concerned. Each type of actuator behaves in a different way and its expressions are presented describing all the assumptions done. If the load is considered, the different steady-state working points depending on the load can be discussed and shown graphically.

Example 2.3. Evaluate the force produced by a hollow cube submerged in water sketched in Figure 2.14.

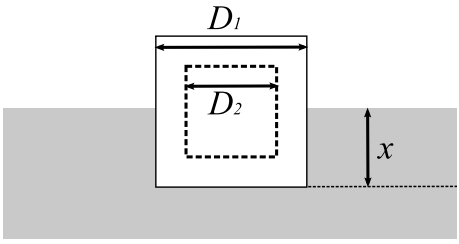

Fig. 2.14 Sketch of the system under analysis in Example 2.3

The force produced by the cube can be expressed as the force due to submerging it into water minus the weight of the cube as

$$F_{cube} = \rho_{water} D_1^2 x g - \rho_{cube} \left(D_1^3 - D_2^3\right) g \tag{2.12}$$

[1] Adaptronics is a term referred to the analysis, design and integration of smart structures and systems.

where $g \approx 9.81$ m/s^2 is the gravity constant . Using the geometric factor $k_1 = D_2/D_1$ and the relative cube density $\nu = \rho_{cube}/\rho_{water}$

$$F_{cube} = \rho_{water} D_1^3 g \left(\frac{x}{D_1} - \nu \left(1 - k_1^3\right) \right) \tag{2.13}$$

where it can be noted that the maximum force is produced for $x \geq D_1$ when the cube is absolutely submerged $F_{cube-max} = \rho_{water} D_1^3 g \left(1 - \nu \left(1 - k_1^3\right)\right)$ and the minimum force is produced for $x = 0$ and yields $F_{cube-min} = -\rho_{water} D_1^3 g \nu \left(1 - k_1^3\right)$ as shown in Figure 2.15. Between these limits the force varies linearly, being exactly equal to zero for $x = D_1 \nu \left(1 - k_1^3\right)$.

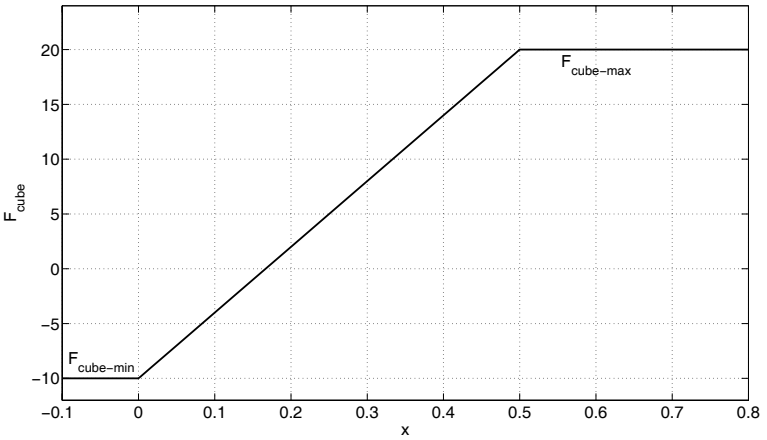

Fig. 2.15 Cube force characteristic of Example 2.3

2.4.2 Steady-State Analysis

The output quantities analysis can be addressed by considering static or steady-state conditions of the system or considering the system dynamics. Depending on the necessary analysis different approaches have to be taken. The steady-state analysis provide useful information about steady operating points, where the actuator and the load find the equilibrium. The steady-state analysis does not consider how the system moves from one equilibrium to another, but it provides very important information to be employed in the design of the actuator. The present section considers steady-state analysis. Some considerations on actuators dynamics are exposed in Section 2.10

In order to establish the characterization plot of the actuator, force-stroke curves and work-stroke curves can be used, taking into account the output quantities as a function of the displacement or stroke of the actuator. The inputs (currents, voltages, pressures, etc.) capable of changing these curves are presented, explaining why and how they can influence the actuator performance. The design parameters cannot be considered inputs and their influence is discussed in following steps.

Example 2.4. Capacitive actuators (Figure 2.16) are a class of electrostatic MEMS actuators. Obtain the force-stroke and work-stoke curves for such actuators.

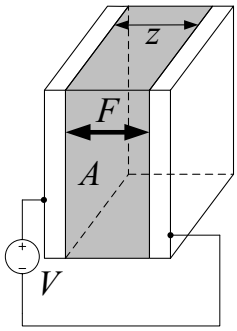

Fig. 2.16 Capacitive actuator of Example 2.4

The energy stored E_C by a capacitor of capacitance C yields $E_C = (1/2)CV^2$ where V is the applied voltage. Considering two opposite parallel plates, the capacitance C can be expressed as $C = \varepsilon A/z$ where ε is the dielectric permittivity , A is the plate surface and z the distance between plates. The force between plates yields:

$$F_C = -\frac{\varepsilon A V^2}{2z^2} \tag{2.14}$$

The work can be expressed as:

$$W_C = \frac{\varepsilon A V^2}{2z} \tag{2.15}$$

Force-stroke and work-stroke curves are plotted in Figures 2.17 and 2.18.

Example 2.5. Considering the capacitive electrostatic actuator of Example 2.4, discuss the evolution of the equilibrium points when changing the voltage if the actuator is attached to an elastic load.

The actuator and load curves are defined by

$$F_{C-actuator} = \frac{\varepsilon A V^2}{2z^2} \tag{2.16}$$

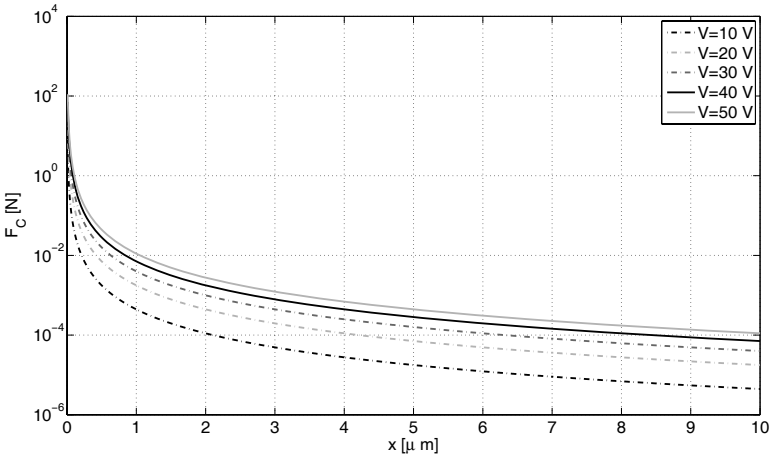

Fig. 2.17 Force-stroke curve of Example 2.4

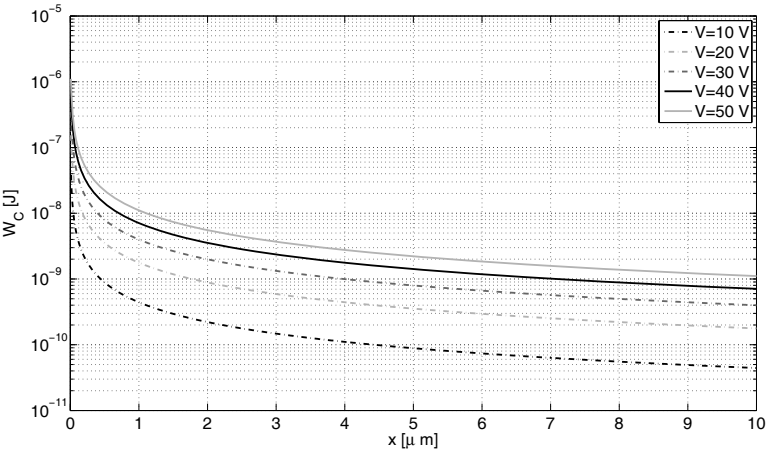

Fig. 2.18 Work-stroke curve of Example 2.4

$$F_{C-load} = k_{Load} z \tag{2.17}$$

The equilibrium if found when $F_{C-actuator} = F_{C-load}$, that is

$$z_{eq} = \sqrt[3]{\frac{\varepsilon A V^2}{2k_{Load}}} \tag{2.18}$$

$$F_{C-load-eq} = F_{C-actuator-eq} = \sqrt[3]{\frac{\varepsilon A V^2 k_{Load}^2}{2}} \tag{2.19}$$

Equilibrium points are plotted in Figure 2.19 using the values $\varepsilon = 8.854 \times 10^{-12}$ F/m, $A = 10^{-6}$ m^2, $k_{Load} = 3 \times 10^5$ N/m and voltage varying from 10 to 50 V.

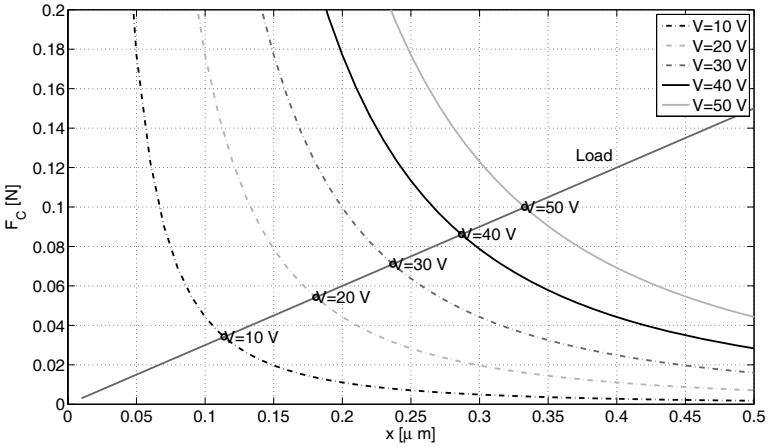

Fig. 2.19 Force-stroke curve equilibrium points of Example 2.5

2.5 Thresholds

Some physical limits (maximum allowed temperature, mechanical resistance etc.) do not allow the actuator output quantities to be increased indefinitely. Since the purpose is to separately deal with the maximum force, stroke and work available in a given size and the performance scalability the allowed quantities and parameters are:

- geometric quantities (reference lengths)
- geometric relationships (geometrical factors, aspect ratios and filling factors)
- material properties (magnetic permeability, resistivity, temperature coefficient, conductivity, etc.)
- universal physics constants (μ_0, ε_0, etc.)
- physical thresholds (maximum temperature, stress, etc.)

Therefore, all the other quantities (currents, magnetic fluxes, pressures, etc.) must be expressed as functions of the mentioned quantities. The physical thresholds limiting the maximum force, stroke and work must be analyzed, showing how they limit the performance of the actuator.

The principle limiting quantities in some common actuators are shown in Table 2.2.

Table 2.2 Actuator limiting quantities

Actuator technology	Actuator limiting quantities
Electromagnetic actuators	Temperature, magnetic saturation, mechanical resistance
Electrostatic actuators	Electrical field, mechanical resistance, temperature
Hydraulic actuators	Mechanical resistance, fluid losses, temperature
Pneumatic actuators	Mechanical resistance, fluid losses, temperature
Thermal expansion actuators	Mechanical resistance, temperature
Piezoelectric actuators	Electrical field, mechanical resistance, temperature
Magnetostrictive actuators	Magnetic saturation, temperature, mechanical resistance
Magnetorheological actuators	Magnetic saturation, temperature, mechanical resistance
Electrorheological actuators	Electrical field, temperature, mechanical resistance
Shape memory alloy actuators	Mechanical resistance, temperature

Example 2.6. Discuss the limiting electrical limiting quantities involved in the electrostatic capacitive actuators studied in Example 2.4.

The maximum applicable voltage V_{max} depends on the maximum allowed electrical field E_{max} and the displacement z as

$$V_{max} = E_{max} z \tag{2.20}$$

Therefore, the more the distance between plates is increased the higher the voltage that can be applied. A reasonable example value for E_{max} could be around $1000\, V/mm$, where it can be noted that this class of actuator may be specially adequate in the micro-range where a voltage of 1 V would correspond to a displacement of 1 μm.

Example 2.7. Analyze the flux flowing in a toroidal inductance and discuss the maximum flux considering the magnetic saturation as the limiting quantity.

The magnetization curve (Figure 2.20) show the relationship between the flux density B and the magnetic field intensity H. It is common to use the expression

$$B = \mu H = \mu_r \mu_0 H \tag{2.21}$$

where μ is the magnetic permeability obtained as the product of the relative permeability μ_r characteristic of each material and the vacuum permeability $\mu_0 = 4\pi 10^{-7} NA^{-2}$. If there was no saturation, μ would be constant regardless the value of H. In practice, this is only the case for operation at low values of H, for higher values saturation effects become more important and μ cannot be considered constant anymore.

Nonlinearities linking B and H have been deeply analyzed in the last decades [17, 15, 14, 13, 12, 6], considering saturation and hysteresis limit cycles. In this example a very simplified μ expression is employed, since the purpose of the example is to illustrate the methodology rather than obtain exact expressions. Expression (2.21) can be for example expressed as

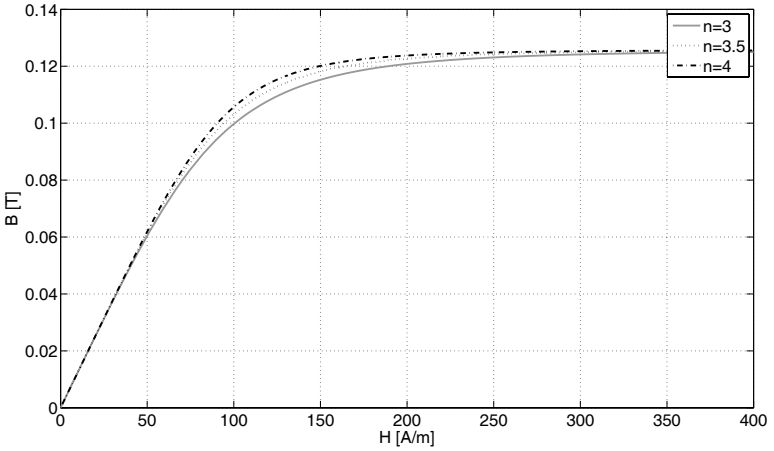

Fig. 2.20 BH saturation curve of Example 2.7

$$B = \mu_0 \mu_r^H k_1 \left(\frac{H^n}{k_0 + H^n} \right)^{\frac{1}{n}} \tag{2.22}$$

where μ_r^H is a constant that corresponds to the value of μ_r for $H = 0$.

The magnetic field intensity H can be defined as $H = Ni/l$, where N is the number of turns of the coil and i is the current flowing in the coil. In order to prevent saturation, a threshold H_{max} has to be defined, implying a limit in the current $i_{max} = H_{max}/N$. The magnetic flux ϕ flowing in the coil can be expressed as $\phi = B/S$ where S is the cross-section. The maximum flux will be given by

$$\phi_{max} = \frac{\mu_0 \mu_r^H k_1}{S} \left(\frac{H_{max}^n}{k_0 + H_{max}^n} \right)^{\frac{1}{n}} \tag{2.23}$$

Similar expressions could be derived using an alternative formulation which links the flux ϕ to the magnetomotive force $\mathfrak{F}$ by defining the magnetic reluctance $\mathfrak{R} = \mathfrak{F}/\phi$. This alternative formulation allows to analyze such a system as an electrical circuit , where flux corresponds to electrical current, magnetomotive force corresponds to voltage and reluctance corresponds to resistance.

2.6 Maximum Target Quantity for a Given Size

The limiting quantities expressions developed in the latter section, can be substituted in the target quantities expressions, allowing them to be maximized for the given

limiting values and design parameters. Such target quantities can range from the output mechanical quantities to other relevant quantities.

2.6.1 Output Mechanical Quantities Maximization

The analysis of a given output quantity, for a given class of actuators, as a function of the design variables, shows (as a rule) a monotonic dependance on certain size variables. For instance, the limit force will typically depend monotonically on the actuator cross section and the actuator stroke on the length. Other design variables will exist (typically some aspect or shape factors) for which the considered output quantity can be maximized. The search of such optimal design variables is very useful, since it enables a fair and effective comparison between actuators of different kinds and can be of essential importance for the optimization of the whole active mechanical system. These expressions are carefully analyzed keeping the size constant.

The limit force, stroke and work available in a given size are studied depending on the different design parameters. The geometric factors, aspect ratios and the materials selected providing the best performance are discussed. This leads to a general expression of the maximum force, stroke and work in a given volume and provides design rules to optimize the actuator's performance with the proper ratios and materials.

The output quantity to be maximized χ can be expressed as a function of a reference length L, limiting quantities $\lambda_1, \lambda_2, ...$, universal constants, material properties $\nu_1, \nu_2, ...$, geometrical factors $k_1, k_2, ..., k_n$, aspect ratios $\eta_1, \eta_2, ...\eta_m$, filling factors k_{ff}.

In many cases it is possible to separate the different kind of terms appearing in the output quantity χ expression, allowing a separated analysis of the different terms. Geometrical factors, aspect ratios and filling factors can be separated from other involved quantities, defining a *design factor*. The maximization of such a design factor implies the maximization of the concerned output quantity by means of an appropriate actuator design.

Moreover, with the purpose of separating all the different factors involved in the output quantities expression the following functions can be defined:

- Universal constants k_{uc}
- Design factor $\vartheta_{df}\left(k_1, k_2, ..., k_n, \eta_1, \eta_2, ...\eta_m, k_{ff}\right)$
- Geometric function $\varsigma_L(L)$
- Limiting quantities function $\varsigma_{lim}(\lambda_1, \lambda_2, ...)$
- Material properties function $\varsigma_{mat}(\nu_1, \nu_2, ...)$

If it is possible to algebraically separate the different previous functions, the selected output quantity to be optimized χ can be represented by

$$\chi_{max} = f\left(k_{uc}, \vartheta_{df}, \varsigma_L, \varsigma_{lim}, \varsigma_{mat}\right) \tag{2.24}$$

In a number of practical cases the previous functions are easily separable and it is possible to express (2.24) as

$$\chi_{max} = k_{uc}\varsigma_L\varsigma_{lim}\varsigma_{mat} \tag{2.25}$$

which has the straightforward property of allowing to maximize or minimize χ by maximizing or minimizing all the terms separately.

Example 2.8. Discuss the maximum force and work in the electrostatic capacitive actuator studied in Examples 2.4 and 2.6.

The previously developed maximum voltage (2.20) can be substituted in (2.16). The maximum output force yields

$$F_{C-max} = -\frac{\varepsilon A E_{max}^2}{2} \tag{2.26}$$

which is the type of (2.25) with:

- $k_{uc} = -1/2$
- $\vartheta_{df} = 1$
- $\varsigma_L = A$
- $\varsigma_{lim} = E_{max}^2$ with $\lambda_1 = E_{max}$
- $\varsigma_{mat} = \varepsilon$

The maximum work:

$$W_{C-max} = \frac{\varepsilon A z E_{max}^2}{2} \tag{2.27}$$

which is again the type of (2.25) with:

- $k_{uc} = 1/2$
- $\vartheta_{df} = 1$
- $\varsigma = Az$
- $\varsigma_{lim} = E_{max}^2$ with $\lambda_1 = E_{max}$
- $\varsigma_{mat} = \varepsilon$

Example 2.9. A given actuator force is expressed as

$$F = AP_{max}k_1^2\eta\left(1-k_1^2\right)(-\eta+1) \tag{2.28}$$

where P_{max} is the maximum limiting pressure, A is the actuator cross-section, k_1 is a geometrical factor and η is an aspect ratio. Discuss the maximum force.

The force expression is similar to (2.25), therefore it will be enough to maximize all the separate terms to maximize the force. Actually, the only non-constant terms are those included in the design factor ϑ_{df}, which can be defined as:

$$\vartheta_{df} = k_1^2\eta\left(1-k_1^2\right)(-\eta+1) \tag{2.29}$$

Analyzing the previous expression a maximum can be found for $k_{1-max} = \sqrt{2}/2$, $\eta_{max} = 1/2$ and $\vartheta_{df-max} = 1/16$ as illustrated in Figure 2.21. The maximum force yields $F_{max} = AP_{max}/16$.

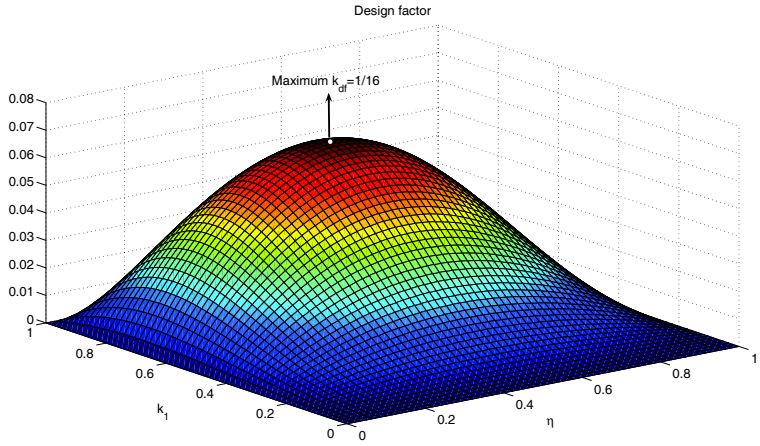

Fig. 2.21 Design factor of Example 2.9

2.6.2 Other Quantities

Other target quantities can be considered instead of the mentioned mechanical output quantities. It may be interesting to address the minimization of the actuator cost or other indices related to economics, maintenance, control or environmental issues. Moreover, in many cases it can be specially useful to study some cost to mechanical quantities ratios, such cost/energy [€/J].

Example 2.10. Discuss the minimum cost/energy ratio β for the actuator studied in Examples 2.4, 2.6 and 2.8.

The actuator cost c can be considered proportional to the n-power of the actuator volume as $c_E = k_c A^n z^n$, where k_c is the proportionality constant between size and cost. The energy expression (2.15) can be employed to compute the cost/energy ratio as

$$\beta = \frac{c_E}{W_C} = \frac{k_c A^n z^n}{\frac{\varepsilon A V^2}{2z}} = \frac{2k_c A^{n-1} z^{n+1}}{\varepsilon V^2} \tag{2.30}$$

Using the maximum voltage from (2.20)

$$\beta = \frac{2k_c A^{n-1} z^{n-1}}{\varepsilon E_{max}^2} \tag{2.31}$$

where it can be noted that the higher the maximum allowed electrical field E_{max} or the electrical permittivity ε the lower the ratio β. Obviously, the ratio β can also be minimized by reducing the parameter k_c. As long as the volume dependance is concerned, this is to be discussed in the following step, which considers the target quantities as functions of the size.

2.7 Scalability

In the fifth step the actuator performance as a function of the size is analyzed and the scalability and application range are discussed. If two geometrically similar passive mechanical systems with a given scale factor are considered, and their mechanical behavior can be described by an approach based on continuum mechanics, they are to be loaded by forces whose ratio is the square of the scale factor in order to produce the same stress and strain distribution and, consequently, a similar displacement field.

A certain actuator class is mechanically scalable if its output quantities follow the same rules, i.e. if (by proportional scaling in all directions) the actuator force is proportional to the square of the size and the actuator displacement is proportional to the size. Usually, a certain actuator class will be mechanically scalable only in a certain size range; beyond this range, the required actuator size changes with respect to the rest of the mechanical system, which can make the use of the considered type of actuator unpractical.

If the force is proportional to the area and the stroke to the length in the whole actuator's domain it follows that the work is proportional to the volume since the work is obtained from the integration of the force between two different strokes. If all these requirements are fulfilled and the actuator is fully scalable significant consequences arise. The structures working in the elastic region are considered fully scalable loads, the expression ruling its behavior $\sigma = E\varepsilon$ shows that the quotient between the stress $\sigma = F/A$ and the strain $\varepsilon = x/L$ is the Young Modulus E without dependance on the size of the structure. Therefore, if the actuator is shown to be scalable and the load is scalable in the sense described above, the whole system (actuator plus load structure) would be scalable, allowing the development of models of easy (normal size) construction as a preliminary step to the construction of large or small systems (inside the scalability range), with the corresponding saving of resources. In this case, the experimental results must be analyzed as non-dimensional numbers and provide information for all the range of sizes where the scalability can be assumed.

Scalability analysis is based on certain assumptions. Since the described assumptions are necessary to consider one actuator scalable, the non-scalability when these assumptions do not hold true has to be also studied.

Example 2.11. The force of a certain actuator is expressed as $F_a = k\pi r^{\gamma}$, where γ is a constant $\gamma > 0$. Discuss the scalability of the actuator as a function of the parameter γ.

It is straightforward to note that the actuator will be scalable in the sense described above as long as $\gamma = 2$. In such a case the actuator force per cross-section will be constant $F_a/\pi r^2 = k$. Considering the general case, the force per cross section yields

$$\frac{F_a}{\pi r^2} = k r^{\gamma-2} \tag{2.32}$$

The force per cross section performance as a function of the parameter γ is plotted in Figure 2.22, where it is shown that for $\gamma = 2$ the force is clearly scalable. For larger γ values, the force per cross section is increased with the size, recommending the use of such actuators for large actuators. On the other side, when $\gamma < 2$, the actuator performance improvement is decreased when the size is increased, recommending its use for applications demanding small actuators.

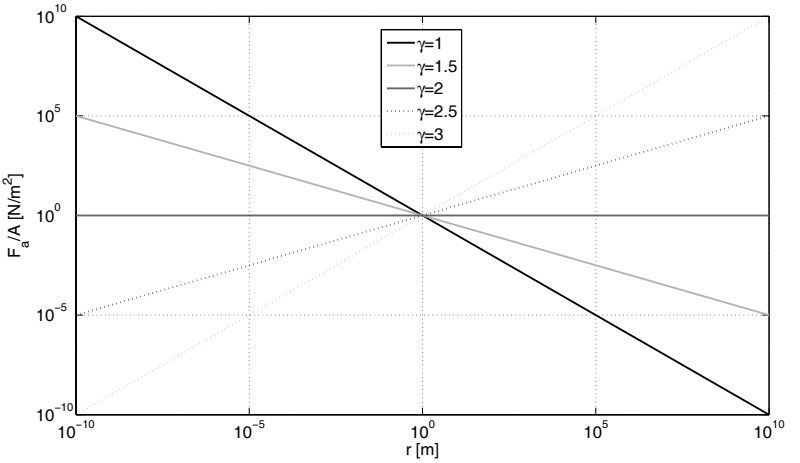

Fig. 2.22 Force per cross section performance as a function of the parameter γ

2.8 Dimensional Analysis

It is not always possible to use analytical methods to derive the expressions ruling actuators. Furthermore, even when analytical methods are feasible it can be convenient to validate such results by means of simulations and experimental validation. Such validations may be complemented (or in some cases even substituted) with the so-called dimensional analysis techniques.

2.8.1 The Buckingham Pi Theorem

Dimensional analysis [18] is based on considering dimensionless groups of quantities to form the analyzed expressions. Such analysis allows to obtain some relationships that can become a valuable complement to other developed analysis and experimentation.

The dimension of a certain quantity u can be expressed as $[u]$. All the quantities can be expressed in some systems containing the basic reference dimensions. The most common systems are:

- Mass-Length-Time MLT
- Force-Length-Time FLT
- Mass-Length-Time-Temperature $MLT\theta$

However, the reference system can be chosen depending on each application. Some usual quantities dimensions can be expressed depending on the reference system as:

- Length, in both MLT and FLT systems yields $[l] = L$
- Time,in both MLT and FLT systems yields $[t] = T$
- Mass, in MLT system $[m] = M$, in FLT system $[m] = FL^{-1}T^2$
- Force, in MLT system $[F] = MLT^{-2}$, in FLT system $[F] = F$
- Volume, in both MLT and FLT systems yields $[V] = L^3$
- Acceleration, in both MLT and FLT systems yields $[a] = LT^{-2}$

The so-called Buckingham Pi Theorem [1] proposes a method of forming dimensionless groups to characterize a certain system. If an equation $f(u_1, u_2, ...u_m) = 0$ is characterized by m quantities $u_i, i = 1..m$, it can be reduced to an equation with $m-n$ dimensionless groups where n is the minimum number of reference dimensions required to characterize the system. The $m-n$ dimensionless groups Π satisfy

$$\phi(\Pi_1, \Pi_2, ...\Pi_{m-n}) = 0 \tag{2.33}$$

The Buckingham Pi Theorem can be applied according to the following steps:

1. List the m quantities involved in the analyzed expression.
2. Define a reference system of n dimensions (MLT, FLT,...) and express the quantities dimensions in such a reference system.
3. Construct a matrix, having n rows and m columns, where the components a_{ij} correspond to the index of dimension j corresponding to the quantity i.
4. Find the $m-n$ dimensionless groups solving the system $\sum_{i=0}^{m} a_{ij} = 0, j = 1..n$
5. Using expression (2.33) substitute the $m-n$ Π dimensionless groups.

Example 2.12. Analyze the force produced by a fluid power actuator using dimensional analysis considering only the force, pressure and area.

The quantities involved can be listed and expressed in the FL system:

- Force $[F] = F$
- Pressure $[P] = FL^{-2}$
- Area $[A] = L^2$

The dimension matrix yields:

$$\begin{array}{c|ccc} & F & P & A \\ \hline F & 1 & 1 & 0 \\ L & 0 & -2 & 2 \end{array} \tag{2.34}$$

Considering $F = KP^aA^b$ the following equations are obtained

$$1 = a \tag{2.35}$$
$$0 = -2a + 2b \tag{2.36}$$

obtaining $a = 1$ and $a = b = 1$. Thus

$$F = KPA \tag{2.37}$$

which matches perfectly with the well known force expression if $K = 1$.

Example 2.13. Analyze the force of an electrostatic capacitive actuator using dimensional analysis.

The quantities involved can be listed and expressed in the FLV system:

- Force (N) $[F] = F$
- Voltage (V) $[V] = V$
- Dielectric permittivity ($C^2N^{-1}m^{-2}$ =N V^{-2}) $[\varepsilon] = FV^{-2}$
- Area (m^2) $[A] = L^2$
- Distance (m) $[z] = L$

The dimension matrix yields:

$$\begin{array}{c|ccccc} & F & V & \varepsilon & A & z \\ \hline F & 1 & 0 & 1 & 0 & 0 \\ L & 0 & 0 & 0 & 2 & 1 \\ V & 0 & 1 & -2 & 0 & 0 \end{array} \tag{2.38}$$

Considering $F = KV^a\varepsilon^bA^cz^d$ the following equations are obtained

$$\begin{array}{lll} 1 = & b & b = 1 \\ 0 = 2c + d & \rightarrow & d = -2c \\ 0 = a - 2b & & a = 2 \end{array} \tag{2.39}$$

Substituting in the previous force expression

$$F = KV^2\varepsilon A^cz^{-2c} \tag{2.40}$$

Therefore, the force can be expressed as

$$F = KV^2\varepsilon\Pi\left(\frac{A}{z^2}\right) \tag{2.41}$$

which matches clearly with the well known expression $F_{C-actuator} = \frac{\varepsilon AV^2}{2z^2}$, using $K = 1/2$ and $\Pi(u) = u$.

Example 2.14. Analyze the force performed by a pneumatic actuator.

Before facing the dimensional analysis problem, some important concepts have to defined:

- The orifice flow expression of a gas entering in a chamber yields

$$\dot{m} = Q\rho = KC_0A\frac{P}{\sqrt{T}} \tag{2.42}$$

  where $\dot{m}$ is the mass flow, Q is the volumetric flow, ρ the gas density, A is the orifice area, P the gas pressure, T the gas temperature and K and C_0 are constants.
- The ideal gases constant yields

$$R = \frac{P}{\rho T} \tag{2.43}$$

- The adiabatic process constant taking place in the cylinder can be expressed as

$$K_{pt} = PT^{\frac{\gamma}{1-\gamma}} \tag{2.44}$$

  where $\gamma = C_P/C_V$ being C_P the specific heat coefficient for constant pressure and C_V is the heat coefficient for constant volume [2].
- The orifice constant can be defined

$$C_0 = \sqrt{\frac{\gamma}{R}\left(\frac{2}{\gamma+1}\right)^{\frac{\gamma+1}{\gamma-1}}} \tag{2.45}$$

It is important to note that the previous expressions are not known before beginning the dimensional analysis. The quantities involved in the dimensional analysis can be listed and expressed in the $FLT\theta$ system:

- Force (N) $[F] = F$
- Position (m) $[x] = L$
- Pressure (Nm^{-2}) $[P] = FL^{-2}$
- Density (Ns^{2}m^{-4}) $[\rho] = FT^2L^{-4}$
- Flow (m^{3}s^{-1}) $[Q] = L^3T^{-1}$
- Temperature (K) $[T] = \theta$
- Ideal gases constant (m^{2}s^{-2}K^{-1}) $[R] = L^2T^{-2}\theta^{-1}$
- Adiabatic process constant (K$^{\frac{\gamma}{1-\gamma}}$N m^{-2}) $[K_{pt}] = FL^{-2}T^{\frac{\gamma}{1-\gamma}}$
- Orifice constant (sK$^{1/2}$m^{-1}) $[C_0] = TL^{-1}\theta^{1/2}$

The dimension matrix yields:

	F	x	P	ρ	Q	T	R	K_{pt}	C_0
F	1	0	1	1	0	0	0	1	0
L	0	1	−2	−4	3	0	2	−2	−1
T	0	0	0	2	−1	0	−2	0	1
θ	0	0	0	0	0	1	−1	$\frac{\gamma}{1-\gamma}$	1/2

(2.46)

Considering $F = Kx^a P^b \rho^c Q^d T^e R^f K_{pt}^g C_0^h$ the following equations are obtained

$$\begin{array}{rcl} 1 = & b+c+g & \\ 0 = a-2b-4c+3d+2f-2g-h & \rightarrow & \begin{array}{l} b = 1-d/2-f+h/2-g \\ a = \quad 2-2d \\ c = \quad d/2+f-h/2 \\ e = \quad f-g\frac{\gamma}{1-\gamma}-h/2 \end{array} \\ 0 = \quad +2c-d-2f+h & & \\ 0 = \quad e-f+\frac{\gamma}{1-\gamma}g+h/2 & & \end{array} \tag{2.47}$$

Therefore, the force can be expressed as

$$F = Kx^{2-2d} P^{1-d/2-f+h/2-g} \rho^{d/2+f-h/2} Q^d T^{f-g\frac{\gamma}{1-\gamma}-h/2} R^f K_{pt}^g C_0^h \tag{2.48}$$

Rearranging, the following force expression using the different non-dimensional groups can be found:

$$\frac{F}{x^2 P} = K\phi\left(\frac{\sqrt{\rho}}{x^2\sqrt{P}}, \frac{\rho RT}{P}, \frac{K_{pt}}{PT^{\frac{\gamma}{1-\gamma}}}, \frac{C_0\sqrt{P}}{\sqrt{\rho T}}\right) \tag{2.49}$$

obtaining the non-dimensional numbers $\Pi_0 = \frac{F}{x^2 P}$, $\Pi_1 = \frac{Q\sqrt{\rho}}{x^2\sqrt{P}}$, $\Pi_2 = \frac{\rho RT}{P}$, $\Pi_3 = \frac{K_{pt}}{PT^{\frac{\gamma}{1-\gamma}}}$ and $\Pi_4 = \frac{C_0\sqrt{P}}{\sqrt{\rho T}}$.

The following set of non-dimensional numbers can be defined:

- $\Pi_a = \Pi_0 = \frac{F}{x^2 P}$ represents the well known relationship between pressure and force $F = PA$.
- $\Pi_b = \Pi_1 \times \Pi_4^{-1} = \frac{Q\sqrt{T}}{C_0 P x^2}$ characterizes the orifice expression (2.42).
- $\Pi_c = \Pi_2 = \frac{\rho RT}{P}$ corresponds to the ideal gases law expressed in (2.43).
- $\Pi_d = \Pi_3 = \frac{K_{pt}}{PT^{\frac{\gamma}{1-\gamma}}}$ matches the adiabatic process expression (2.44).
- $\Pi_e = \Pi_4 \times \Pi_2^{1/2} = C_0\sqrt{R}$ which corresponds to the orifice constant (2.45).

The final expression can be represented as

$$\frac{F}{x^2 P} = K\phi\left(\frac{Q\sqrt{T}}{C_0 P x^2}, \frac{\rho RT}{P}, \frac{K_{pt}}{PT^{\frac{\gamma}{1-\gamma}}}, C_0\sqrt{R}\right) \tag{2.50}$$

2.8.2 Non-Dimensional Numbers

Non-dimensional numbers are useful to characterize certain behaviors that are not easily established by a given quantity. Some non-dimensional numbers are well established in different engineering disciplines, ranging from thermal to fluid dynamics engineering. Representative non-dimensional numbers employed in fluid dynamics are:

- The *Reynolds number* defines the relationship between the inertial and viscous forces in a moving fluid. It yields

$$Re = \frac{\rho v d}{\mu} \tag{2.51}$$

where ρ is the fluid density, v is the fluid velocity, d is significant length and μ is the absolute fluid viscosity.

- The *Euler number* characterized the ratio between pressure and inertia forces in a fluid. It yields

$$Eu = \frac{2P}{\rho v^2} \tag{2.52}$$

where P is the pressure, ρ is the fluid density and v is the fluid velocity.

Some well-known thermal transfer non-dimensional numbers:

- The *Nusselt number* defines forced convection, being established as

$$Nu = \frac{h_c L}{\lambda} \tag{2.53}$$

where h_c is the convection coefficient, L is a characteristic length and λ is the thermal conductivity of the fluid producing the forced convection.

- The *Fourier number* quantifies heat conduction. It yields

$$Fo = \frac{\alpha t}{R^2} \tag{2.54}$$

where α is the thermal diffusivity, t a characteristic time and R the physical length where conduction is being produced.

- The *Grashof number* characterizes free convection. It yields

$$Gr = \frac{g\beta\left(T_s - T_\infty\right)L^3}{\nu^2} \tag{2.55}$$

where g is the gravity acceleration, β the volumetric thermal expansion coefficient, T_s the source temperature, T_∞ the quiescent temperature, ν the kinematic viscosity and L a characteristic length.

- The *Prandtl number* quantifies the relationship between viscous and thermal diffusion rate. It is usually expressed as

$$Pr = \frac{c_p \mu}{\lambda} = \frac{\nu}{\alpha} \tag{2.56}$$

where c_p is the specific heat, μ is the viscosity, λ the thermal conductivity, ν is kinematic viscosity and α is the thermal diffusivity.

- The *Rayleigh number* establishes the ratio between buoyancy and viscous forces in free convection. It yields

$$Ra = \frac{g\beta\,(T_s - T_\infty)\,L^3}{\nu\alpha} \tag{2.57}$$

satisfying $Ra = GrPr$

Other well-known non-dimensional numbers are:

- The *Poisson ratio* ν is employed in mechanical engineering and links the deformations ε produced in different axes as

$$\nu = -\frac{\varepsilon_x}{\varepsilon_y} \tag{2.58}$$

- The *power factor* $cos\varphi$ is employed in electrical engineering and defines the relationship between active P power and reactive Q power in an alternating current circuit as

$$cos\varphi = \frac{P}{\sqrt{P^2 + Q^2}} \tag{2.59}$$

2.9 Validation

The seventh and final methodology step validates the obtained results by means of prototyping and/or simulation and/or comparison with industrial devices. This will usually allow the designer to decide whether the actuator is the optimum or if it is convenient to introduce new modifications and to start again all the design procedure.

2.9.1 Prototype Construction

The classical approach of results validation is based on the construction of a prototype and the validation of the theoretically developed expressions with such a real prototype. The scalability of the actuator discussed in Step 5 can be used to build scale actuators and structures and generalize conclusions for different sizes.

2.9.2 Industrial Actuators

Comparison with data of industrial actuator can provide very relevant information. Firstly, it will illustrate whether the actuator behaves similarly to other actuators of the same class. On the other hand, the designer will be able to decide if the actuator performs better than other competing actuators or whether the same performance is achieved but at lower cost, weight or volume.

2.9.3 Simulation

The simulation of the system under study can provide relevant information in order to validate the conclusions extracted in the previous steps. Moreover, computer aided engineering (CAE) tools allow the designer to test the proposed actuators without the need for building a real prototype. Different particular cases can be studied by using the obtained optimal geometries and dimensions. In such cases, not only the relevant output quantities can be validated, assuring that the obtained analytic expressions hold for a particular case, but also the assumed limiting quantities can be checked and it can be observed which are the most critical areas of the actuator.

Finite element analysis (FEA) [19, 7, 16] employs the finite element method (FEM) to deal with a broad range of engineering applications. There are a number of finite element simulation packages like COMSOL®, ALGOR®, ANSYS®, NASTRAN®, etc. Most of such packages are based on the virtual work principle or the minimum total potential energy principle. Finite Element Analysis was firstly proposed in 1943 by Richard Courant who established the mathematical basis. In the 1950s and 1960s it started to be employed in engineering applications, starting with mechanical engineering. Nowadays, finite element analysis is a fundamental tool for systems simulation, since it has changed deeply the way engineers approach the design of their applications.

In order to simulate using finite element analysis a certain actuator along with the system and structure where it is integrated, the following steps have to be followed:

1. Definition of all the constants involved in the simulation, including the so-called universal constants but also the material properties assumed. Most packages include material library where the different material properties are already included.
2. Definition of the assumed symmetries in order to simplify the analysis. The higher the complexity of the system under study, the more important to consider symmetries, studying a single portion and extract conclusions for the overall system.
3. Drawing (or import) of the system under analysis. In order to obtain relevant results it is extremely important to have an accurate drawing of the studied actuator. The drawings can be also imported from common CAD packages.
4. Specification of the boundary conditions. Typically the surrounding of the system has to be included in the drawing, since it also plays an important role in the physical system. Air, for example has a certain magnetic permeability, so that the magnetic flux can flow through it. The surrounding system limits have to be clearly defined stating their boundary conditions. For example, in an system analyzed from the electromagnetism point of view, it is common to establish electrical or magnetic isolation as boundary conditions.
5. Specification of the physics laws to be considered in the analysis. Each system part is ruled by different physics laws. It has to be clearly established what is the physical law ruling each system block.

6. Definition of the finite element mesh, considering different types of mesh according to the importance of the region. Most critical regions have to have the finest a mesh.
7. Problem solving. Once all the previous steps have been properly addressed, the system can be solved, by firstly tuning the solver appropriately, specifying what kind of analysis is to be done.
8. Post-processing. The obtain results can be plotted so that the desired results can be easily graphically seen.

All these steps are illustrated with a simple system containing a permanent magnet and a levitating ball:

1. Constant definition. The following constants have been defined: permeability of vacuum $\mu_0 = 4\pi 10^{-7} NA^{-2}$, permanent magnet magnetization $M_{pm} = 750 \times 10^3 A/m$ and the magnetic relative permeability $\mu_r = 15000$.
2. Definition of the assumed symmetries. In this examples no symmetries are considered, since it is a very simple system.
3. Drawing. The drawing can be seen in Figure 2.23. The permanent magnet is a block of 40 mm$\times$ 40 mm $\times$ 50 mm, the ball is a sphere of radius 20 mm whose closest point to the permanent magnet is placed at 5 mm.
4. Specification of the boundary conditions. The air surrounding the permanent magnet and the ball includes a large region, whose boundary conditions establish magnetic isolation as shown in Figure 2.23.
5. Specification of the physics laws to be considered in the analysis. The air and the ball are ruled by
$$-\nabla \cdot \mu_0 \mu_r \nabla V_m = 0 \tag{2.60}$$
where V_m is the so-called magnetic potential. The so-called constitutive law yields $B = \mu_0 \mu_r H$ with the difference that while the ball has a high $\mu_r = 15000$, the air has $\mu_r = 1$. The permanent magnet is governed by
$$-\nabla \cdot (\mu_0 \nabla V_m - \mu_0 M_{pm}) = 0 \tag{2.61}$$
with the constitutive law $B = \mu_0 H + \mu_0 M_{pm}$. The stress and force in the ball are the relevant output quantity, therefore it has to be specified that such electromagnetic stress and force is to be computed.
6. Definition of the finite element mesh. As illustrated in Figure 2.24, the system mesh is performed, considering a finer mesh for the permanent magnet and the ball.
7. Problem solving. The system is solved using the stationary linear solver.
8. Post-processing. The obtained results are graphically shown as illustrated in Figure 2.25 using streamlines for the magnetic flux and boundary colors for the ball electromagnetic stresses, Figure 2.26 using boundary colors and arrows related to the Maxwell tensor stresses, Figure 2.27 where slices are used to plot the magnetic flux density and Figure 2.28 where the a number of isosurfaces show the points having the same magnetic flux density.

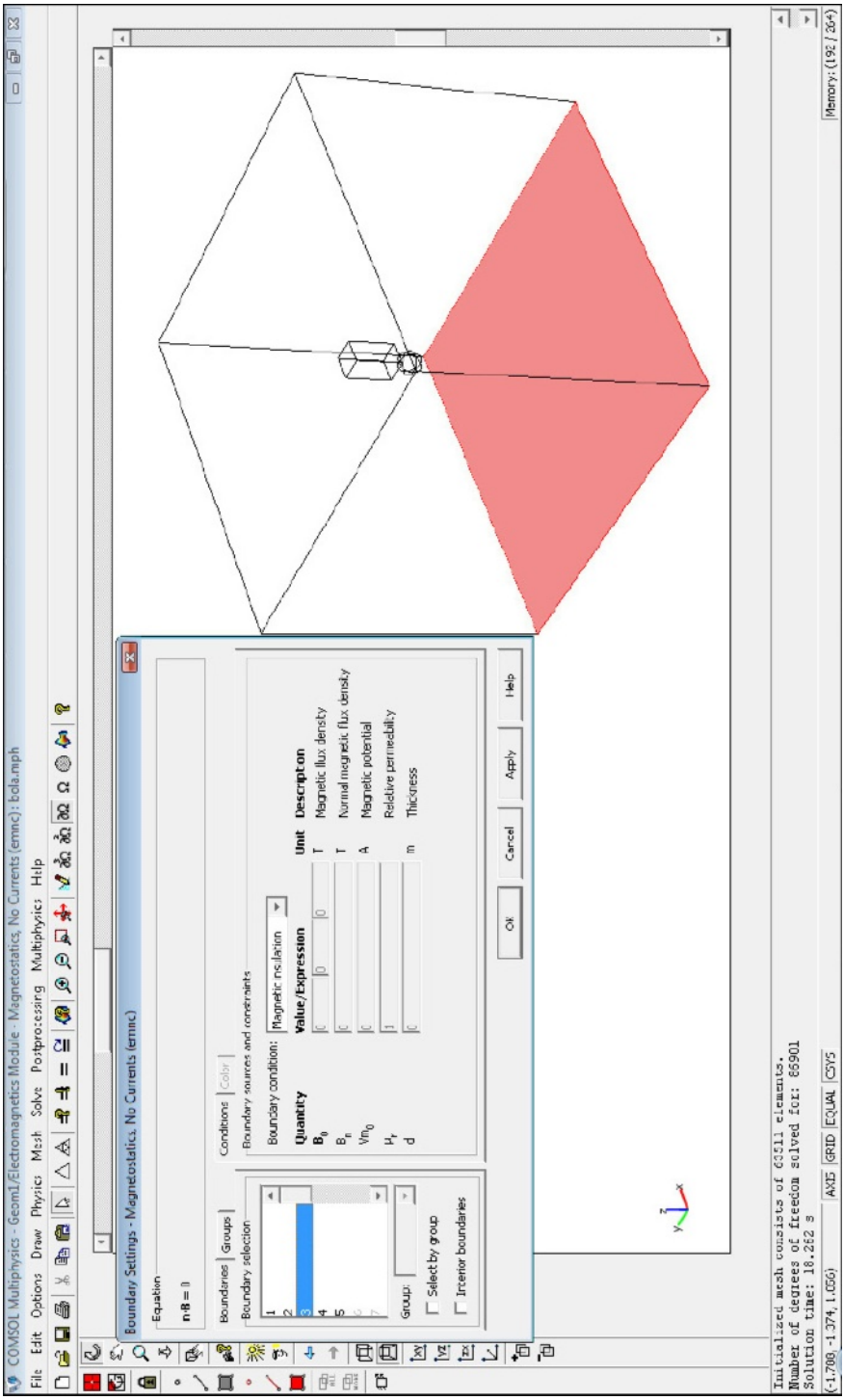

Fig. 2.23 Typical screen of a finite analysis software (COMSOL® by COMSOL AB) of the example of the permanent magnet and the levitating ball

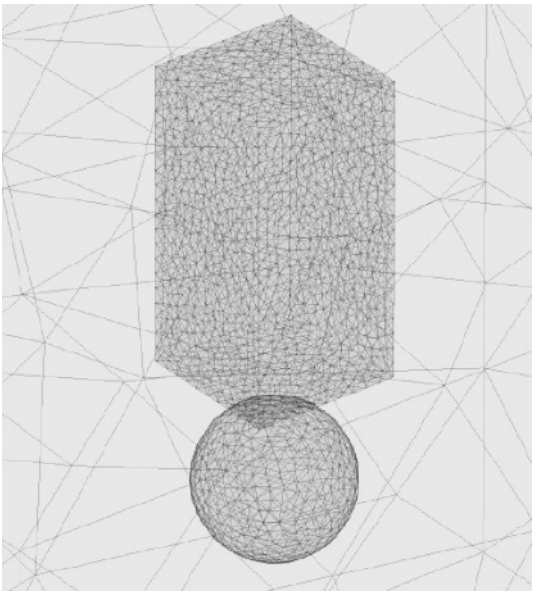

Fig. 2.24 Example element mesh using COMSOL® by COMSOL AB. It can be noted that the permanent magnet and the ball are finer meshed that the surrounding air

Example 2.15. Analyze the force-position characteristic of ball levitating due to the attraction of a permanent magnet.

The force expression of a permanent magnet attracting a levitating ball cannot be easily expressed analytically. A simplified expression can be used

$$F_M = \frac{1}{\sum_{i=0}^{N} a_i z^i} \tag{2.62}$$

In order to determine the optimum degree N and the coefficients a_i different simulations have been developed for different distances z. The obtained results are shown in Table 2.3 and Figure 2.29.

Table 2.3 Force-position data obtained using FEA

z [mm]	0	0.5	1	1.5	2	3	5	7	10	15	20	30
F [N]	36.2	31.71	27.66	24.25	21.45	16.46	10.1	6.2	3.13	1.12	0.45	0.1

Using standard regression techniques, FEA results can be analyzed with different degree polynomials. It can be observed in Figure 2.30 that the best matching is obtained for $N = 5$. The obtained force expression yields

$$F_M(z) = \frac{1}{c_0 + c_1 z + c_2 z^2 + c_3 z^3 + c_4 z^4 + c_5 z^5} \tag{2.63}$$

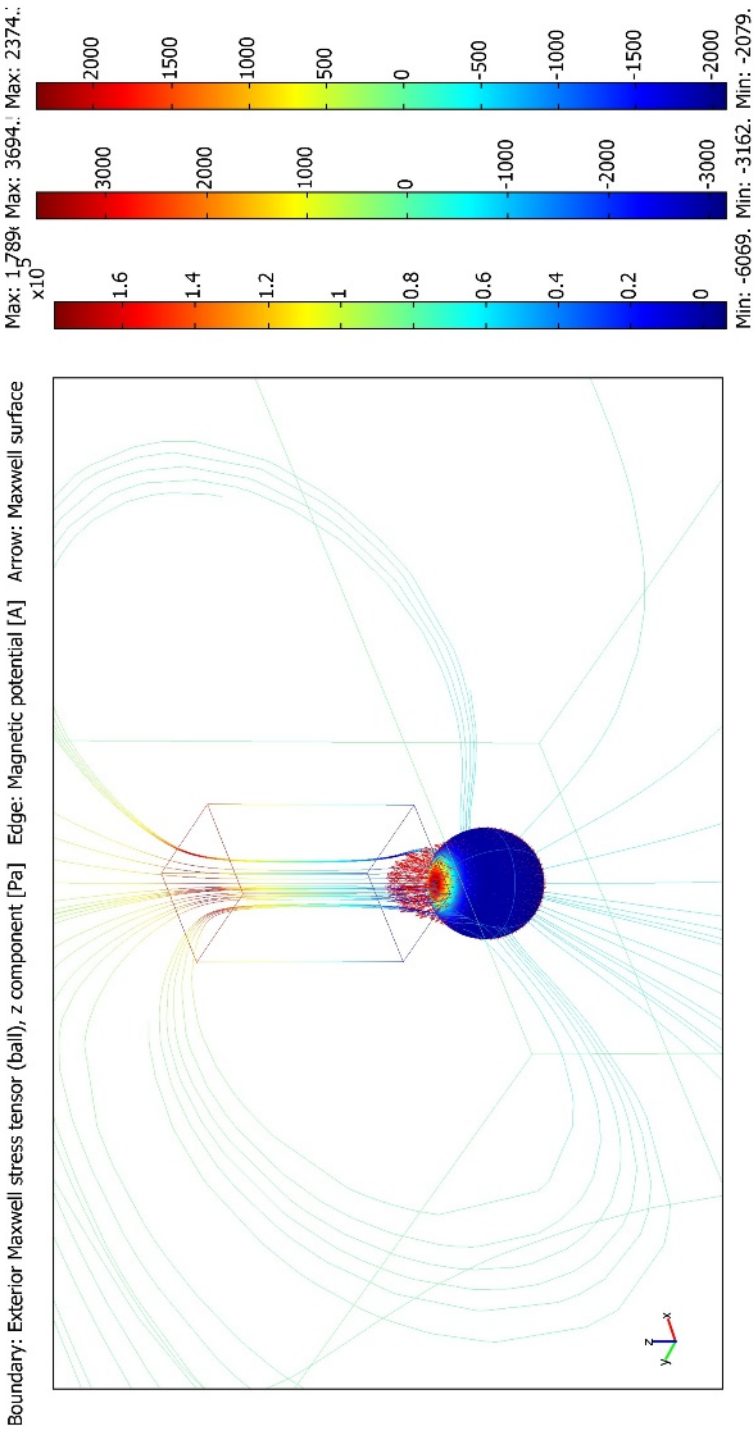

Fig. 2.25 Post-processing of the solved examples. The streamlines show the magnetic flux flow

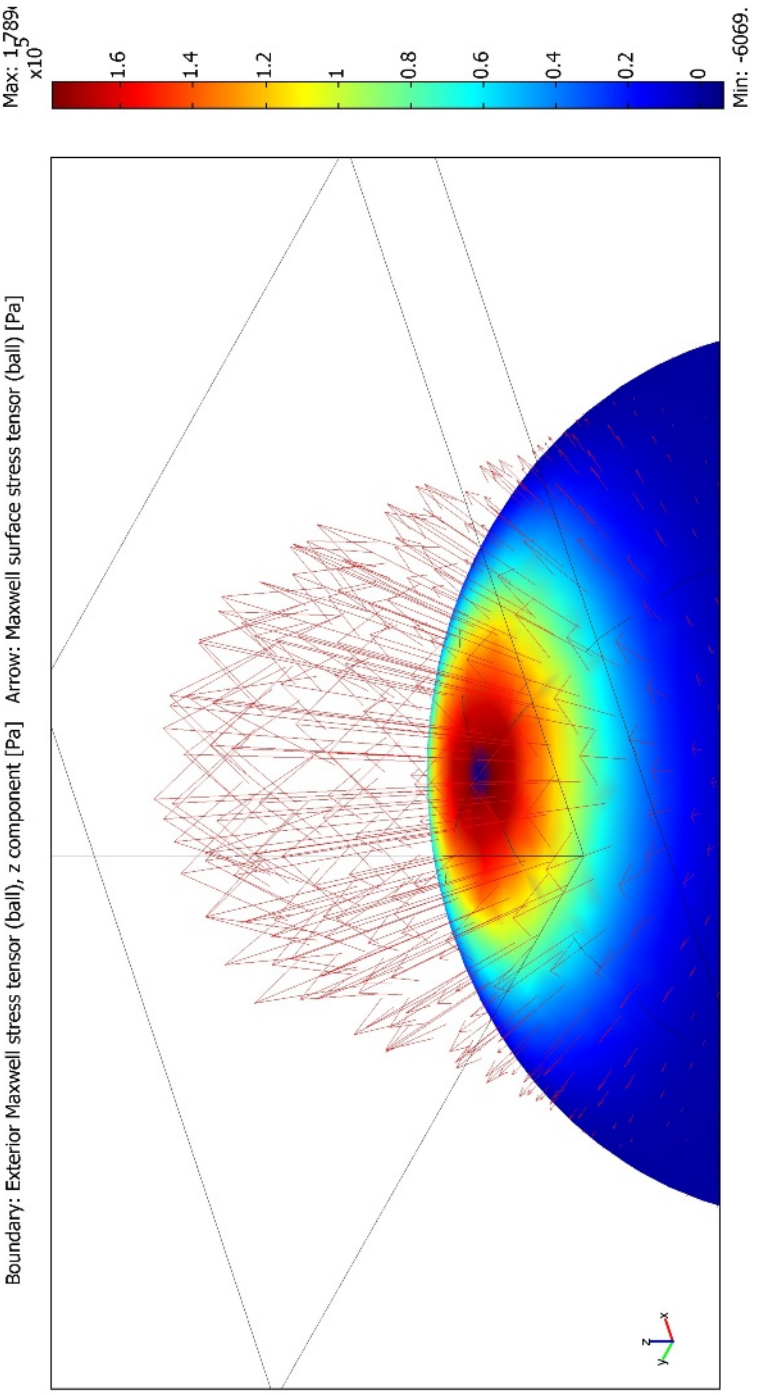

Fig. 2.26 Post-processing of the solved examples. The ball colors and arrows show the different Maxwell tensor stresses in the ball

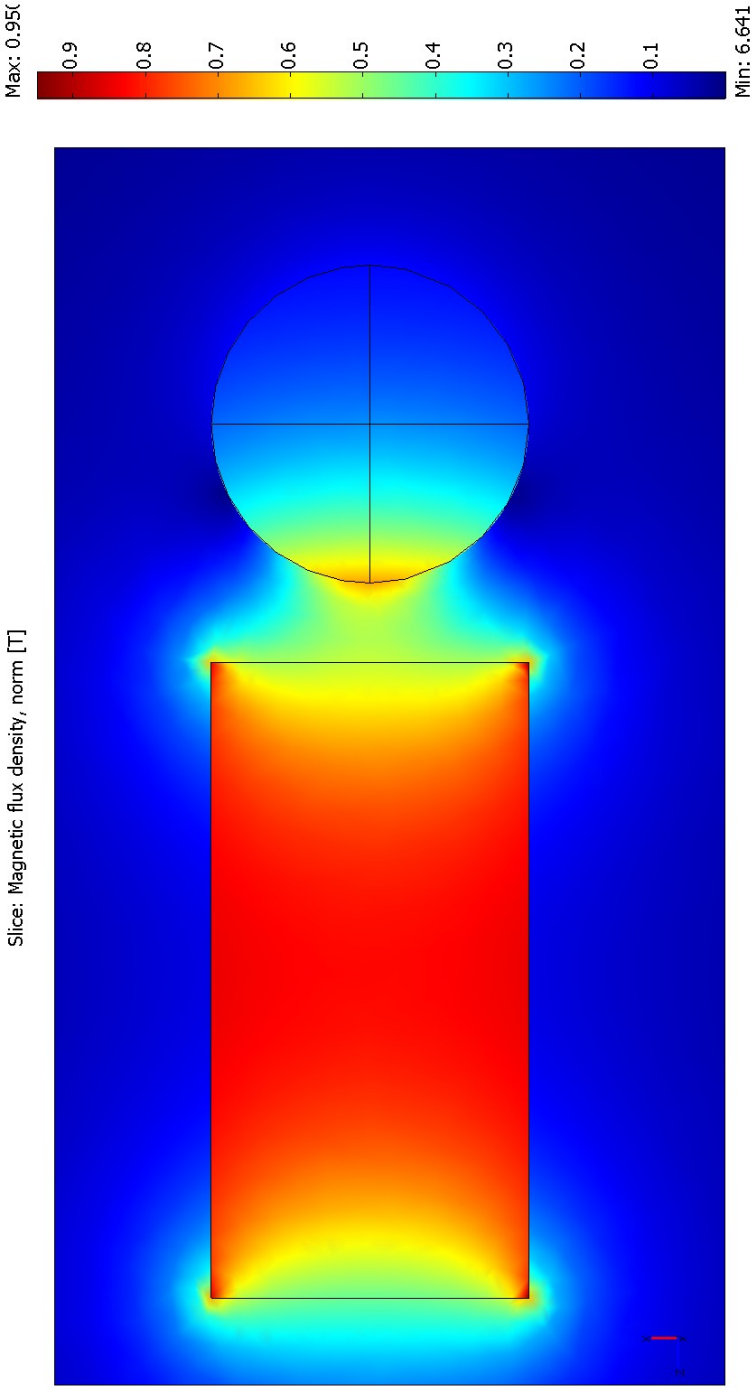

Fig. 2.27 Post-processing of the solved examples. The slices show the different values of magnetic flux density

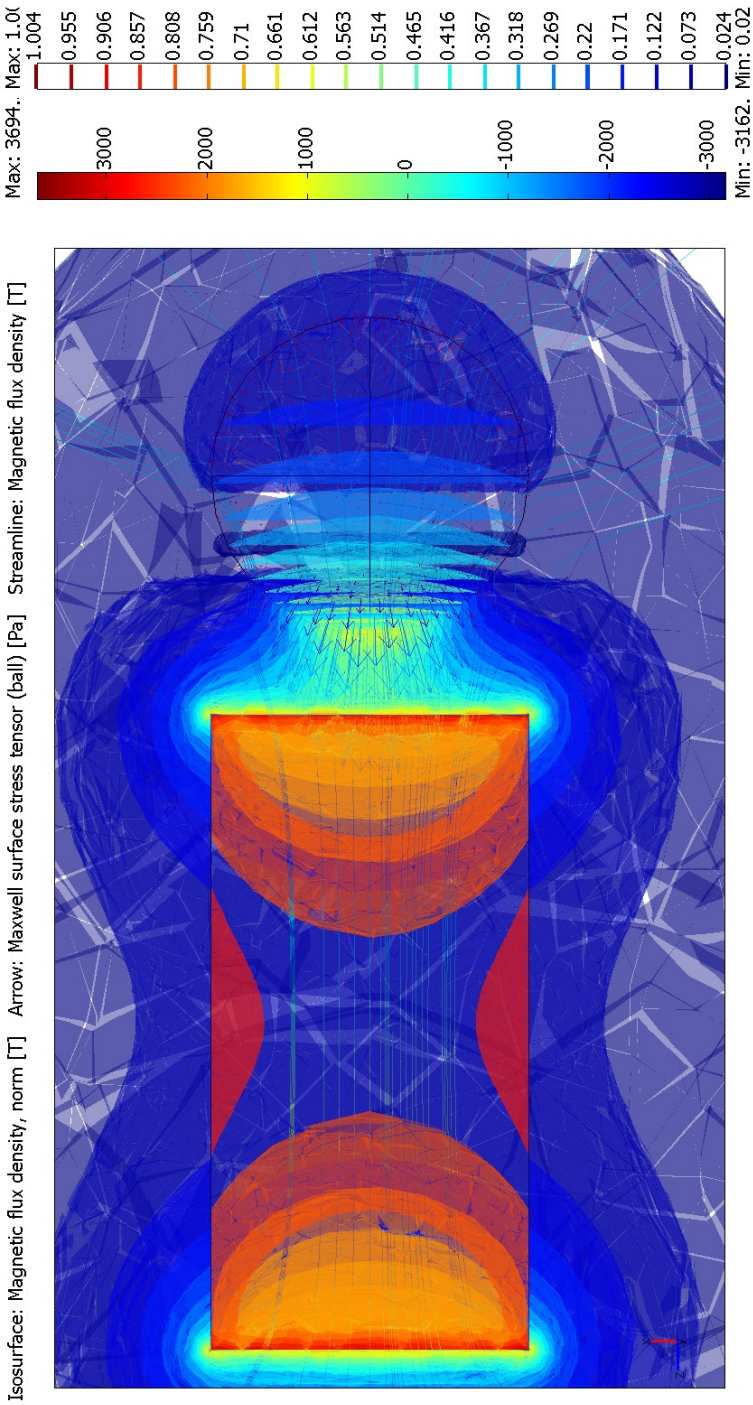

Fig. 2.28 Post-processing of the solved examples. The isosurface show the different surfaces having the same magnetic flux density

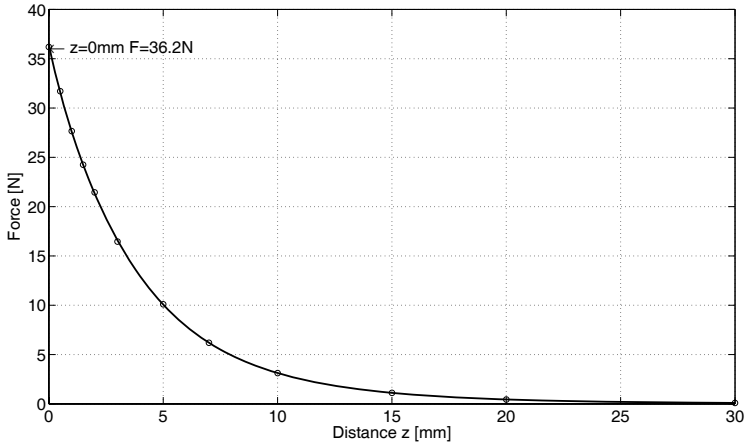

Fig. 2.29 Obtained FEA results for the permanent magnet and ball system of Example 2.15

with $c_0 = 1.47 \times 10^{-7}$, $c_1 = 5.14 \times 10^{-6}$, $c_2 = 3.35 \times 10^{-5}$, $c_3 = 0.0013$, $c_4 = 0.0066$ and $c_5 = 0.028$.

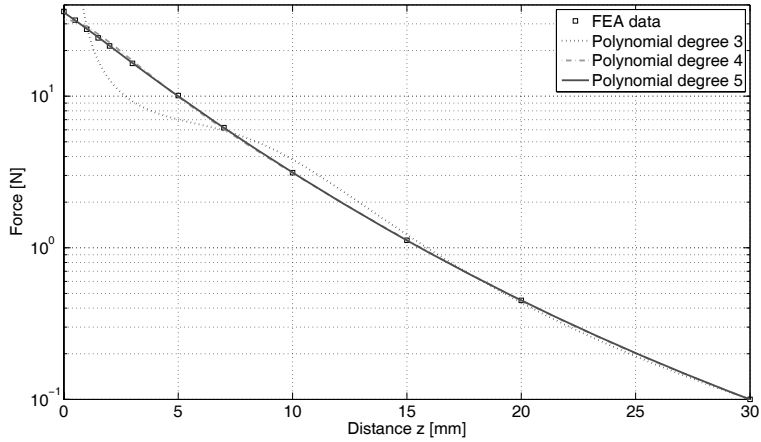

Fig. 2.30 Comparison of the different polynomials proposed to model the force-displacement curve of Example 2.15

2.10 Considerations on Actuators Dynamics

2.10.1 Dynamical Analysis

If the dynamical quantities are considered, it is necessary to consider not only the actuator but the load attached to it. A typical linear load can be characterized by an elastic constant k_L, damping coefficient b_L and mass m_L. Considering the actuator force $F_a(t)$, the dynamics differential equation yields:

$$F_a(t) = m_L\ddot{x}(t) + b_L\dot{x}(t) + k_L x(t) \tag{2.64}$$

where $x(t)$ is the actuator displacement.

The transfer function between the displacement and the force can be expressed as

$$\frac{X(s)}{F_a(s)} = \frac{1}{m_L s^2 + b_L s + k_L} \tag{2.65}$$

where s is the Laplace operator and $X(s)$ and $F_a(s)$ are the Laplace transforms of $x(t)$ and $F_a(t)$.

Analyzing the transfer system poles according to linear systems theory [8], the following system poles are obtained:

$$s_{12} = \frac{-b_L \pm \sqrt{b_L^2 - 4m_L k_L}}{2m_L} \tag{2.66}$$

where it can be clearly noted that the system dynamics will importantly depend on

$$b_L^2 - 4m_L k_L \tag{2.67}$$

The natural frequency $\omega_0 \geq 0$ and the damping ratio ζ may be defined as

$$\omega_0 = \sqrt{\frac{k_L}{m_L}} \tag{2.68}$$

$$\zeta = \frac{b_L}{2\sqrt{k_L m_L}} \tag{2.69}$$

Substituting (2.68) and (2.69) in (2.66) the poles yield

$$s_{12} = \omega_0 \left(-\zeta \pm \sqrt{\zeta^2 - 1}\right) \tag{2.70}$$

Depending on the value of ζ different system behaviors can be considered:

- $\zeta = 1$ The system is critically damped. There is double pole at $-\omega_0\zeta$, assuring stability for $\omega_0 > 0$. The homogenous solution of the system dynamic yields

$$x(t) = (k_1 + k_2 t)\, e^{-\omega_0 t} \tag{2.71}$$

where k_1 and k_2 depend on the initial conditions $x(0)$ and $\dot{x}(0)$.

- $\zeta > 1$: the system is over-damped. Both poles are real and the system will be stable as long as both poles have negative real part. Hence, it will always be stable since

$$-\zeta \pm \sqrt{\zeta^2 - 1} < 0 \tag{2.72}$$

for any $\zeta > 1$. The homogenous solution of the system dynamic yields

$$x(t) = k_1 e^{-\omega_0\left(-\zeta - \sqrt{\zeta^2-1}\right)t} + k_2 e^{-\omega_0\left(-\zeta + \sqrt{\zeta^2-1}\right)t} \tag{2.73}$$

where k_1 and k_2 depend on the initial conditions $x(0)$ and $\dot{x}(0)$.

- $\zeta < 1$ The system is under-damped. The poles yield

$$-\zeta\omega_0 \pm j\omega_0\sqrt{1-\zeta^2} \tag{2.74}$$

where the pole negative real part for $\zeta > 0$ guarantees stability. The homogenous solution of the system dynamic yields

$$x(t) = e^{-\zeta\omega_0 t}\left(k_1 \cos\left(\omega_0\sqrt{1-\zeta^2}t\right) + k_2 \sin\left(\omega_0\sqrt{1-\zeta^2}t\right)\right) \tag{2.75}$$

where k_1 and k_2 depend on the initial conditions $x(0)$ and $\dot{x}(0)$.

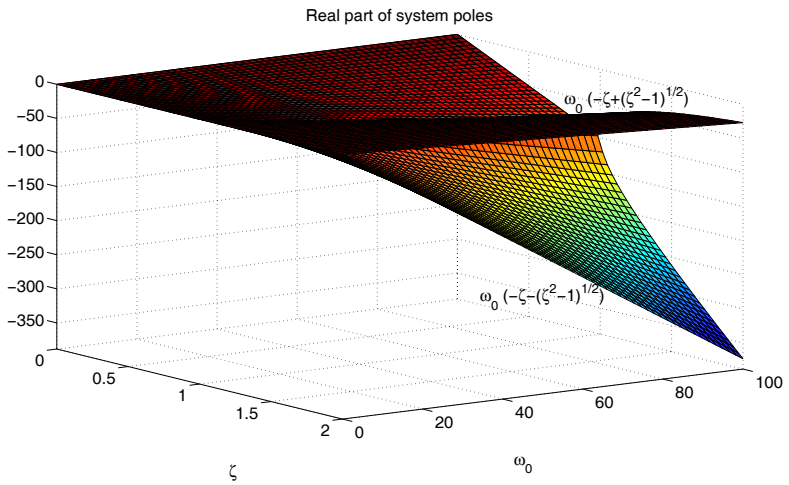

Fig. 2.31 Real part of the poles of (2.70)

The system poles for the different poles can be observed in Figures 2.31 and 2.32. The step response of under, over and critical damped systems is illustrated in Figure 2.33 for different values of ζ and $\omega_0 = 10$ rad/s. It can be noted that there is only one case for $\zeta = 0$ where the displacement oscillates permanently since it has

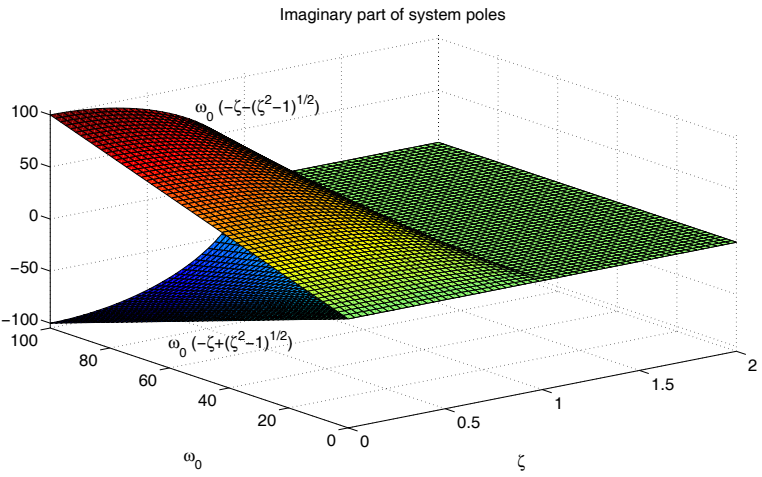

Fig. 2.32 Imaginary part of the poles of (2.70)

both poles with real part equal to zero. The frequencial response is illustrated in the bode diagram of Figure 2.34, where it can be noted that the resonance frequency of the system corresponds to the natural frequency ω_0, and it is important for poorly damped systems.

2.10.2 Control System

In previous Section 2.10, the dynamics of the load have been described. When the whole system considering also the actuator is to be analyzed, it is important to include the control system. The control system can be either an *open loop* control system or a *closed loop* control system:

- In open loop, the actuator input quantities are established arbitrarily without feedback and therefore without verifying that the control output quantity is actually achieving the desired value. Most open loop applications are undertaken in open loop because no sensor for the output quantity is needed, with the cost reduction involved. The main drawback is the lack of precision. A typical open loop system is sketched in Figure 2.35.
- Closed loop system measure or estimate the output quantity and feed it back to the control system in order to eliminate the so-called controller error. A typical closed loop system is sketched in Figure 2.36.

The block diagrams of Figures 2.35 and 2.36 illustrate typical open loop and closed loop control systems. The main elements are:

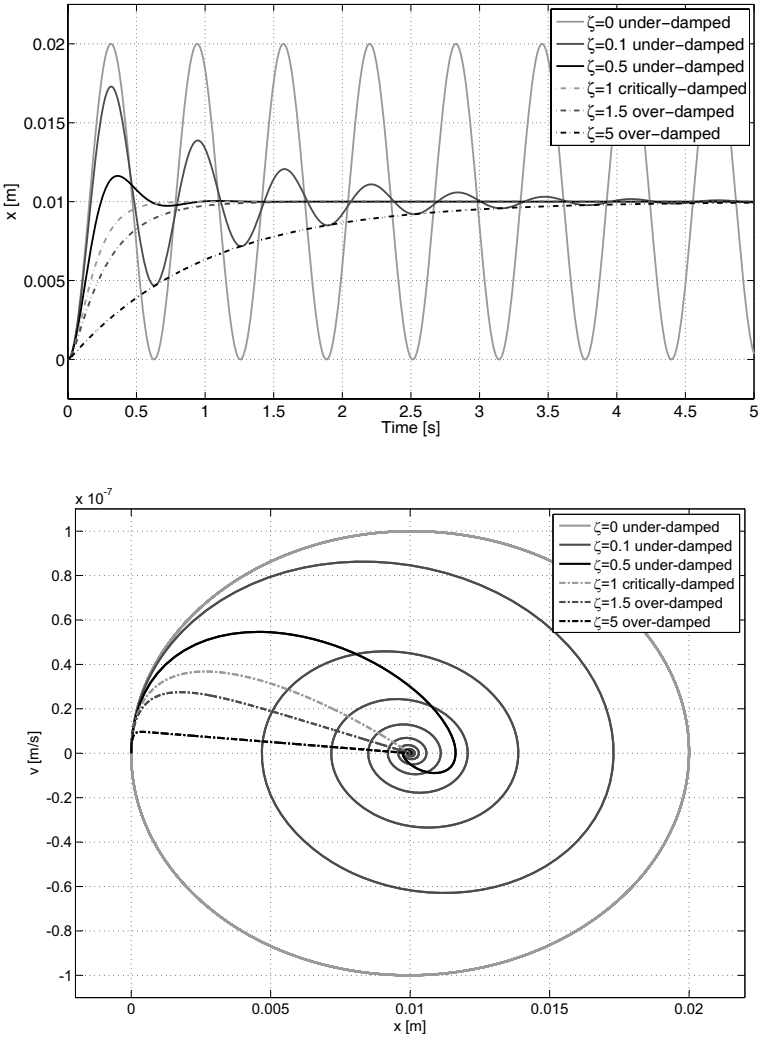

Fig. 2.33 Dynamic step response of the system with different ζ and $\omega_0 = 10$ rad/s

- The *power grid* (1) provides the energy needed to drive the *actuator* (3). It can be by means of electricity, fluid power, heat, etc.
- The *power conversion* (2) unit takes the output of the control system (5) and drives the actuator. Typical examples of converters are electrical inverters or hydraulic proportional valves.
- The *actuator* (3) transforms the energy supplied into the mechanical energy applied to the load (4).

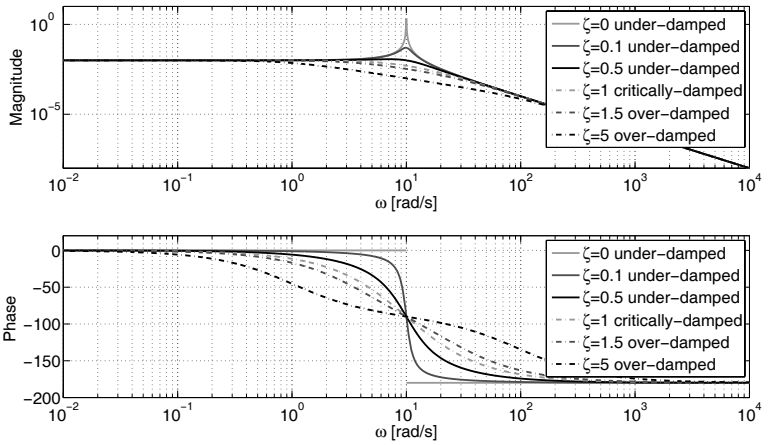

Fig. 2.34 Bode plot of the system for different ζ and $\omega_0 = 10$ rad/s

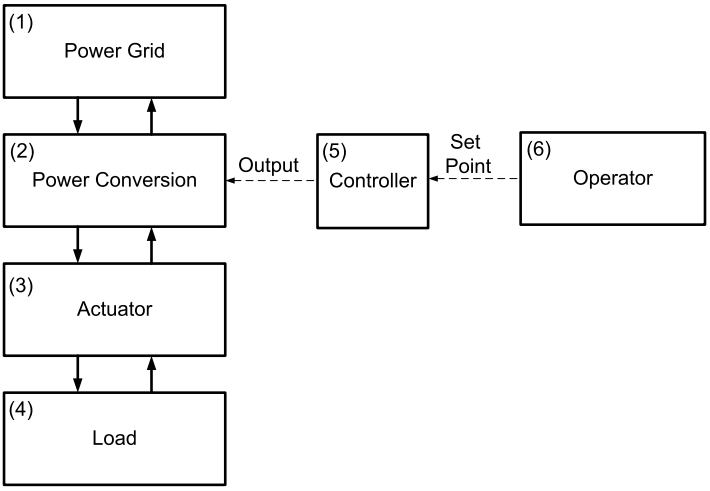

Fig. 2.35 Typical open loop control block diagram of a mechatronic system

- The *controller* (5) takes the set point values referenced by the *operator* (6) and applies the obtained control effort output to the power conversion unit (2).

It can be noted that the energy can flow in both directions in many applications. Although actuators are designed to behave transforming a certain energy source into mechanical energy in some occasions they have to operate as generators and transform mechanical energy in the source energy. Actuators featuring such bidirectional energy flow allow to brake or return to the original position without the need for ex-

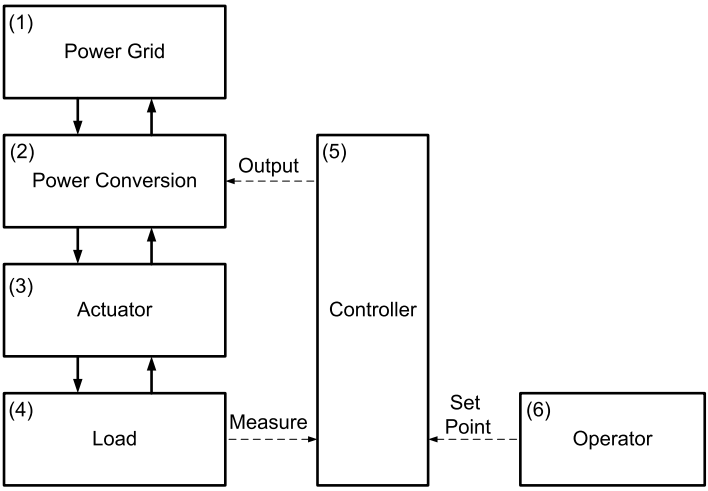

Fig. 2.36 Typical closed loop control block diagram of a mechatronic system

ternals brakes. Furthermore, they are more efficient since part of the energy may be returned to the power grid. A typical example of these efficient reversible machines are electrical machines.

The object of the present book is not to delve into control aspects of dynamical systems, and hence some assumptions can be done in order to simplify the analysis:

1. The controller can be executed in continuous time. It is important to remark that it is not the case when digital discrete time systems are concerned. To delve into such discrete time systems [10] can be consulted.
2. The analyzed systems are considered linear[8], i.e. the state variables $x(t)$ of the system can be expressed as functions of the inputs $u(t)$ as

$$\dot{x}(t) = Ax(t) + Bu(t) \tag{2.76}$$
$$y(t) = Cx(t) + Du(t) \tag{2.77}$$

where $y(t)$ is the system output and A,B,C and D are the system matrixes. If at least one of such matrixes vary with time, the system is considered *Linear Time-Varying (LTV)* or *Linear Parameter-Varying (LPV)*, otherwise if the four matrixes do not vary with time, a *Linear Time-Invariant (LTI)* system is considered. If the system is not linear, it can be linearized used standard linear systems tools [8].
Nonlinear systems are carefully studied in [9]. Their state variables can be expressed in the general form:

$$\dot{x}(t) = \phi(x(t), u(t)) \tag{2.78}$$

where it can be noted that the function ϕ represent a number of different non-linearities. Depending on the function ϕ, the appropriate analysis procedure can be used [9].
3. No perturbations are considered.
4. The control effort (controller output to be applied by the actuator) is unbounded or its bounds are not overcome during the analyzed time. To consider systems not satisfying such assumption, see [3].

Although control theory is an extremely broad engineering discipline, and there exist numerous different controllers to be applied in active systems, it is common define the error $\varepsilon(t) = x^*(t) - x(t)$ as the difference between the reference value $x^*(t)$ and the measured value $x(t)$ and the output control effort as function of such an error as

$$y = f\left(\varepsilon(t), \dot{\varepsilon}(t), \int \varepsilon(t)dt\right) \tag{2.79}$$

According to the previous assumptions, the system (2.64) can be studied

$$f\left(\varepsilon(t), \dot{\varepsilon}(t), \int \varepsilon(t)dt\right) = m_L\ddot{x}(t) + b_L\dot{x}(t) + k_L x(t) \tag{2.80}$$

Although there are a number of available families of controllers, the simpler and more extensively used controllers are the so-called PID controllers. Such controllers compute the output as

$$f\left(\varepsilon(t), \dot{\varepsilon}(t), \int \varepsilon(t)dt\right) = K_P\varepsilon(t) + K_I\int \varepsilon(t)dt + K_D\dot{\varepsilon}(t) \tag{2.81}$$

where K_P, K_I and K_D are controller constant, which are to be designed analyzing carefully the system under study.

Example 2.16. Consider a control law

$$f\left(\varepsilon(t), \dot{\varepsilon}(t), \int \varepsilon(t)dt\right) = k_p\varepsilon(t) \tag{2.82}$$

with a reference value $x^*(t) = 0$. Discuss how the controller can modify the response of the system.

Substituting the control law in the system (2.80)

$$-k_p x(t) = m_L\ddot{x}(t) + b_L\dot{x}(t) + k_L x(t) \tag{2.83}$$

It is straightforward to note that the new system dynamics will be the same as the unactuated system with a modified elastic constant

$$k'_L = k_L + k_p \tag{2.84}$$

The new system dynamics will be characterized by:

$$\omega_0 = \sqrt{\frac{k_L + k_p}{m_L}} \tag{2.85}$$

$$\zeta = \frac{b_L}{2\sqrt{(k_L + k_p)\, m_L}} \tag{2.86}$$

allowing to freely choose the system response by choosing the adequate constant k_p. Note that the while the sign of k_p can be chosen the system will be stable as long as $k_p > -k_L$.

References

1. Buckingham E (1914) On physically similar systems: Illustrations of the use of dimensional equations. Phys Rev 4:345–376
2. Holman J (1980) Thermodynamics, 3rd edn. McGraw-Hill, Kogakusha
3. Hu T, Lin Z (2001) Control Systems with Actuator Saturation: Analysis and Design. Birkhauser
4. Huber J (1998) Ferroelectrics: Models and applications. PhD thesis, University of Cambridge
5. Huber JE, Fleck NA, Ashby MF (1997) The selection of mechanical actuators based on performance indices. Proc R Soc Lond A 453:2185–2205
6. Jack A, Mecrow B (1990) Methods for magnetically nonlinear problems involving significant hysteresis and eddy currents. IEEE Transactions on Magnetics 26(2):424–429, DOI 10.1109/20.106344
7. Jin J (1993) The finite element method in electromagnetics. Wiley New York
8. Kailath T (1980) Linear systems. Prentice-Hall
9. Khalil H (2002) Nonlinear systems. Prentice Hall Upper Saddle River, NJ
10. Kuo B (1992) Digital Control Systems. Oxford university press
11. Kuribayashi K (1993) Criteria for the evaluation of new actuators as energy converters. Advanced robotics 7(4):289–307
12. Kyriakides E, Heydt G, Vittal V (2005) Online parameter estimation of round rotor synchronous generators including magnetic saturation. IEEE Transactions on Energy Conversion 20(3):529–537, DOI 10.1109/TEC.2005.847951
13. Levi E (1997) Modelling of magnetic saturation in smooth air-gap synchronous machines. IEEE Transactions on Energy Conversion 12(2):151–156, DOI 10.1109/60.629697
14. Nandi S (2004) A detailed model of induction machines with saturation extendable for fault analysis. IEEE Transactions on Industry Applications 40(5):1302–1309
15. Novotnak R, Chiasson J, Bodson M (1999) High-performance motion control of an induction motor with magneticsaturation. IEEE Transactions on Control Systems Technology 7(3):315–327
16. Reddy J (1993) An introduction to the finite element method. McGraw-Hill Singapore
17. Sullivan C, Kao C, Acker B, Sanders S (1996) Control systems for induction machines with magnetic saturation. IEEE Transactions on Control Industrial Electronics 43(1):142–152
18. Taylor E (1974) Dimensional analysis for engineers. Clarendon Press Oxford
19. Zienkiewics O, Taylor R, Nithiarasu P, Zhu J (2005) The Finite Element Method. Elsevier/Butterworth-Heinemann

Part II
Conventional Actuators

Chapter 3
Design Analysis of Solenoid Actuators

3.1 Design Parameters

The solenoid actuators provide motion exciting a magnetic field where a plunger (movable part) tries to minimize the reluctance (i.e. the air gap) moving to the less reluctance position. A typical geometry is shown in Figure 3.1.

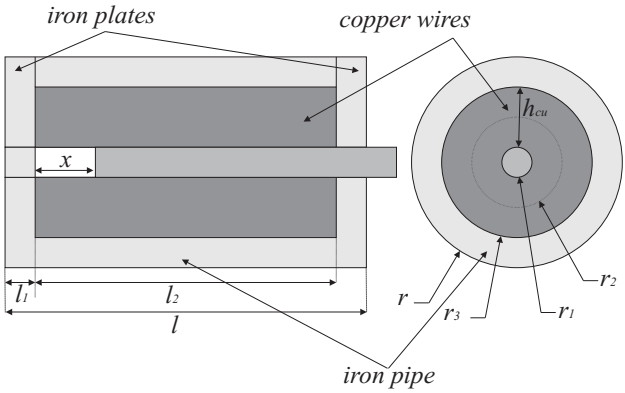

Fig. 3.1 Solenoid actuator sketch

The geometric constants and aspect ratios can be defined as [4, 5, 3]:

$$k_{ri} = \frac{r_i}{r} \tag{3.1}$$

$$k_{li} = \frac{l_i}{l} \tag{3.2}$$

$$\eta = \frac{l}{r} \tag{3.3}$$

where the non-dimensional constants associated to the radial lengths correspond to k_{ri}, while the axial lengths constants correspond to k_{li}.

The filling factor can be computed as the ratio between the profitable copper section S_{use} and the overall actuator section S_{total} as

$$k_{ff} = \frac{S_{use}}{S_{total}} = \frac{NA_w}{S_{total}} \tag{3.4}$$

where A_w is the single copper wire section and N is the number of turns.

3.2 Output Quantities

The solenoid force is produced for the change of reluctance due to the change of the air gap distance. Its expression can be derived from the energy stored in a solenoid

$$W_m = \int id\lambda = \int Nid\Phi \tag{3.5}$$

Before evaluating the energy stored in the solenoid, it is necessary to compute the magnetic flux. The magnetic flux flowing inside a solenoid can be derived from the reluctance expression

$$\Phi = \frac{F_{mm}}{\Re} \tag{3.6}$$

were F_{mm} is the magneto-motive force, equal to the number of turn N times the current i and $\Re$ is the reluctance expressed as a function of the magnetic properties of the iron μ_r, the length l_2, the cross-section of the plunger $S = \pi r_1^2$ and the length l_{eq}, which is the plunger length with a reluctance equivalent to the reluctance of the plates and the pipe.

It can be written as:

$$\Phi = \frac{F_{mm}}{\Re} = \frac{Ni}{\frac{x}{\mu_0 S} + \frac{l_2 + l_{eq} - x}{\mu_r \mu_0 S}} = \frac{Ni\mu_r\mu_0 S}{l_2 + l_{eq} + x(\mu_r - 1)} \tag{3.7}$$

Using the obtained magnetic flux expression, the stored energy yields:

$$W_m = \int id\lambda = \int \frac{SN^2 i^2 \mu_r^2 \mu_0}{2\left(l_2 + l_{eq} + (\mu_r - 1)x\right)^2} dx \tag{3.8}$$

The solenoid actuator force can be derived as:

$$F = \frac{dW_m}{dx} = \frac{SN^2 i^2 \mu_r^2 \mu_0}{2\left(l_2 + l_{eq} + (\mu_r - 1)x\right)^2} \tag{3.9}$$

The energy can be obtained integrating the force (3.9) between a given displacement x and 0 as:

$$W = \int_0^x F dx = \frac{SN^2 i^2 \mu_r^2 \mu_0 x}{2\left(l_2 + l_{eq} + (\mu_r - 1)x\right)\left(l_2 + l_{eq}\right)} \tag{3.10}$$

It can be seen that W is the total energy which the actuator stores in each position. This energy is transformed in work against a load and kinetic energy $W_k = (1/2)mv^2$, since this work focuses on the static behavior of the studied actuators, a quasi-static movement is considered. Therefore, if it is not otherwise stated all the energy is assumed to be transformed into work. The force and work curves are shown in Figures 3.2 and 3.3.

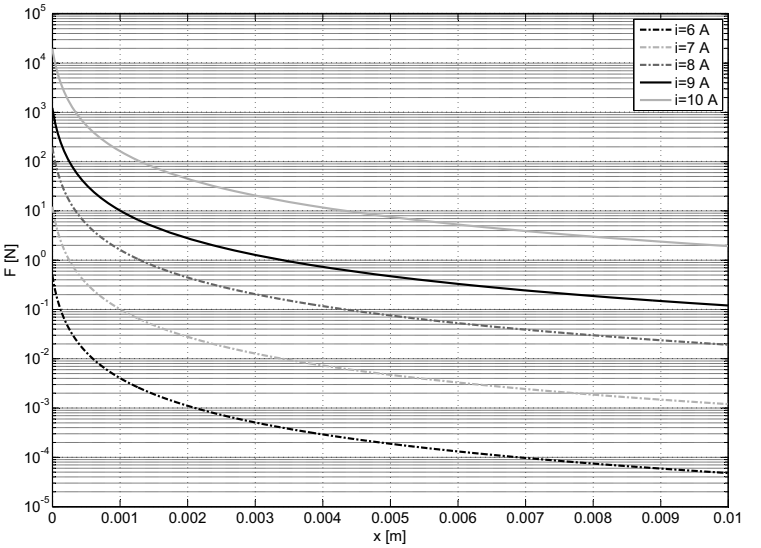

Fig. 3.2 Force-displacement curves for the solenoid actuator

The force-stroke curves (Figure 3.4) are presented when the input quantity (electrical current) is changed for different loads (one elastic load, equivalent to a structure, and one constant load). It can be seen that for a constant force load the equilibrium point x_eq are established for

$$x_{eq} = \frac{\sqrt{\frac{SN^2 i^2 \mu_r^2 \mu_0}{2F_{load}}} - l_2 - l_{eq}}{\mu_r - 1} \tag{3.11}$$

If the actuator is attached to an elastic load with $F_load(x) = F_0 - k_e x$, the equilibrium point yields

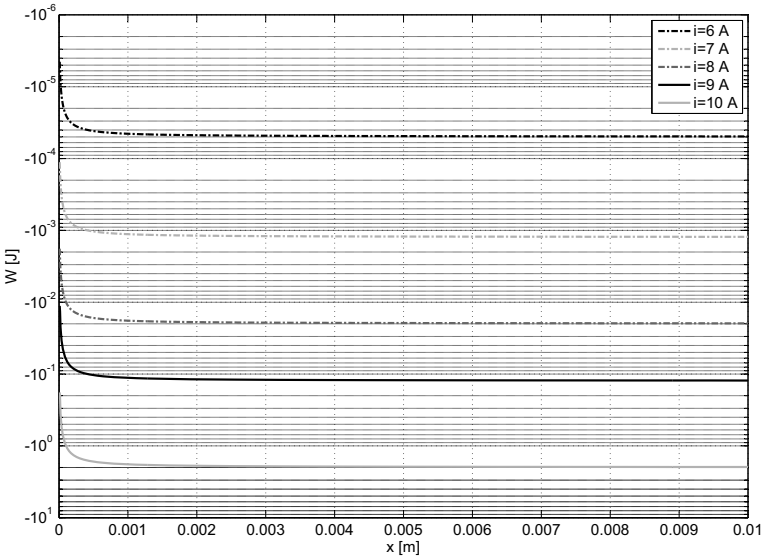

Fig. 3.3 Work-displacement curves for the solenoid actuator

$$F_0 - k_e x_{eq} = \frac{SN^2 i^2 \mu_r^2 \mu_0}{2\left(l_2 + l_{eq} + (\mu_r - 1)\, x_{eq}\right)^2} \tag{3.12}$$

where x_{eq} can be found as the solution of a three-degree equation.

It can be seen in Figure 3.4 how the operating points are changing depending on the input quantity and the load, when the current is increased working against an elastic load the working point is moving from E1 to E5. From the initial working point the load can be moved to the other points depending on the input current. The work against a constant load presents more difficulties. When the current is not large enough the actuator cannot begin to move and remains blocked at the initial position, needing a minimum current to begin the traction.

3.3 Thresholds

The main limiting quantity considered in this chapter is the maximum allowed actuator temperature. To analyze how the maximum temperature implies a limitation in the actuator electrical current a detailed analysis of the heat transfer phenomena taking place in the solenoid actuator has to be performed.

First of all, the resistance of the coils of all the actuators is expressed as a function of the geometrical dimensions and the copper resistivity as:

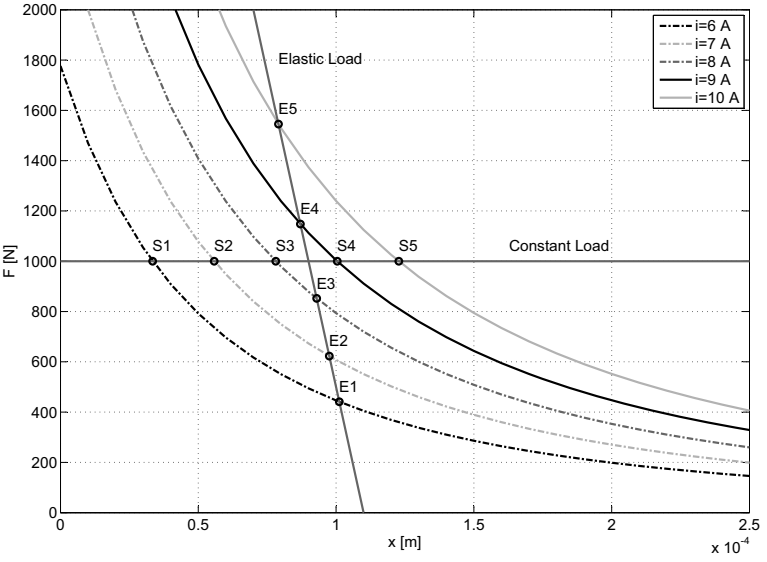

Fig. 3.4 Force-displacement curves for elastic and constant loads

$$R = \frac{\delta_{res} l_w}{A_w} = \frac{\delta_0 (1 + \gamma \Delta T) l_w}{A_w} \tag{3.13}$$

where γ is the resistivity temperature coefficient, δ_0 the resistivity at a given temperature T_0, $\Delta T = T_{max} - T_0$ the temperature increment, and l_w and A_w the length and cross-section of the wire. The steady-state heating balance equals the heat power produced in the coils due to the Joule effect with the heat power which the actuator can dissipate by means of conduction and convection as:

$$Ri^2 = \dot{Q} = \frac{\Delta T}{\vartheta_{cond} + \vartheta_{conv}} \tag{3.14}$$

where ϑ_{cond} is the thermal resistance by means of conduction and ϑ_{conv} is the thermal resistance by means of convection . The thermal resistance is defined in [1] as the temperature increment ΔT divided into the heat flow $\dot{Q}$. Since the solenoid actuator studied in this work presents cylindrical shape, only this actuator shape will be considered. If the heat produced in the coils flows radially, the thermal resistances can be written as:

$$\vartheta_{cond} = \frac{\log(r/r_3)}{2\pi l \lambda_{iron}} = \frac{\log(1/k_{r3})}{2\pi l \lambda_{iron}} \tag{3.15}$$

$$\vartheta_{conv} = \frac{1}{2\pi l r h_c} \tag{3.16}$$

where l is the length of the actuator, λ_{iron} the conductivity of the iron, h_c the convection coefficient between the iron surface and the air, and r_3 and r the internal and external radium of the pipe surrounding the actuator. If no pipe is surrounding the actuator there will be no heat transfer by means of conduction, and therefore, less thermal resistance.

From the heating balance (3.14) an expression of the maximum allowed current is obtained. The maximum current can be expressed as:

$$i_{max} = \sqrt{\frac{\Delta T}{R(\vartheta_{cond} + \vartheta_{conv})}} \tag{3.17}$$

Substituting the resistance obtained in (3.13) and the thermal resistances from (3.15) and (3.16) in the last expression, the maximum current can be written as:

$$i_{max} = \sqrt{\frac{A_w 2\pi l \Delta T}{\delta_0 (1+\gamma\Delta T) l_w (\frac{\log\left(\frac{1}{k_{r3}}\right)}{\lambda_{iron}} + \frac{1}{r h_c})}} \tag{3.18}$$

The conduction coefficient λ is a material property, but the convection coefficient h_c depends on the non-dimensional Nusselt number which may be expressed as:

$$Nu_L = \frac{h_c l}{\lambda_{air}} \tag{3.19}$$

The maximum allowed current can be expressed substituting the convection coefficient using the Nusselt number as

$$i_{max} = \sqrt{\frac{A_w 2\pi l \Delta T}{\delta_0 (1+\gamma\Delta T) l_w (\frac{\log\left(\frac{1}{k_{r3}}\right)}{\lambda_{iron}} + \frac{2}{Nu_L \lambda_{air}})}} \tag{3.20}$$

3.4 Maximum Output Quantities

Before evaluating the maximum output quantities, the different relevant expressions obtained can be summarized as the maximum current obtained in (3.18), the convection coefficient of (3.19) and the geometrical expressions of (3.3). As far as the number of turns N is concerned, it can be expressed as a function of the actuator dimensions as:

$$N = \frac{h_{cu} l_2 k_{ff}}{A_w} \tag{3.21}$$

where h_{cu} is the thickness of copper, l_2 the coil's length, k_{ff} the filling factor described in (3.4) and A_w the cross-section of a single wire.

Replacing (3.18), (3.21), (3.19) and (3.3) in (3.9), the maximum force (obtained when $x = 0$) can be expressed as:

$$\frac{F_{max}}{S_{act}} = \frac{\lambda_{air}\mu_0 \Delta T \mu_r^2}{\delta_0 (1+\gamma \Delta T)} \frac{k_L^2 k_{r1}^2 \left(\frac{k_{r3}-k_{r1}}{k_{r2}}\right) k_{ff}}{\left(\frac{2k_\lambda \lambda_{air}}{\lambda_{iron}} + \frac{4}{Nu_L \eta}\right)} \tag{3.22}$$

with $k_\lambda = \log(1/k_{r3})$ and $k_L = l_2/(l_2 + l_{eq})$. The equivalent length ratio can be expressed as:

$$\frac{l_{eq}}{l} = \frac{k_{r1}^2(1-2k_{l1})}{1-k_{r3}^2} + \frac{k_{r1}^2 \eta^2 \log \frac{1}{k_{r1}}}{k_{l1}} \tag{3.23}$$

It can be noted that the maximum force divided into the cross-section of the actuator is expressed as a function of material constants, physical thresholds and geometrical relationships. A design factor depending on the design parameters can be defined from (3.22) as:

$$q_f = \frac{k_L^2 k_{r1}^2 \left(\frac{k_{r3}-k_{r1}}{k_{r2}}\right) k_{ff}}{\left(\frac{2k_\lambda \lambda_{air}}{\lambda_{iron}} + \frac{4}{Nu_L \eta}\right)} \tag{3.24}$$

Substituting all the terms in the last expression it can be written as:

$$q_f = \frac{2k_{l2}^2 k_{r1}^2 k_{ff} \frac{k_{r3}-k_{r1}}{k_{r3}+k_{r1}}}{\left(k_{l2} + \frac{k_{r1}^2 k_{l2}}{1-k_{r3}^2} + \frac{k_{r1}^2 \eta^2 \log \frac{1}{k_{r1}}}{(1-k_{l2})/2}\right)^2 \left(\frac{2k_\lambda \lambda_{air}}{\lambda_{iron}} + \frac{4}{Nu_L \eta}\right)} \tag{3.25}$$

The expression (3.25) has been analyzed numerically. The best design parameterization has been found for values $k_{r1} = 0.29$, $k_{r2} = 0.535$, $k_{r3} = 0.78$, $k_{l1} = 0.25$, $k_{l2} = 0.50$ and $\eta = 0.7$. The optimized found design factor is $q_f = 0.2299$.

In Figure 3.5 the design factor q_f depending on the ratios k_{r1} and k_{r3} is plotted. The aspect ratio η, the ratio r_{l1} and the filling factor are kept constant to allow a three-dimensional plot. The filling factor k_{ff} is typically around 0.75 and can be considered independent of the other design parameters.

Regarding the aspect ratio, it is shown in Figures 3.6 and 3.7 that the best performance aspect ratio is achieved for $\eta = 0.7$.

The dependance on the factor k_{l2} is shown in Figure 3.8 where it is clearly shown that the best performance is achieved for $k_{l2} = 0.5$.

The maximum displacement is l_2 and is proportional to the length of the actuator l since $l_2 = k_{l2} l$. The maximum volumetric work is achieved when the whole displacement is done. It can be obtained integrating the force. The maximum work expression found yields:

$$\frac{W_{max}}{V_{act}} = \frac{q_{fW} \lambda_{air} \mu_0 \Delta T \mu_r^2}{\delta_0 (1+\gamma \Delta T) \left(\frac{2k_\lambda \lambda_{air}}{\lambda_{iron}} + \frac{4}{Nu_L \eta}\right)} \tag{3.26}$$

with the work design factor

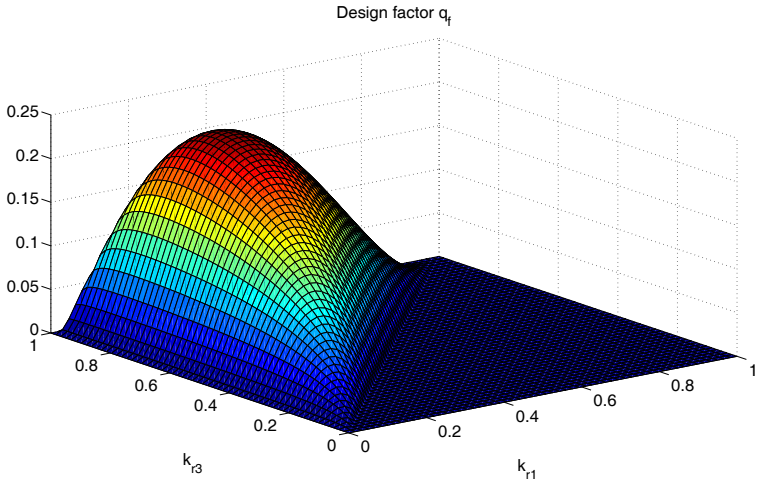

Fig. 3.5 Solenoid force design factor depending on k_{r1} and k_{r3} with $k_{l2} = 0.5$ and $\eta = 0.7$

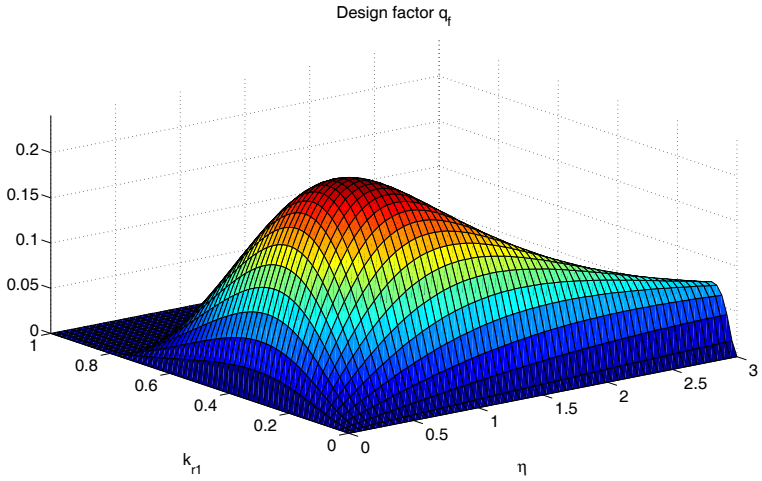

Fig. 3.6 Solenoid force design factor depending on η and k_{r1} with $k_{l2} = 0.5$ and $k_{r3} = 0.78$

$$q_{fW} = \frac{2k_{l2}^2 k_{r1}^2 k_{ff} \frac{k_{r3}-k_{r1}}{k_{r3}+k_{r1}} \left(\frac{2k_\lambda \lambda_{air}}{\lambda_{iron}} + \frac{4}{Nu_L \eta} \right)^{-1}}{\left(k_{l2} + \frac{k_{r1}^2 k_{l2}}{1-k_{r3}^2} + \frac{k_{r1}^2 \eta^2 \log \frac{1}{k_{r1}}}{(1-k_{l2})/2} \right) \left(k_{l2} + \frac{k_{r1}^2 k_{l2}}{1-k_{r3}^2} + \frac{k_{r1}^2 \eta^2 \log \frac{1}{k_{r1}}}{(1-k_{l2})/2} + \mu_r - 1 \right)} \tag{3.27}$$

The evaluation of the expression (3.27) shows that the best design parameterization is achieved for $k_{r1} = 0.39$, $k_{r2} = 0.625$, $k_{r3} = 0.86$, $k_{l1} = 0.125$, $k_{l2} = 0.75$ and $\eta = 1.01$. The optimized found work design factor is $q_{fW} = 0.0015$.

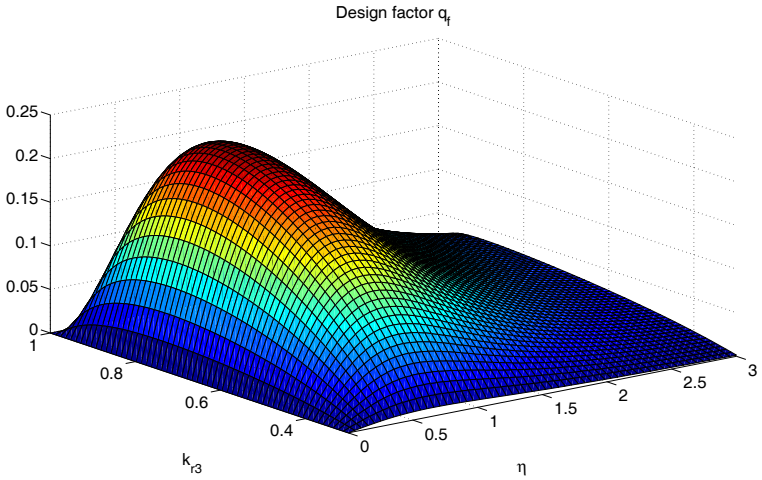

Fig. 3.7 Solenoid force design factor depending on η and k_{r3} with $k_{l2} = 0.5$ and $k_{r1} = 0.29$

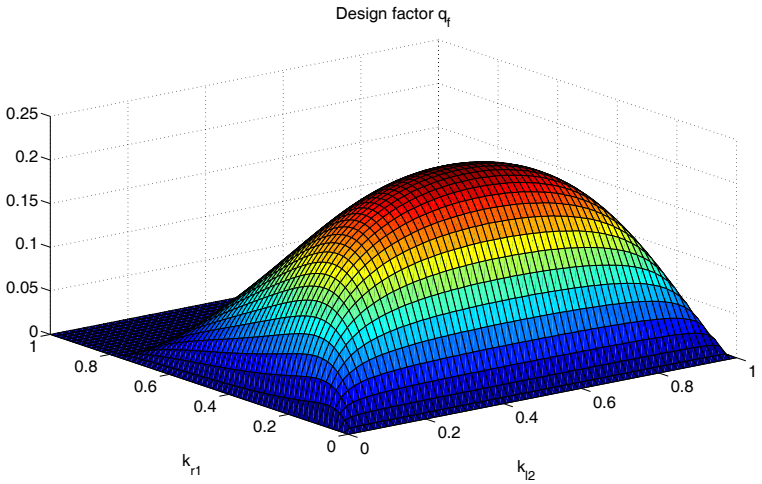

Fig. 3.8 Solenoid force design factor depending on k_{l2} and k_{r1} with $\eta = 0.7$ and $k_{r1} = 0.29$

In Figure 3.9 the work design factor q_{fW} depending on the ratios k_{r1} and k_{r3} is plotted. In order to analyze the influence of the aspect ratio, it is shown in Figures 3.10 and 3.11 that the best performance aspect ratio is achieved for $\eta = 1.01$. The dependance on the factor k_{l2} is shown in Figure 3.12 where it is shown that the best performance is achieved for $k_{l2} = 0.75$.

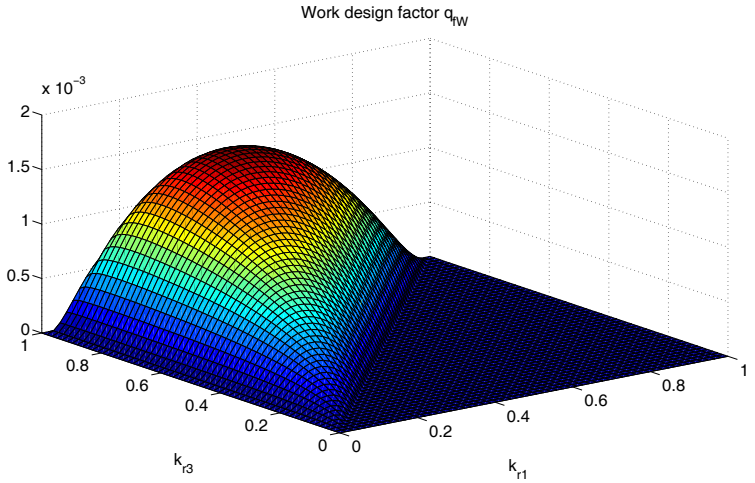

Fig. 3.9 Solenoid work design factor depending on k_{r1} and k_{r3} with $k_{l2} = 0.75$ and $\eta = 1.01$

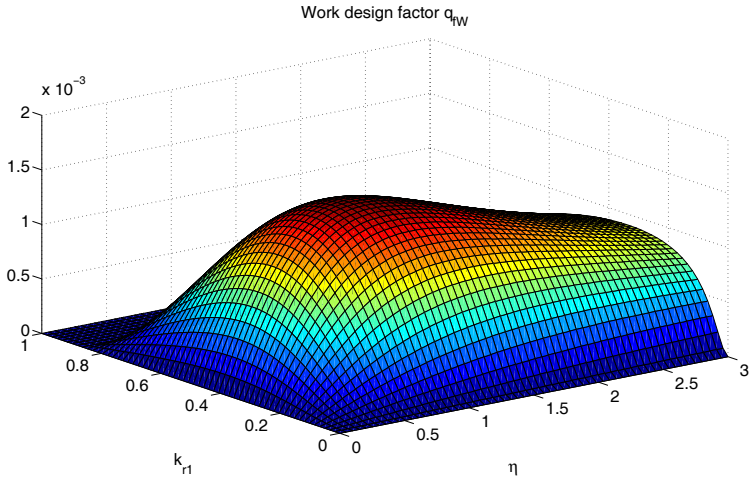

Fig. 3.10 Solenoid work design factor depending on η and k_{r1} with $k_{l2} = 0.75$ and $k_{r3} = 0.86$

3.5 Scalability

If the l_{eq}/l ratio is kept constant in (3.22) and (3.26), scalability will depend only on the Nusselt number.

The Nusselt number can be written as a function of Reynolds, Prandtl and Grashof numbers, in [6] it is presented as:

$$N_u = CR_e^m P_r^n G_r^p \tag{3.28}$$

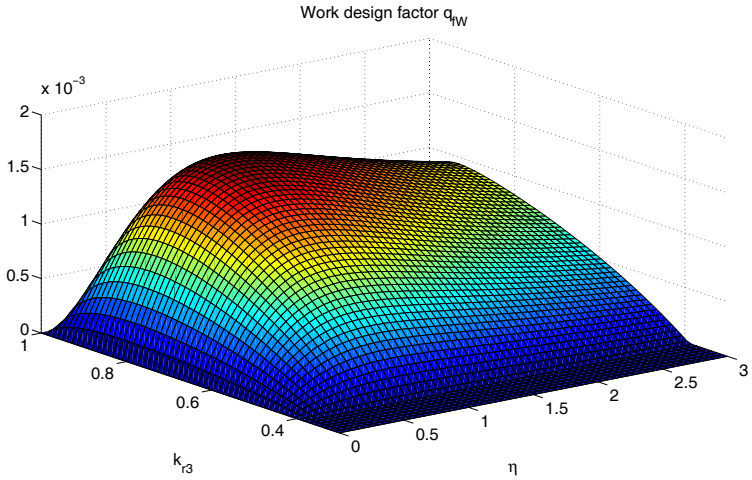

Fig. 3.11 Solenoid work design factor depending on η and k_{r3} with $k_{l2} = 0.75$ and $k_{r1} = 0.39$

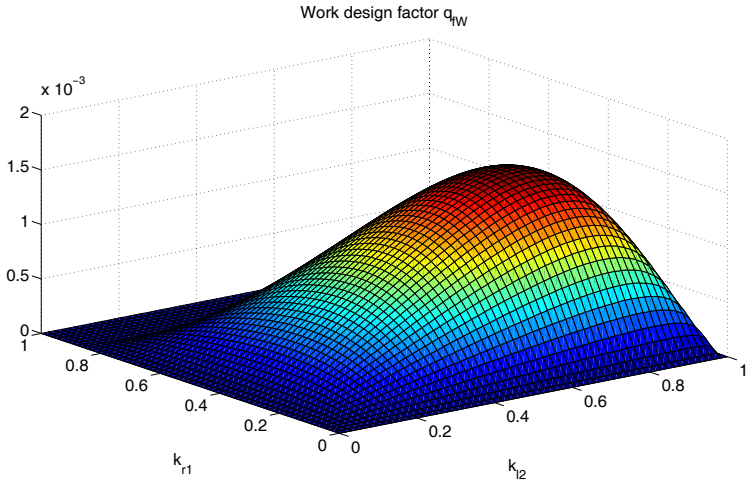

Fig. 3.12 Solenoid work design factor depending on k_{l2} and k_{r1} with $\eta = 1.01$ and $k_{r1} = 0.39$

where R_e is the Reynolds number ($\rho vL/\eta$) which shows the relationship between the inertial forces and the viscous forces in the dynamics of a fluid, P_r is the Prandtl number ($\eta c/\lambda$) which characterizes the regime of convection, G_r is the Grashof number($\beta g \Delta T L^3/\nu^2$) analog to the Reynolds number when natural convection is concerned and C, m, n and p can take different values in forced convection ($C < 1, m < 1, n = 1/3, p = 0$) and natural convection ($C < 1, m = 0, n < 1/3, p < 1/3$). The Nusselt number can be in all the cases expressed as:

$$N_{u-r} = K_{Nu} r^{\alpha} \tag{3.29}$$

where K_{Nu} and α must be discussed in each case.

If the Nusselt number is assumed to be constant ($\alpha = 0$), the force will be independent of the actuator length and it will be proportional to the cross-section. The work will be proportional to both the length and the cross-section, and therefore to the volume so that a constant volumetric energy will be shown. Such an assumption cannot generally be done when studying the different convection cases. With a positive value of α (which is the behavior observed) the actuator force and work are not scalable anymore and their maximum performance values are increased when the size is increased. In such a case the maximum force per cross-section can be expressed as:

$$\frac{F_{max}}{S_{act}} = k_a \frac{r^\alpha}{k_b + r^\alpha} \tag{3.30}$$

It can be noted that for high values of r the maximum force tends to be scalable since $\lim_{r\to\infty} k_a r^\alpha / (k_b + r^\alpha) = k_a$, as it is observed in Figure 3.13. For tiny actuators the force and work performance becomes worse. It may explain that these actuators are not used when a small actuator is required.

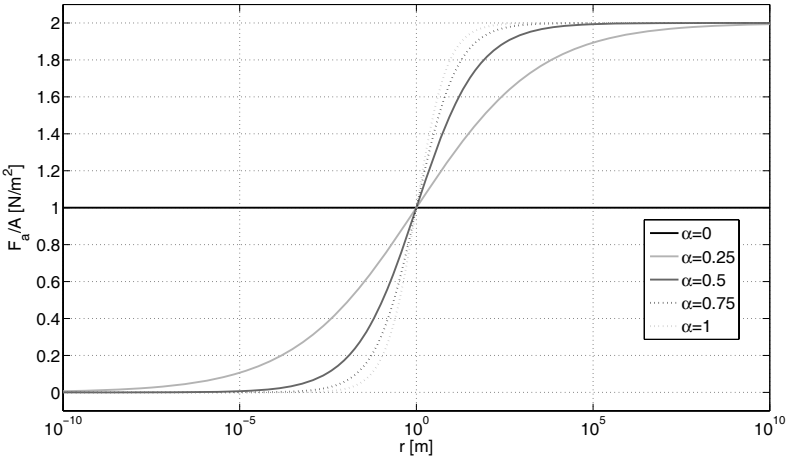

Fig. 3.13 Solenoid force scalability for different α coefficients in the Nusselt number expression

3.6 Dimensional Analysis

The force provided by these actuators can be analyzed with dimensional analysis using the Buckingham Pi Theorem [2], the quantities involved are shown in the Table 3.1. The $FLTI\theta$ (force – length – time – current – temperature) system is used.

Table 3.1 Solenoid actuator dimensional analysis quantities

F	Force	$[F]$
x	Position	$[L]$
μ	Permeability	$[FI^{-2}]$
h_c	Convection coef.	$[FL^{-1}T^{-1}\theta^{-1}]$
λ	Conduction coef.	$[FT^{-1}\theta^{-1}]$
δ	Resistivity	$[FL^2I^{-2}T^{-1}]$
T	Temperature	$[\theta]$

Table 3.2 Dimension matrix for the solenoid force analysis

	F Force	x Position	μ Permeability	h_c Convection	λ Conduction	δ Resistivity	T Temperature
F	1	0	1	1	1	1	0
L	0	1	0	-1	0	2	0
T	0	0	0	-1	-1	-1	0
I	0	0	-2	0	0	-2	0
θ	0	0	0	-1	-1	0	1

The dimension matrix is shown in Table 3.2. Since there are seven involved quantities and a five dimension $FLTI\theta$ (force – length – time – current – temperature) system, the number of non-dimensional groups will be 7-5=2.

Considering $F = x^a \mu^c h_c^d \lambda^e \delta^f \theta^g$ the following equations are obtained:

$$\left\{\begin{array}{c} 1 = c+d+e+\mathrm{f} \\ 0 = \mathrm{a}-\mathrm{d}+2f \\ 0 = -\mathrm{d}-\mathrm{e}-\mathrm{f} \\ 0 = -2c-2f \\ 0 = -\mathrm{d}-\mathrm{e}+\mathrm{g} \end{array}\right\} \rightarrow \left\{\begin{array}{c} c = 1 \\ \mathrm{a} = +\mathrm{d}+2 \\ e = 1-d \\ f = -1 \\ \mathrm{g} = 1 \end{array}\right\} \tag{3.31}$$

Therefore

$$F = x^{2+d} \mu h_c^d \lambda^{1-d} \delta^{-1} \theta \tag{3.32}$$

The maximum force can be expressed as:

$$\frac{F\delta}{x^2 \mu \theta \lambda} = \phi\left(\frac{x h_c}{\lambda}\right) = \phi\left(Nu\right) \tag{3.33}$$

Arranging the terms:

$$\frac{F}{x^2} = K \frac{\mu T \lambda}{\delta} \Phi\left(N_u\right) \tag{3.34}$$

where it can be observed that it matches perfectly with (3.22) since $\delta = \delta_0\left(1+\gamma \Delta T\right)$ and μ_r and all the geometrical constants are adimensional. The results obtained for the work match with the expression (3.26), the maximum work given by dimensional analysis can be expressed as:

$$\frac{W}{x^3} = K \frac{\mu T \lambda}{\delta} \Phi\left(N_u\right) \tag{3.35}$$

3.7 Finite Element Analysis

The configuration featuring the maximum work performance has been simulated using Finite Element Analysis software COMSOL® by COMSOL AB in order to validate the obtained expression. The optimal configuration found in the previous steps for values $k_{r1} = 0.39$, $k_{r2} = 0.625$, $k_{r3} = 0.86$, $k_{l1} = 0.125$, $k_{l2} = 0.75$ and $\eta = 1.01$ has been analyzed, considering the material properties:

- $\lambda_{air} = 0.0257\ W/Km$
- $\lambda_{iron} = 80\ W/Km$
- $\mu_0 = 1.25664 \times 10^{-6}\ Tm/At$
- $\Delta T = 50\ K$
- $\mu_r = 200$
- $\rho_0 = 1.68 \times 10^{-8}\ \Omega m$
- $\gamma = 0.0068\ \Omega m/K$
- Nu=60

Considering an actuator radius of 5 cm, the actuator dimensions used in the FEA analysis yield:

- l =5.05 cm
- r_1=1.95 cm
- r_2=3.125 cm
- r_3=4.3 cm
- l_1=3.79 cm
- l_2=0.63 cm

A sketch of the actuator can be seen in Figure 3.14, where it can be noted that only half a section of the actuator is considered due to the cylindrical symmetry of the actuator under analysis.

To use Finite Element Analysis, the current density of the copper has to be computed. The maximum current density can be expressed as:

$$J_{max} = \frac{Ni_{max}}{S_{cu}} = \frac{i_{max}}{k_{ff} A_w} \tag{3.36}$$

where S_{cu} is the overall copper section and A_w the single wire section. Using (3.20), it can be expressed as

$$J_{max} = \sqrt{\frac{2\pi l \Delta T}{k_{ff}^2 A_w \delta_0 (1+\gamma\Delta T) l_w (\frac{\log\left(\frac{1}{k_{r3}}\right)}{\lambda_{iron}} + \frac{2}{Nu_L \lambda_{air}})}} \tag{3.37}$$

substituting $l_w = 2\pi r_2 N$ and $N = (r_3 - r_1) l_2 k_{ff}/A_w$ in the previous expression:

$$J_{max} = \frac{1}{r}\sqrt{\frac{\Delta T}{k_{ff}^3 \delta_0 (1+\gamma\Delta T) k_{r2}(k_{r3} - k_{r1}) k_{l2} (\frac{\log\left(\frac{1}{k_{r3}}\right)}{\lambda_{iron}} + \frac{2}{Nu_L \lambda_{air}})}} \tag{3.38}$$

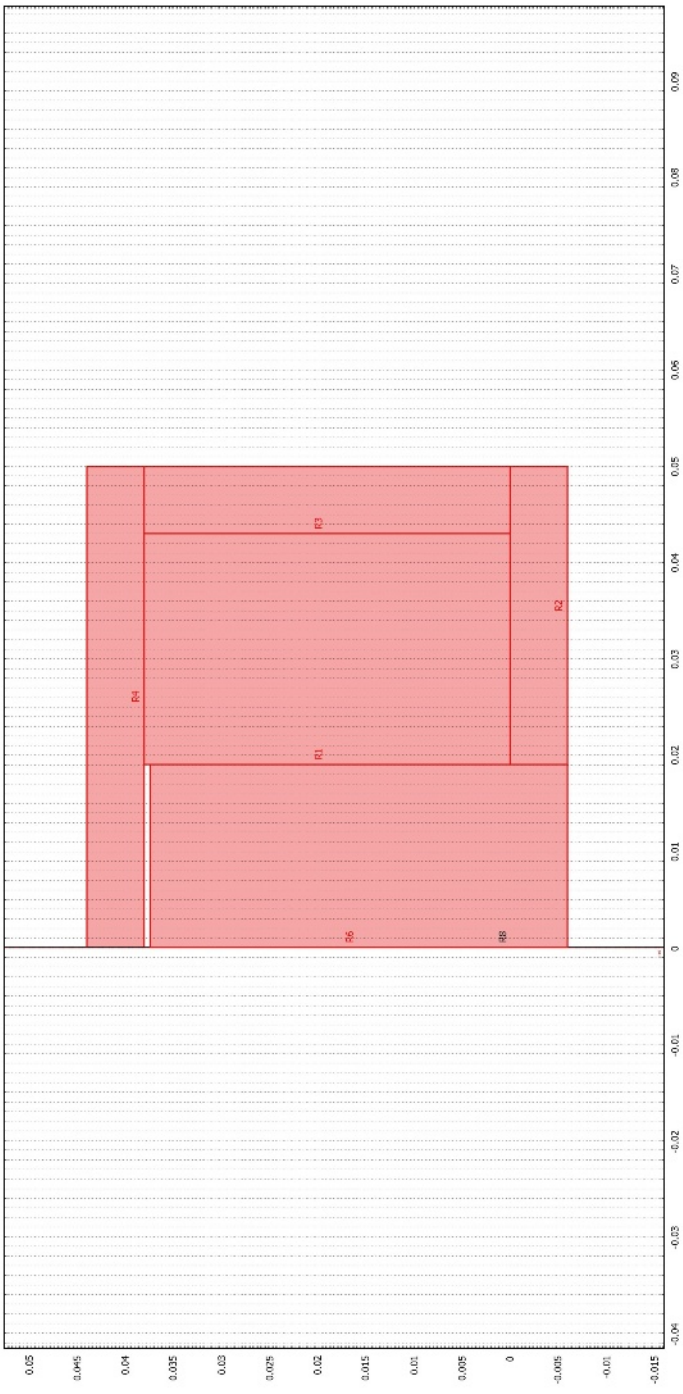

Fig. 3.14 Geometry of the actuator analyzed with COMSOL®

which corresponds to a current density of 2.7303×10^7 Am^{-2}. The effective current density to be applied in the FEA model corresponds to $k_{ff}J_{max} = 2.025 \times 10^7$ Am^{-2}.

The FEA mesh of the analyzed actuator is shown in Figure 3.15. The results illustrating the magnetic flux densities along with the maxwell tensor stresses are presented in Figures 3.16 and 3.17. The force obtained is 100.52 N.

The maximum force using the analytic procedure described in Step 4 can be evaluated as:

$$\frac{F_{max}}{S_{act}} = \frac{\lambda_{air}\mu_0 \Delta T \mu_r^2}{\rho_0 (1+\gamma \Delta T)} \frac{k_L^2 k_{r1}^2 \left(\frac{k_{r3}-k_{r1}}{k_{r2}}\right) k_{ff}}{\left(\frac{2k_\lambda \lambda_{air}}{\lambda_{iron}} + \frac{4}{Nu_L \eta}\right)} \tag{3.39}$$

Substituting the values and using a solenoid radius of 5 cm (and the corresponding length l=5.05 cm for the aspect ratio $\eta = 1.01$), the maximum force obtained is 102.1 N, which matches reasonably well with the FEA analysis result.

3.8 Comparison with Industrial Actuators

The comparison of different actuators using available industrial actuator data can provide relevant information. The present section presents an analysis of data from different manufacturers of solenoid actuators. A typical solenoid datasheets is illustrated in Figure 3.18.

Since electromagnetic actuators are often cooled with air by means of free convection, a numerical analysis is presented assuming natural convection. In such case the Nusselt number can be written as a function of the Rayleigh number in the form $N_{uD} = CR_a^n$ where C and n are to be discussed for different values of R_a as it is exposed in [6]. It has been found (assuming an air temperature of 293 K and a temperature increment of 50 K) that for diameters between 2.6 mm and 0.124 m the coefficients $C = 0.48$ and $n = 1/4$ can be used, while for diameters between 0.124 m and 5.75 m, $C = 0.125$ and $n = 1/3$ can be used. This range of diameters covers all the industrial electromagnetic actuators found, but other ranges can be considered using other coefficients. The Nusselt numbers can be written as:

$$\begin{aligned} N_{u_D} &= 129.20 \times D^{1/4} \quad 0.0026 < D < 0.124\ m \\ N_{u_D} &= 217.25 \times D^{1/3} \quad 0.124 \leq D < 5.75\ m \end{aligned} \tag{3.40}$$

Different manufactured industrial solenoids actuators have been studied. Its output mechanical quantities compared to the maximum quantities developed in this work are shown in Figures 3.19 and 3.20. The maximum quantities have been calculated using the design factor $q_f = 0.04$.

The data from industrial actuators have been analyzed and approached using a linear regression after taking logarithms of the quantities concerned. The force provided by the solenoid actuators has been approached with the function

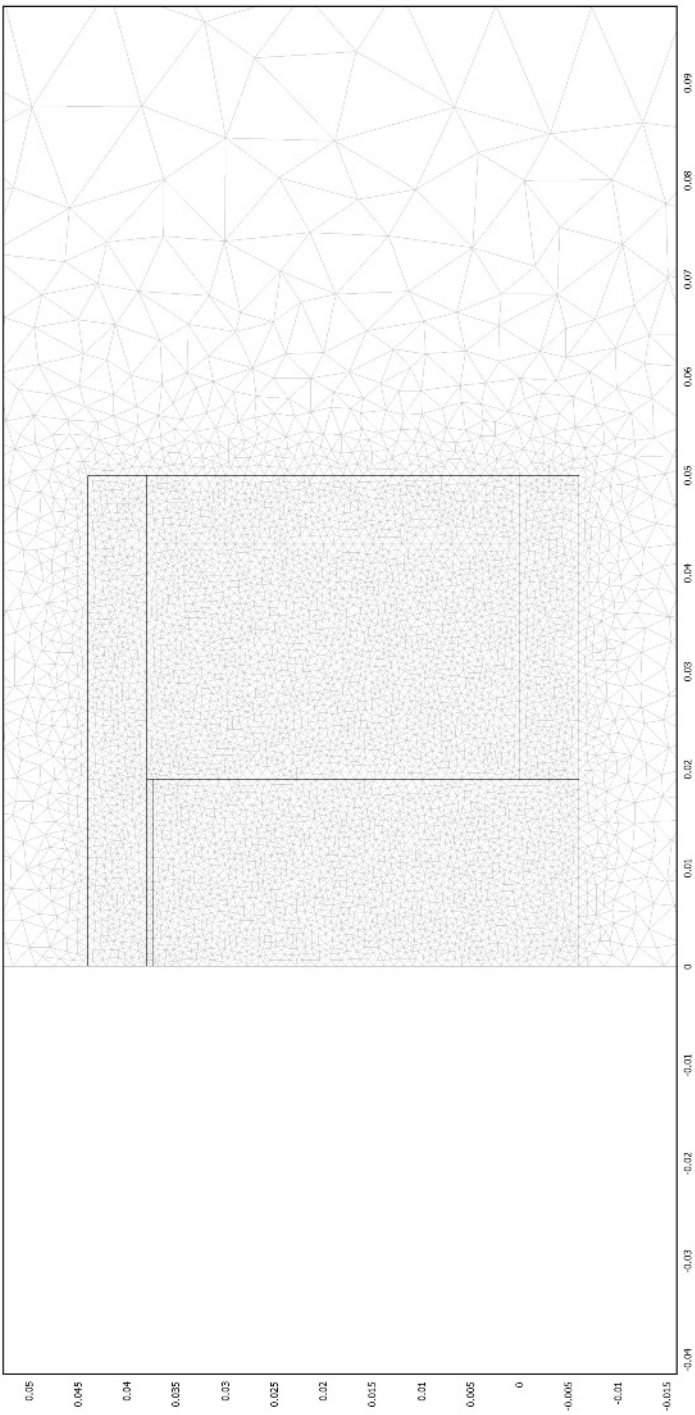

Fig. 3.15 Finite element mesh of the actuator analyzed with COMSOL®

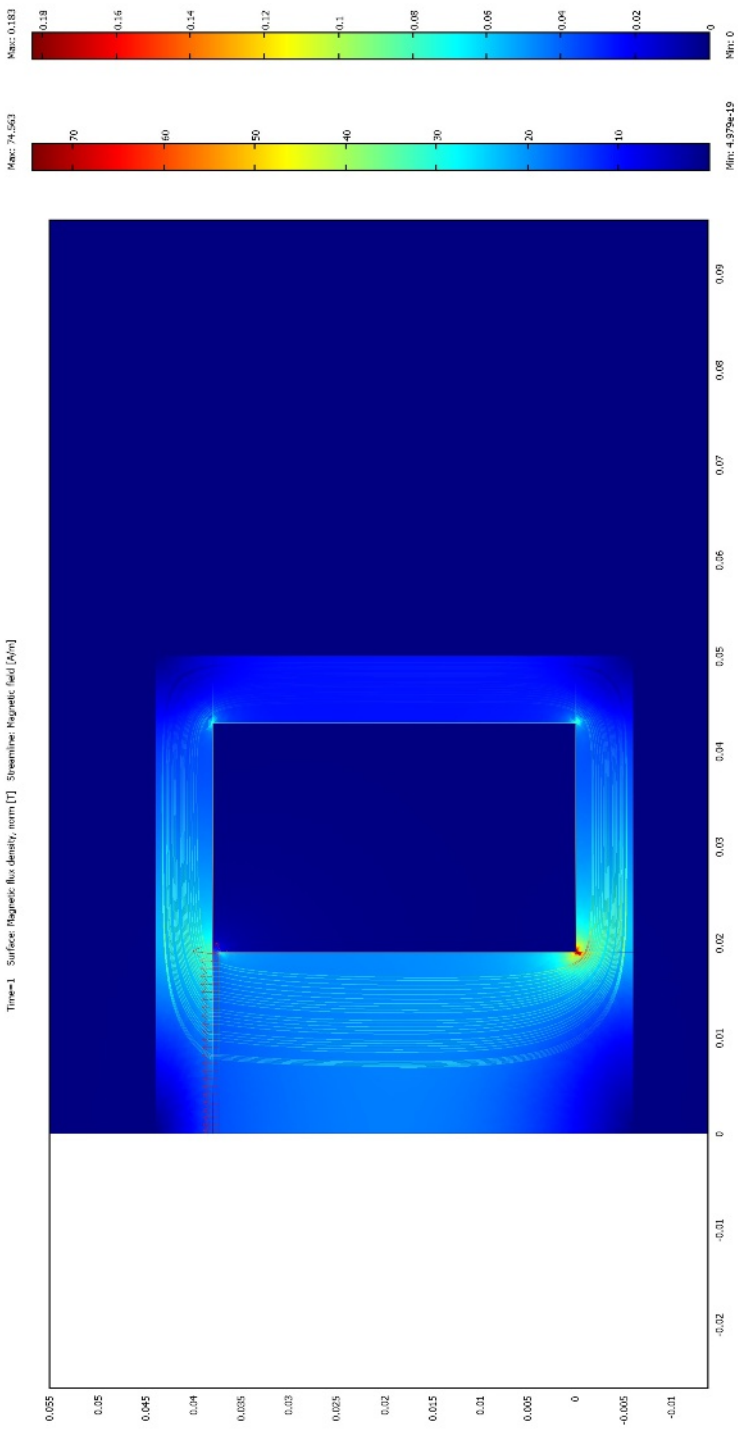

Fig. 3.16 Flux densities and Maxwell tensor stresses in the analyzed actuator

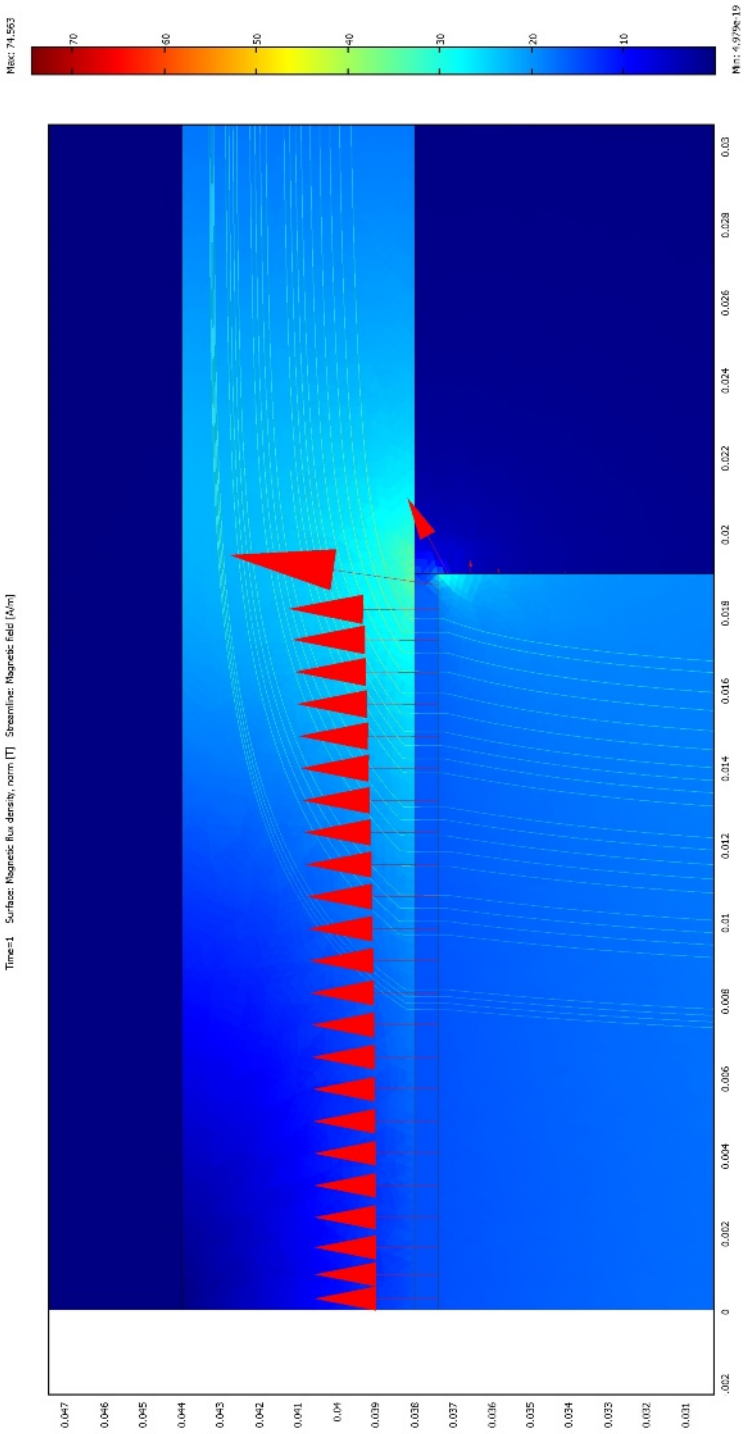

Fig. 3.17 Detail of the airgap flux densities and Maxwell tensor stresses in the analyzed actuator

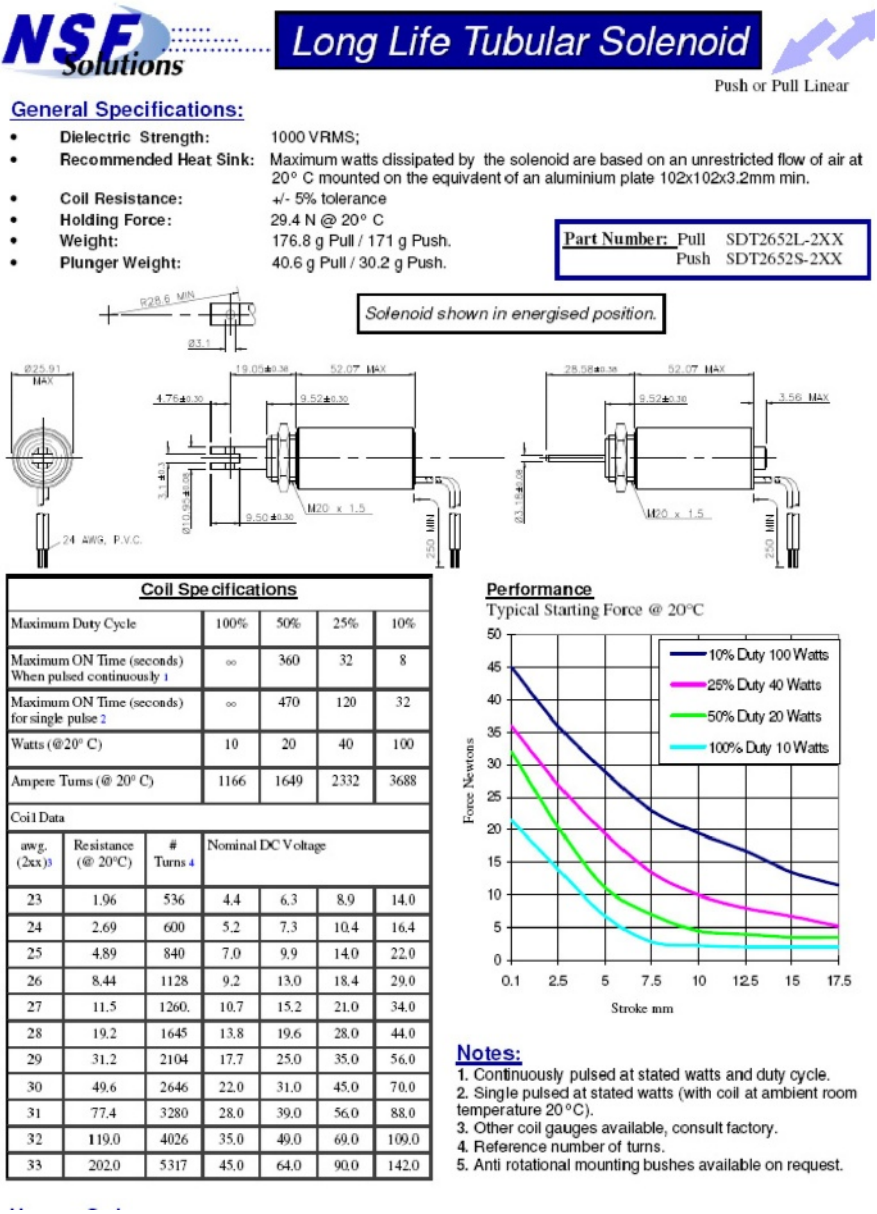

Fig. 3.18 Datasheet of an industrial solenoid actuator. Courtesy of NSF Controls Ltd

$9.35 \times 10^6 r^{2.3336}$. It has been stated that the limiting force for the solenoid holds $F \propto r^2 Nu$. Therefore, the α coefficient should be located between 2.25 and 2.333

(according to (3.40), $2+1/4$ and $2+1/3$). It matches with the α coefficient 2.3336 obtained with the regression.

The solenoid work has been fitted with $1.369 \times 10^5 V^{1.167}$, where the coefficient is close to the expected between 1.083 and 1.111 ($1+\frac{1/4}{3}$ and $1+\frac{1/3}{3}$).

As shown in the regression analysis and in Figures 3.19 and 3.20, it can be concluded that the behavior of industrial solenoid actuators follows the trends developed theoretically.

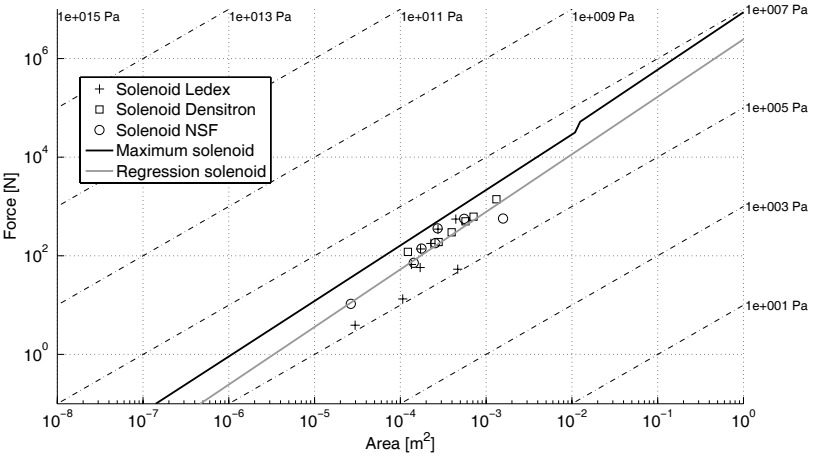

Fig. 3.19 Industrial electromagnetic actuator force-area comparison

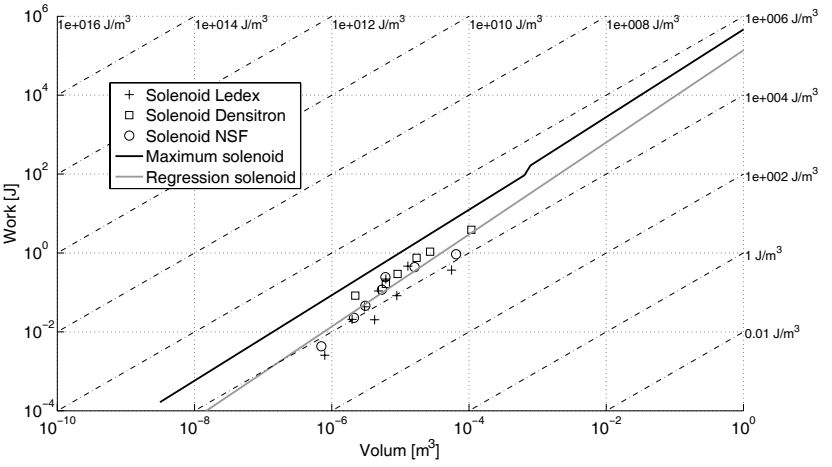

Fig. 3.20 Industrial electromagnetic actuator work-volume comparison

3.9 Dynamics

Although the proposed methodology focuses on the statical output mechanical quantities, some considerations on actuator dynamics are very important for most applications. As it has been stated in Section 2.10, the dynamic behavior does not depend only on the actuator but in the load attached to it and the controller governing the overall system. The present section presents examples of some classical applications employing solenoid actuators. A brief example dealing with a complete system comprising a solenoid actuator, the attached load and a linear controller is shown.

3.9.1 System Modeling

As it has been shown in Section 3.2, the solenoid actuator force stated in (3.9) can be written as

$$F(x,i,t) = \frac{\kappa_{sol} i(t)^2}{\left(\kappa_\mu + x(t)\right)^2} \tag{3.41}$$

where

$$\kappa_{sol} = \frac{SN^2 \mu_r^2 \mu_0}{2(\mu_r - 1)} \tag{3.42}$$

and

$$\kappa_\mu = \frac{l_2 + l_{eq}}{(\mu_r - 1)} \tag{3.43}$$

Although different loads can be considered as it has been shown in 2.10, it is common to consider the system (2.64)

$$F(x,i,t) = m_L \ddot{x}(t) + b_L \dot{x}(t) + k_L x(t) \tag{3.44}$$

Using the solenoid force it can be rewritten as

$$\frac{\kappa_{sol} i(t)^2}{\left(\kappa_\mu + x(t)\right)^2} = m_L \ddot{x}(t) + b_L \dot{x}(t) + k_L x(t) \tag{3.45}$$

where it can be noted that the system is nonlinear and it is not possible to derive the Laplace transformation of such a differential equation in order to analyze its properties.

3.9.2 Open Loop Simulation

Before dealing with control issues, the system can be simulated in open loop as illustrated in Figure 3.21 applying certain currents to the actuator and analyzing the system response. The system has been simulated using the following parameters:

- $\kappa_{sol} = 1.983 \times 10^{-4}$ N m^2 A^{-2}
- $\kappa_{\mu} = 2.6 \times 10^{-4}$ m
- $m_L = 0.1$ Kg
- $b_L = 41$ N s m^{-1}
- $k_L = 100101$ N m^{-1}

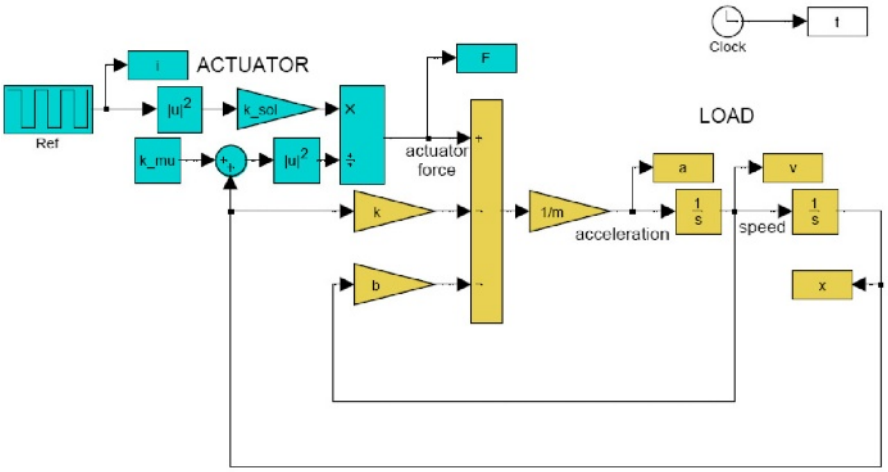

Fig. 3.21 Simulated solenoid actuator scheme

The system response is shown in Figures 3.22–3.24. The speed-position curves of Figure 3.24 show the difference between the transition from the zero equilibrium point to the equilibrium point where the actuator is excited. This transition is provoked by the solenoid force and is much faster (see also Figure 3.22) than the return to the initial position. The return is performed by the structure itself, since the actuator does not provide any return force.

3.9.3 Control Design

Although the current $i(t)$ cannot be applied instantaneously, it is commonly assumed that the current dynamics are much faster than the motion dynamics and hence the transients needed to establish the reference currents are neglected.

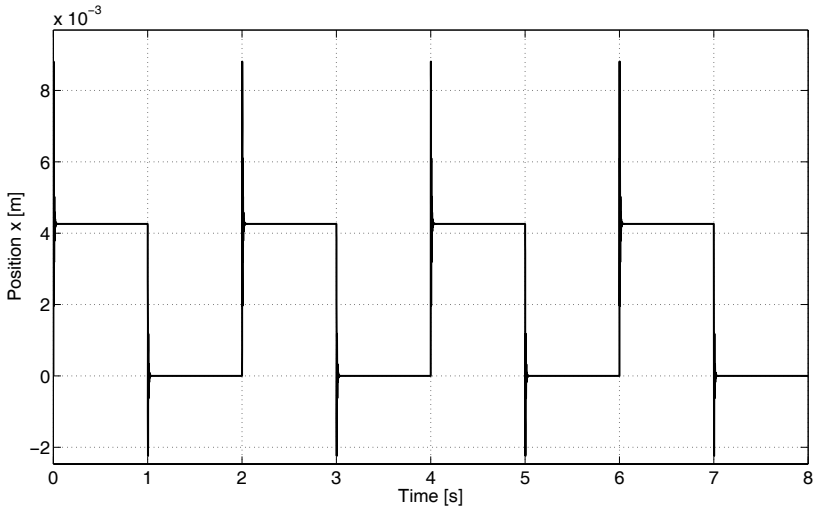

Fig. 3.22 Position response of the solenoid actuator to an open loop simulation

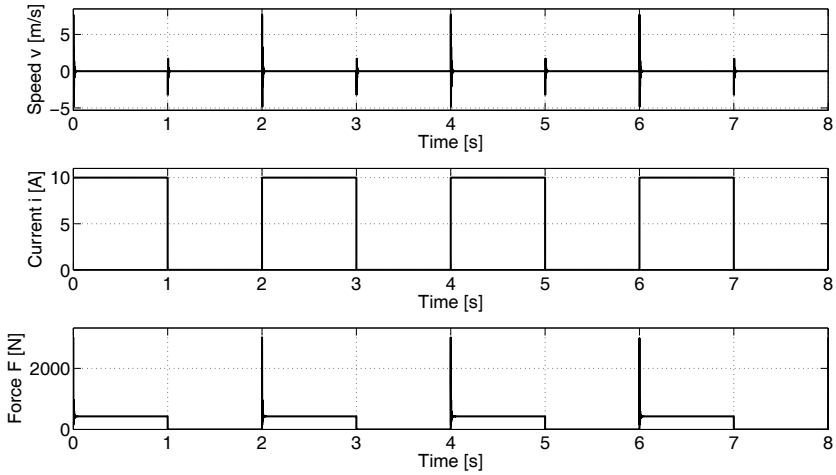

Fig. 3.23 Speed, current and force response of the solenoid actuator to an open loop simulation

The system (3.45) is nonlinear due to force dependance on the inverse square of the actuator position. Hence, it is not possible to use linear standard techniques [7] to study such a system and to design an optimal controller. Several nonlinear approaches may be used[8], but they are out of the scope of this work. A very simple linear PI controller is proposed as an example of the system under analysis.

The current to be applied to the actuator is therefore computed as:

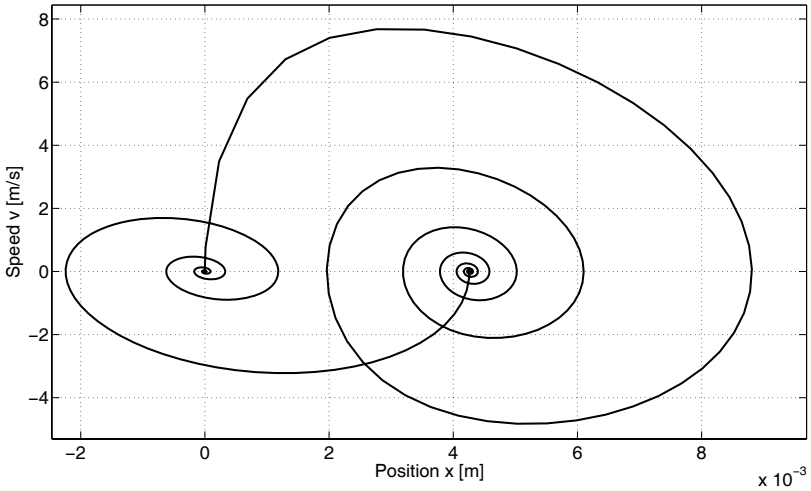

Fig. 3.24 Position-speed curve response of the solenoid actuator to an open loop simulation

$$i^*(t) = k_p\,(x(t) - x^*(t)) + k_i \int (x(t) - x^*(t))\,dt \tag{3.46}$$

where k_p and k_i are the proportional and integral constants of the PI controller, which are adjusted linearizing the system close to the operating point $x = 5$ mm.

3.9.4 Closed Loop Simulation

The system under analysis has been simulated with Simulink® according to the scheme sketched in Figure 3.25. The following parameters have been used:

- $\kappa_{sol} = 1.983 \times 10^{-4}$ N m^2 A^{-2}
- $\kappa_\mu = 1.005 \times 10^{-4}$ m
- $m_L = 0.1$ Kg
- $b_L = 39$ N s m^{-1}
- $k_L = 10201$ N m^{-1}
- $k_p = 110$ A m^{-1}
- $k_i = 28000$ A s^{-1} m^{-1}

Different simulations have been performed for rectangular, triangular and sinusoidal tracking functions. The system responses are shown in Figures 3.26–3.31.

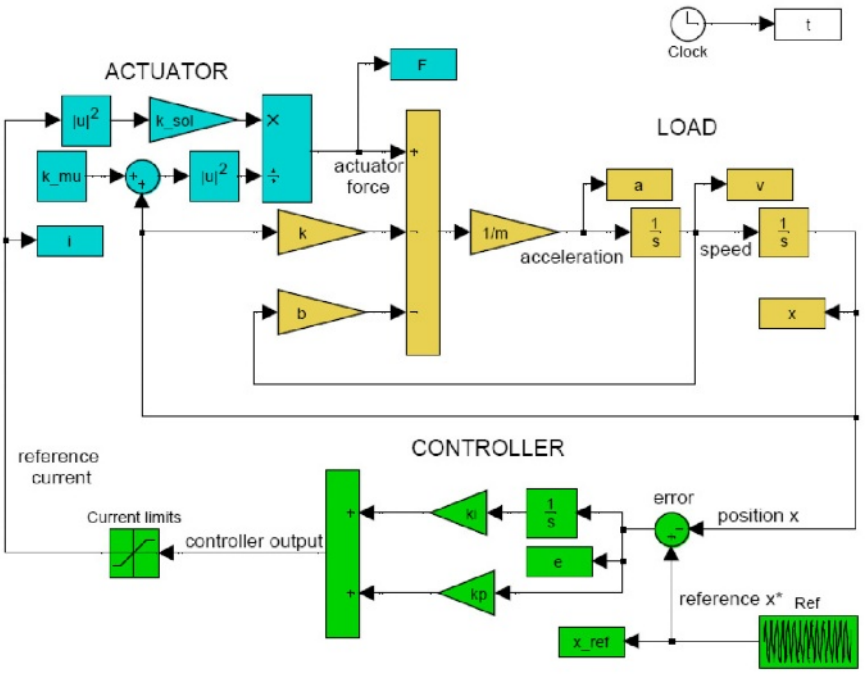

Fig. 3.25 Simulated solenoid actuator scheme

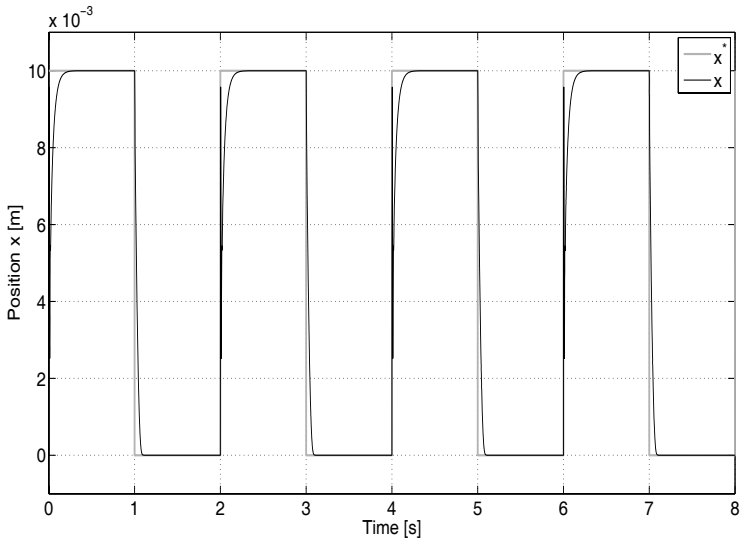

Fig. 3.26 Solenoid actuator response tracking a rectangular reference

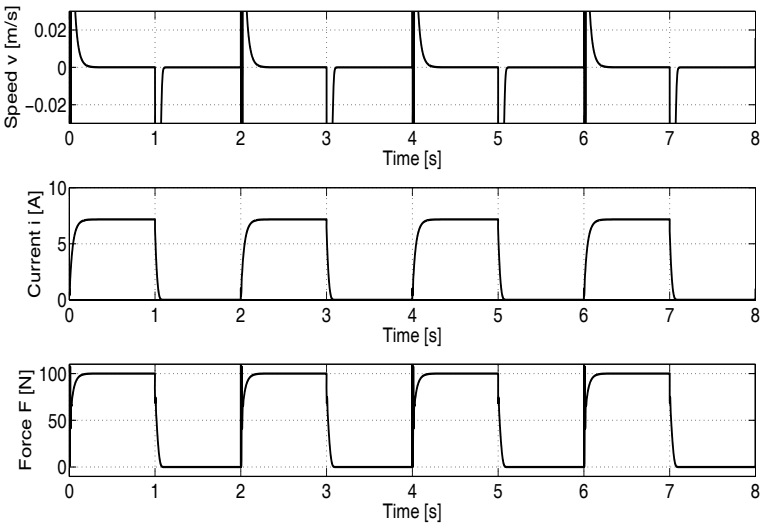

Fig. 3.27 Speed, current and force of the solenoid actuator tracking a rectangular reference

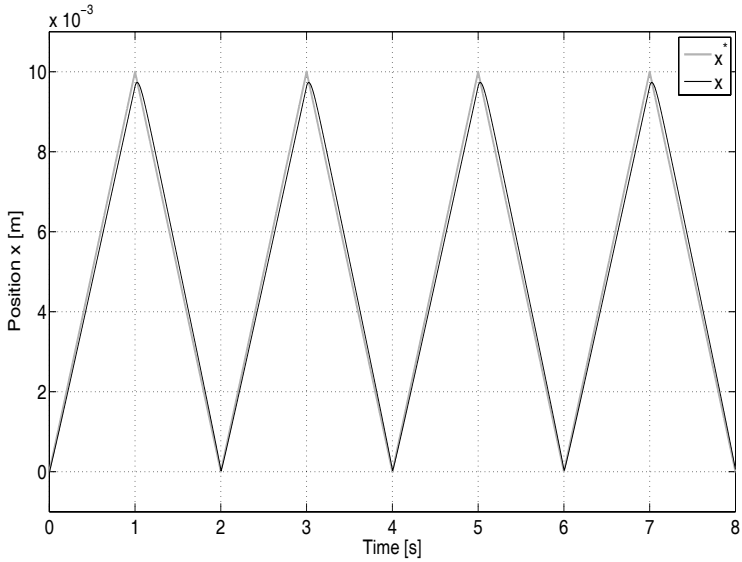

Fig. 3.28 Solenoid actuator response tracking a triangular reference

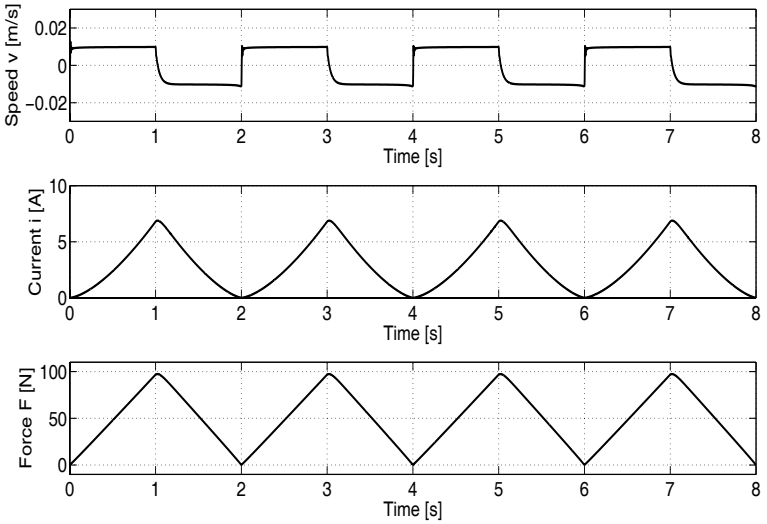

Fig. 3.29 Speed, current and force of the solenoid actuator tracking a triangular reference

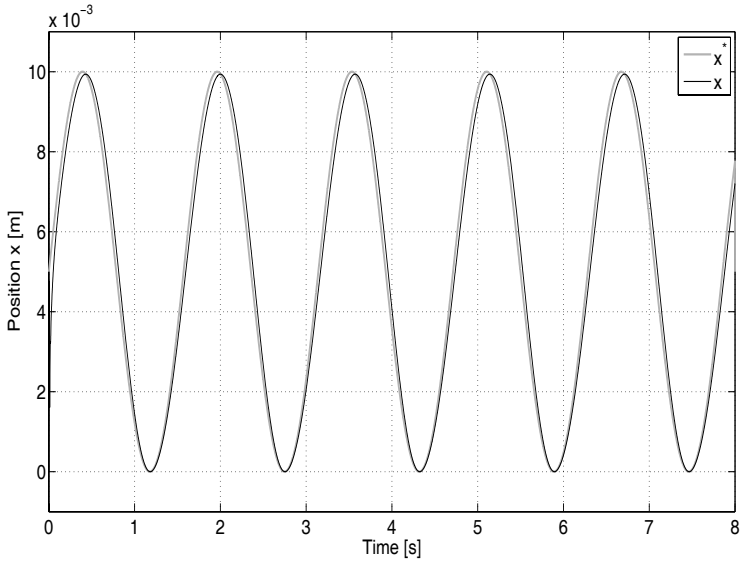

Fig. 3.30 Solenoid actuator response tracking a sinusoidal reference

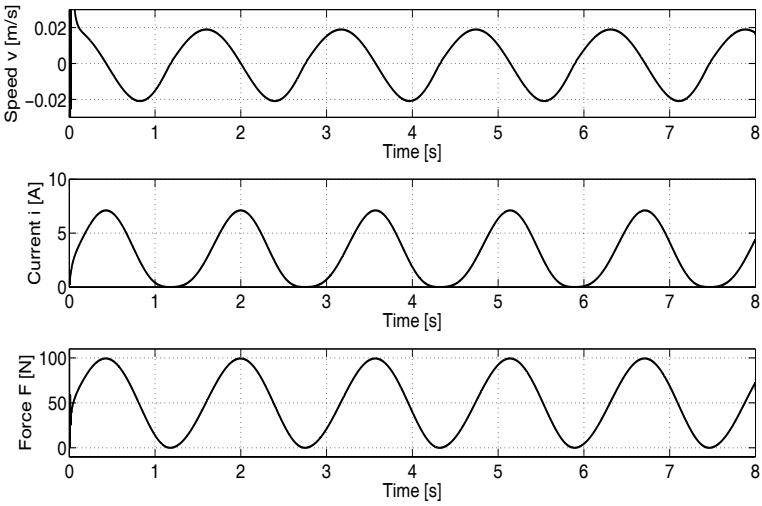

Fig. 3.31 Speed, current and force of the solenoid actuator tracking a sinusoidal reference

References

1. Bonals L, Ruiz R (1994) Transmissió de calor. Edicions UPC, Barcelona
2. Buckingham E (1914) On physically similar systems: Illustrations of the use of dimensional equations. Phys Rev 4:345–376
3. Gomis-Bellmunt O (2007) Design, modeling, identification and control of mechatronic systems. PhD thesis, Technical University of Catalonia
4. Gomis-Bellmunt O, Galceran-Arellano S, Sudrià-Andreu A, Montesinos-Miracle D, Campanile LF (2007) Linear electromagnetic actuator modeling for optimization of mechatronic and adaptronic systems. Mechatronics 17:153–163
5. Gomis-Bellmunt O, Campanile F, Galceran-Arellano S, Montesinos-Miracle D, Rull-Duran J (2008) Hydraulic actuator modeling for optimization of mechatronic and adaptronic systems. Mechatronics 18:634–40
6. Incropera F, DeWitt D (1990) Introduction to heat transfer. Wiley, New York
7. Kailath T (1980) Linear systems. Prentice-Hall
8. Khalil H (2002) Nonlinear systems. Prentice Hall Upper Saddle River, NJ

Chapter 4
Design Analysis of Moving Coil Actuators

4.1 Design Parameters

Moving coil actuators are based on the interaction of a magnetic flux provided by a permanent magnet and the electrical current flowing in the so-called moving coil.

The geometric dimensions are shown in Figure 4.1. For the sake of simplicity and without loss of generality it has been assumed that $l_1 = l_2 = l_3$.

The geometric constants and aspect ratios are defined as [3, 4, 2]

$$k_{ri} = r_i/r \tag{4.1}$$

$$k_{li} = l_i/l \tag{4.2}$$

$$\eta = \frac{l}{r} \tag{4.3}$$

where the non-dimensional constants associated to the radial lengths correspond to k_{ri}, while the axial lengths constants correspond to k_{li}.

The filling factor can be computed similarly to the solenoid actuator as the ratio between the profitable copper section S_{use} and the overall actuator section S_{total} as

$$k_{ff} = \frac{S_{use}}{S_{total}} = \frac{NA_w}{S_{total}} \tag{4.4}$$

where A_w is the single copper wire section and N is the number of turns.

4.2 Output Quantities

Moving coil actuators use the force produced by the interaction of perpendicular magnetic field and electrical current, described in the Lorenz force law. It yields:

$$F = Bl_w i \tag{4.5}$$

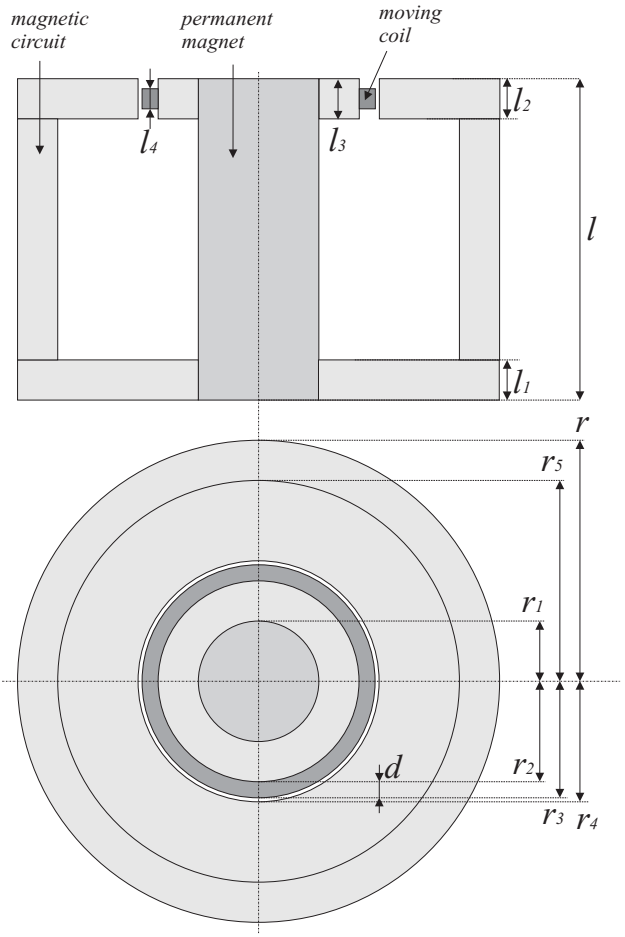

Fig. 4.1 Moving coil actuator sketch

where B is the field density provided by the permanent magnet, l_w is the length of the wire and i the current flowing in the wire.

The present work assumes that the moving coil stroke is limited to the region where the flux is flowing, so that the force-stroke curve presents a constant force depending linearly on the current applied to the coil. The work is obtained by the integration of a constant function. Without the assumption of limited stroke, the length of wire l_w being crossed by magnetic flux decreases as the coil is moving outside the flux region, whereas the flux density and the current are kept constant since the copper permittivity can be considered equal to the air permittivity.

The flux density B in the coil can be derived from the reluctance expression. In this case the magneto-motive force is provided by the permanent magnet $F_{mm} = H_c l$, where H_c is the coercitive field (a magnet constant). The reluctance can be

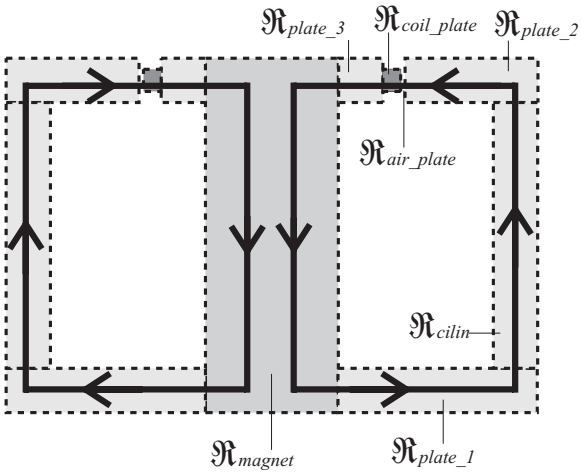

Fig. 4.2 Moving coil actuator reluctances

calculated as the series association of all the reluctances sketched in Figure 4.2. The total reluctance of the magnetic circuit can be expressed as:

$$\mathfrak{R} = \frac{\log\left(\frac{k_{r2}^{\frac{1}{k_{l1}}-\frac{\mu_r}{\mu_{cu}k_{l4}}}k_{r4}^{\frac{\mu_r-1}{k_{l1}}}}{k_{r1}^{\frac{2}{k_{l1}}}k_{r3}^{\frac{\mu_r}{k_{l1}}-\frac{\mu_r}{\mu_{cu}k_{l4}}}}\right) + \frac{2(1-2k_{l1})}{(1-k_{r5}^2)\eta^2} + \frac{2}{\frac{\mu_m}{\mu_r}k_{r1}^2\eta^2}}{\mu_r\mu_0 2\pi l} \tag{4.6}$$

The flux density ($B = \Phi/S$) can be written as:

$$B = \frac{H_c l/\mathfrak{R}}{r_3 l_4} = \frac{H_c}{r\mathfrak{R}k_{r3}k_{l4}} \tag{4.7}$$

The number of turns can be expressed as a function of the actuator dimensions as:

$$N = \frac{dl_4 k_{ff}}{A_w} = \frac{(r_3 - r_2)l_4 k_{ff}}{A_w} \tag{4.8}$$

The length l_w used in (4.5) can be expressed as:

$$l_w = 2\pi\frac{r_3 + r_2}{2}N = \pi r^2 l\frac{(k_{r3}^2 - k_{r2}^2)k_{l4}k_{ff}}{A_w} \tag{4.9}$$

Since the permanent magnet is always providing the same magneto-motive force, and the length of wire crossed by the flux is constant, the force from (4.5) can be considered proportional only to the current.

4.3 Thresholds

The main limiting quantity considered for the moving coil actuator is the maximum allowed actuator temperature. The heat transfer taking place in the moving coil actuator is related mainly to convection, since the coil producing heat is surrounded directly by air.

Using the resistance expression (3.13), the heat transfer equilibrium is found for

$$Ri^2 = \dot{Q} = \frac{\Delta T}{\vartheta_{conv}} \tag{4.10}$$

where ϑ_{conv} is the thermal resistance by means of convection. The maximum current can be expressed as:

$$i_{max} = \sqrt{\frac{\Delta T}{R(\vartheta_{conv})}} \tag{4.11}$$

The maximum current can therefore be expressed as:

$$i_{max} = \sqrt{\frac{A_w \Delta T \pi (r_{out}^2 - r_{in}^2) h_c}{\delta_0 (1+\gamma \Delta T) l_w}} \tag{4.12}$$

The previously developed expression of the convection coefficient $N_{u-r} = \frac{h_c r}{\lambda_{air}}$ can be used in order to express the maximum current as function of the non-dimensional Nusselt number as:

$$i_{max} = \frac{A_w}{\sqrt{rl}} \sqrt{\frac{\Delta T N_u \lambda_{air}}{2\eta \delta_0 (1+\gamma \Delta T) k_{l4} k_{r3} k_{ff}}} \tag{4.13}$$

4.4 Maximum Output Quantities

Using the maximum current from (4.13), the length from (4.9) and the flux density from (4.7), the force expression (4.5) turns into:

$$\frac{F_{max}}{S_{act}} = q_f H_c \mu_r \mu_0 \sqrt{\frac{\Delta T N_u \lambda_{air}}{2\eta \delta_0 (1+\gamma \Delta T)}} \tag{4.14}$$

where q_f is the design factor which can be expressed as:

$$q_f = \frac{\frac{2\pi}{\eta}(k_{r3}^2 - k_{r2}^2)\sqrt{\frac{k_{ff}}{k_{r3}^3 k_{l4}}}}{\log\left(\frac{k_{r2}^{\frac{1}{k_{l1}} - \frac{\mu_r}{\mu_{cu} k_{l4}}} k_{r4}^{\frac{\mu_r - 1}{k_{l1}}}}{k_{r1}^{\frac{2}{k_{l1}}} k_{r3}^{\frac{\mu_r}{k_{l1}} - \frac{\mu_r}{\mu_{cu} k_{l4}}}}\right) + \frac{2(1-2k_{l1})}{(1-k_{r5}^2)\eta^2} + \frac{2}{\frac{\mu_m}{\mu_r} k_{r1}^2 \eta^2}} \tag{4.15}$$

The expression (4.15) has been analyzed numerically in order to obtain the most optimum parameterization. It has been found with values $k_{r1} = k_{r2} = 0.72$, $k_{r3} = k_{r4} = k_{r5} = 0.94$, $k_{l1} = k_{l4} = 0.50$ and $\eta = 2.08$. The optimized design factor obtained is $q_f = 0.0054$.

In Figure 4.3 the design factor q_f depending on the ratios k_{r1} and η is plotted. The filling factor and the other geometric relationships are kept constant to allow a three-dimensional plot. The filling factor k_{ff} is typically around 0.75 and can be considered independent of the other design parameters.

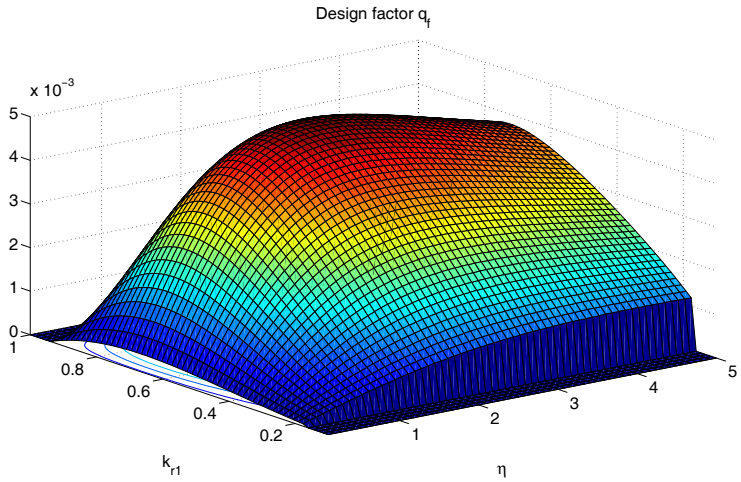

Fig. 4.3 Moving coil design factor depending on η and k_{r1} with $k_{r3} = 0.94$ and $k_{l1} = k_{l4} = 0.5$

It has been assumed that the coil movement is limited to the region where the whole coil is being crossed by the magnetic flux provided by the permanent magnet. Therefore, the available stroke is $l_1 - l_4$, which can be written as $l\,(k_{l1} - k_{l4})$. Since the force does not depend on the displacement in this region, the work can be easily obtained multiplying the force times the displacement as:

$$\frac{W_{max}}{V_{act}} = F_{max}\,(k_{l1} - k_{l4}) \tag{4.16}$$

A modified design factor $q_{fW} = q_f\,(k_{l1} - k_{l4})$ is to be analyzed to obtain the best performance design concerning the work. It can be easily seen that the design parameters providing maximum force produce no work because they are using the maximum coil width $k_{l4} = k_{l1} = 1/2$, allowing no stroke. A numerical analysis has been undertaken to obtain the optimum modified design factor. The best performance values has been found with $k_{r1} = k_{r2} = 0.78$, $k_{r3} = k_{r4} = k_{r5} = 0.94$, $k_{l1} = 0.50$, $k_{l4} = 0.07$ and $\eta = 1.1$. The optimized design factor obtained is $q_{fW} = 0.0023$.

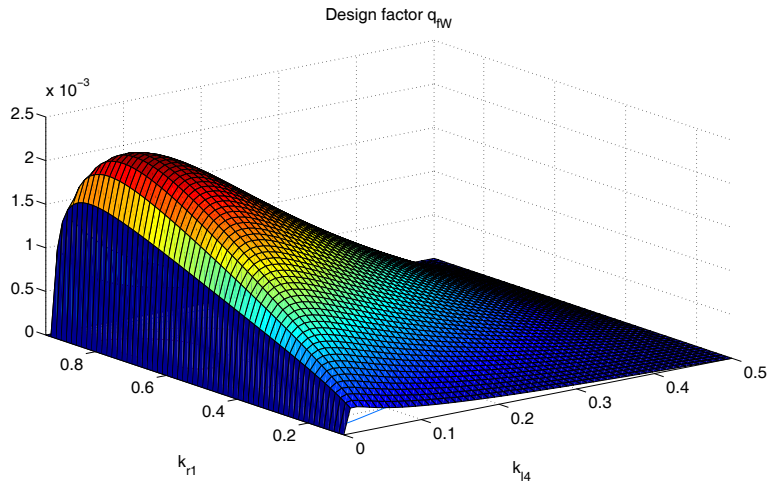

Fig. 4.4 Moving coil work modified design factor depending on k_{r1} and k_{l4} with $k_{l1} = 0.5$ and $\eta = 1.1$

4.5 Scalability

Regarding the scalability, it can be seen that the force and work depend on the Nusselt number, while the stroke can be considered completely scalable. As it has been discussed for the solenoid actuator, if the Nusselt number is considered constant all the output mechanical quantities can be considered scalable. Nonetheless, this assumption cannot be done and it is observed that both the force per cross-section and the volumetric work density depend linearly on $\sqrt{N_u}$. Hence, the cited output quantities present a linear dependance on $r^{\alpha/2}$, implying an improvement of the performance when the size is increased and not allowing the use of these actuators for tiny applications.

4.6 Dimensional Analysis

The force provided by these actuators can be analyzed with dimensional analysis using the Buckingham Pi Theorem [1]. The quantities involved are shown in the Table 4.1. The $FLTI\theta$ (force – length – time – current – temperature) system is used.

The dimension matrix is shown in Table 4.2. Since there are eight involved quantities and a five dimension $FLTI\theta$ (force – length – time – current – temperature) system, the number of non-dimensional groups will be $8 - 5 = 3$.

Considering the expression

Table 4.1 Moving coil actuator dimensional analysis quantities

F	Force	$[F]$
x	Position	$[L]$
μ	Permeability	$[FI^{-2}]$
H	Magnetic Field Intensity	$[IL^{-1}]$
h_c	Convection Coef.	$[FL^{-1}T^{-1}\theta^{-1}]$
λ	Conduction Coef.	$[FT^{-1}\theta^{-1}]$
δ	Resistivity	$[FL^2I^{-2}T^{-1}]$
T	Temperature	$[\theta]$

Table 4.2 Dimension matrix for the moving coil force analysis

	F	x	μ	h_c	λ	δ	T	H
	Force	Position	Permeability	Convection	Conduction	Resistivity	Temperature	Magnetic F.
F	1	0	1	1	1	1	0	0
L	0	1	0	-1	0	2	0	-1
T	0	0	0	-1	-1	-1	0	0
I	0	0	-2	0	0	-2	0	1
θ	0	0	0	-1	-1	0	1	0

$$F = x^a \mu^c h_c^d \lambda^e \delta^f T^g H^h \tag{4.17}$$

the following equations are obtained:

$$\left\{ \begin{array}{c} 1 = c + d + e + \mathrm{f} \\ 0 = \mathrm{a} - \mathrm{d} + 2f - h \\ 0 = -\mathrm{d} - \mathrm{e} - \mathrm{f} \\ 0 = -2c - 2f + h \\ 0 = -\mathrm{d} - \mathrm{e} + \mathrm{g} \end{array} \right\} \rightarrow \left\{ \begin{array}{c} c = 1 \\ \mathrm{a} = +d + 2 \\ \mathrm{f} = -\mathrm{g} \\ \mathrm{h} = 2 - 2g \\ \mathrm{e} = g - d \end{array} \right\} \tag{4.18}$$

Therefore

$$F = x^{2+d} \mu^1 h_c^d \lambda^{g-d} \delta^{-g} T^g H^{2-2g} \tag{4.19}$$

The maximum force can be written as

$$\frac{F}{x^2} = \mu H^2 \phi \left(\frac{x h_c}{\lambda}, \frac{\lambda T}{\delta H^2} \right) \tag{4.20}$$

Rearranging the terms and using the Nusselt number

$$\frac{F}{x^2} = \mu H^2 \phi \left(Nu, \frac{1}{H} \sqrt{\frac{\lambda T}{\delta}} \right) \tag{4.21}$$

The maximum force can be finally expressed as

$$\frac{F}{x^2} = K \mu H \sqrt{\frac{T \lambda N_u}{\delta}} \tag{4.22}$$

where it can be observed that it matches perfectly with (4.14) since $\delta = \delta_0 (1 + \gamma \Delta T)$ and μ_r and all the geometrical constants are non-dimensional.

The maximum work can be derived similarly. It can be expressed as:

$$\frac{W}{x^3} = K \mu H \sqrt{\frac{T \lambda N_u}{\delta}} \tag{4.23}$$

which matches with Expression 4.16.

4.7 Finite Element Analysis

The configuration featuring best work design factor performance have been chosen to be validates using Finite Element Analysis. The chosen configuration geometric constants yield $k_{r1} = k_{r2} = 0.78$, $k_{r3} = k_{r4} = k_{r5} = 0.94$, $k_{l1} = 0.50$, $k_{l4} = 0.07$ and $\eta = 1.1$. Considering a reference length $r = 5$ cm it implies:

- $l = 4.5$ cm
- $r_1 = r_2 = r_3 = 3.9$ cm
- $r_4 = r_5 = 4.7$ cm
- $l_1 = l_2 = l_3 = 2.25$ cm
- $l_4 = 0.31$ cm

The material properties considered yield:

- $\lambda_{air} = 0.0257\ W/Km$
- $\lambda_{iron} = 80\ W/Km$
- $\mu_0 = 1.25664 \times 10^{-6}\ Tm/At$
- $\Delta T = 50\ K$
- $\mu_r = 200$
- $\rho_0 = 1.68 \times 10^{-8}\ \Omega m$
- $\gamma = 0.0068\ \Omega m/K$
- Nu=60
- $H_c = 0.5 \times 10^6\ A/m$
- $\mu_c = \mu_m = 1$

A sketch of the moving coil actuator can be seen in Figure 4.5. As in the analysis of the solenoid actuator, before applying finite element analysis it is necessary to compute the maximum current density of the copper as:

$$J_{max} = \sqrt{\frac{2\pi l \Delta T}{k_{ff}^2 A_w \delta_0 (1 + \gamma \Delta T)\, l_w (\frac{2}{Nu_L \lambda_{air}})}} \tag{4.24}$$

substituting $l_w = 2\pi r_2 N$ and $N = (r_3 - r_1) l_2 k_{ff} / A_w$:

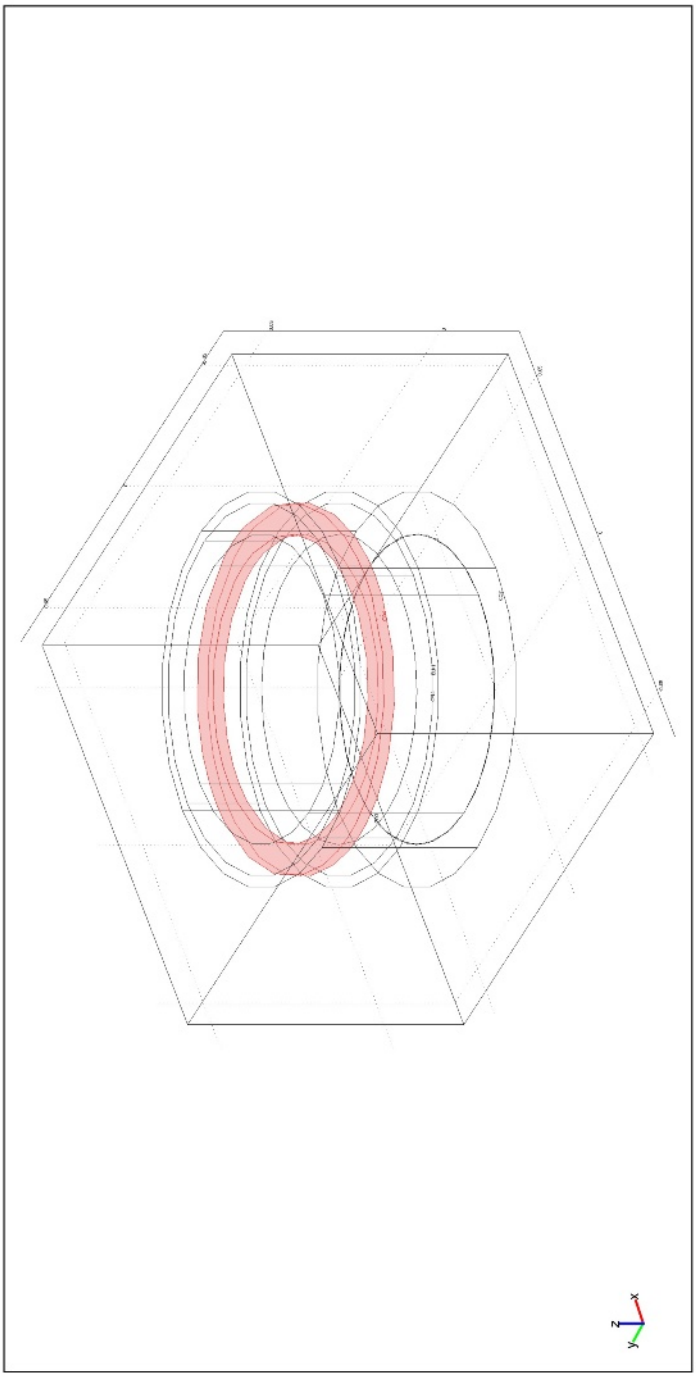

Fig. 4.5 Geometry of the actuator analyzed with COMSOL®

$$J_{max} = \frac{1}{r}\sqrt{\frac{\Delta T N u_L \lambda_{air}}{2k_{ff}^3 \delta_0 (1+\gamma\Delta T) k_{r2}(k_{r3}-k_{r1})k_{l2}}} \tag{4.25}$$

The FEA mesh of the analyzed actuator is shown in Figure 4.6. The results illustrating the magnetic flux densities and Maxwell tensor stresses are presented in Figures 4.7 and 4.8 .

4.8 Comparison with Industrial Actuators

The present section presents an analysis of data from different manufacturers of moving coil actuators. A typical datasheet is illustrated in Figure 4.9.

Similarly as described in Section 3.8, moving coil actuators can be considered to be cooled by means of natural convection. The Nusselt number can be written[5] as:

$$\begin{aligned} N_{u_D} &= 129.20 \times D^{1/4} \;\; 0.0026 < D < 0.124\ m \\ N_{u_D} &= 217.25 \times D^{1/3} \;\;\; 0.124 \leq D < 5.75\ m \end{aligned} \tag{4.26}$$

Different manufactured industrial moving coil actuators have been studied. Their output mechanical quantities compared to the maximum quantities previously stated are shown in Figures 4.10 and 4.11. The maximum quantities have been calculated using design factors $q_f = 0.0108$ and $q_{fW} = 0.0029$.

Data analysis has shown that moving coil actuator can be approached with the function $4.59 \times 10^4 r^{2.1270}$. The force holds $F \propto r^2\sqrt{Nu}$ and therefore $\alpha = 2.1270$ coefficient is located between 2.125 and 2.166. The moving coil work has been approached with $8.775 \times 10^3 V^{1.129}$, slightly higher than the expected between 1.041 and 1.056.

As shown in Figures 4.10 and 4.11, the behavior of the moving coil industrial actuators follows the trends developed theoretically.

4.9 Dynamics

The present section presents simple examples of some classical applications employing moving coil actuators.

4.9.1 System Modeling

The force performed by a moving coil actuator can be derived from Expression 4.5 as

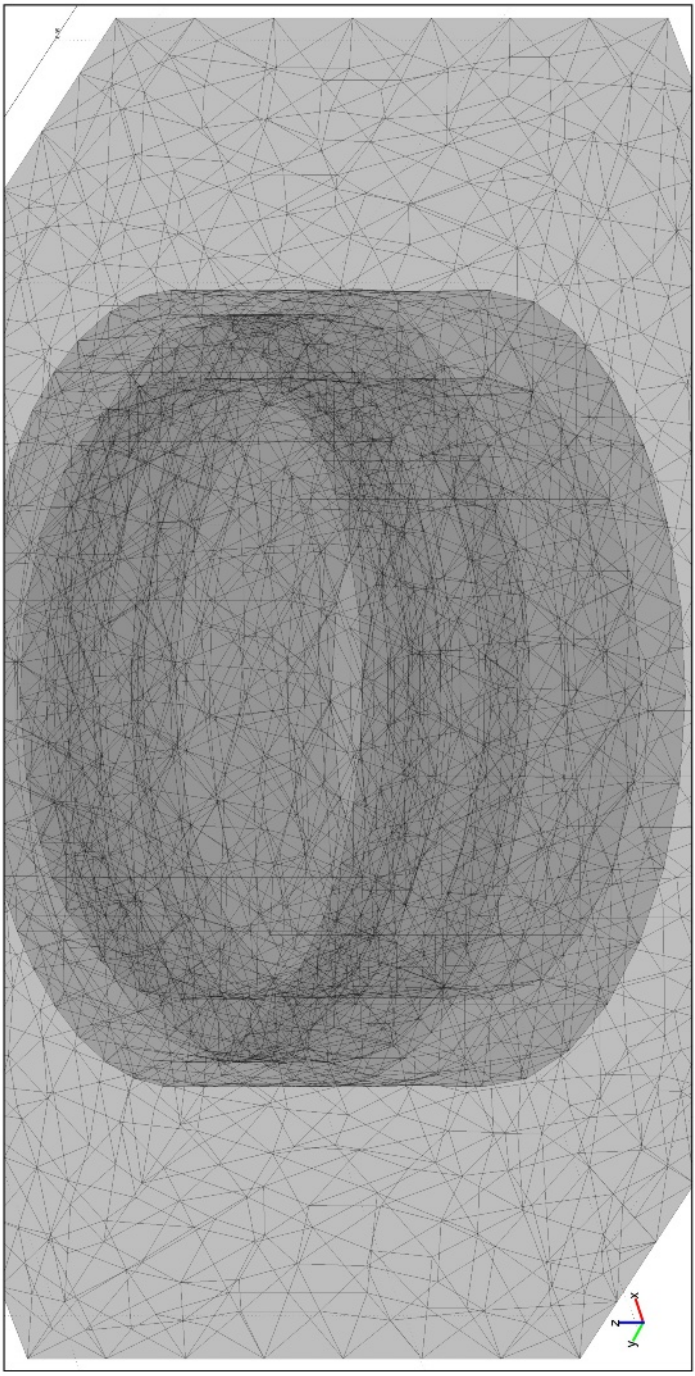

Fig. 4.6 Finite element mesh of the actuator analyzed with COMSOL®

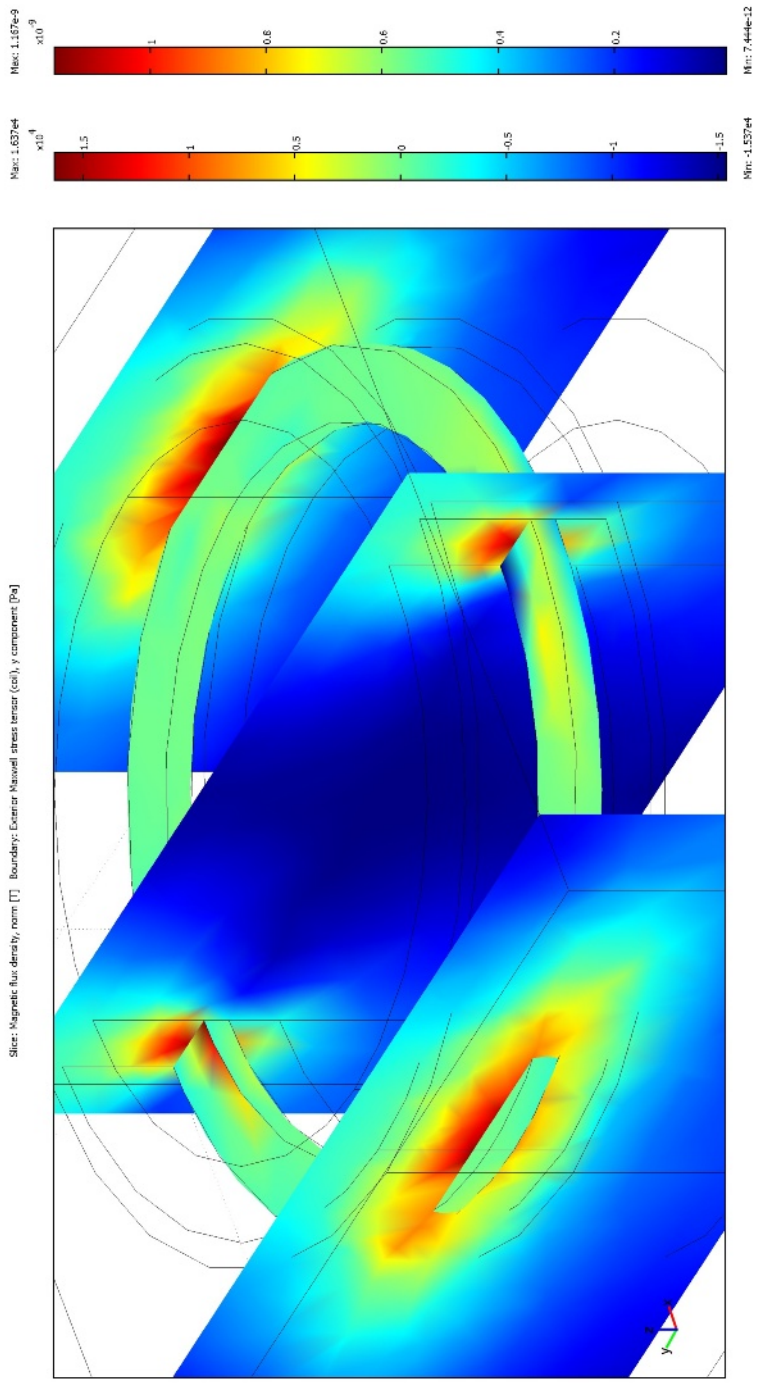

Fig. 4.7 Flux densities of the analyzed actuator

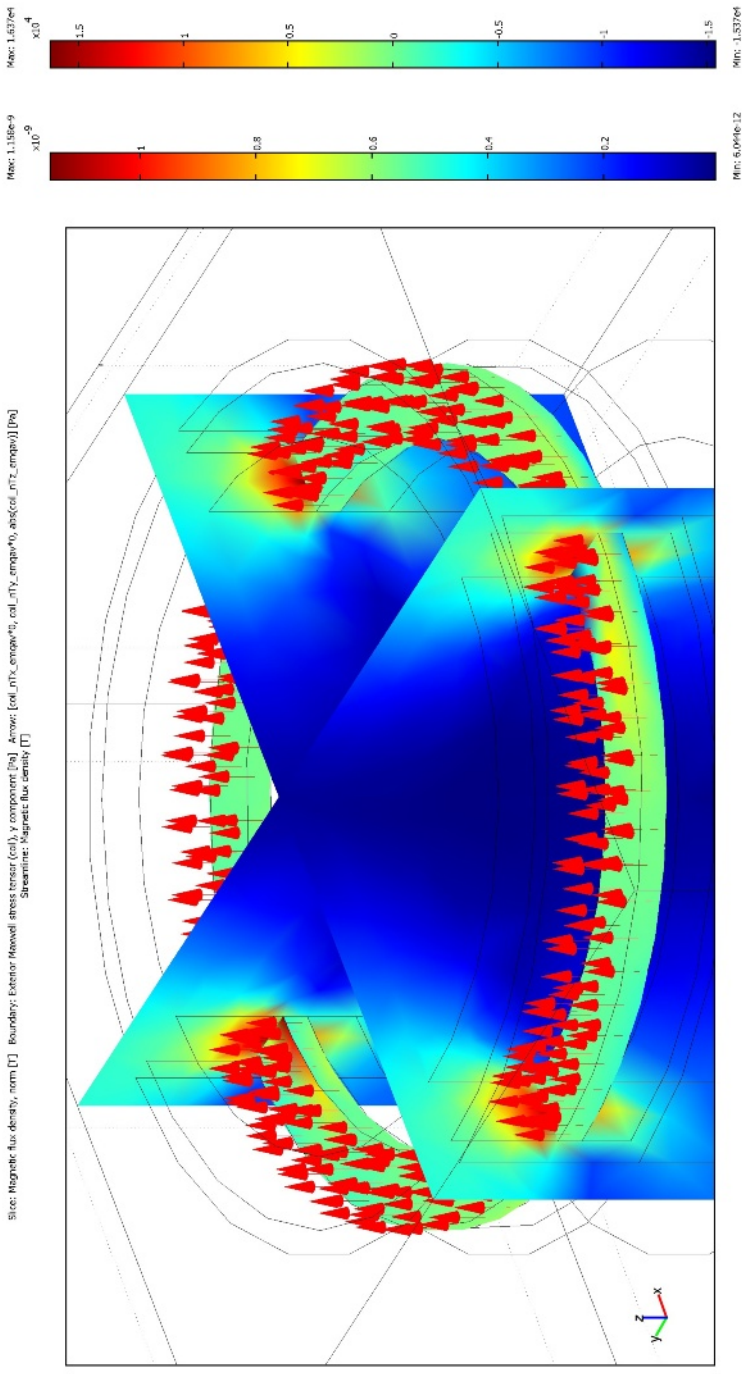

Fig. 4.8 Flux densities and Maxwell tensor stresses in the analyzed actuator

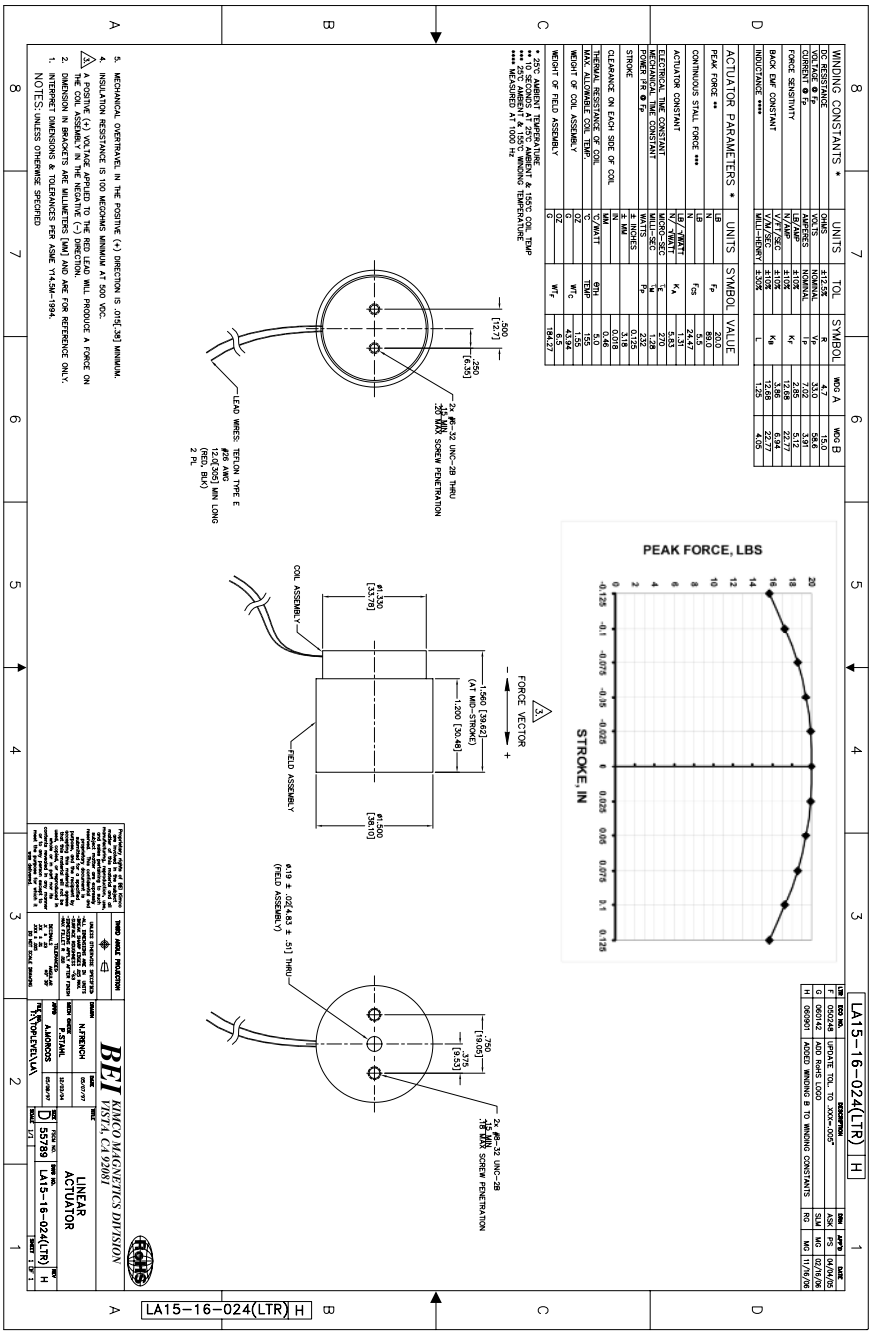

Fig. 4.9 Datasheet of an industrial moving coil actuator. Courtesy of BEI Kimco Magnetics

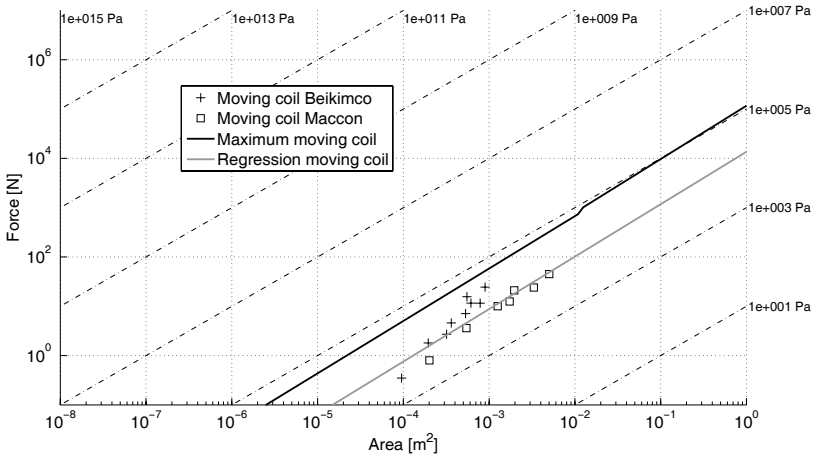

Fig. 4.10 Industrial electromagnetic actuator force-area comparison

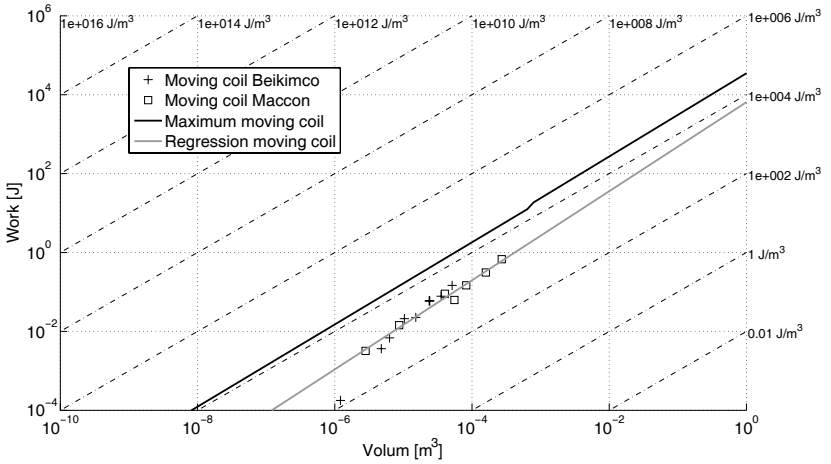

Fig. 4.11 Industrial electromagnetic actuator work-volume comparison

$$F(i,t) = \kappa_{Bl} i(t) \tag{4.27}$$

where

$$\kappa_{Bl} = Bl_w \tag{4.28}$$

Considering the load attached to a flexible structure, the system equation yield

$$F(i,t) = m_L \ddot{x}(t) + b_L \dot{x}(t) + k_L x(t) \tag{4.29}$$

Using the moving coil force it can be rewritten as

$$\kappa_{Bl} i(t) = m_L \ddot{x}(t) + b_L \dot{x}(t) + k_L x(t) \tag{4.30}$$

Applying the Laplace transformation with initial null position and speed:

$$\kappa_{Bl} I(s) = m_L X(s) s^2 + b_L X(s) s + k_L X(s) \tag{4.31}$$

The system transfer function can be stated as

$$\frac{X(s)}{I(s)} = \frac{\kappa_{Bl}}{m_L s^2 + b_L s + k_L} \tag{4.32}$$

Analogously to the developments of Section 2.10 the transfer system poles can be analyzed according to linear systems theory [6]. The following system poles are obtained:

$$s_{12} = \frac{-b_L \pm \sqrt{b_L^2 - 4 m_L k_L}}{2 m_L} \tag{4.33}$$

where it can be clearly noted that the system dynamics will importantly depend on $b_L^2 - 4 m_L k_L$. The natural frequency $\omega_0 \geq 0$ and the damping ratio ζ may be defined as

$$\omega_0 = \sqrt{\frac{k_L}{m_L}} \tag{4.34}$$

$$\zeta = \frac{b_L}{2\sqrt{k_L m_L}} \tag{4.35}$$

Substituting (4.34) and (4.35) in (4.33) the poles yield

$$s_{12} = \omega_0 \left(-\zeta \pm \sqrt{\zeta^2 - 1} \right) \tag{4.36}$$

where depending on the vale of ζ the system can be considered under-damped, critically damped or over-damped as discussed in Section 2.10.

4.9.2 Control Design

In the present example, the closed loop control system is considered. Considering a controller whose transfer function is $G(s)$ the system equations in the Laplace domain yield

$$\kappa_{Bl} G(s) \left(X(s) - X^*(s) \right) = m_L X(s) s^2 + b_L X(s) s + k_L X(s) \tag{4.37}$$

which can be rearranged as

$$\frac{X(s)}{X^*(s)} = \frac{-\kappa_{Bl} G(s)}{m_L s^2 + b_L s + k_L - \kappa_{Bl} G(s)} \tag{4.38}$$

Using a PI controller $G(s) = k_p + \frac{k_i}{s}$

$$\frac{X(s)}{X^*(s)} = \frac{-\kappa_{Bl} k_p s + k_i}{m_L s^3 + b_L s^2 + (k_L - \kappa_{Bl} k_p) s + k_i} \tag{4.39}$$

4.9.3 Closed Loop Simulation

The considered system parameters:

- $\kappa_{Bl} = 23.1$ N A^{-1}
- $m_L = 0.1$Kg
- $b_L = 39$N s m^{-1}
- $k_L = 10201$N m^{-1}

The PI controller can be designed by assigning appropriate poles to the closed loop system. The obtained PI constants are $k_p = 15.21 \times 10^3$ A m^{-1} and $k_i = 20.11 \times 10^3$ A s m^{-1}.

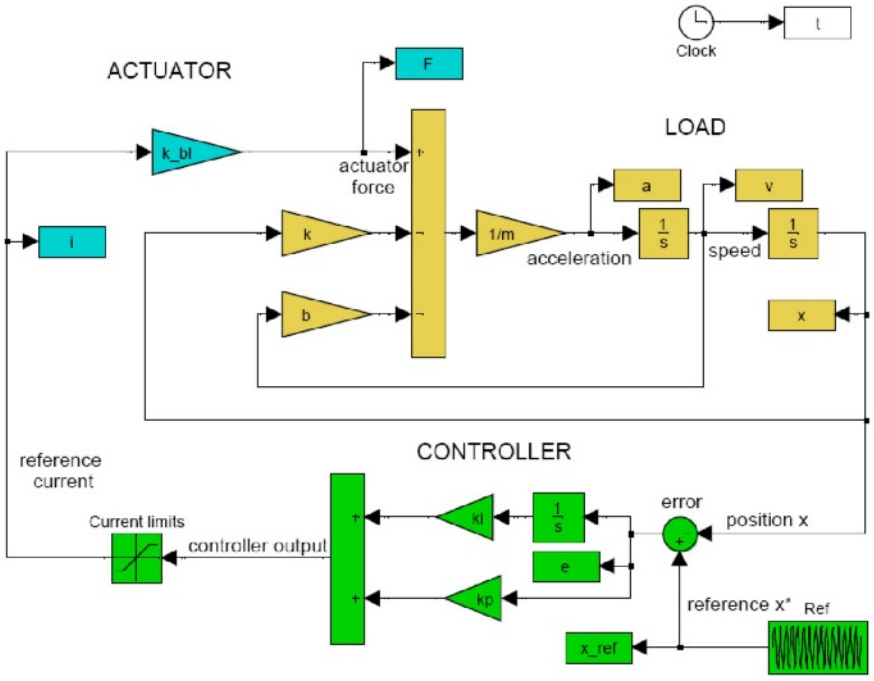

Fig. 4.12 Simulated moving coil actuator scheme

The system has been simulated with MATLAB® Simulink® according to the scheme sketched in Figure 4.12. Different simulations have been performed for rectangular, triangular and sinusoidal tracking functions. The system response are shown in Figures 4.13–4.18.

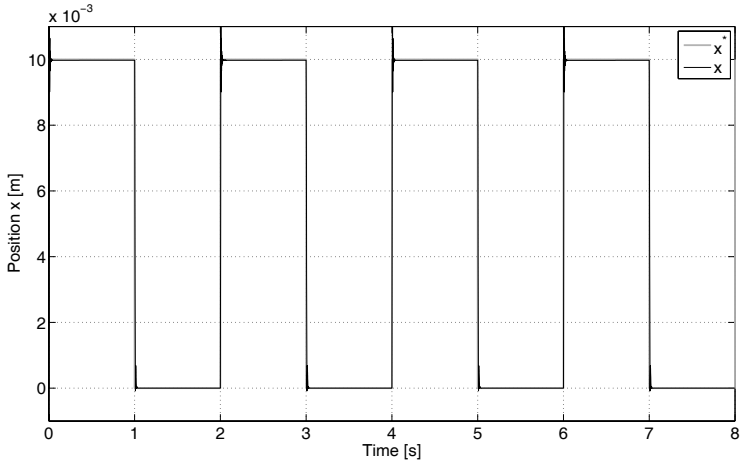

Fig. 4.13 Moving coil actuator response tracking a rectangular reference

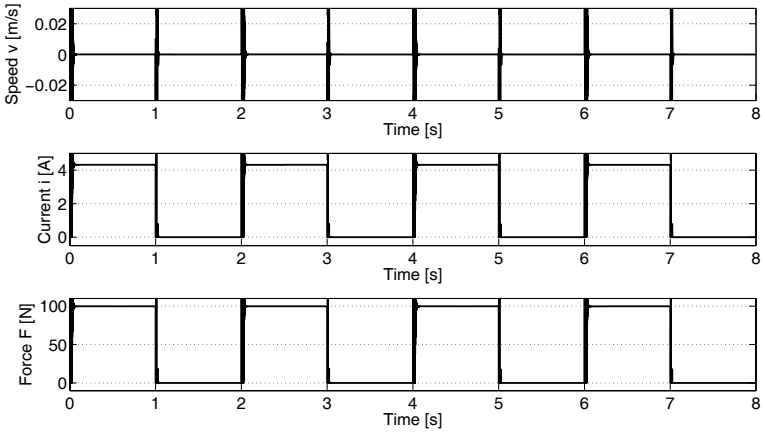

Fig. 4.14 Speed, current and force of the moving coil actuator tracking a rectangular reference

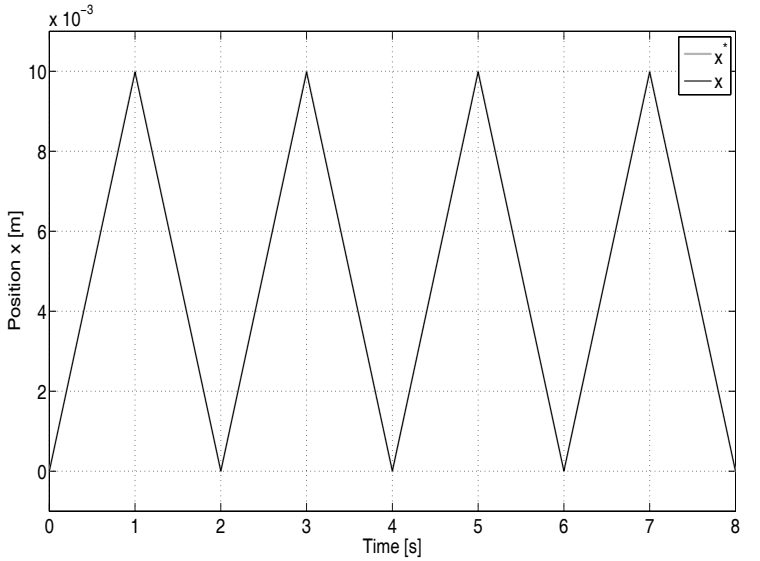

Fig. 4.15 Moving coil actuator response tracking a triangular reference

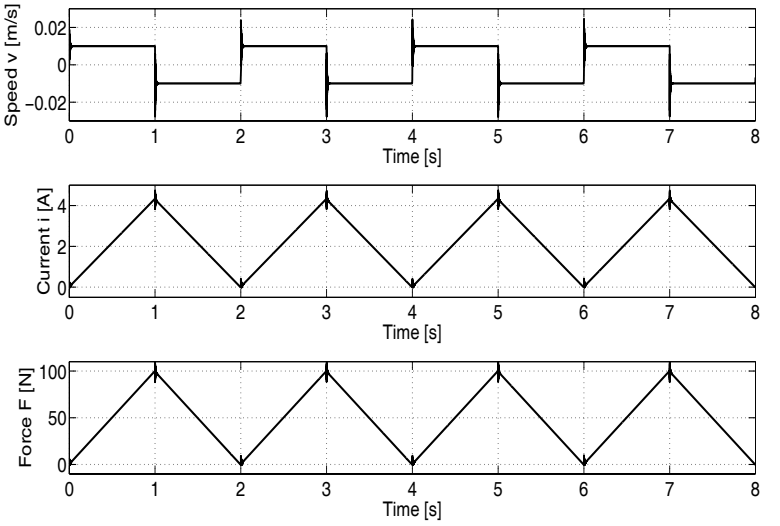

Fig. 4.16 Speed, current and force of the moving coil actuator tracking a triangular reference

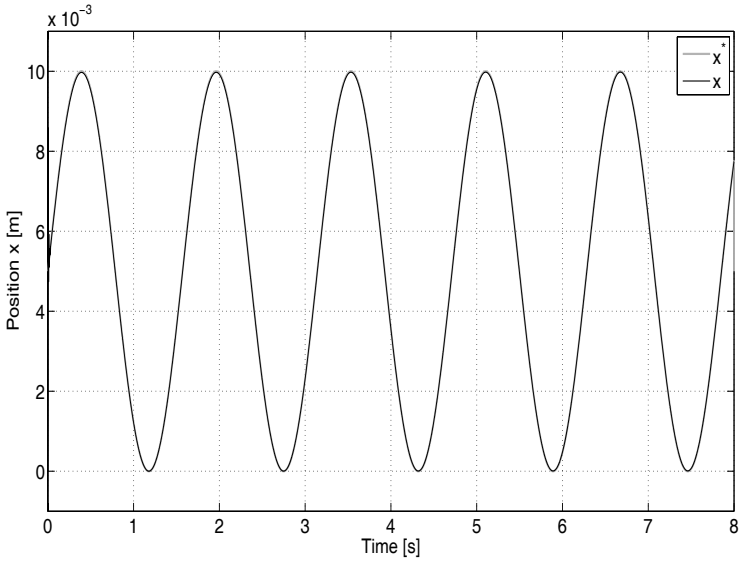

Fig. 4.17 Moving coil actuator response tracking a sinusoidal reference

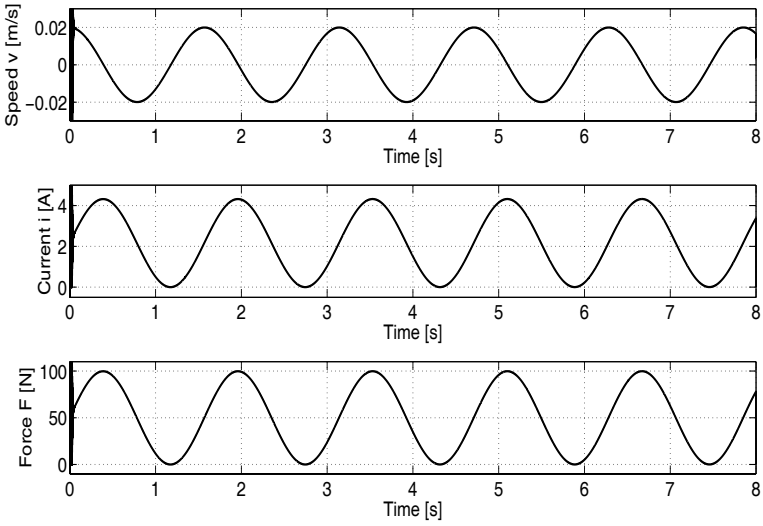

Fig. 4.18 Speed, current and force of the moving coil actuator tracking a sinusoidal reference

References

1. Buckingham E (1914) On physically similar systems: Illustrations of the use of dimensional equations. Phys Rev 4:345–376
2. Gomis-Bellmunt O (2007) Design, modeling, identification and control of mechatronic systems. PhD thesis, Technical University of Catalonia
3. Gomis-Bellmunt O, Galceran-Arellano S, Sudrià-Andreu A, Montesinos-Miracle D, Campanile LF (2007) Linear electromagnetic actuator modeling for optimization of mechatronic and adaptronic systems. Mechatronics 17:153–163
4. Gomis-Bellmunt O, Campanile F, Galceran-Arellano S, Montesinos-Miracle D, Rull-Duran J (2008) Hydraulic actuator modeling for optimization of mechatronic and adaptronic systems. Mechatronics 18:634–40
5. Incropera F, DeWitt D (1990) Introduction to heat transfer. Wiley, New York
6. Kailath T (1980) Linear systems. Prentice-Hall

Chapter 5
Design Analysis of Hydraulic Actuators

5.1 Design Parameters

In the present chapter, hydraulic actuators are studied. However, some of the results obtained also apply for their pneumatic counterparts.

An ideal power supply with no losses will be considered. It implies that the load will not change the supplied pressure. This fact can be assumed with no loss of generality as long as the power of the power supply is much larger than the nominal power consumed by the actuator.

In Figure 5.1 a hydraulic actuator is sketched [3]. It can be seen that for $x = 0$ both orifices are completely closed, when $x > 0$ follows $P_1 > P_2$ since $P_s > P_r$, and the plunger moves forward, when $x < 0$ follows $P_2 < P_1$ and it moves backward. The sections can be written as

$$A_1 = \frac{\pi}{4} D_1^2 \tag{5.1}$$

$$A_2 = \frac{\pi}{4} \left(D_1^2 - D_2^2 \right) \tag{5.2}$$

where D_1 is the diameter of the cylinder and D_2 is the diameter of the rod which guides the plunger.

The geometry of hydraulic cylindrical actuators is shown in Figure 5.2. The same geometry would be valid for pneumatic actuators, with the only difference of the fluid used and the corresponding limitations.

5.2 Force-Stroke and Work-Stroke Characteristic

The cylinder force can be expressed as [5, 4, 7]

$$F = P_1 A_1 - P_2 A_2 \tag{5.3}$$

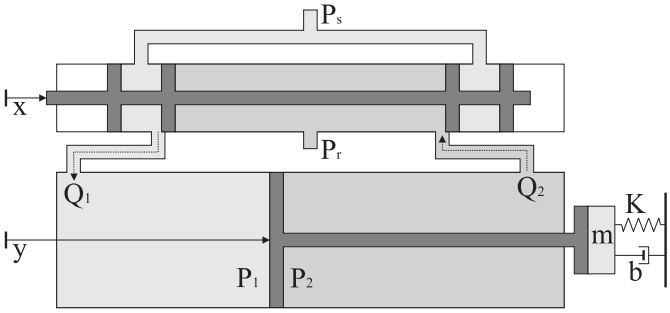

Fig. 5.1 Hydraulic actuator

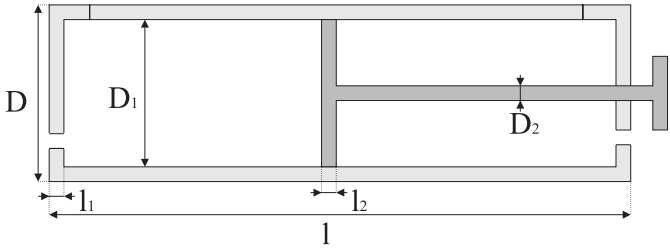

Fig. 5.2 Geometry of a hydraulic actuator

where P_i is the pressure in the chamber i and A_i is the effective section of the piston. It can be expressed as:

$$F = P_1 \pi \frac{D_1^2}{4} - P_2 \pi \frac{\left(D_1^2 - D_2^2\right)}{4} \tag{5.4}$$

The force performed by the cylinder in steady-state conditions depends on whether the movement is done forward or backward, since the section is different. Assuming $P_2 = P_r = 0$ and $P_1 = P_s$, the forward force can be expressed as:

$$F_f = P_s \frac{\pi}{4} D_1^2 \tag{5.5}$$

Concerning the backward force, $P_2 = P_s$ and $P_1 = P_r = 0$. The force yields:

$$F_b = P_s \frac{\pi}{4} \left(D_1^2 - D_2^2\right) \tag{5.6}$$

Assuming quasistatic behavior the work can be obtained assuming the force is constant during the time and therefore multiplying the force times the displacement.

5.3 Thresholds

The maximum allowed shear stress is the main quantity limiting the available mechanical force and work. It can be expressed using the Mohr circle as half the difference between the radial and tangential stresses. The radial stress in a thick walled cylinder can be written from [6] as a function of the position r in the wall as follows:

$$\sigma_{rr} = \frac{PD_1^2}{D^2 - D_1^2}\left(1 - \frac{D^2}{4r^2}\right) \tag{5.7}$$

The tangential stress in a thick walled cylinder from [6] yields:

$$\sigma_{\theta\theta} = \frac{PD_1^2}{D^2 - D_1^2}\left(1 + \frac{D^2}{4r^2}\right) \tag{5.8}$$

The equivalent shear stress can be derived from (5.7) and (5.8) as:

$$\tau_{eq} = \frac{\sigma_{rr} - \sigma_{\theta\theta}}{2} = \frac{PD_1^2}{D^2 - D_1^2}\frac{D^2}{4r^2} \tag{5.9}$$

It can be clearly seen in (5.9) that the maximum shear stress is produced for the minimum value of r, i.e. $r = D_1/2$. Using the defined geometric relationships the maximum shear stress yields:

$$\tau_{eq} = \frac{P}{1 - k_{D1}^2} \tag{5.10}$$

Hence, to not overcome the shear stress threshold, the maximum pressure must be established as:

$$P_{L1} = \tau_{eq}\left(1 - k_{D1}^2\right) \tag{5.11}$$

For backward motion, there arises another fact: there exists a maximum axial stress σ_{aa} in the rod attaching the load. It implies another pressure limitation:

$$P_{L2} = \sigma_{aa} k_{D2}^2 \tag{5.12}$$

Then, the maximum pressure for backward motion P_{Lb} can be written as:

$$P_{Lb} = min\{P_{L1}, P_{L2}\} = min\{\tau_{eq}\left(1 - k_{D1}^2\right), \sigma_{aa} k_{D2}^2\} \tag{5.13}$$

Defining $\varphi = \sigma_{aa}/\tau_{eq}, \varphi > 0$, it may be expressed as:

$$P_{Lb} = \tau_{eq} min\{\left(1 - k_{D1}^2\right), \varphi k_{D2}^2\} \tag{5.14}$$

5.4 Maximum Force, Stroke and Work

5.4.1 Forward Motion

Using (5.11) and (5.5), the maximum available force per cross-section can be expressed for the forward motion as:

$$\frac{F_f}{\pi D^2/4} = \tau_{eq}\left(1-k_{D1}^2\right)k_{D1}^2 \tag{5.15}$$

The design factor q_f can be defined as:

$$q_f = \left(1-k_{D1}^2\right)k_{D1}^2 \tag{5.16}$$

and is the factor to be maximized in the design.

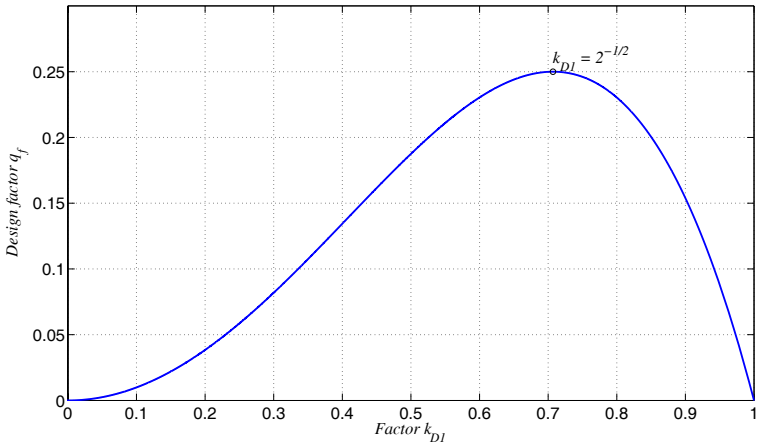

Fig. 5.3 Forward force design factor

Analyzing the latter expression, it can be seen that for a given size the forward force is maximized for $k_{D1} = 1/\sqrt{2}$ performing a force per cross section of $\tau_{eq}/4$ with a design factor $q_f = 1/4$. Graphical results may be seen in Figure 5.3.

5.4.2 Backward Motion

Using (5.14) and (5.6), the maximum available force per cross-section can be expressed for the backward motion as:

$$\frac{F_f}{\pi D^2/4} = \tau_{eq} min\{\left(1-k_{D1}^2\right), \varphi k_{D2}^2\} \left(k_{D1}^2 - k_{D2}^2\right) \tag{5.17}$$

An alternative formulation yields:

$$\begin{aligned} \frac{F_f}{\pi D^2/4} &= \tau_{eq} \left(1-k_{D1}^2\right) \left(k_{D1}^2 - k_{D2}^2\right) \; 1-k_{D1}^2 < \varphi k_{D2}^2 \\ \frac{F_f}{\pi D^2/4} &= \tau_{eq} \varphi k_{D2}^2 \left(k_{D1}^2 - k_{D2}^2\right) \; 1-k_{D1}^2 \geq \varphi k_{D2}^2 \end{aligned} \tag{5.18}$$

The design factor $q_f = 4F_f/\tau_{eq}\pi D^2$ may be defined as:

$$\begin{aligned} q_f &= \left(1-k_{D1}^2\right) \left(k_{D1}^2 - k_{D2}^2\right) \; 1-k_{D1}^2 < \varphi k_{D2}^2 \\ q_f &= \varphi k_{D2}^2 \left(k_{D1}^2 - k_{D2}^2\right) \; 1-k_{D1}^2 \geq \varphi k_{D2}^2 \end{aligned} \tag{5.19}$$

Analyzing the expression (5.19), the maximum design factor may be found by using $1-k_{D1}^2 = \varphi k_{D2}^2$ or its equivalent formulation $k_{D2} = \sqrt{\left(1-k_{D1}^2\right)/\varphi}$. In such a case:

$$q_f = \left(1-k_{D1}^2\right) \left(k_{D1}^2 - 1 + k_{D1}^2/\varphi\right) \tag{5.20}$$

It can be expressed as:

$$q_f = -\frac{\varphi+1}{\varphi} k_{D1}^4 + \frac{2\varphi+1}{\varphi} k_{D1}^2 - 1 \tag{5.21}$$

To obtain the maximum design factor:

$$\dot{q}_f = -4\frac{\varphi+1}{\varphi} k_{D1}^3 + 2\frac{2\varphi+1}{\varphi} k_{D1} \rightarrow 4\frac{\varphi+1}{\varphi} k_{D1max}^3 = 2\frac{2\varphi+1}{\varphi} k_{D1max} \tag{5.22}$$

The maximum k_{D1max} yields:

$$k_{D1max} = \sqrt{\frac{2\varphi+1}{2\varphi+2}} \tag{5.23}$$

It can be demonstrated that it is maximum, since $\ddot{q}_f(k_{D1max}) = -12\frac{\varphi+1}{\varphi} k_{D1}^2 + 2\frac{2\varphi+1}{\varphi} = -4\frac{2\varphi+1}{\varphi}$ which is $\ddot{q}_f(k_{D1max}) < 0, \forall \varphi > 0$. The maximum design factor yields:

$$q_{fmax} = \frac{1}{4} \frac{1}{\varphi^2+1} \tag{5.24}$$

And k_{D2}:

$$k_{D2max} = \sqrt{\frac{1}{2\varphi(\varphi+1)}} \tag{5.25}$$

For $\varphi = 1$, $k_{D1max} = \sqrt{3}/2$ and the maximum design factor $q_f = 1/8$ for $k_{D2} = 1/2$. It can be noted that the maximum design factor is half the value of the one found for forward motion. Graphical results may be seen in Figure 5.4. It is shown how the maximum design factors may be found in the value stated previously for $\varphi = 1$.

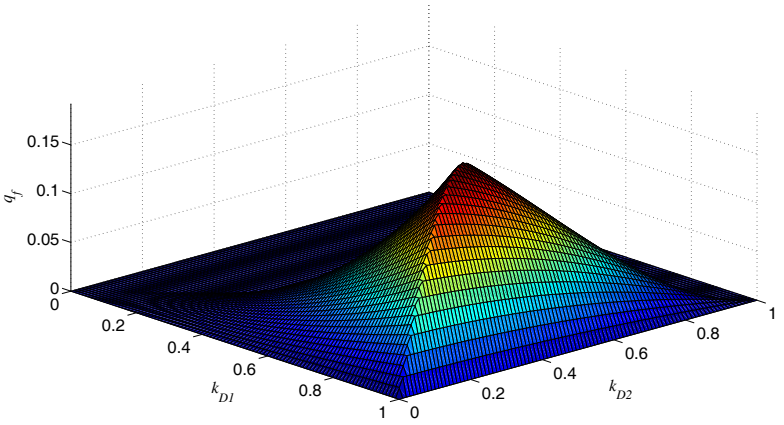

Fig. 5.4 Backward force design factor, $\varphi = 1$

5.4.3 Considering Forward and Backward Motion

In practical cases, both forward and backward motion are used. If the average force including forward and backward motion are considered:

$$\frac{F_{fb}}{\pi D^2/4} = \frac{\tau_{eq}}{2}\left[min\{\left(1-k_{D1}^2\right), \varphi k_{D2}^2\}\left(k_{D1}^2 - k_{D2}^2\right) + \left(1-k_{D1}^2\right)k_{D1}^2\right] \quad (5.26)$$

An alternative formulation yields:

$$\frac{F_f}{\pi D^2/4} = \tau_{eq}\left(1-k_{D1}^2\right)k_{D1}^2 + \left(1-k_{D1}^2\right)\left(k_{D1}^2 - k_{D2}^2\right) \; 1-k_{D1}^2 < \varphi k_{D2}^2$$

$$\frac{F_f}{\pi D^2/4} = \tau_{eq}\left(1-k_{D1}^2\right)k_{D1}^2 + \varphi k_{D2}^2\left(k_{D1}^2 - k_{D2}^2\right) \; 1-k_{D1}^2 \geq \varphi k_{D2}^2 \quad (5.27)$$

A detailed analysis (similar to the developed for the backward motion, and excluded here) show that the maximum can be derived from (5.27), by differentiating against k_{D1} and k_{D2} and equaling to zero. The following system of equations is ob-

tained:

$$k_{D2} - k_{D1}\frac{1}{\sqrt{2}} = 0 \tag{5.28}$$

$$\varphi k_{D2}^2 - 2k_{D1}^2 = -1 \tag{5.29}$$

Solving, the maximum is shown for:

$$k_{D1max} = \sqrt{\frac{2}{4-\varphi}} \tag{5.30}$$

$$k_{D2max} = \sqrt{\frac{1}{4-\varphi}} \tag{5.31}$$

Taking $\varphi = 1$, graphical results may be seen in Figure 5.5.

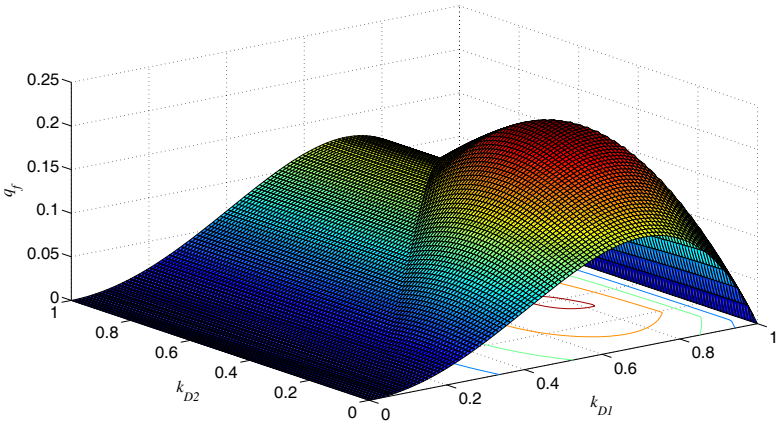

Fig. 5.5 Forward-backward averaged force design factor, $\varphi = 1$

5.4.4 Stroke and Work

The stroke is given by $l - 2l_1 - l_2$. For the sake of simplicity, and without lost of generalization, l_1 can be considered equal to $l_1 = l_2 = (D - D_1)/2$, since they correspond to the wall thickness. The stroke is then $l - 3l_1 = l - (3/2)D(1 - k_{D1}) = l\,(1 - 3\eta(1 - k_{D1}))$. It will be maximized for $\eta = 0$, which is clearly not possible, due to the fact that no force would be performed for such an aspect ratio. In this case,

the force criterion would be dominant, while trying to obtain the smaller aspect ratio η for stroke maximization purposes.

Similar conclusions can be extracted analyzing the work. The maximum forward work per volume can be expressed as:

$$\frac{W_f}{\pi l D^2/4} = \tau_{eq}\left(1-k_{D1}^2\right)k_{D1}^2\left(1-3\eta(1-k_{D1})\right) \tag{5.32}$$

As it has been highlighted for the stroke, the work is maximized for $\eta = 0$. Concerning the dependance on k_{D1}, the maximum volumetric work can be found as the solution k_{D1} of the equation:

$$\begin{aligned}-2k_{D1}^3(1-3\eta(1-k_{D1}))+2(1-k_{D1}^2)k_{D1}(1-3\eta(1-k_{D1}))\\ +3(1-k_{D1}^2)k_{D1}^2\eta = 0\end{aligned} \tag{5.33}$$

whose solution is omitted because of its length. For $\eta = 0$, it yields:

$$k_{D1max} = \frac{\sqrt{2}}{2} \tag{5.34}$$

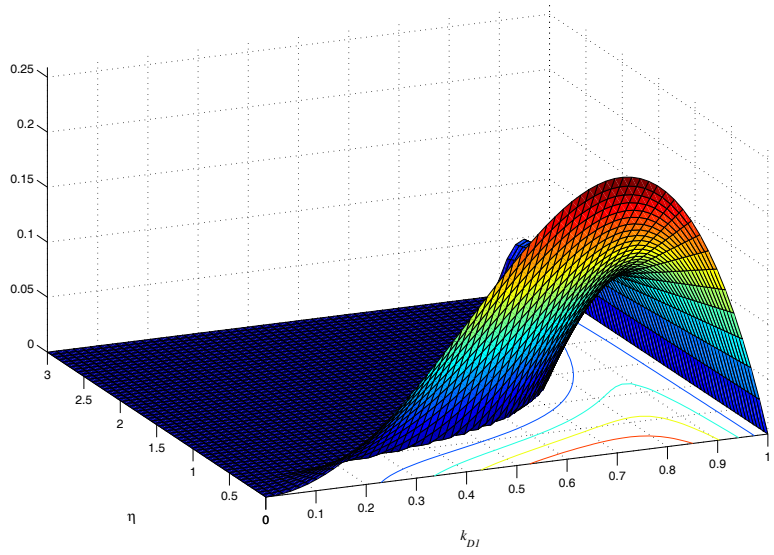

Fig. 5.6 Forward work design factor

Graphical results may be seen in Figure 5.6. It can be noted that only the forward motion has been addressed. Similar effects to those observed with the force when dealing with backward and averaged forward and backward motion appear also with the work.

5.5 Scalability

Regarding the scalability, the static behavior of hydraulic actuators does not have the dependance on size-dependant numbers such as the Nusselt number (as happened with electromagnetic actuators [2]). Hence, as long as the static behavior is concerned the scalability criterion applies for the usual industrial range of dimensions.

5.6 Dimensional Analysis

The force provided by these actuators can be analyzed with dimensional analysis using the Buckingham Pi Theorem [1]. The quantities involved are shown in the Tables 5.1 and 5.2. The FL (force-length) system is used.

Table 5.1 Hydraulic actuator dimensional force analysis quantities

F	Force	$[F]$
x	Length	$[L]$
σ	Stress	$[FL^{-2}]$

Table 5.2 Hydraulic actuator dimensional work analysis quantities

W	Work	$[FL]$
x	Length	$[L]$
σ	Stress	$[FL^{-2}]$

The results show that the maximum force can be expressed as:

$$\frac{F}{x^2} = K\sigma \tag{5.35}$$

where it can be observed that it matches perfectly with previous analytical results. The results obtained for the work match with the previous results. The maximum work given by dimensional analysis can be expressed as:

$$\frac{W}{x^3} = K\sigma \tag{5.36}$$

5.7 Industrial Actuators

The results obtained analytically are compared with industrial actuators in the present section. Actuators from different manufacturers including *Bosch Rexroth*

AG, *Parker* and *Enerpac* have been studied, taking into account their dimensions, maximum allowed pressures, strokes, etc.

The comparison between the inner-output diameter ratio of the analyzed actuators and the optimum extracted analytically from the equations show that the matching is remarkable. It can be seen in Figure 5.7. It can be noted that the real actuator data regression lies between the optimum for forward and backward motion. It is placed very close to the forward motion optimum.

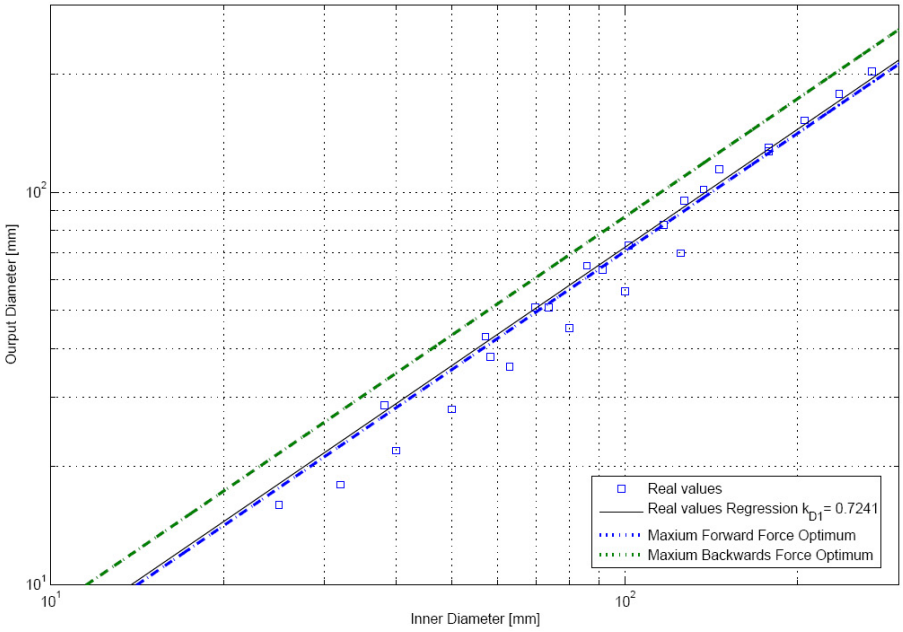

Fig. 5.7 Comparison between the input to output diameter ratio existing in industrial actuators and the results of the present work

The force-cross section relationship analyzed in Section 5.4 has proven to apply for the real actuators. In Figure 5.8 it can be noted that the real actuator performance for different actuators is below the maximum threshold. The regression analysis of each class of actuator shows that the relationship between the force and the cross-section can be found as the considered operating pressure.

5.8 Dynamics

Although the proposed methodology focuses on the statical output mechanical quantities, some considerations on actuator dynamics may be relevant for most applications. As it has been stated in Section 2.10, the dynamic behavior does not depend

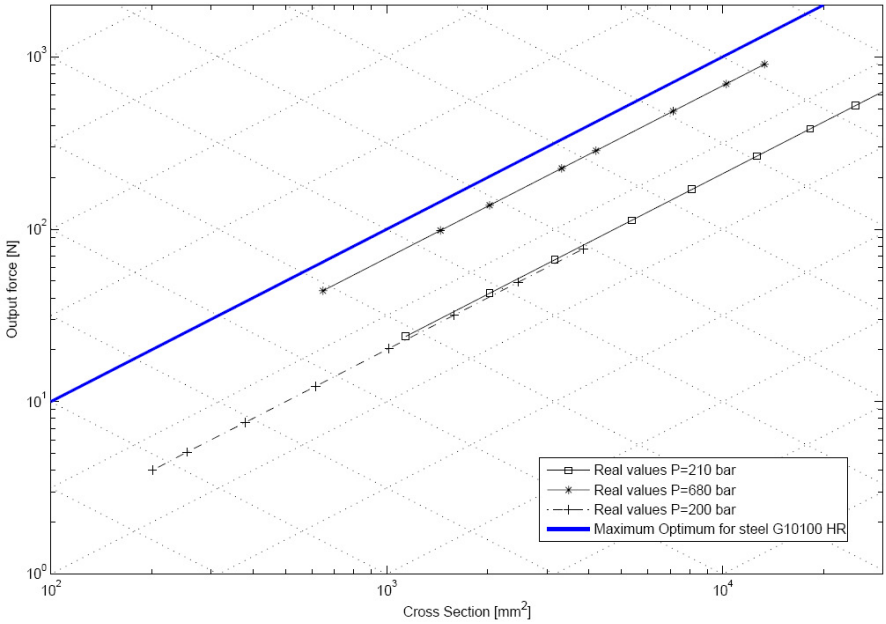

Fig. 5.8 Industrial hydraulic actuator force-area performance

only on the actuator but in the load attached to it and the controller governing the overall system. The present section presents examples of some classical applications employing the described hydraulic actuators.

The presented examples do not include any discussion on control issues. The discussion on control developed in Section 2.10.2 can be applied to this class actuators.

5.8.1 System Modeling

As it is sketched in Figure 5.1, x corresponds to the cylinder orifice aperture and it can be controlled in order to control the actuator motion. For x=0 both orifices are completely closed, when x¿0 the cylinder 1 is connected to the pressure supply P_s allowing the flow to go into the chamber 1 and thus making the cylinder move from 1 to 2. In the other hand, when $x < 0$ the cylinder 2 is connected to P_s and the motion is produced in the opposite direction.

The orifices expressions depend on the sign of x. If $x > 0$, they yield:

$$Q_1 = C_{orif} x w_{orif} \sqrt{\frac{2(P_s - P_1)}{\rho_1}} \tag{5.37}$$

$$Q_2 = -C_{orif} x w_{orif} \sqrt{\frac{2(P_2 - P_r)}{\rho_2}} \tag{5.38}$$

where C_{orif} is the orifice discharge coefficient, w_{orif} is the orifice width and ρ_i is the density of the fluid in the chamber i.

If $x < 0$:

$$Q_2 = -C_{orif} x w_{orif} \sqrt{\frac{2(P_s - P_2)}{\rho_2}} \tag{5.39}$$

$$Q_1 = C_{orif} x w_{orif} \sqrt{\frac{2(P_1 - P_r)}{\rho_1}} \tag{5.40}$$

Although the changes are typically very small, the fluid density can be either considered variable. The isothermal bulk modulus establishes the linkage between pressure and density as

$$\beta = \rho_0 \left| \frac{\partial P}{\partial \rho} \right|_{P_0, T_0} \tag{5.41}$$

where ρ_0 corresponds to the initial density with pressure P_0 and temperature T_0.

The cylinder displacement y implies a chamber expansion of the chamber connected to the pressure P_s and a compression of the other chamber. Such expansion and compression implies a small density variation of the fluid according to (5.41).

If it is considered that the fluid density is constant over the fluid and allowed to change with time according to the bulk modulus expression, it is possible to apply the conservation of mass principle in order to obtain the following mass flows expressions:

$$\dot{m}_1 = \rho_1 A \dot{y} \tag{5.42}$$

$$\dot{m}_2 = -\rho_2 A \dot{y} \tag{5.43}$$

The corresponding volumetric flows yield:

$$Q_1 = A \dot{y} \tag{5.44}$$

$$Q_2 = -A \dot{y} \tag{5.45}$$

Although different loads can be considered as it has been shown in 2.10, the following dynamics equation can be considered:

$$(P_1 - P_2) A = m_L \ddot{y}(t) + b_L \dot{y}(t) + k_L y(t) \tag{5.46}$$

5.8.2 Open Loop Simulation

5.8.2.1 Simulation 1

The system has been evaluated in open loop applying a rectangular signal to the orifice aperture x between -1 cm and 1 cm. A general scheme is shown in Figure 5.9. The system has been simulated using the following parameters:

- $C_{orif} = 0.6$
- $w_{orif} = 10^{-2}$ m
- $\beta = 10^9$ Pa
- $A = 5 \times 10^{-4}$ m^2
- $P_s = 10^6$ Pa
- $P_r = 0$ Pa
- $\rho_0 = 1000$ Kg m^{-3}
- $m_L = 0.1$ Kg
- $b_L = 400$ N s m^{-1}
- $k_L = 10000$ N m^{-1}

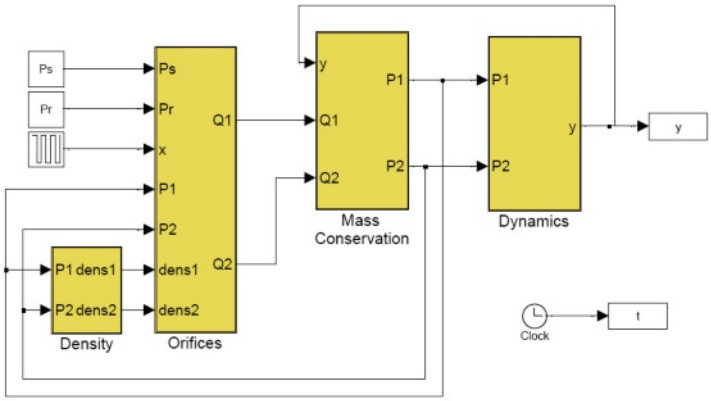

Fig. 5.9 Simulated hydraulic actuator scheme

The system response is shown in Figures 5.10–5.13. Figure 5.10 shows the position y evolution when changing the orifice aperture x. It can be noted that the transient is smooth without peaks due to the high damping of the system. In Figure 5.10 also the speed $\dot{y}$ response is plotted. A detail of a position and speed transient is illustrated in Figure 5.11, also showing the position-speed curve. The mass flow and pressure responses are plotted in Figures 5.12 and 5.13.

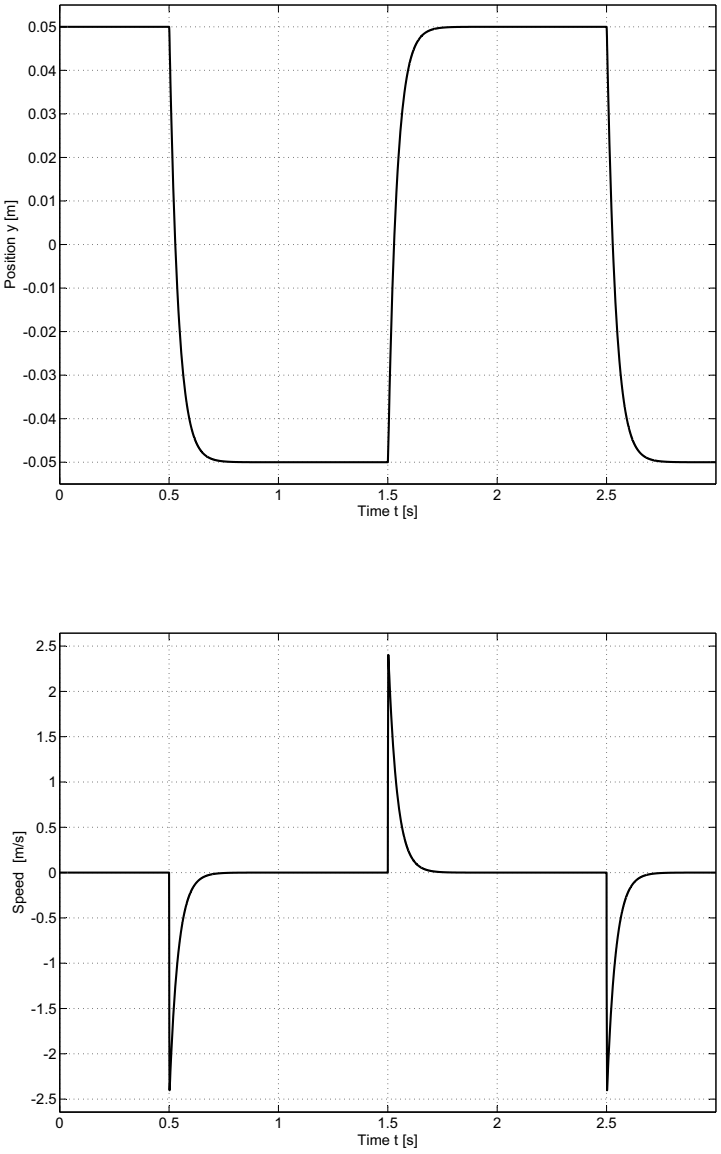

Fig. 5.10 Position and speed response of the hydraulic actuator to an open loop simulation. Simulation 1

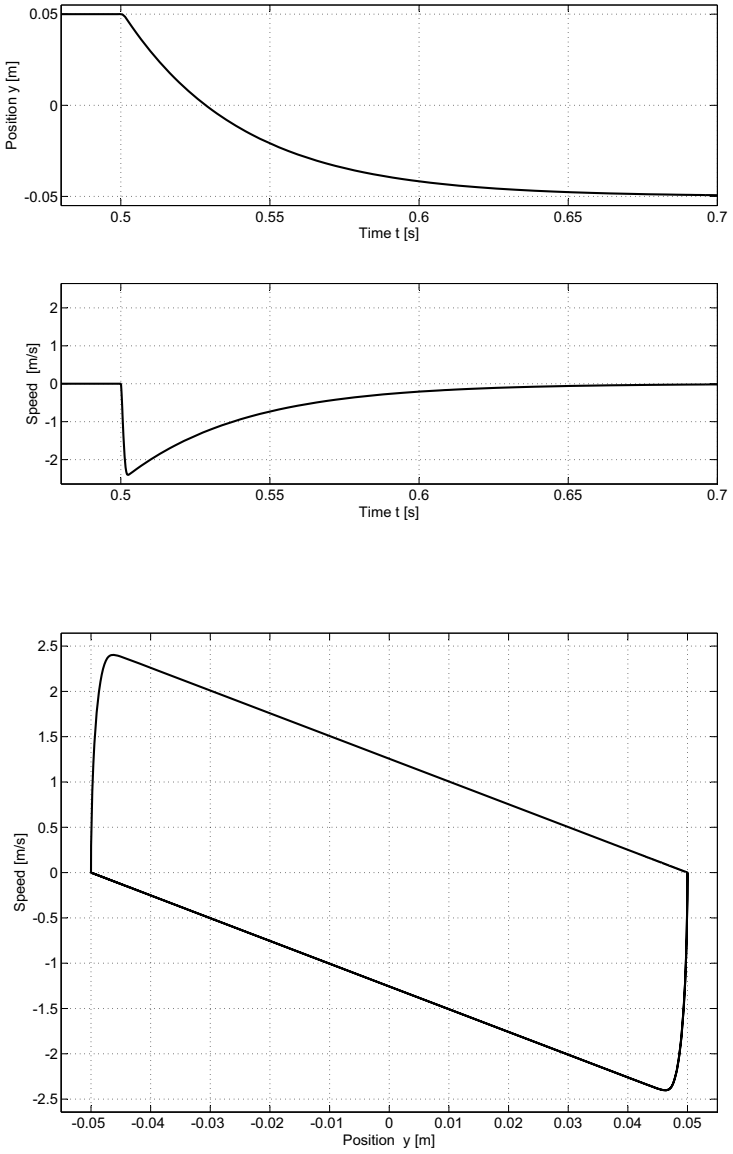

Fig. 5.11 Transient of the position and speed response. Simulation 1

5.8.2.2 Simulation 2

Another simulation establishing a poorer damping has been performed, in order to illustrate the importance of the load attached to the actuator. This second simulation has been done with the following parameters:

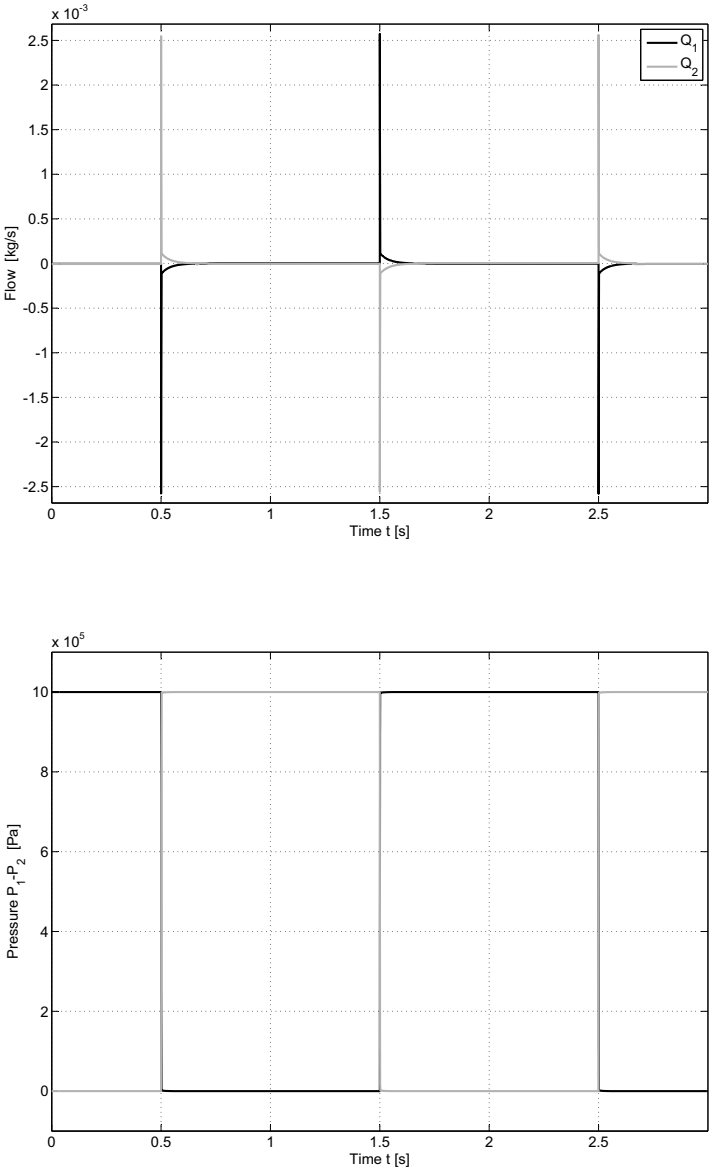

Fig. 5.12 Mass flow and pressure response of the hydraulic actuator to an open loop simulation. Simulation 1

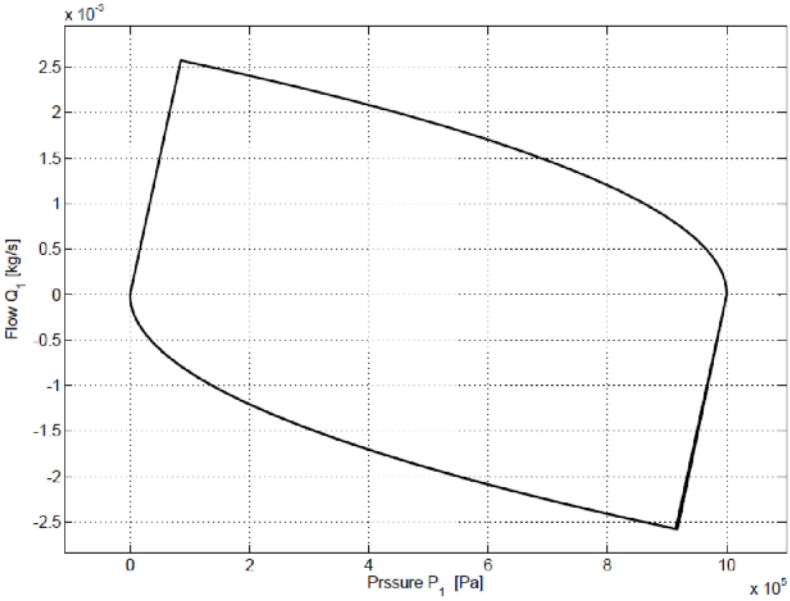

Fig. 5.13 Pressure-flow curve response of the hydraulic actuator to an open loop simulation. Simulation 1

- $C_{orif} = 0.6$
- $w_{orif} = 10^{-2}$ m
- $\beta = 10^9$ Pa
- $A = 5 \times 10^{-4}$ m^2
- $P_s = 10^6$ Pa
- $P_r = 0$ Pa
- $\rho_0 = 1000$ Kg m^{-3}
- $m_L = 0.1$ Kg
- $b_L = 10$ N s m^{-1}
- $k_L = 10000$ N m^{-1}

The system response is shown in Figures 5.14–5.17. Figure 5.14 shows the position y evolution when changing the orifice aperture x. It can be noted that the transient is not smooth like in the previous example due to the poor damping of the system. In Figure 5.14 also the speed $\dot{y}$ response is plotted. The position and speed transients are illustrated in Figure 5.15, where it can be noted how the steady-state point is reached. The position-speed curve is also plotted in Figure 5.15. The mass flow and pressure responses are plotted in Figures 5.16 and 5.17.

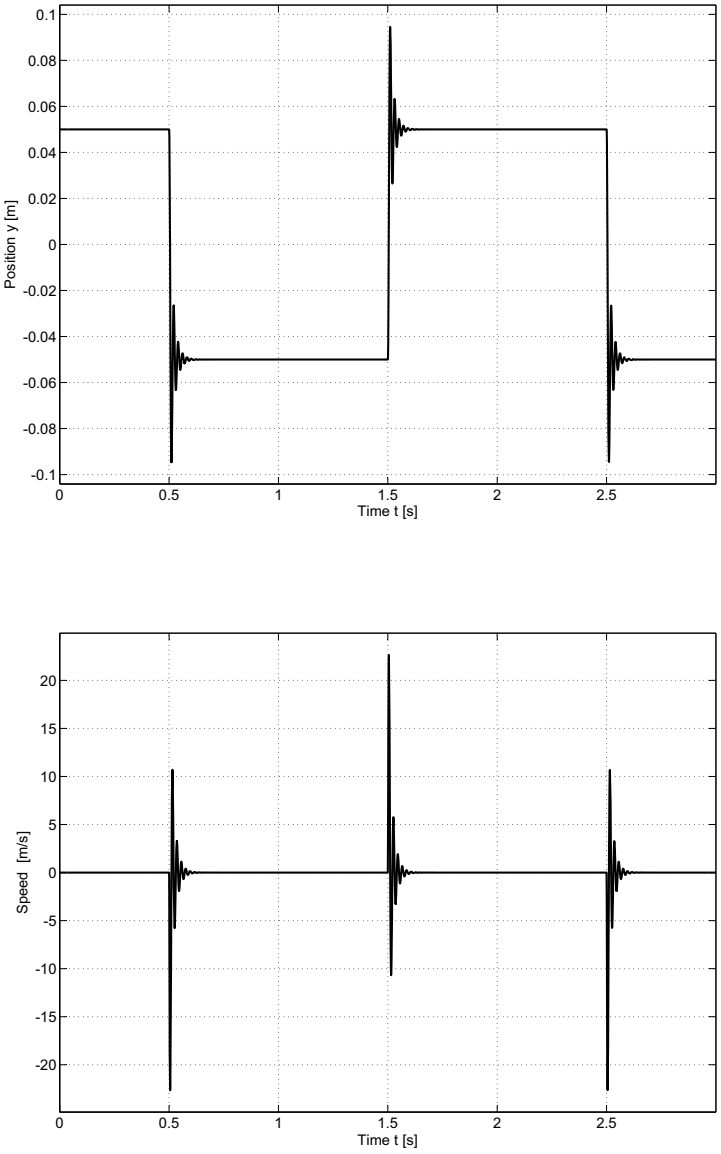

Fig. 5.14 Position and speed response of the hydraulic actuator to an open loop simulation. Simulation 2

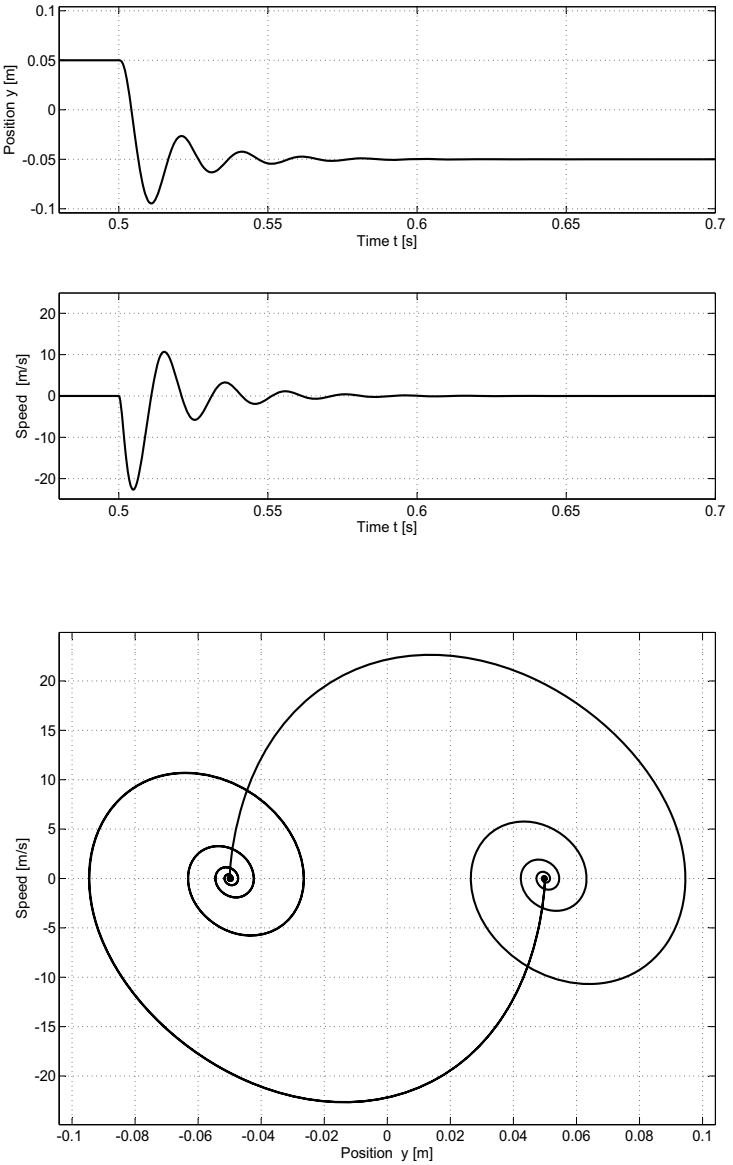

Fig. 5.15 Transient of the position and speed response. Simulation 2

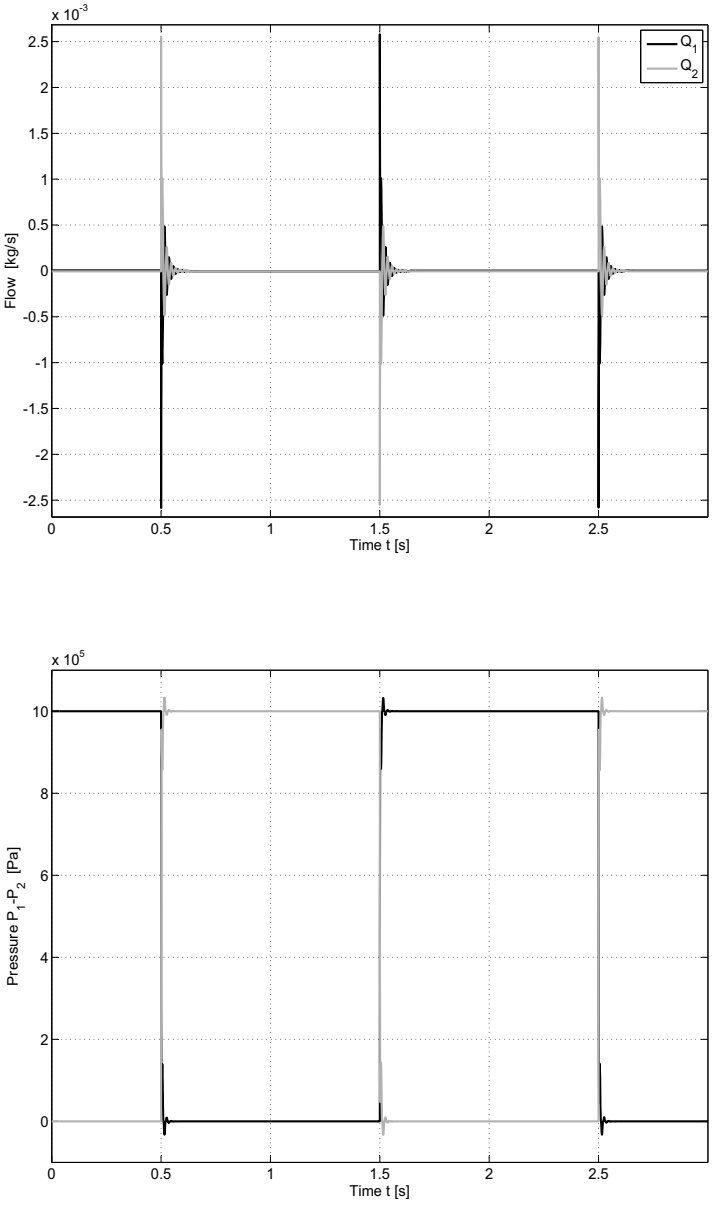

Fig. 5.16 Mass flow and pressure response of the hydraulic actuator to an open loop simulation. Simulation 2

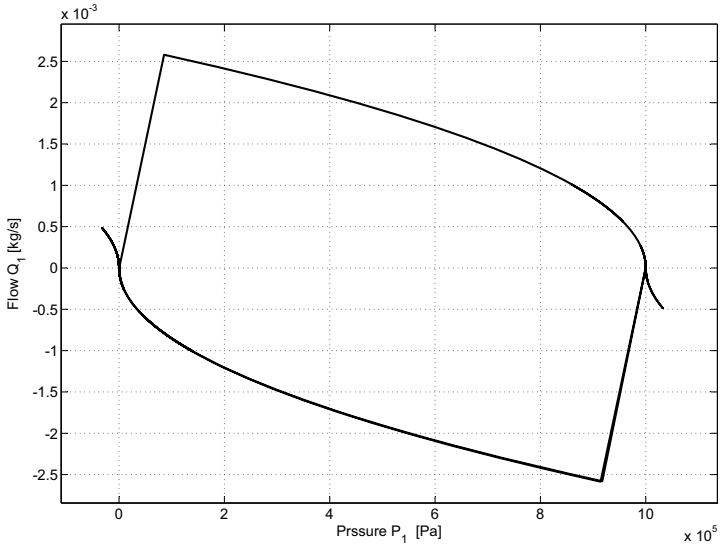

Fig. 5.17 Pressure-flow curve response of the hydraulic actuator to an open loop simulation. Simulation 2

References

1. Buckingham E (1914) On physically similar systems: Illustrations of the use of dimensional equations. Phys Rev 4:345–376
2. Gomis-Bellmunt O, Galceran-Arellano S, Sudrià-Andreu A, Montesinos-Miracle D, Campanile LF (2007) Linear electromagnetic actuator modeling for optimization of mechatronic and adaptronic systems. Mechatronics 17:153–163
3. Gomis-Bellmunt O, Campanile F, Galceran-Arellano S, Montesinos-Miracle D, Rull-Duran J (2008) Hydraulic actuator modeling for optimization of mechatronic and adaptronic systems. Mechatronics 18:634–40
4. Jelali M, Kroll A (2003) Hydraulic servo-systems. Springer
5. Merrit H (1967) Hydraulic Control Systems. John Wiley & Sons
6. Timoshenko S, Young DH (1962) Elements of Strength of Materials, 4th edn. Princeton, NJ
7. Watton J (2007) Modelling, Monitoring and Diagnostic Techniques for Fluid Power Systems. Springer-Verlag

Part III
Solid-State Actuators

Chapter 6
Design Principles for Linear, Axial Solid-State Actuators

6.1 Complexity Levels in Modeling Solid-State Actuators

A complete description of the behavior of solid-state actuators requires a multi-field approach, which involves full coupling with the non-mechanical field quantities (of electrical or thermal nature, for instance). Powerful simulation tools like COMSOL® allow for such an accurate multi-field analysis for an actuator device of given geometry and material distribution. The complexity (and accurateness) of a multi-field approach depend on the number of feedback loops which are considered in the analysis. In the case of a shape memory actuator (SMA) heated by Joule effect, for instance, the activation can be modeled by prescribing the temperature in the SMA-element, the heating power, the electrical current or the electrical tension. Even in the latter case, which includes the full thermo-mechanical modeling of the SMA actuator as well as the modeling of its electrical resistance as a function of temperature and transformation state, the analysis is still incomplete since it neglects the coupling with the supply circuitry and the control system. The simplest modeling option in this sense is the direct prescription of a given induced strain. The only feedback which is considered by this option is the mechanical one, which converts the imposed induced strain into the actual strain by means of the stress-strain relationship of the active material. This option is often denoted as "thermal analogy", since it is equivalent to the prescription of a temperature change in a material subject to thermal expansion (with anisotropic thermal expansion properties in order to allow for generating a non-hydrostatic strain state). Usually, the stress-strain relationship of the active material is linearized, which is consequent with the superposition principle implicit in the prescribed induced strain approach (actual strain = induced strain + elastic strain).

6.2 Limits and Advantages of a Linear Theory of Solid-State Actuation Based on Prescribed Induced Strain

Despite of its simplicity, the prescribed induced strain approach catches the relevant aspects of solid-state actuation in most practical cases with an accuracy level which is adequate for preliminary design and optimization purposes. The theories and design rules presented in the following are based on this approach. Extensions to higher levels of complexity are beyond the scopes of this book. The reader interested in the fascinating topic of multi-field based constitutive models of active materials will find plenty of details in specialised publications and textbooks, e.g. [3, 8]. Although simple and of limited validity, the prescribed induced strain approach is of high practical relevance, for the same reason for which the preliminary design of a steel bridge can be brought to a quite advanced level without requiring a micromechanical analysis of the employed steel. Thousands of text books on mechanical design de facto reduce the high complexity of the behavior of construction steel to two essential scalar parameters: the elasticity modulus and the allowable stress. This approach just extends this claim to the class of active materials by adding the maximum induced strain to the list of essential material parameters. As mentioned above, the induced strain approach allows for a simple analysis of the actuator performance as a function of its geometry and size. It additionally provides very useful material-related quantities like the volume related and the weight related energy density. It also essentially simplifies the treatment of hybrid actuators (consisting of a passive linear elastic component and a solid-state actuator) by introducing equivalent material-related quantities. In the following, special focus is given to solid-state actuators interfaced with a linear elastic system, since this is the common case for smart structures applications. Other kind of external loads (e.g. a constant force) will be treated in a short fashion for the sake of completeness.

The theory of single-stroke linear solid-state actuators, which is treated in Chapter 6.3, can be applied to virtually any solid-state actuator behaving linearly (as far as the stress-strain relationship is concerned) and whose interaction with the host mechanical system can be essentially reduced to a self-equilibrated couple of concentrated forces. Typical examples are piezoelectric stack actuators and Shape Memory Wires directly interfaced with a structural system at their ends. Integrated actuators like glued piezoelectric patches, surface-bonded Shape Memory thin films and embedded wires can be treated as well, in many cases, as single-stroke actuators since the most part of the load transfer with the host structure is localized near the ends. The models and relationships presented for hybrid actuators can be typically applied to pre-stressed piezoceramic stacks as well as to a large range of linear actuators consisting of active and passive components.

6.3 Theory of Single-Stroke Linear Solid-State Actuators

6.3.1 Definitions and Symbols

As mentioned before, a single-stroke actuator interfaces with its mechanical environment (or host mechanical system) through two scalar variables, the actuator force and the actuator stroke. The actuator force F has the nature of an internal axial reaction or a zero moment couple. It is defined as positive if the actuator exerts a tension load on the host system (i.e. if it is subjected to compression loading by external forces). The actuator stroke u is the relative displacement of the actuator's end points and is positive if their relative distance increases (see Figure 6.1).[1]

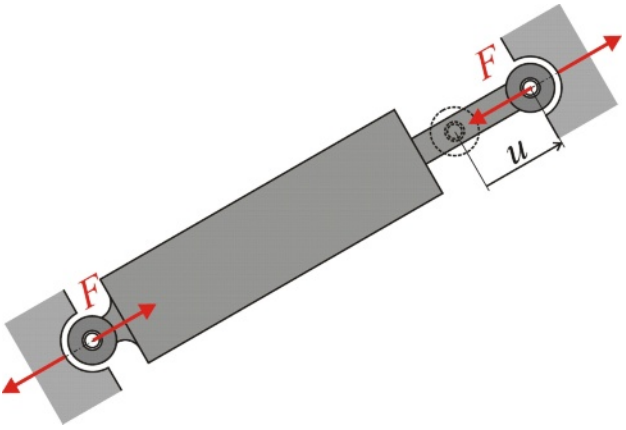

Fig. 6.1 Actuator force and stroke

Mathematically, the actuator can be described by a parametric relationship between force and stroke:

$$f(F,u,\alpha)=0 \tag{6.1}$$

The parameter α represents the actuator input quantity – usually of non-mechanical nature [2] – which allows controlling the actuator by modifying the force which the actuator makes available for a given stroke or, conversely, the stroke provided by the actuator for a given force.

[1] In the following, we will apply the word stroke also to passive mechanical components to denote, in general, a positive or negative elongation, i.e. the change of the distance between two points. The word force will be used, as a rule, in the sense of an internal axial reaction (tension or compression).

[2] In the case of a piezoceramic actuator, this can be the voltage applied to the electrodes; for a shape-memory wire, the wire temperature or the electrical current in the wire are possible choices for the input quantity.

In a solid-state actuator the relationship between actuator force and stroke is substantially ruled by the passive mechanical behavior of the actuator material (stress-strain relationship). In order to give this fact proper relevance, we can specify Equation 6.1 as

$$h(F,u,X_i(\alpha)) = 0 \tag{6.2}$$

where X_i represents a quantity of mechanical nature (displacement or force) which is induced by the input quantity α. The function h is directly related to the mechanical behavior of the actuator material. For a solid-state actuator with a linear mechanical behavior Equation 6.2 can be further specified as

$$F + ku - F_i(\alpha) = 0 \tag{6.3}$$

with $F_i(\alpha)$ as *induced force*, or

$$F + k[u - u_i(\alpha)] = 0 \tag{6.4}$$

with $u_i(\alpha)$ as *induced stroke*.

Most solid-state actuators are *strain-inducing*, i.e. activation primarily results in material strain; stresses – and, consequently, forces – are produced only secondarily, if the active strain is somehow constrained. In those cases, the second formulation is physically more appropriate. From a strictly formal point of view, however, both formulations are equivalent [3], since the induced stroke u_i can always be converted into an induced force of value ku_i. Nevertheless, the induced-force representation (6.3), is often preferred, since it is customary to prescribe forces rather than displacements while analyzing mechanical systems. If the actuator stiffness k vanishes, Equation 6.3, becomes:

$$F = F_i(\alpha) \tag{6.5}$$

which represents an *ideal force generator*, i.e. an actuator providing a constant force, defined by the value of the input variable independently of the actuator stroke. On the other hand, if the stiffness of an induced-stroke actuator tends to infinity, the actuator degenerates into an *ideal stroke generator*:

$$u = u_i(\alpha) \tag{6.6}$$

i.e. an actuator which is able to supply a constant stroke independently of the actuator force. Finally, by setting the induced quantities to zero, both Equations 6.3 and 6.4 turn into

$$F + ku = 0 \tag{6.7}$$

[3] This equivalence holds only as long as the mere relationship between actuator force and stroke is considered. If the internal loading of the actuator material is of concern, the application of the induced-force representation to a strain-inducing solid-state actuator can be misleading. If such an actuator, for instance, is operated without external load ($F = 0, u = u_i$), the active material is stress-free. By regarding it as a spring of stiffness k loaded by the induced force F_i (according to (6.3)), however, the solid-state actuator is subject to a tension or compression loading (depending on the sign of the induced stroke) equal to F_i.

which describes a linear elastic spring.

We will assign to these special cases the symbols represented in Figure 6.2. The symbols used for the ideal generators recall the graph of their respective characteristic curve in the Fu-plane.

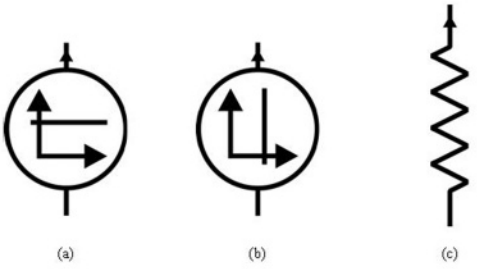

Fig. 6.2 Symbols for (a) ideal force generator , (b) ideal stroke generator and (c) linear elastic spring

These symbols will be used in the following to graphically represent active mechanical systems in a similar way used by the theory of electrical circuits. In this analogy, forces replace electric currents and strokes correspond to electric voltages (forces "flow" through components and strokes are measured between terminals). Wires and nodes will be used to build circuits out of the above mentioned components: wires transfer forces unchanged in value and have zero stroke, while nodes connect three or more terminals. The *node law* which translates the equilibrium conditions requires the sum of all forces "flowing" into a node to be zero. The *loop law* results from compatibility considerations and states that the sum of all strokes of the components building a closed loop must vanish.

In this form, the electric analogy only applies to mechanical systems in which the involved quantities (forces and strokes) can be treated as scalars (like electric voltages and currents in the theory of circuits). This requires all mechanical components to be arranged axially, co-axially or in an equivalent fashion (forces and displacements at terminals must have the same spatial direction).

The small triangle near the top of each symbol allows distinguishing positive and negative forces in the graph: a compression (positive) force is represented by a current flowing toward the triangle, whereas a tension (negative) force "flows" in the opposite direction (from the triangle towards the other terminal). A positive stroke (elongation) is represented by a positive voltage measured from the terminal with the triangle to the other one, while a negative voltage represents a negative stroke (shortening). According to this convention, the circuits of Figure 6.3, which look similar, represent two different mechanical systems (see Figure 6.4).

Further, we will introduce symbols for ideal stroke and force sensors, to provide the graphs with the corresponding indications (see Figure 6.5(a)). The attribute "ideal" refers to the fact that the force in the stroke sensor as well as the stroke of

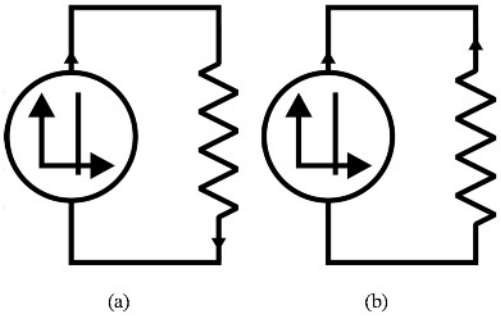

Fig. 6.3 Circuits representing (a) a serial arrangement of an ideal stroke generator and a spring between two rigid walls and (b) a parallel arrangement of the same two components, with one end fixed

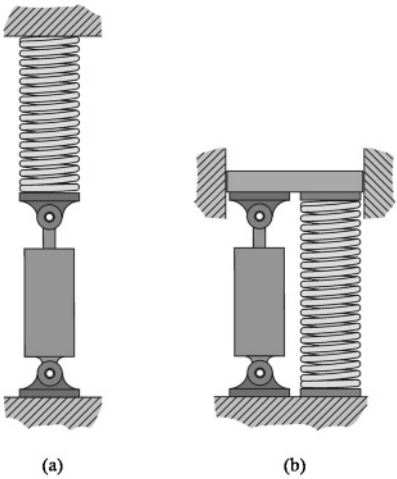

Fig. 6.4 Drawings of the mechanical systems of Figure 6.3, in the same order, (a) a serial arrangement of an ideal stroke generator and a spring between two rigid walls and (b) a parallel arrangement of the same two components, with one end fixed

the force sensor is assumed to be zero. The sensors work like a voltmeter and an ammeter, respectively and are provided with a plus mark to relate the sign of the measured quantity to the displayed value (if, for instance, the force "flows" towards the plus sign, the sensor outputs a positive value. In the case of Figure 6.5(a) the stroke and force sensors are expected to provide values of opposite signs. Stroke

and force sensors can be integrated into the symbols of ideal generators as shown in Figures 6.5(b) and 6.5(c). In such cases the plus mark is omitted with the convention that the measurement direction conforms with the positive direction of the force or stroke generation as identified by the triangle in the generator symbol. If necessary, the spring symbol can be completed by the indication of the stiffness value (see Figure 6.8 as an example).

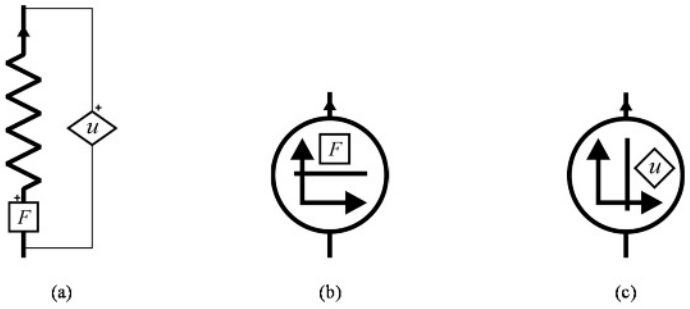

Fig. 6.5 Spring element with (a) stroke and force indications, (b) ideal stroke and (c) force generators with integrated sensors

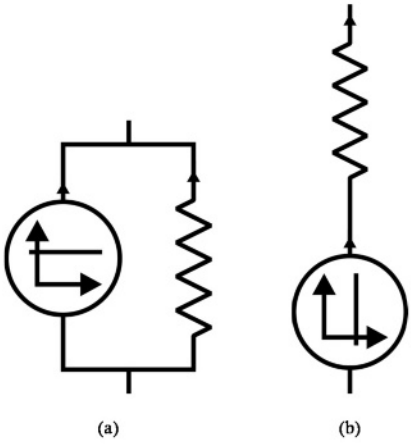

Fig. 6.6 Circuits representing (a) an induced-force actuator and (b) an induced-stroke actuator

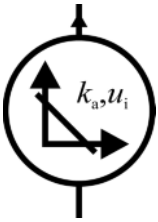

Fig. 6.7 Symbol for an induced-stroke actuator

The induced-force actuator as described by Equation 6.3 can be obtained by arranging an ideal stroke generator and a spring in parallel, while the induced-stroke actuator (6.4) results by a serial arrangement of an ideal stroke generator and a spring (see Figure 6.6). Since, as mentioned before, an induced-force actuator can always be converted into an induced-stroke actuator, we will only consider induced-stroke actuators in the following. To render the graphic representation more compact, we will mostly replace the sub-graph of Figure 6.6(b) by the symbol of Figure 6.7.

6.3.2 Free Stroke and Blocking Force

The induced stroke u_i of an induced-stroke actuator can be unequivocally determined by choosing the value of the input variable α. The actual value of the actuator stroke, however, as well as the value of the actuator force, depends on the load, i.e. on the rest of the circuit in which the actuator is inserted. The stroke produced by the actuator in an open-loop configuration (see Figure 6.8(a)) is denoted as *free stroke* and is equal to the induced stroke: since no force is present in an open-loop circuit, the stroke of the spring element is zero and the overall stroke is equal to the stroke of the ideal stroke generator. If, conversely, the actuator is shorted (Figure 6.8(b)), its stroke vanishes and its force amounts to

$$F_b = ku_i \tag{6.8}$$

which is known as the actuator's *blocking force*. The limit cases of free and blocked actuator define the ranges of stroke and force which can be made available by the actuator for the considered value of induced stroke, provided that the actuator is interfaced with a passive mechanical system without pre-stress or pre-strain [4]. In presence of pre-stress or when other active elements are included in the host system, forces beyond the boundaries of the interval $[0, F_b]$ as well as strokes outside the interval $[0, U_i]$ are possible.

[4] Since a pre-strain state can be represented by an equivalent pre-stress state (see also 6.3.6) we will not distinguish, in the following, between the two conditions. For the sake of brevity, the term *pre-stress* will mostly be used to denote any of the two states.

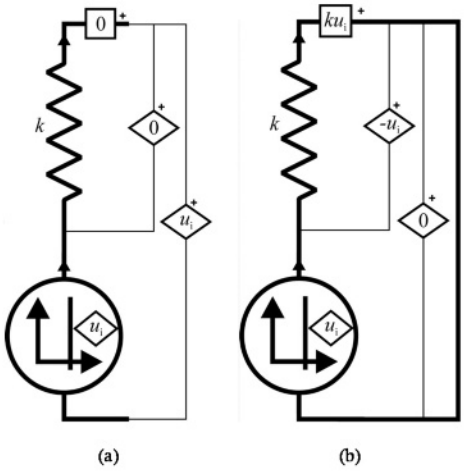

Fig. 6.8 Actuator (a) in open-loop configuration and (b) in shorted configuration

6.3.3 Actuator Coupled with a Linear Elastic Structure

The graph of Figure 6.9 represents the case of an actuator interfaced with a linear elastic structure. The actuator's characteristic (4) is represented, in the Fu-plane, by a straight line as shown in Figure 6.10(a). Figure 6.10(b) shows the graph of Equation 6.7, which provides the characteristic of the linear spring. Since, however, the forces in the two elements have different signs (according to the node rule the sum of the actuator force and of the spring force must be zero), one of the curves has to be mirrored with respect to the u-axis in order to be plotted on the same plane of the other one. If the plane of the actuator force and stroke is chosen (actuator force: F; spring force: -F), both curves are represented as in Figure 6.10(c). The intersection point supplies the values of the actual actuator force and stroke and lies somewhere between the free-stroke and the blocking condition. The slopes of the curves correspond to the respective values of the stiffness. The higher the stiffness ratio is (structure's stiffness k_s over actuator's stiffness k_a), the closer the point of intersection will be to the blocking condition; the lower the ratio, the closer it will come to the free-stroke condition (see Figure 6.11).

The actual values for force and stroke are computed by simultaneously solving the equations

$$F + k_a (u - u_i) = 0 \tag{6.9}$$

$$F = k_s u \tag{6.10}$$

Equation 6.9 corresponds to (6.4) and Equation 6.10 is obtained by (6.7) while taking into account the above mentioned change in sign for the force. It results:

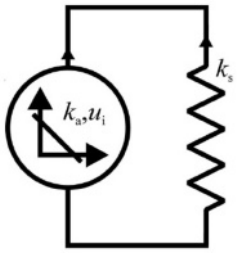

Fig. 6.9 Actuator coupled with a linear elastic structure

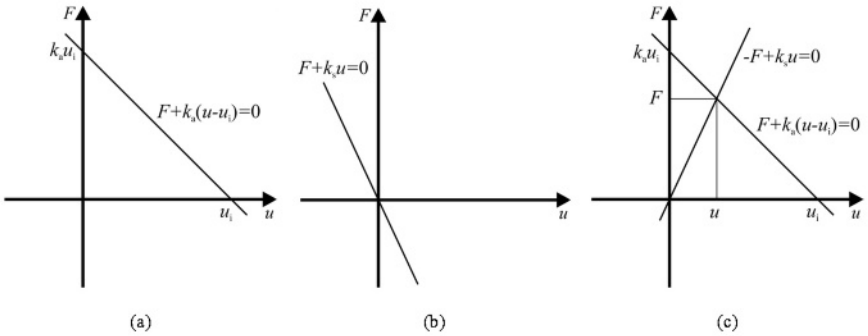

Fig. 6.10 Characteristic curves of (a) an actuator and (b) of a linear spring in the respective Fu-planes. (c) Interaction of both curves in the same Fu-plane (F=actuator force)

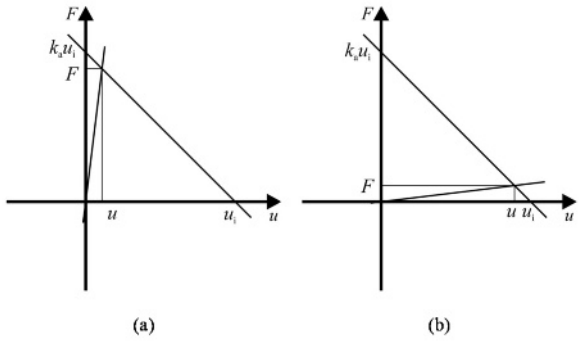

Fig. 6.11 Interaction of the characteristic curves of actuator and structure (a) for $k_s \gg k_a$ and (b) for $k_s \ll k_a$

$$u = \frac{k_a}{k_s + k_a} u_i \tag{6.11}$$

$$F = \frac{k_s k_a}{k_s + k_a} u_i \tag{6.12}$$

6.3.4 Activation Boundary

The above reported considerations about free stroke, blocking force and coupling with a linear elastic structure can be repeated for each single value of the induced stroke, while a change in the induced stroke corresponds to a translation of the actuator's characteristic (see Figure 6.12(a)) in the Fu-plane. The minimum and maximum allowed value of the induced stroke identify the activation boundary of the actuator. In general, and without considering other restrictions, every point of the (infinitely long) strip delimited by the activation boundary can be reached by proper loading. If only coupling with passive structures without pre-stress is considered, however (like in the case of Figure 6.9) the operation domain of the actuator restrict to the regions in the first and third quadrant (Figure 6.12(b)).

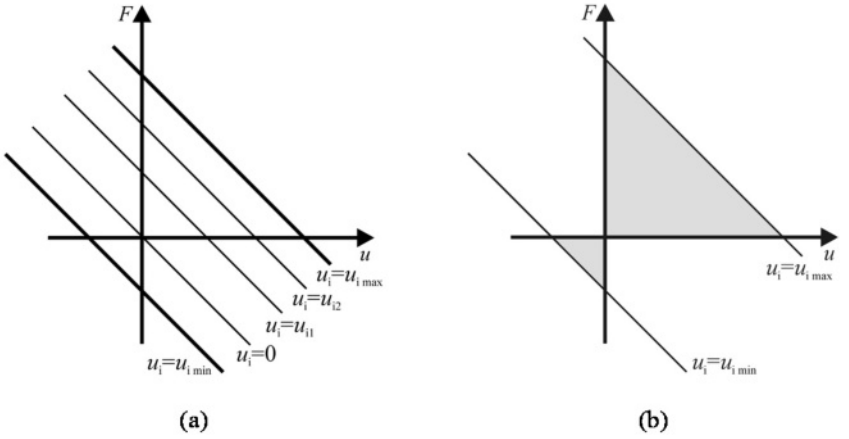

Fig. 6.12 (a) Actuator characteristic curves for different values of the induced strain. (b) Activation boundary. The shaded area represents the operation domain of the actuator when coupled with a passive structure without pre-stress

6.3.5 Strength Boundary

Besides the activation boundary, the actuator force and/or stroke can be limited by strength or stability consideration . For instance, a piezoelectric stack actuator cannot be significantly loaded in tension (see Figure 6.13 a), and a thin wire actuator (e.g. SMA wire) is not able to produce significant positive force (compression load). Together with the activation boundary, the strength boundary defines the operation domain of the actuator (Figure 6.13).

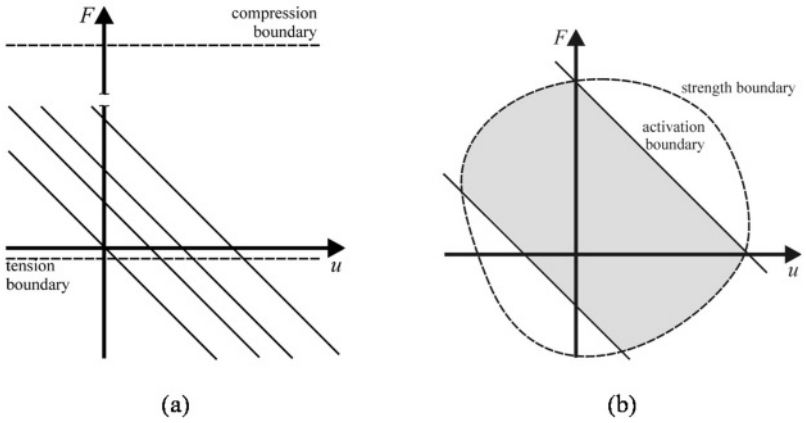

Fig. 6.13 (a) Typical strength boundary of a piezoelectric stack actuator. (b) Operation domain (shaded area) as defined by the strength and the activation boundaries

6.3.6 Stroke Work

The product of the actuator's blocking force and his free stroke (or induced stroke)

$$W_n = F_b u_i \tag{6.13}$$

has the dimension of energy and will be denoted as *nominal stroke work* in the following. This quantity is related to the amount of work which can be performed by the actuator under particular conditions. Let us now consider the case of an actuator with an induced stroke ranging from 0 to a given value u_i and which is coupled with a passive structure without pre-stress. As already mentioned, in this case the actuator can only operate within a triangular domain of the Fu-plane. We will also assume

that the strength boundaries are *passive*, i.e. external to such triangular domain and therefore do not affect the actuator's operation domain. While the induced stroke is increased from zero to u_i, the point on the plane which is identified by the actuator force and stroke will move on the characteristic curve of the host structure. The mechanical work performed by the actuator (*effective stroke work*) will then be given by the portion of the actuator's operation domain which is below the structure's characteristic curve (see Figure 6.14(a)). It is evident that the area of the activation domain

$$\frac{1}{2}W_n = F_b u_i = k_a u_i^2 \tag{6.14}$$

represents the maximum possible amount of work which can be performed by the actuator (in a single activation process from zero to the given value of induced strain) under the given conditions. If the host structure has a linear characteristic (see Figure 6.14(b)), the effective stroke work will be given by the area of a triangular region:

$$W = \frac{1}{2}Fu \tag{6.15}$$

with F and u as the actual values of the actuator force and stroke when the induced stroke reaches the value u_i. For a given solid-state actuator and a given value of the induced strain, the effective stroke work depends on the stiffness of the host structure. In particular, if the stiffness of the host structure vanishes, the effective stroke work vanishes as well (the actuator works under free stroke condition, which implies $F = 0$). For $k_2 \to \infty$ (blocked actuator), the stroke work is, again, zero (vanishing actuator stroke). Between these limit cases it holds $W > 0$ and a maximum must therefore exist. By inserting the expressions (6.11) and (6.12) into (6.15) we obtain

$$u = \frac{1}{2}\frac{k_s k_a^2}{(k_s + k_a)^2}u_i^2 \tag{6.16}$$

and the maximum is identified by the condition

$$\frac{dW}{dk_\mathrm{s}} = 0 \Rightarrow \frac{d}{dk_\mathrm{s}}\left(\frac{k_\mathrm{s}}{(k_\mathrm{s}+k_\mathrm{a})^2}\right) \Rightarrow (k_\mathrm{s}+k_\mathrm{a})^2 = 2k_\mathrm{s}(k_\mathrm{s}+k_\mathrm{a}) \tag{6.17}$$

which yields

$$k_s = k_a \tag{6.18}$$

Hence, the actuator effective stroke work reaches its maximum value in the case in which the stiffness of the host structure matches the actuator's stiffness. By inserting (6.18) into (6.11) and (6.12), respectively, we obtain

$$u = \frac{u_i}{2} \tag{6.19}$$

$$F = k_a\frac{u_i}{2} = F_b 2 \tag{6.20}$$

i.e. when the condition (6.18) is verified, the actuator force produced for a given value of the induced stroke amounts to the half of the corresponding blocking force, and the actuator stroke is the half of the free stroke. The maximum effective stroke work amounts to

$$W_{max} = \frac{1}{2}\frac{F_b}{2}\frac{u_i}{2} = \frac{1}{8}W_n \tag{6.21}$$

From Figures 6.14(a) and (b) it is evident that by loading a solid-state actuator in a nonlinear fashion its work output can be increased by up to a factor four. Lesieutre et al. [5] studied a special device to be interfaced with a piezoceramic actuator in order to attain this purpose. The condition (6.18) (stiffness matching condition) is of basilar importance for the design of solid state actuators. We summarize it:

The maximum effective stroke work of a linear solid-state actuator:

- which works against the stiffness of a linear passive structure
- without pre-stress
- and with passive strength boundaries

amounts to one eighth of the nominal stroke work.

This result can also be applied in presence of active strength boundaries, if they do not intersect the stiffness matching path (see Figure 6.14(b)). If strength boundary and stiffness matching path intersect, the maximum effective stroke work is lower. For the case represented in Figure 6.14(c), in which the strength boundary is a simple force limit (independent of the actuator stroke):

$$F \leq F_{lim} \tag{6.22}$$

the maximum effective stroke work amounts in this case to

$$W_{max} = \frac{1}{2}F_{lim}u_i\left(1 - \frac{F_{lim}}{F_b}\right) \tag{6.23}$$

In the case in which the strength limit force is very low with respect to the blocking force:

$$F_{lim} \ll F_b \tag{6.24}$$

it holds

$$W_{max} \simeq \frac{1}{2}F_{lim}u_i \tag{6.25}$$

The condition (6.24) is typical for active materials with high active strain, like Shape Memory Alloys (SMA).

The considered case of an actuator working against a linear stiffness without pre-stress covers only a part of the conceivable application scenarios. The reader could ask, for instance, which is the maximum work output of an actuator working against a constant load (like in the case in which the actuator is used to lift a weight) or against a load with a constant and a stroke-proportional component (like in the case in which a pre-stress is, indeed, present or when the actuator interfaces with a structural system on which an external constant load acts). We will see that under these load conditions the maximum effective work output is not defined: if

no strength boundary is taken into account, the work output of a solid-state actuator can be arbitrarily high[5].

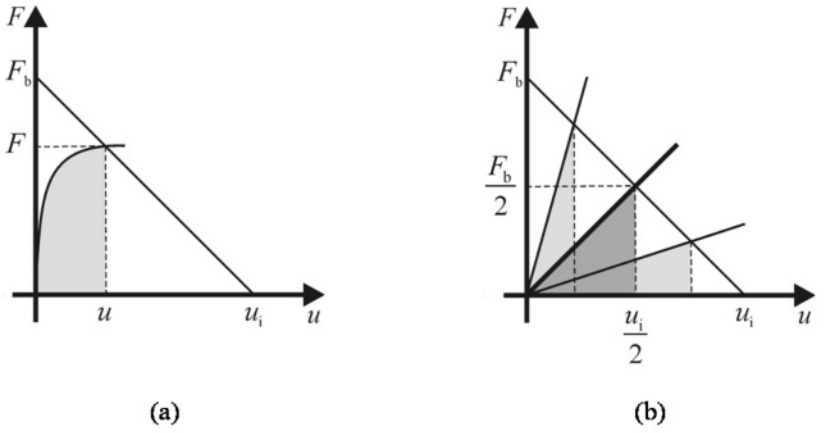

Fig. 6.14 (a) Mechanical work performed by the actuator while interfaced with a passive structure without pre-stress. (b) Work produced against linear structures of different stiffness; stiffness matching condition (thick line, dark shaded area)

The graphs of the above mentioned loading configurations are reported in Figure 6.16. Please note that the cases represented in Figure 6.16(b) and (c) (pre-strain and pre-stress) can be made equivalent by choosing a proper relationship between the generated force, the generated stroke and the spring constant:

$$F_p = k_s u_p \tag{6.26}$$

Let us consider the case of Figure 6.16(a) first. Due to the node law, the actuator force is kept constant by the force generator, independently of the induced stroke:

$$F = F_p \tag{6.27}$$

By increasing the induced stroke from zero to the value u_i, the actuator performs the work

$$W = F_p u_i \tag{6.28}$$

[5] The above reported analysis of the work output of a solid-state actuator interfaced with a passive linear structure without pre-stress is a standard content of the literature dealing with solid-state actuation (e.g. [4]). Interestingly, in the cited contributions the other loading scenarios are – despite of their relevance – not discussed at all.

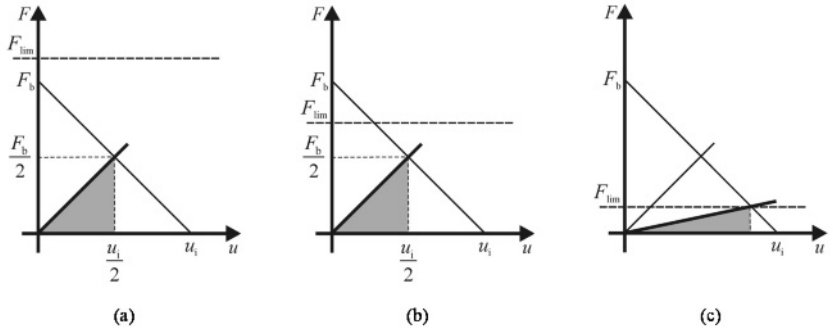

Fig. 6.15 Maximum effective stroke work against a linear structure without pre-stress while considering the strength boundaries: (a) Passive strength boundary, (b) active strength boundary, without intersection with the stiffness matching path and (c) active strength boundary intersecting the stiffness matching path

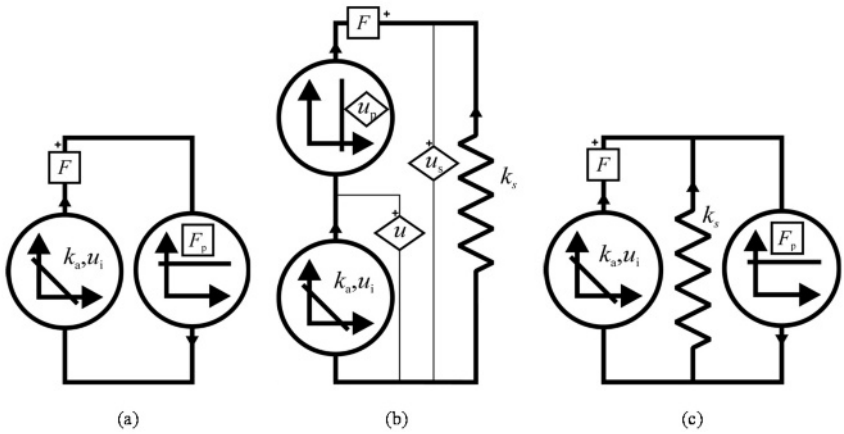

Fig. 6.16 Graphs of (a) an actuator working against a constant load, (b) coupled with a structure with pre-strain and (c) coupled with a structure with pre-stress or loaded by an external constant force

represented by the shaded area in Figure 6.17(a). In the case of Figure 6.6(b), the loop law requires

$$u + u_p = u_s \tag{6.29}$$

while the values of the actuator and the structure strokes are related to the force in the circuit by the respective characteristics:

$$F + k_a(u - u_i) = 0 \tag{6.30}$$

$$-F + k_s u_s = 0 \tag{6.31}$$

Solving the system (6.29)–(6.31) for F and u gives

$$u = \frac{u_i - \frac{k_s}{k_a} u_p}{1 + \frac{k_s}{k_a}}; \quad F = \frac{k_s}{1 + \frac{k_s}{k_a}} \left(u_i + u_p\right) \tag{6.32}$$

and the stroke work – represented by the shaded area in Figure 6.17(b) – reads

$$W = \int_0^{u_i} F\left(\bar{u}_i\right) du = \int_0^{u_i} F\left(\bar{u}_i\right) \frac{du}{du_i} d\bar{u}_i = \frac{1}{1 + \frac{k_s}{k_a}} \int_0^{u_i} F\left(\bar{u}_i\right) d\bar{u}_i \tag{6.33}$$

$$W = \frac{k_s u_i}{\left(1 + \frac{k_s}{k_a}\right)^2} \left(u_p + \frac{u_i}{2}\right) \tag{6.34}$$

As mentioned before, the pre-stress case (Figure 6.16(c)) is equivalent to the above treated pre-strain case. It is evident from the graph of Figure 6.17 that under the considered conditions no inherent limit to the actuator's stroke work exists. The amount of work performed by the actuator can be indefinitely increased by increasing the external load (force or pre-strain).

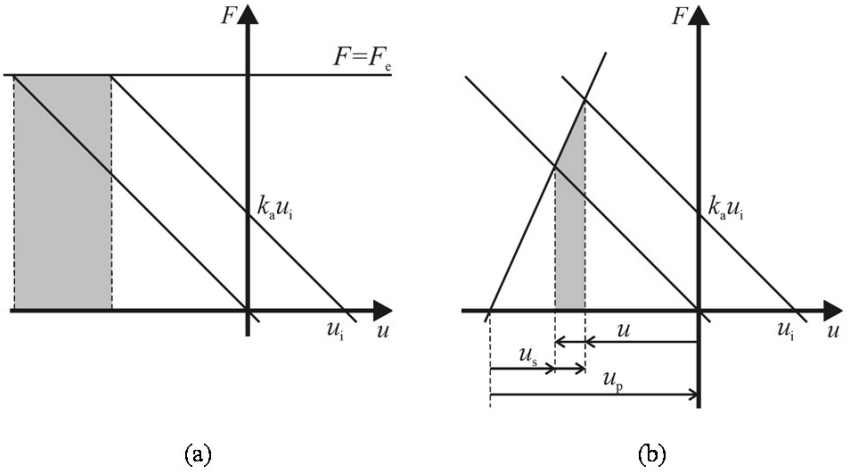

Fig. 6.17 Mechanical work performed by the actuator (a) against a constant load and (b) against a structure with pre-strain

6.3.7 Hybrid Actuators

A linear solid-state actuator can be combined with passive components in such a way that the resulting system can be treated as a new linear solid-state actuator with modified properties. This requires:

- the new system to interface with the mechanical environment through a single force and a single stroke as defined in Section 6.3.1;
- the passive component to be linear elastic.

We will now examine the most common hybrid configurations and derive the characteristic of the hybrid actuator (identified by its free stroke and blocking force) as a function of the characteristic of the original actuator as well as of the passive component's stiffness. Due to the system's linearity, it will suffice to determine the behavior of the hybrid actuator in the two characteristic loading states (open loop and shorted). A simple serial arrangement is typically used to take into account the finite stiffness of attachment parts as well as of mechanically passive, functional components in stacked configurations (e.g. electrodes and insulation layers in piezoceramic stack actuators). In the open-loop loading case (Figure 6.18(a)), the force in all components is zero. It results that the solid-state actuator keeps its free stroke in the hybrid configuration:

$$\hat{u}_i = u_i \tag{6.35}$$

In the shorted case, the stroke of the original actuator and the one of the spring k_h are equal in absolute value and opposite in sign. The force in both components is equal to the blocking force of the hybrid actuator $\hat{F}_b$. It holds

$$\hat{F}_b = k_h u \tag{6.36}$$

$$\hat{F}_b = -k_a(u - u_i) \tag{6.37}$$

Eliminating u following relationship is obtained from (6.36) and (6.37):

$$\hat{F}_b = -k_a\left(\frac{\hat{F}_b}{k_h} - u_i\right) \tag{6.38}$$

$$\hat{F}_b = \frac{k_h k_a}{k_h + k_a} u_i \tag{6.39}$$

and with (6.8)

$$\hat{F}_b = \frac{k_h}{k_h + k_a} F_b \tag{6.40}$$

which shows that the blocking force of the hybrid actuator is reduced by the factor $k_h/(k_a + k_g)$ with respect to the blocking force of the original actuator. In the case of passive strength boundaries, the stroke work (nominal or effective) is reduced by the same factor. If the strength boundaries are active and remain active after the reduction of the blocking force, the maximum stroke work remains unchanged.

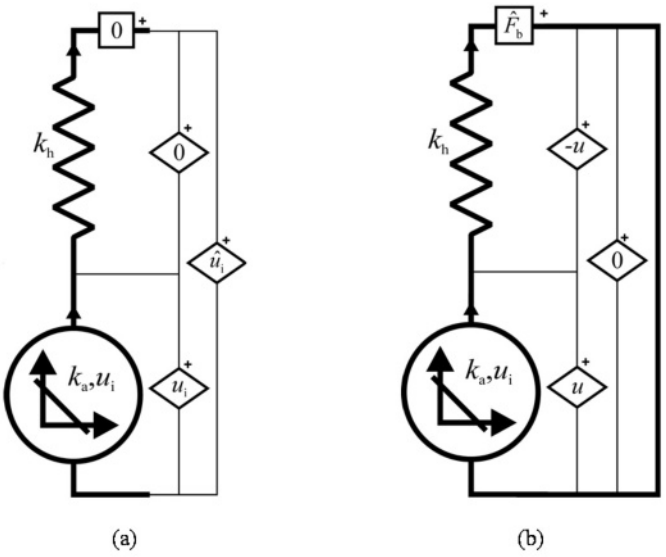

Fig. 6.18 Hybrid actuator in simple serial arrangement, (a) open-loop and (b) shorted

A parallel arrangement (Figure 6.19) is usually employed to protect the solid-state actuator from improper loading. In most cases it is used to apply pre-strain or pre-stress: a typical case is represented by pre-compressed stack actuators in order to enable a tension loading of the hybrid actuator while keeping the stack actuator under a compression state.

In the shorted case (Figure 6.19(b)) all stroke values are zero. It follows that the actuator keeps its blocking force in a parallel configuration:

$$\hat{F}_b = F_b \tag{6.41}$$

Conversely, the actuator's free stroke is reduced. From the open-loop graph (Figure 6.19(a)) it results that the forces in the original solid-state actuator and in the spring are equal in absolute value and opposite in sign. It holds

$$F = k_h \hat{u}_i \tag{6.42}$$

$$F = -k_a(\hat{u}_i - u_i) \tag{6.43}$$

Elimination of F yields

$$\hat{u}_i = \frac{k_a}{k_h + k_a} u_i \tag{6.44}$$

which provides a reduction factor of $k_a/(k_a + k_h)$ for the actuator's free stroke and, as a consequence, for the stroke work.

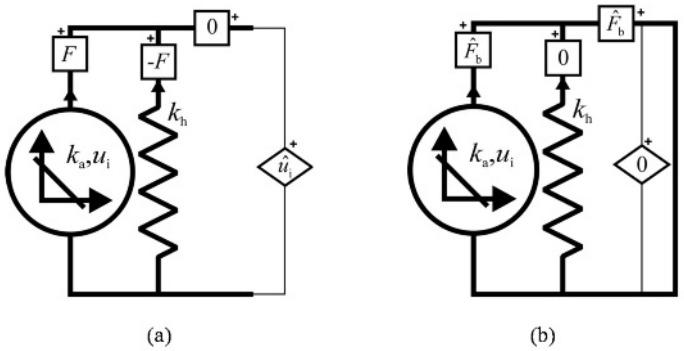

Fig. 6.19 Hybrid actuator in simple parallel arrangement, (a) open-loop and (b) shorted

Another relevant hybrid arrangement is represented by the combination of a solid-state actuator and a leverage system. Only ideal leverage systems need to be considered, since real ones (with mechanical efficiency lower than unity) can be represented by adding serial and/or parallel springs (see below). While combining a solid-state actuator with an ideal leverage system, the actuator's free stroke is increased by the *stroke amplification factor* and the blocking force is reduced by the same factor. The actuator's stroke work remains unchanged.

All configurations (serial and parallel) can be combined together. A relevant case of combined hybrid configuration is represented by solid state actuators integrated into compliant mechanisms for stroke amplification and conversion (see Section 6.4.4). The compliant nature of the mechanism causes some losses of energy in both loading cases, which calls for a serial and a parallel arrangement of springs (Figure 6.20). Please take note that no additional symbol for the leverage system was introduced in the graph; the actuator's output quantities have been properly adjusted instead.

6.4 Design Principles and Rules

6.4.1 Actuator Performance as a Function of Geometry

While studying the relationship between the actuator performance quantities and its geometrical dimensions, we will refer to the case of a homogeneous body of

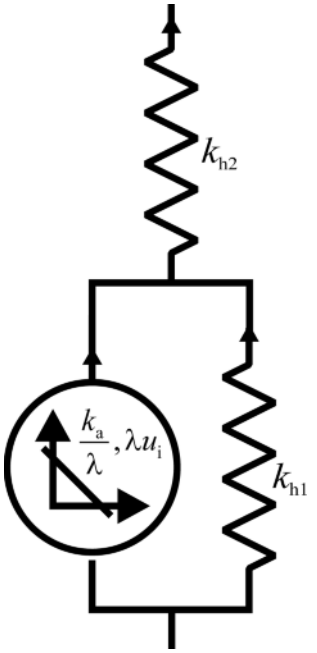

Fig. 6.20 Graph of a solid-state actuator integrated into a compliant mechanism

active material which experiences a constant strain in a given spatial direction (*axial direction*). Strain components in other directions can be also present, but they are generally not used. All the examined performance properties (free stroke, blocking force and stroke work) will be then a function of the actuator's geometry, of material properties (modulus of elasticity and maximum allowable stress) as well as of the above mentioned strain (induced strain). In most cases, solid-state actuators are of prismatic shape, with the prism's axis corresponding to the direction of the active strain. Then, if l is the actuator dimension in axial direction (actuator length) and A the area of the cross-section normal to it, it can be stated:

Elimination of F yields

$$u_i = \varepsilon_i l \tag{6.45}$$

$$F_b = \frac{AE}{l} u_i = AE\varepsilon_i \tag{6.46}$$

with ε_i as the *induced strain*. Equation 6.46 is obtained by (6.8) and by the expression of the axial stiffness of a prismatic bar

$$k = \frac{AE}{l} \tag{6.47}$$

An important consequence of the laws (6.45) and (6.46) is that the nominal stroke work (see (6.13)) for a given induced strain value is directly proportional to the

actuator's volume:

$$W_n = F_b u_i = AlE\varepsilon_i^2 = VE\varepsilon_i^2 \tag{6.48}$$

The proportionality constant

$$w_n = E\varepsilon_i^2 \tag{6.49}$$

will be denoted as *nominal volume-specific stroke work* in the following. If the maximum allowable induced strain for the used material is considered in (6.49), the nominal volume-specific stroke work is a mere material constant and is called *nominal energy density* for the given active material.

In this case, and for the above examined case of an actuator working against a linear stiffness without pre-stress and with passive strength boundaries (or strength boundaries which do not intersect the stiffness matching path) the maximum effective stroke work reads

$$W_{max} = \frac{1}{8}W_n = \frac{1}{8}w_n V \tag{6.50}$$

with

$$W_{max} = \frac{1}{8}w_n = \frac{1}{8}E\varepsilon_i^2 \tag{6.51}$$

as the *effective energy density* of the active material.

A special case of practical relevance is the already examined case of a strength-related force boundary (see Figure 6.14(c)) in which the boundary results from the allowable axial stress of the material. In this case Equations 6.23 and 6.25 read respectively

$$W_{\max} = \frac{1}{2}\sigma_{\lim}\varepsilon_{\mathrm{i}}\left(1 - \frac{\sigma_{\lim}}{E\varepsilon_{\mathrm{i}}}\right)V \tag{6.52}$$

$$W_{\max} \simeq \frac{1}{2}\sigma_{\lim}\varepsilon_{\mathrm{i}}V \tag{6.53}$$

so that the maximum effective stroke work can be, again, expressed as the product of a material constant and the actuator's volume.

The design relevance of the results (6.50) and (6.52)–(6.53) is given by the fact that if the mechanical work to be produced by the actuator is known, the minimum amount (volume) of active material needed for actuation is definite independently of the actuator geometry.

If the actuator's cross-section varies along the length, the above discussed relationships need to be adapted. If a class of actuators is considered in which the cross-section area varies with a given law

$$A = A_{\mathrm{ref}}\gamma(\xi) \tag{6.54}$$

with ξ as a dimensionless length coordinate ranging from 0 to 1, the key findings of this section keep their validity after correction with a factor depending from the function $\gamma(\xi)$.

Finally, some special cases of hybrid configurations should be considered here. The first one is the case of a serial prismatic arrangement of an active and a passive

material with overall lengths

$$l_a = \eta l \tag{6.55}$$

$$l_h = (1-\eta) l \tag{6.56}$$

and with Young's modulus E_a and E_a, respectively. The hybrid actuator has the cross-section area A. It does not matter, in this context, whether the materials are arranged in two separate blocks or in a larger number of alternate layers. The latter option is the more common in practice (stacked actuators).

From (6.45) and (6.55) the actuator's free stroke can be computed as

$$u_i = \varepsilon_i \eta l \tag{6.57}$$

which can be reported back to (6.45) by introducing the equivalent active strain

$$\hat{\varepsilon}_i = \varepsilon_i \eta \tag{6.58}$$

The blocking force can be computed from (6.40) and (6.47) as

$$\hat{F}_\mathrm{b} = \frac{\eta E_\mathrm{h} E_\mathrm{a}}{(1-\eta) E_\mathrm{a} + \eta E_\mathrm{h}} A \varepsilon_i = \frac{E_\mathrm{h} E_\mathrm{a}}{(1-\eta) E_\mathrm{a} + \eta E_\mathrm{h}} A \hat{\varepsilon}_i \tag{6.59}$$

which leads to the equivalent modulus of elasticity or

$$\hat{E} = \frac{E_\mathrm{h} E_\mathrm{a}}{(1-\eta) E_\mathrm{a} + \eta E_\mathrm{h}} \tag{6.60}$$

The equivalent specific stroke work is then

$$\hat{E} \hat{\varepsilon}_\mathrm{i}^2 = \frac{\eta E_\mathrm{h}}{(1-\eta) E_\mathrm{a} + \eta E_\mathrm{h}} E_a \varepsilon_\mathrm{i}^2 \tag{6.61}$$

By using the equivalent values for the elasticity modulus and the induced strain in (6.48), (6.49), (6.51), (6.52) and (6.53) the results of this section can be directly applied to the hybrid actuator of the described kind. In (6.52) and (6.53) the lowest of the two limit stresses is to be used.

The second case concerns a parallel arrangement of prismatic passive and active elements of the same length . The overall cross-section areas of the active and of the passive elements are

$$A_\mathrm{a} = \eta A \tag{6.62}$$

$$A_\mathrm{h} = (1-\eta) A \tag{6.63}$$

respectively. According to (6.44), (6.45) and (6.47) it reads

$$\hat{u}_\mathrm{i} = \frac{\eta E_a}{(1-\eta) E_\mathrm{h} + \eta E_a} \varepsilon_\mathrm{i} l \tag{6.64}$$

which leads to the induced strain

$$\hat{\varepsilon}_\mathrm{i} = \frac{\eta E_a}{(1-\eta)E_\mathrm{h} + \eta E_a}\varepsilon_\mathrm{i} \tag{6.65}$$

while from (6.46) and (6.62) -(6.63) the equivalent modulus results

$$\hat{E} = \eta E_\mathrm{a} + (1-\eta)E_\mathrm{h} \tag{6.66}$$

The equivalent specific stroke work is in this case

$$\hat{E}\hat{\varepsilon}_\mathrm{i}^2 = \frac{\eta^2 E_a}{(1-\eta)E_\mathrm{h} + \eta E_a}E_a\varepsilon_\mathrm{i}^2 \tag{6.67}$$

While using (6.52) and (6.53) an equivalent limit stress has to be used as well. If the hybrid actuator produces no external force (open loop, see Figure 6.19(b)) the force in the active element is, according to (6.42) and (6.44)

$$F_\mathrm{a1} = k_\mathrm{h}\frac{k_a}{k_\mathrm{h}+k_a}u_i \tag{6.68}$$

If the actuator is loaded by an external force F, an additional force F_{a2} acts on the active element while the passive element is loaded by a force equal to $F - F_{as}$. Since the stroke has to remain the same in both elements, it holds

$$\frac{F_\mathrm{a2}}{E_\mathrm{a}A_\mathrm{a}} = \frac{F - F_\mathrm{a2}}{E_\mathrm{h}A_\mathrm{h}} \tag{6.69}$$

$$F_\mathrm{a2} = \frac{E_\mathrm{a}A_\mathrm{a}}{E_\mathrm{a}A_\mathrm{a} + E_\mathrm{h}A_\mathrm{h}}F \tag{6.70}$$

By adding both forces and with (6.47) the relationship between actuator force of the hybrid actuator and force in the active element is obtained

$$F = \frac{E_\mathrm{h}A_\mathrm{h} + E_\mathrm{a}A_\mathrm{a}}{E_\mathrm{a}A_\mathrm{a}}F_\mathrm{a} - E_\mathrm{h}A_\mathrm{h}\varepsilon_i \tag{6.71}$$

and from this the expression of the equivalent limit stress

$$\hat{\sigma}_\mathrm{lim} = \left(\frac{E_\mathrm{h}}{E_\mathrm{a}}(1-\eta) + \eta\right)\sigma_\mathrm{lim} - E_\mathrm{h}(1-\eta)\varepsilon_i \tag{6.72}$$

Finally, in the case of an actuator equipped with a ideal leverage system of stroke amplification factor λ, the expressions for stroke and force are modified as

$$u_\mathrm{i} = \lambda\varepsilon_\mathrm{i}l \tag{6.73}$$

$$F_\mathrm{b} = \frac{1}{\lambda}AE\varepsilon_i \tag{6.74}$$

and the corresponding equivalent material parameters are

$$\hat{\varepsilon}_\mathrm{i} = \lambda \varepsilon_\mathrm{i} \tag{6.75}$$

$$\hat{E} = \frac{E}{\lambda^2} \tag{6.76}$$

6.4.2 The Stiffness-Matching Paradigm

In the last section it was stated that the mechanical work to be produced by an actuator against a linear stiffness and without pre-stress determines the minimum volume of the actuator. Its actual volume, however, can be much higher than this minimum threshold if the actuator geometry is not properly chosen. The design criterion is in this case the stiffness matching principle: the actuator is to be designed such to match the stiffness of the host structure to minimize its volume for a given amount of mechanical work. If the actuator is much weaker than the host structure, it must be designed for a very high free stroke in order to reach the required stroke under load. This results in a very long actuator; conversely, an actuator which would be much stiffer than the structure would need a very large cross section area to develop enough force when loaded. In both cases, the actuator works inefficiently, i.e. a much larger amount of active material is required as compared to the stiffness matching case. While discussing this principle in the following, we will explicitly refer to the case of a prismatic actuator without strength limits; extensions to actuators of other shapes and with active strength boundaries can be made according to what explained in the previous section.

Figure 6.21(a) shows a given characteristic of the host structure (solid line) and a point on it, which is to be reached by the actuator to be designed. An infinite number of actuators (dashed lines) made of a given active material (i.e. with given values of the maximum induced strain ε_i and of the Young's modulus E) are conceivable which, when loaded by coupling them with the structure, would provide the required values of force and stroke (given by the coordinates of the point in the figure). All the actuators differ in their values of the blocking force and free stroke, and consequently in their length and cross-section area. From (6.30), (6.45) and (6.46) the relationship between actuator's length and cross-section area is obtained

$$A = -\frac{F}{E}\frac{l}{(u - \varepsilon_\mathrm{i} l)} \tag{6.77}$$

with u and F as given values of the actuator's stroke and force to be reached. While taking the actuator's length as the design variable, the volume of the actuator can be expressed as

$$V = -\frac{F}{E}\frac{l^2}{(u - \varepsilon_\mathrm{i} l)} \tag{6.78}$$

By minimizing the volume as a function of the actuator length the value

$$l_{\text{opt}} = \frac{2u}{\varepsilon_{\text{i}}} \tag{6.79}$$

is obtained, and from (6.77)

$$A_{\text{opt}} = \frac{2F}{E\varepsilon_{\text{i}}} \tag{6.80}$$

which corresponds to the stiffness matching condition (Figure 6.21(b)), in which the actual actuator stroke amounts to half of the free stroke and the actual force to half of the blocking force.

It is clear from the derivation of (6.79)–(6.80) that this result can be extended also to the case in which the actuator does not work against a linear stiffness, but is in general required to reach given values of stroke and force when loaded (see Figure 6.21(c)). In this case the term "stiffness matching" refers to an imaginary linear structure whose characteristic crosses the given work point.

For $l \to \infty$ the cross-section area tends to F/E. In this limit case (horizontal line in Figure 6.21(a)) the actuator works under blocking condition. Conversely, for $l \to u/\varepsilon_i$ (free stroke condition, vertical line) the actuator cross-section area tends to infinity. The practical relevance of these limit cases is that actuators working near their blocking or free-stroke condition are quite ineffective and tend to be very voluminous as compared to the optimal case.

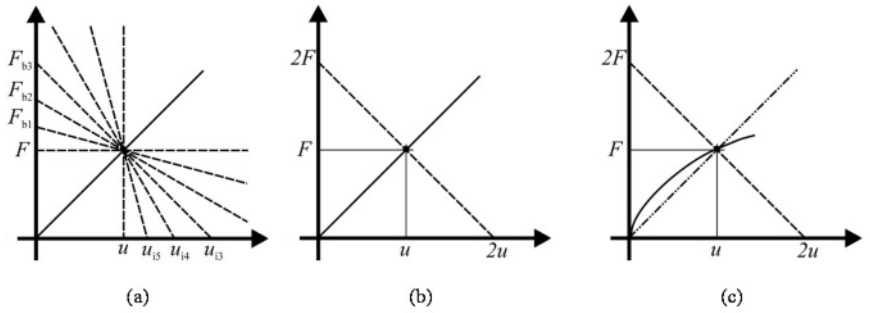

Fig. 6.21 (a) Host structure characteristic with working point and characteristics of actuators providing the required output quantities. (b) Characteristic of the optimal actuator according to the stiffness matching principle. (c) Extension to the case of a general load

6.4.3 Design of Hybrid Actuators

Most actuators are built in hybrid configuration. Piezoelectric stack actuators, pre-stressed actuators as well as actuators integrated in a compliant mechanism for stroke amplification and/or conversion are among the most common configurations.

Design for minimum volume as introduced in the previous chapter can be extended to hybrid configurations by referring to the equivalent material parameter introduced in Section 6.3.7. For instance, an actuator in parallel design with a given area ratio η can be optimized according to (6.79)–(6.80) by taking into account the expressions (6.65)–(6.66) for the Young's modulus and the induced strain. The resulting design will have the minimal overall volume among all actuators with the given η and able to supply the assigned output quantities under load. With respect to the use of pure active material, the optimal volume will increase, being inversely proportional to the factor on the right end side of (6.67).

In the special case of the design of a pre-stressed actuator, the design will therefore include some volume (or weight) penalty due to the need of realizing a given pre-stress. The design of the passive parallel component is ruled by *strength* considerations: it must carry the assigned pre-stress force plus the active force (6.43) present in the open-loop (free-stroke) state. Since the volume penalty is essentially influenced by the *stiffness* of the passive element, it is advantageous to choose materials with a high ratio between strength and Young's modulus (or equivalent spring constructions with high strength and low stiffness).

6.4.4 Solid-state Actuator in a Compliant Frame

One of the advantages of solid-state actuations is their monolithic nature. Motion generation does not require moveable parts. If stroke amplification or re-direction is required, a solution which is fully consistent with this nature is the use of a compliant mechanism to this purpose. In this way, the typical advantages of the monolithic design (no wear and backlash, no need for lubrication, high scalability, low weight) are kept at the level of the complete actuator. As a counterpart, the design process becomes quite challenging, mainly due to the inherent complexity of the design of the compliant frame.

In this section, we will directly refer to the so-called *fish-mouth actuator* [2] as a representative example for this class of actuators. Most of the concepts and results can be, however, applied or adapted to other cases.

Beyond the primary function of redirecting the actuator force and stroke and/or converting its output (stroke or force amplification), the compliant frame can perform one or more of the following additional tasks:

- *providing the actuator with an own stiffness*: for most applications, especially in the field of adaptive structures, actuators are required to provide some level of structural stiffness, since the twofold function of the actuator as an active and a

passive element helps saving structural weight; additionally, the actuator's own stiffness can contribute to increase its precision: load fluctuations which cannot be actively compensated (e.g. due to the limited dynamics of the control system or sensor's resolution) are equilibrated in a passive way;
- *pre-stressing the active component*: some solid-state actuators can only work under a compression loading state (like piezoceramic stack actuators) or under a tension state (like shape-memory wires); pre-stress enables a bi-directional function and increases indirectly the actuator's stiffness by fully exploiting the contribution of the active material;
- *restoring the activation mechanism*: this is relevant for active materials which require a (pseudoplastic) pre-strain to perform their activation task (typically Shape-Memory Alloys).

The fish-mouth actuator uses a bundle of Shape-Memory wires as active element. The compliant frame is a prismatic composite spring with a closed section (see Figure 6.22). The section mean line consists of two half ellipses joined by straight lines. The elliptical regions bend during activation and provide the mechanism with the desired compliance. The fish-mouth actuator was conceived to realize a high effective strain (more than 25%) by employing Shape Memory wires with 2% active strain. The effective strain is defined as the ratio between the induced strain and the thickness of the actuator measured in the activation direction:

$$\varepsilon_{\text{eff}} = \frac{u_{\text{i}}}{h} \tag{6.81}$$

or, with (6.73)

$$\varepsilon_{\text{eff}} = \lambda \frac{l}{h} \varepsilon_{\text{i}} \tag{6.82}$$

where ε_i is the active strain of the Shape Memory Wires.

According to (6.82), the strain increase is due to two contributions: the actual stroke amplification λ and the re-orientation of the stroke in the transversal direction, which involves a further factor l/h (in the final design of the fish-mouth actuator these factors amount to 2 and 6.75, respectively).

Similar hybrid actuator concepts were developed for piezo-stack actuators [7][6].

While analyzing the hybrid actuator, the compliant frame can be seen as a two-degrees-of-freedom system (see Figure 6.23). The input degree of freedom concerns the force P and stroke v produced by the active element; the output degree of freedom refers to the force F and stroke u of the hybrid actuator. The signs of the input quantities are defined in coherence with the conventions of Section 6.3 with respect to the active element (SMA wires). Expansion of the wires leads to a positive stroke v and compression in the wires to a positive force P. The arrows in Figure 6.23 represent forces acting on the frame (note that forces acting on the frame and displacements are of different signs on the output side).

In order to perform its task, the compliant frame must simultaneously fulfill several mechanical requirements, which are partially in conflict with another:

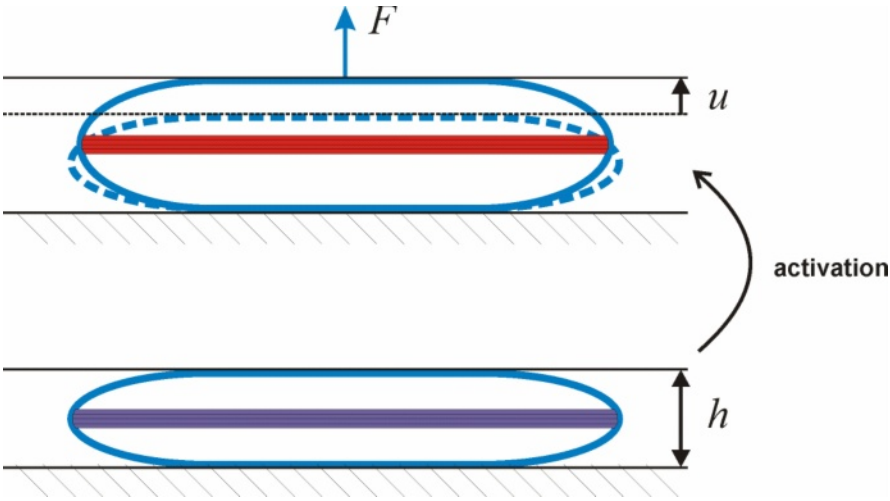

Fig. 6.22 The fish-mouth actuator

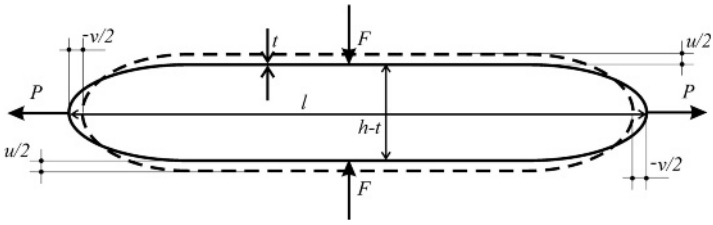

Fig. 6.23 The fish-mouth actuator spring as a two-degrees-of-freedom system

- *Deformability*. The frame has to allow the deformation which is required to transfer/convert the stroke of the active component to the output degree of freedom under free-stroke conditions. Since no force is prescribed but only displacements, this results in a merely kinematic condition. The relevant material parameter is the allowable strain of the passive material. If – like in the case of the fish-mouth actuator – the compliant frame relies on bending elements and the mean line geometry is given, the deformability condition results in an upper limit for the thickness of the flexible parts.
- *Flexibility*. This property concerns the *primary stiffness* of the compliant frame, i.e. the stiffness

$$k_I = \left.\frac{dP}{dv}\right|_{F=0} \tag{6.83}$$

measured at the input interface with the output port unloaded (free-stroke condition). In the representation of Figure 6.20, the primary stiffness is proportional to the stiffness of the spring arranged in parallel to the solid-state actuator (see below). According to (6.44), it reduces the actuator's free stroke and should be therefore kept low.

- *Stiffness*. The *secondary stiffness* of the compliant frame

$$k_{II} = -\left.\frac{dF}{du}\right|_{v=0} \tag{6.84}$$

  is the stiffness measured at the output interface with the input port blocked (i.e. with the stroke of the active element equal to zero). In the model of Figure 6.20, it corresponds to the stiffness of the spring arranged in series to the solid-state actuator (k_{h2}). According to (6.40), it affects the actuator's blocking force and must be as high as possible to keep the blocking force of the hybrid actuator close to the one of the amplified solid-state actuator.
- *Strength*. Loading the actuator at the output interface $F > 0$ creates an additional stress state as compared to the free-stroke operation which is the object of the deformability requirement. Ideally, the compliant frame should be designed such that the strength boundary remains passive (i.e. no point on the activation boundary should lead to a critical stress state). At least, the strength boundary should be determined in order to avoid mechanical overload.

Beyond the mentioned mechanical requirements, the compliant frame is expected to convert forces and strokes by given factors:

$$\gamma_s = \frac{u}{v}; \quad \gamma_f = \frac{F}{P} \tag{6.85}$$

Both factors are negative since the compliant mechanism also inverts the sign of forces and strokes.

The force-deformation behavior of the compliant frame, which rules the amplification factors and the stiffness values, is, as a rule, nonlinear due to large deformations. In order to comply with the hypotheses at the basis of the theory presented in 6.3, we will assume that the behavior of the compliant frame can be linearized about a suitable point. In this case, the equivalent spring model Figure 6.20 can be used.

Concerning the amplification factors, it should be pointed out that a compliant system, unlike a conventional mechanism, has a mechanical efficiency lower than unity, which involves that the stroke conversion factor is not necessarily the reciprocal of the force conversion factor. Besides this, the conversion factors depend on the loading. Due to the reciprocity property of conservative systems, however, the stroke amplification factor for unloaded output ($F = 0$) is equal to the reciprocal of the force amplification factor for blocked input ($v = 0$).

This can be seen by writing the force-displacement relationship of the compliant frame as a two-degrees-of-freedom system

$$\begin{bmatrix} P \\ F \end{bmatrix} = \begin{bmatrix} a & b \\ -b & -c \end{bmatrix} \begin{bmatrix} v \\ u \end{bmatrix} \tag{6.86}$$

where a, b and c are positive constants.
$F = 0$ implies

$$bv = -cu \Rightarrow u = -\frac{b}{c}v \Rightarrow \gamma_s|_{F=0} = -\frac{b}{c} \tag{6.87}$$

whereas $v = 0$ leads to

$$F = -\frac{c}{b}P \Rightarrow \gamma_f|_{v=0} = -\frac{c}{b} \tag{6.88}$$

While recalling the spring model of Figure 6.20, it should be noted that the force provided by the solid-state actuator in the graph (which is already ideally stroke-amplified by the factor λ) amounts to P/λ and its stroke to λv.

The parallel spring constant is $k_I\lambda^2$ and the serial spring constant is equal to the secondary stiffness k_{II}, since in the open-loop configuration of the hybrid actuator (Figure 6.24(a)) the parallel spring defines the relationship

$$\frac{P}{\lambda} = \frac{k_I}{\lambda^2}\lambda v \Rightarrow P = k_I v \tag{6.89}$$

which corresponds to the definition of the primary stiffness (6.83), whereas in the case of shorted input (Figure 6.24(b)), the ratio between output force and output displacement is directly given by the serial stiffness

$$F = -k_{II}u \tag{6.90}$$

In the open-loop case, the displacement produced by the solid-state actuator corresponds to the overall displacement of the hybrid actuator:

$$\lambda v = u \tag{6.91}$$

while in the case of shorted input the force of the solid-state actuator equates the force of the hybrid actuator:

$$\frac{P}{\lambda} = F \tag{6.92}$$

This leads to the conclusion that the ideal amplification factor in the graph corresponds the stroke amplification factor for unloaded output $\gamma_s|_{F=0}$ (and its reciprocal to the force amplification factor for blocked input $\gamma_f\big|_{v=0}$). This result appears evident if one considers the fact that in both examined loading configurations the springs in the equivalent system are not loaded and therefore cannot influence the system's behavior. The mechanism behaves therefore as an ideal amplification device.

For a general loading (given output force F, see Figure 6.24(c)) it holds

$$F = \frac{P}{\lambda} - \frac{k_I}{\lambda^2}\lambda v \tag{6.93}$$

and the force amplification factor is therefore

$$\gamma_f = \frac{1}{\lambda}\left(1 - k_I\frac{v}{P}\right) \tag{6.94}$$

Equation 6.94 suggests that the force amplification factor of the compliant frame decreases for decreasing loading of the input port. If v reaches the value k_I/P (which implies $F = 0$ according to (6.83)) the force amplification factor drops to zero.

The stroke amplification factor is obtained for the general loading case from

$$u = \lambda v - \frac{F}{k_{II}} \Rightarrow \frac{u}{v} = \lambda - \frac{u}{v}\frac{F}{uk_{II}} \Rightarrow \gamma_f = \frac{u}{v} = \frac{\lambda}{1 + \frac{F}{uk_{II}}} \tag{6.95}$$

Analogously to the force amplification factor, the stroke amplification factor decreases for increasing loading at the output port and reaches zero for $u = 0$.

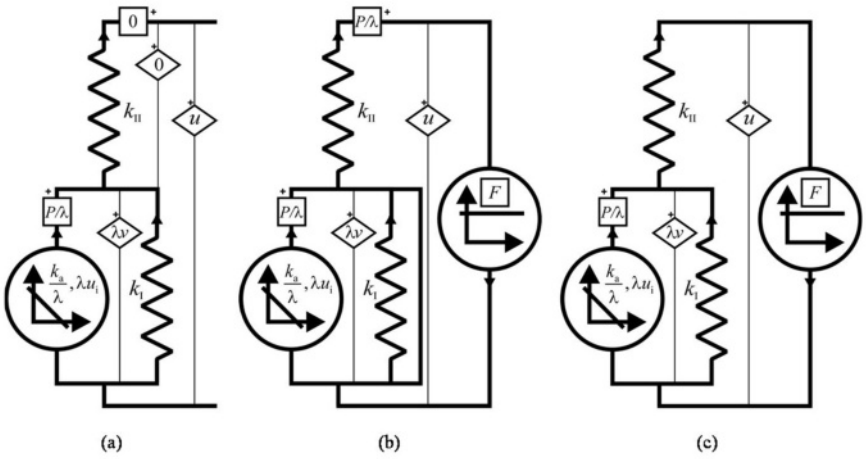

Fig. 6.24 Graph of the hybrid solid-state actuator with (a) open-loop output, (b) shorted input and (c) general loading

The above presented consideration help in the design process of the hybrid actuator to couple the design analysis (analysis of performance as a function of the design variables) of the solid-state actuator itself – which can be carried on according to 6.4.1 – and the one of the compliant frame.

The design of the compliant frame will consist of a kinematic analysis, a stiffness analysis and a strength analysis. In the first one the amplification factors will be analyzed as a function of the design variables, in the second one the stiffness values and in the third one the limit loads which the compliant part can carry. Typically, there will be requirement conflicts between the stroke-related properties (deformability and flexibility, which tend to reduce the cross section and the length of the flexible parts) and the load-related properties (stiffness and strength, which favour solutions with short and thick springs). Simplified analytical models are very useful to manage the trade-off, at least in a preliminary design phase. More accurate

modeling and experimental analysis can help to refine the design. In some cases it can be appropriate to support the design procedure by means of formal optimization algorithms, especially in the coupled design phase (compliant frame and solid-state actuator).

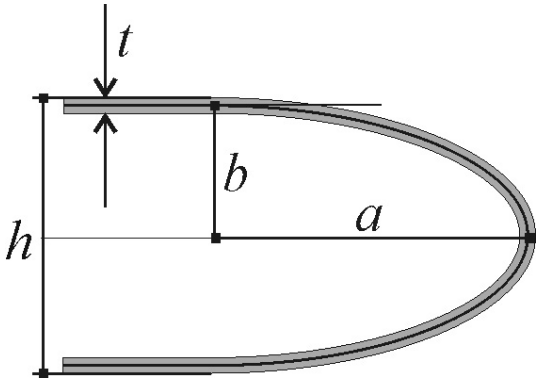

Fig. 6.25 The elliptical region of the fish-mouth actuator spring

In the case of the fish-mouth actuator, the kinematics of the compliant frame is essentially ruled by the mean line geometry of the composite spring. Several simplified analytical models were formulated and compared to another as well as to FEM analysis results. The most accurate proved to be the so-called circle-arc model, in which the elliptical regions of the spring were approximated by circle arcs and supposed to keep a circular shape after bending [2]. This model provides the expression of the stroke amplification ratio

$$\gamma_s = \frac{1 - 2\mu \arctan\left(\frac{1}{\mu}\right)}{\mu - (\mu^2 - 1)\arctan\left(\frac{1}{\mu}\right)} \tag{6.96}$$

where

$$\mu = \frac{a}{b} \tag{6.97}$$

is the axis ratio of the spring ellipse (see Figure 6.25). The expression (6.96) can be simplified for large aspect ratios by Taylor approximation as

$$\gamma_s \simeq -\frac{3}{4}\lambda \tag{6.98}$$

which provides for $\lambda \geq 2$ the amplification factor with an (overestimation) error less than 7%.

The spring's primary stiffness is essentially related to the bending stiffness of the elliptical regions. Here simple models on the basis of the Bernoulli-Euler beam theory supply a useful basis for the design analysis. As far as the secondary stiffness

is concerned it could be necessary to take into account membrane deformations of the composite spring to properly evaluate its behavior.

Finally, the strength analysis deals with a quite complex stress distribution in the flexible region and should be therefore supported by a thorough experimental analysis. The collapse mechanisms will be profoundly different in the free-stroke operation and in the blocking-force operation and need to be analyzed separately for the two loading cases. A linear superposition of the results with the aim of predicting the full strength boundary (i.e. the strength limit for an arbitrary loading through coupling with a host structure of given stiffness) can be considered as a preliminary basis, but it should be completed by experimental determination of the actual strength limit for an adequate number of loading conditions.

The blocking force rupture mode is quite complex to be analyzed theoretically in order to obtain a useful design relationship for the limit force as a function of the design parameters. As far as the free stroke strength limit is concerned, however, the assumption of a classical bending collapse due to a strain level beyond the allowable limit can be taken as a criterion, resulting in an upper boundary for the laminate thickness. According to the circle-arc model the corresponding restriction can be written

$$t \leq \frac{2}{\frac{1}{R} - \frac{1}{R_0}} \varepsilon_{\text{all}} \tag{6.99}$$

with as the material's allowable strain. The radii and are known functions of the geometrical design variables as well as of the required actuator stroke.

While analyzing a hybrid actuator with a compliant frame for stroke and force amplification and/or conversion, the simple relationships obtained in Section 6.4.1 for the case of a prismatic block of active material are of course no longer valid and have to be adapted. For instance, increasing the cross-section area of the fish-mouth actuator (normal to the direction of the output force and stroke) do not influence only the blocking force, but has a more complex effect on all performance parameter (the length of the active element increases and consequently the stroke at the input port; in addition, the amplification factors as well as the stiffness values are concerned by the resulting changes in the spring geometry).

6.4.5 The Actuator's Own Stiffness as a Design Requirement

As mentioned before, a solid-state actuator can be required – beyond its primary performance features like free stroke and blocking force – to supply the host structure with a given amount of stiffness. One of the advantages of solid-state actuators is represented by their inherent stiffness which results by their strain-inducing actuator principle; conventional force-generating devices like electromagnetic actuators do not provide the host mechanical system with a stiffness contribution (see also Section 6.4.1).

In general, three different levels of stiffness contributions can be identified while analyzing a solid-state actuator:

1. The mere stiffness contribution of the passive component (if this exists, i.e. for the case of an actuator in hybrid design).
2. The stiffness contribution resulting from the passive stiffness of the active material, supported by the one of the passive component (if available).
3. The stiffness contribution of the actuator in connection with a feedback control system.

The third level can realize – as a matter of principle – arbitrarily high level of stiffness (a theoretically infinite stiffness can be realized by a feedback control system which keeps the actuator stroke at a constant value). The stiffness contribution due to the feedback control, however, disappears when the actuator is not active and is limited in its dynamics by the reaction time constants of the control algorithm and hardware. The second level is always present as long as the active element keeps its integrity. In the case of a collapse, the stiffness level drops to level one.

The contribution provided by the passive stiffness of the active material, which is essential to level two, can be estimated by simple considerations of solid mechanics, involving the element's geometry and the material's modulus of elasticity, as already made in 6.4.1. However, this constitutes an approximate approach since it neglects the feedback effects which stem from the typical multi-field nature of active materials. Considering for instance a piezoceramic actuator, together with the so-called *inverse* piezoelectric effect which is at the basis of the actuator function, a *direct* piezoelectric effect is always present which rules the sensor function of the piezoceramic element. Both effects are described by the piezoelectric equations

$$\mathbf{S} = \mathbf{s}\mathbf{T} + \mathbf{d}\mathbf{E} \tag{6.100}$$

$$\mathbf{D} = \mathbf{d}^{\mathbf{T}}\mathbf{T} + \varepsilon\mathbf{E} \tag{6.101}$$

with:

- **T** as the vector including the six components of the mechanical stress.
- **S** as the vector of mechanical strain, correspondingly arranged.
- **E** as the vector including the three components of the electric field.
- **D** as the vector with the components of the electric displacement.
- **s**, **d** and ε as matrices of material-dependent coupling constants (elasticity, piezoelectric and electrostatic constants, respectively).

From Equations 6.100 and 6.101 is evident that the change in mechanical stress does not determine, alone, the mechanical strain in the component. An exact determination of the stiffness contribution of the active material can only be obtained if the electrostatic variables are eliminated from the equations, which, in turn, requires taking into account the properties of the electrical circuit behind the piezoelectric element.

In the case of a Shape Memory Actuator the relevant coupling effect which is to be considered is of thermo-mechanical nature. The stiffness of the Shape-Memory element depends on the tangent elasticity modulus of the shape-memory material, which is a complex function of stress and temperature in the wire as well as of the

loading history, due to the pronounced hysteresis which characterize the behavior of shape-memory alloys. Shape-memory constitutive model from the several ones available in the literature (see for instance [1]) can be used in order to describe this relationship. Such a model supplies – for a given alloy – one relationship between stress, strain and temperature. The system keeps two degrees of freedom, i. e. nothing can be said about the infinitesimal change of stress for a given infinitesimal change of strain if it is not defined how the temperature is allowed to change. For this reason the tangent modulus and, as a consequence, the actuator transversal stiffness for a given load case depends on a *temperature evolution law* which can, in turn, be directly or indirectly coupled with the actuator mechanics.

For slow load fluctuations and no wire activation the *isothermal* condition can be taken as temperature evolution law. For fast load fluctuations (e.g. in the case in which the actuator stiffness is needed for dynamic purposes) an *adiabatic* temperature evolution should be considered, which takes into account the latent heat of the martensitic transformation and relates the temperature change with the stress or the strain change in the wire. If the shape-memory wires are electrically activated by Joule effect, the evolution of the electrical resistance in the wire has to be taken into account in the temperature evolution law. Finally, if the actuator is feedback-controlled, the control law influences significantly the actuator stiffness behavior. In evaluating the actuator's transversal stiffness attention must be paid to the fact that the stiffness values can differ for loading and unloading due to the hysteretic behavior of the shape-memory alloy.

The maximum conceivable stiffness contribution at level two for an actuator in hybrid design is given by an active element which – due for instance to the action of a feedback controller which keeps the stroke of the active element at a constant value – blocks the input port. In this case the actuator provides a stiffness contribution which is equal to the above introduced secondary stiffness. This case is not to be confused with the above mentioned case of a controller acting on the overall actuator stroke, which is virtually able to realize an infinite stiffness (level three).

6.4.6 Coupled Design of Actuator and Host Structure

In some cases, particularly while designing active shape-adaptable systems based on the integration of solid-state actuators in compliant structures, the actuator design is to be directly coupled with the design of the host structure itself. Like in the case of a compliant frame as a part of a hybrid actuator, a shape adaptable host structural system is subject to conflicting requirements, like providing given load-carrying capabilities (stiffness and strength) and at the same time offering a required amount of deformability (defined as the maximum deformation of the compliant structure which is compatible with the allowable strain of the material) in order to accommodate the desired shape changes. In some cases, this leads to a problem definition which requires a given contribution of the solid-state actuator to offer feasible solutions at all.

It is important to note here that the presence of a solid-state actuator with a given amount of own stiffness is the key element to solve such requirement conflicts by introducing essential additional design variables: the stiffness which can be subject to an upper limit due to the deformability requirement is the stiffness of the host structure, which is different from the stiffness of the complete system "seen" by the external load, i.e. the system consisting of solid-state actuator and structure. In other words: by increasing the size of the solid-state actuator the load-carrying capabilities of the overall system are enhanced without any influence on the deformability of the compliant part.

An example in which a coupled structure-actuator design is essential is reported in the following. A shape-adaptive wind-tunnel model had to be designed and realized [1]. The required geometry changes included, among others, a hinge less trailing-edge flap. The concept which was adopted for the hinge less flap is schematically described in Figure 6.26. This design responded very well to manufacturing and aerodynamic requirements as well as to the restrictive space constraints. Shape memory alloy wires were chosen for actuation. A minimum swing angle was prescribed for the active flap as well as the maximum allowed deviation from the target contour under load. Destined to operate in two-dimensional flows, the wind-tunnel model was additionally required to have constant deformation behavior in span direction. This called for a prismatic geometry of the compliant system and virtually reduced the design variables to the ones defining cross-section geometry thickness and material of one single leaf spring. The spring length was set to the largest value compatible with the space constraints: beyond this limit the airfoil thickness at the spring end would have become too small to accommodate the attachment between actuator wires and structure without causing manufacturing problems and leading to unacceptably low values of the actuator lever arm. In the considered case, therefore, the deformability-versus-stiffness trade-off is essentially ruled by just one design variable, namely the spring thickness (some influence is exerted by the material choice, but within narrow limits).

In this case, deformability and stiffness are directly conflicting qualities: ensuring proper deformability means setting an upper bound to the spring thickness, while the stiffness requirement implies a lower bound for it. It can therefore happen that the design problem admits no solution if limited to the passive compliant system. If the stiffness contribution of the actuator is taken into account, however, any required level of overall stiffness can be reached – without affecting deformability – by properly choosing the cross section of the wire bundle.

This effect is exemplarily illustrated by the design domain graphs of Figure 6.27. The graphs are traced on the $h-a$-plane, with h as the leaf-spring width and a as the cross section of the actuator wire bundle per unit width in span direction. If the actuator's stiffness contribution is not considered (Graph a), the actuator cross section does not come into play and the feasible design domain, identified by the restrictions $h \leq h_d$ and $h \geq h_s$, is an empty set (no feasible solutions) if $h_d < g_s$. The contribution of the actuator material to the overall stiffness modifies the corresponding restriction boundary to a curve of the kind $h^2 + Ba = h_s^3$, which always intersects the boundary of the deformation restriction, providing a finite region of feasible de-

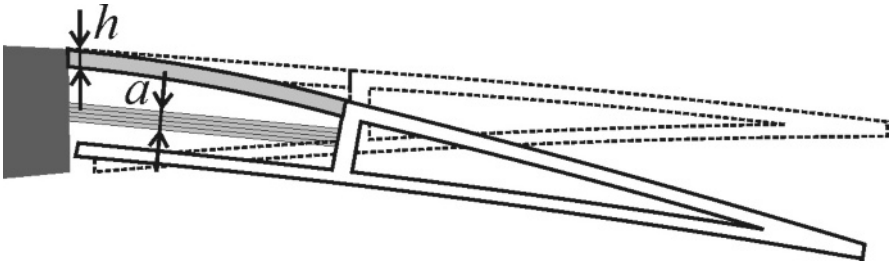

Fig. 6.26 Design of a hinge less trailing-edge flap

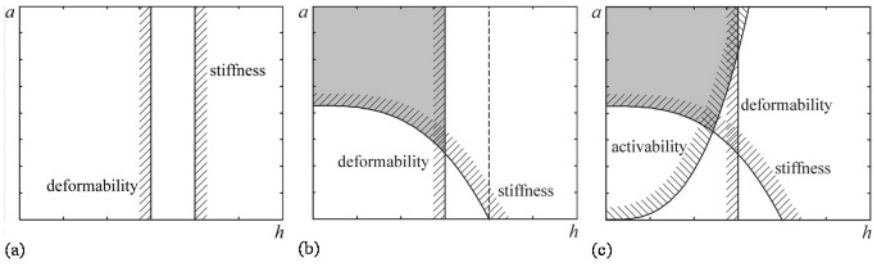

Fig. 6.27 Design space graphs for the hinge less trailing-edge flap

signs (Graph b). A possible reduction of the feasible design domain (Graph c) can result from the activability restriction, which requires the actuator wire bundle to provide enough active force to bend the leaf spring by the required amount and takes the form $a/h^2 \geq C > 0$.

6.4.7 Simultaneous Optimization of Actuator Position and Geometry

A large amount of contributions can be found in literature, which deal with the optimization of the actuators' position in active structures, most of them in dynamic applications. In most cases, however, an interaction with the actuator design is not considered. A usual optimization target is the claim of minimal actuator force for a given effect on the active structure (static or dynamic response). What is often overlooked in this context is that reducing the actuator force do not necessarily reduces its size, and that the relationship between actuator force and stroke needs to be taken into account. The force-related criterion is the more appropriate, the closer the actuator behaves to an ideal force generator. If conventional electromagnetic actuators are used, for instance, this kind of approach reveals correct.

As discussed before, a solid state actuator always behaves between an ideal force generator and an ideal stroke generator. While operating in the neighborhood of the

blocking condition (actuator own stiffness negligible as compared to the stiffness of the host structure), the actuator closely resembles in its behavior an ideal force generator. While operating near the free-stroke condition (large actuator stiffness as compared to the structure stiffness) the behavior is similar to the one of an ideal stroke generator. In the limit case of an ideal stroke generator, minimizing the actuator force while optimizing the actuator position would lead to misleading results: more appropriate locations could then be found in points with conventionally unfavorable leverage conditions, in which activations requires large forces and small strokes.

Even if – as usual – the actuators operate in quasi-blocking condition, it leads, as before discussed, to a quite inefficient actuator design according to the stiffness matching paradigm. In the limit case (blocking condition) the required actuator volume would approach infinity in order to provide a finite stroke.

To simultaneously optimize position and geometry of the actuators, it can therefore be convenient to adopt an energetical approach, which virtually de-couples the two optimization steps. In the static case, and if the conditions for the application of the stiffness-matching paradigm are fulfilled, the required actuator's volume is unequivocally determined by the mechanical energy which is to be transmitted to the host structure. The optimization can hence be carried out stepwise:

1. search of the actuator position or positions which require a minimum of mechanical work to reach the desired static response; determination of the required actuator force and stroke to perform activation in the optimal actuator point or points.
2. optimization of the actuator geometry according to the stiffness matching paradigm (see 6.4.2).

6.5 Extension to the Dynamic Case

6.5.1 Work Produced by a Solid-State Actuator in Cyclic Operation

In 6.3.6 the energy output of a linear solid-state actuator interacting with a linear stiffness was analyzed. The stroke work introduced there was defined as the maximum possible amount of work which can be performed by the actuator in a single activation process from zero to a given value of induced strain. If the reduced strain is reported to zero, the curve on the force-stroke plane is described in the opposite direction, energy flows from the structure to the actuator and the total amount of work produced by the actuator over the activation *cycle* is zero.

By coupling the actuator with a different kind of load (e.g. a nonlinear mechanism or a structural element with hysteretic behavior) a positive amount of work could be extracted by the actuator. In this case the area of the actuator's operation domain (see Figure 6.13(b)) represents the theoretically maximum cyclic work of

the actuator. The actual value of the cyclic work depends on the force-displacement characteristic of the load.

A particularly relevant kind of load in this context is a linear oscillating system. We consider the case of a system excited by the sinusoidal force

$$F(t) = F_0 + F_\mathrm{d} \sin \omega t \tag{6.102}$$

with the static term F_0 and the oscillating term $F_d \sin \omega t$. The response of the oscillating system will have in general the following form

$$u(t) = u_0 + u_\mathrm{d} \sin(\omega t + \varphi) \tag{6.103}$$

The static term of the response will be determined by the static stiffness of the load:

$$u_0 = \frac{F_0}{k_\mathrm{s}} \tag{6.104}$$

while the dynamic part of the response (without taking into account transient effects) will be given by the dynamic stiffness of the host system at the given frequency. By expressing the sinusoidal parts of excitation and response in complex terms

$$F_\mathrm{d} \sin \omega t = \mathrm{Re}\left[\hat{F}_\mathrm{d} e^{i\omega t}\right] \tag{6.105}$$

$$u_\mathrm{d}(\sin \omega t + \varphi) = \mathrm{Re}\left[\hat{u}_\mathrm{d} e^{i\omega t}\right] \tag{6.106}$$

the dynamic stiffness is defined by

$$\hat{k}_\mathrm{d}(\omega) = \frac{\hat{F}_\mathrm{d}}{\hat{u}_\mathrm{d}} = k_\mathrm{d} e^{i\varphi} \tag{6.107}$$

with

$$k_d(\omega) = \frac{F_\mathrm{d}}{u_\mathrm{d}} \tag{6.108}$$

as the modulus and $\varphi(\omega)$ as the phase of the dynamic stiffness (i.e. the phase difference between response and excitation; please note that by definition the phase of the excitation is zero, so the phase of the dynamic stiffness coincides with the phase of the response). We will choose to define the phase angle in the range

$$-\pi < \varphi \leq \pi \tag{6.109}$$

For a given static offset F_0 (and the resulting value of the static response u_0), a particular value of the dynamic stiffness (which is unequivocally determined by the nature of the host dynamic system and the activation frequency) identifies on the force-stroke plane a family of elliptical trajectories (see Figure 6.28). All ellipses of the family have the centre, the axis ratio as well as the direction of the axes in common. Additionally, a sense of description is assigned to the trajectories, depending on the phase angle. For $0 < \varphi < \pi$ the trajectories are traced counter clockwise, for

$0 < \varphi > -\pi$ clockwise. In the cases $\varphi = 0$ and $\varphi = \pi$ the ellipses degenerate in segments of the straight lines

$$F = k_d u \tag{6.110}$$

$$F = -k_d u \tag{6.111}$$

respectively.

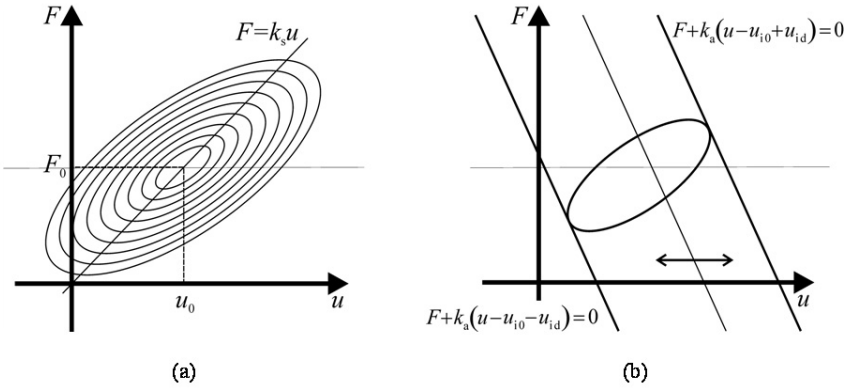

Fig. 6.28 (a) Family of elliptical trajectories for an oscillating host system and (b) trajectory described for a given oscillating induced stroke

Within a given trajectory family a particular curve can be identified by a given value of the dynamic stroke or force amplitude (only one of them can be freely chosen since Equation 6.108 must be fulfilled).

Now we assume that the force and stroke of the dynamically operating solid-state actuator are related one another as in the static case, i.e. they fulfill the relationship (6.30). This assumption is realistic if the activation frequency is far lower than the actuator's first resonance frequency.

By inserting (6.102) and (6.103) into (6.30) we obtain

$$u_i = u_{i0} + u_{\mathrm{id}} \sin(\omega t + \psi) \tag{6.112}$$

with

$$u_{i0} = \frac{F_0}{k_a} + u_0 \tag{6.113}$$

$$u_{\mathrm{id}} = \sqrt{\left(\frac{F_{\mathrm{d}}}{k_a}\right)^2 + 2u_{\mathrm{d}}\frac{F_{\mathrm{d}}}{k_a}\cos\varphi + u_{\mathrm{d}}^2} \tag{6.114}$$

$$\cos\psi = \frac{\frac{F_\mathrm{d}}{k_a} + u_\mathrm{d}\cos\varphi}{u_\mathrm{id}} \qquad \sin\psi = \frac{u_\mathrm{d}\sin\varphi}{u_\mathrm{id}} \tag{6.115}$$

which shows that an oscillating induced stroke produces an actuator force and a stroke compatible with (6.102) and (6.103). Equation 6.113 identifies together with (6.104) the static offset of the actuator force (and stroke), while (6.108) and (6.114) define the dynamic amplitude and hence determine which one of the elliptical trajectories is described.

$$u_0 = \frac{u_{i0}}{1+\frac{k_\mathrm{s}}{k_a}} \tag{6.116}$$

$$F_0 = \frac{k_\mathrm{s} u_{i0}}{1+\frac{k_\mathrm{s}}{k_a}} \tag{6.117}$$

$$u_\mathrm{d} = \frac{u_\mathrm{id}}{\sqrt{\left(\frac{k_\mathrm{d}}{k_a}\right)^2 + 2\frac{k_\mathrm{d}}{k_a}\cos\varphi + 1}} \tag{6.118}$$

$$F_\mathrm{d} = \frac{k_\mathrm{d} u_\mathrm{id}}{\sqrt{\left(\frac{k_\mathrm{d}}{k_a}\right)^2 + 2\frac{k_\mathrm{d}}{k_a}\cos\varphi + 1}} \tag{6.119}$$

According to Equation 6.112, the actuator characteristic performs a harmonic translation on the force-stroke plane and describes a strip limited by the straight lines

$$F + k_a\,(u - u_{i0} - u_\mathrm{id}) = 0 \tag{6.120}$$

$$F + k_a\,(u - u_{i0} + u_\mathrm{id}) = 0 \tag{6.121}$$

which are tangent to the traced elliptical trajectory (see Figure 6.28(b)).

The area of the ellipse corresponds to the work performed by the solid-state actuator during a cycle. It holds

$$\Omega = \int_0^{2\pi/\omega} F_d \frac{du}{dt} dt = F_d u_d \int_0^{2\pi/\omega} \sin(\omega t + \varphi) dt = -F_d u_d \pi \sin\varphi \tag{6.122}$$

The average power is obtained by dividing the cyclic work by the period:

$$\Pi = \frac{-F_\mathrm{d} u_\mathrm{d} \pi \sin\varphi}{\frac{2\pi}{\omega}} = \frac{-F_\mathrm{d} u_\mathrm{d} \omega \sin\varphi}{2} \tag{6.123}$$

6.5.2 Maximum Cycle Work and Power Output

For a given actuator, a given excitation frequency, a given phase angle and a given amplitude of the dynamic induced stroke u_{id}, the value of the mechanical power transferred from the solid-state actuator to the host structure depends on the modulus

of the host structure's dynamic stiffness. The power output is maximum when the product $F_d u_d$, expressed as a function of k_d, reaches a maximum.

From (6.118) and (6.119) one obtains

$$F_{\mathrm{d}} u_{\mathrm{d}} = \frac{k_{\mathrm{d}} u_{\mathrm{id}}^2}{\left(\frac{k_{\mathrm{d}}}{k_a}\right)^2 + 2\frac{k_{\mathrm{d}}}{k_a}\cos\varphi + 1} \tag{6.124}$$

The first derivative of the function (6.124) with respect to k_d vanishes when

$$\left(\frac{k_{\mathrm{d}}}{k_a}\right)^2 + 2\frac{k_{\mathrm{d}}}{k_a}\cos\varphi + 1 = 2k_{\mathrm{d}}\left(\frac{k_{\mathrm{d}}}{k_a^2} + \frac{1}{k_a}\cos\varphi\right) \tag{6.125}$$

$$K_a^2 = k_d^2 \tag{6.126}$$

$$k_a = k_d \tag{6.127}$$

Equation 6.127 is the stiffness matching condition for the dynamic case. According to this condition, the output cycle work of the solid-state actuator (and, as a consequence, its output power) reaches its maximum value when the modulus of the host structure's stiffness matches the actuator's stiffness.

Inserting (6.127) into (6.118)–(6.119) the dynamic force and stroke amplitudes are obtained:

$$u_{\mathrm{d}} = \frac{u_{\mathrm{id}}}{\sqrt{2\,(1+\cos\varphi)}} \tag{6.128}$$

$$F_{\mathrm{d}} = \frac{k_{\mathrm{a}} u_{\mathrm{id}}}{\sqrt{2\,(1+\cos\varphi)}} \tag{6.129}$$

The corresponding cycle work and average power amount to

$$\Omega_{\max} = -\frac{\pi\sin\varphi}{2\,(1+\cos\varphi)} k_{\mathrm{a}} u_{\mathrm{id}}^2 \tag{6.130}$$

$$\Pi_{\max} = -\frac{\omega\sin\varphi}{4\,(1+\cos\varphi)} k_{\mathrm{a}} u_{\mathrm{id}}^2 \tag{6.131}$$

In the resonance case:

$$\varphi = \pm\frac{\pi}{2} \tag{6.132}$$

Equations 6.128–6.131 respectively read

$$u_{\mathrm{d}} = \frac{\sqrt{2}}{2} u_{\mathrm{id}} \tag{6.133}$$

$$F_{\mathrm{d}} = \frac{\sqrt{2}}{2} k_{\mathrm{a}} u_{\mathrm{id}} \tag{6.134}$$

$$\Omega_{\max} = \mp \frac{\pi}{2} k_a u_{id}^2 \tag{6.135}$$

$$\Pi_{\max} = \mp \frac{\omega}{4} k_a u_{id}^2 \tag{6.136}$$

The resonance case is particularly relevant for vibration control. When $\varphi = -\pi/2$, positive work is made by the actuator on the structure (resonance excitation), while in the case $\varphi = \pi/2$ the work is negative (resonance damping). The amount of mechanical work which can be extracted from the oscillating system in one vibration cycle defines the capability of the solid-state actuator to actively damp the vibration.

In resonance and in the typical case in which the amplitude of the dynamic induced stroke is half the maximum induced stroke for static activation:

$$u_{id} = u_{i0} = \frac{u_{i,stat}}{2} \tag{6.137}$$

from (6.13), (6.19), (6.20), (6.21) and (6.135) it can be written:

$$|\Omega_{\max}| = \frac{\pi}{8} W_n = \pi W_{\max} \tag{6.138}$$

6.5.3 Design Principles and Rules for the Dynamic Case

Due to the relationship (6.138), many results presented in 6.4 can be extended to the considered dynamic case. The nominal and effective energy density of an active material, for instance, allow for estimation of the minimum amount of actuator volume if the needed cycle work (or power, for a given activation frequency) is known.

While designing an actuator for dynamic applications, the stiffness-matching paradigm, applied to the dynamic quantities, helps reducing or even minimizing the actuator volume by choosing a proper actuator geometry.

Finally, a simultaneous optimization of actuator position and geometry for dynamic applications can be carried on, analogously to the static case, in an energy-related way. As a first step, the actuator position or positions are identified which require minimum power to reach the desired dynamic response; subsequently, the actuator geometry is optimized according to the stiffness matching paradigm.

References

1. Campanile L, Sachau D, Seelecke S (1999) Ein adaptives Windkanalmodell für einen adaptiven Tragflügel. In: (in German) Proc. "Deutscher Luft- und Raumfahrtkongress", Berlin, Germany, pp 19–28

2. Campanile LF, Keimer R, Breitbach EJ (2004) The ”fish-mouth” actuator: Design issues and test results. Journal of Intelligent Material Systems and Structures 15:711–719
3. Gandhi MV, Thomson BS (1992) Smart materials and structures. Chapman and Hall, London
4. Giurgiutiu V, Rogers CA (1996) Energy based comparision of solid state induced strain actuators. Journal of intelligent material systems and structures 7
5. Lesieutre GA, Loverich J, Koopmann G, Mockensturm E (2002) Enhancement of mechanical work output of a piezo-stack using a non-linear motion transmission mechanism. In: 13th International Conference on Adaptive Structures and Technologies (ICAST), pp 631–643
6. Letty RL, Claeyssen F, Barillot F, Lhermet N (2003) Amplified piezoelectric actuators. In: AMAS Workshop on Smart Materials and Structures, Jadwisin
7. Niezrecki C, Brei D, Balakrishnan S, Moskalik A (2001) Piezoelectric actuation: State of the art. The Shock and Vibration Digest 33:269–280
8. Uchino K (1998) Piezoelectric actuators and ultrasonic motors. Kluwer Academic Publishers, Boston

Index